Investigation of Gravity Drainage in Fractured Porous Media

by

Sohrab Zendehboudi

A thesis
presented to the University of Waterloo
in fulfillment of the
thesis requirement for the degree of

Doctor of Philosophy

in

Chemical Engineering

Waterloo, Ontario, Canada, 2010

Author's Declaration

I hereby declare that I am the sole author of this thesis. This is a true copy of the thesis, including any required final revisions, as accepted by my examiners.

I understand that my thesis may be made electronically available to the public.

Abstract

The oil production from well fractured carbonate reservoirs is a considerable part of the total oil production in the world. The petroleum resource base in naturally fractured reservoirs is estimated to be in the range of billions of barrels in the U.S and in addition, a multibillion- barrel international oil resource base exists in naturally fractured reservoirs.

Gravity drainage is important in some of oil recovery processes, either acting as the driving force in processes using horizontal wells or altering the displacement patterns during water-flooding, chemical flooding, CO_2 flooding and other EOR methods. The gravity drainage process has a major effect on oil recovery from oil reservoirs. Gravity drainage driven oil production in naturally fractured and other complex reservoirs falls into two regimes: the balk flow regime and the film flow regime. Oil recovery by gravity drainage in a fractured reservoir strongly depends on the capillary height of the porous medium. Capillarity and gravity forces are usually the major driving forces in fractured reservoirs.

This PhD thesis consists of two main parts namely: 1) Experimental works on gravity drainage, and 2) Modeling and simulation of the gravity drainage processes using COMSOL® software.

An appropriate design of experiment (DOE) method was selected to find the most important parameters contributing in gravity drainage and then conduct the experiments in a useful as well as economic manner. A two-dimensional experimental setup was employed to investigate free fall gravity drainage (FFGD) and controlled gravity drainage (CGD) using unconsolidated glass beads fractured porous media having various fractures configurations. Flow visualization measurements were carried out. Following the flow visualization experiments, parametric sensitivity analysis was performed considering the effects of different system parameters such as fracture aperture, matrix height, permeability, and fluid properties on the dependent variables including drainage rate, critical pumping rate, maximum drainage rate, recovery factor and so on. These experiments enabled us to capture some aspects of the recovery mechanism and the flow communication between matrix block and fracture during gravity drainage. After analyzing the experimental data for the FFGD test runs, it was found that the rate of liquid flowing from matrix to fracture is proportional to the difference of liquid levels in the matrix and in the fracture. In addition, the characteristic rate and the maximum liquid drainage rate from the fractured models were determined for such a stable gravity-dominated process. The experiments showed that the presence of fracture is more influential in lower matrix permeability systems. For a given fracture-matrix system with different initial liquid saturation conditions, it was seen that the production history can be correlated by plotting the fraction of recoverable liquid as a function of time. Furthermore, the recovery factor can be correlated using dimensionless numbers such as the Bond number and the dimensionless time.

For the controlled gravity drainage (CGD) test runs conducted, the experimental results indicated that higher pumping rates cause a higher difference between the liquid levels in the fracture and

in the matrix, thus the gas breakthrough happens sooner. Moreover, it was found that as long as the porous medium is drained with a constant liquid pumping rate but lower than critical rate, the height difference between the G-L interfaces in matrix and fracture remains constant. In this study, a new concept of "Critical Pumping Rate" (CPR) was defined at which each particular porous medium has recovery factor equal to the recovery factor for higher rates just before gas breakthrough. The difference between liquid levels in fracture and matrix remains unchanged at rates higher than CPR. Known this particular withdrawal rate, there are two main advantages, namely: 1) choosing a pumping rate lower than it to drain the reservoir without getting gas breakthrough; and 2) understanding the physics of pumping behaviour from fractured media and extending the concept to the real cases. In addition, the maximum liquid pumping rate from each physical model was studied and it was found that the rate depends strongly on the storage capacity of the fractures, petrophysical properties of each model as well as physical properties of test fluids. The critical rate, maximum rate, recovery factor at gas breakthrough and difference of gas liquid interface positions in matrix and fracture were correlated by dimensionless numbers such as Bond number, Capillary, and the ratio of permeabilities. Linear regression correlations presented in this study can predict production history and flow behaviour in the fractured porous media for a wide range of dimensionless numbers.

The COMSOL® software was used to numerically simulate the gravity drainage processes in the two-dimensional flow experiments for fractured porous media. The parameters of the model were based on theory, as well as on the results of the two-dimensional gravity drainage experiments. The simulation results for the gravity drainage processes compared favourably with the experimental results, as a good match between the numerical solution and the experimental data was found. The simulation model developed provides a basis for further modeling of gravity drainage process in more complicated porous media.

Acknowledgements

I am heartily thankful to my supervisor, Professor Ioannis(John) Chatzis, whose encouragement, guidance and support from the initial to the final level enabled me to develop an understanding of the subject. I am indebted to him more than he knows.

Furthermore, I would like to thank greatly the other members of the supervising committee, Dr. Farhad Ein-Mozaffari, Dr. Xianshe Feng**,** Dr. Rajinder Pal, Dr. Ali Elkamel, and Dr. Jon F. Sykes, for their time and invaluable comments.

I also appreciate and value Dr. Maurice B. Dusseault for his great assistance and detailed technical attention.

I gratefully acknowledge National Iranian Oil Company (NIOC) and the Natural Science and Engineering Research Council (NSERC) of Canada for their financial support.

I wish to thank the technical staff of the Chemical Engineering and Mechanical Engineering Machine Shop. The advice and support of Ravindra Singh, Bert Habicher, Rick Hectus, S. Ganeshalingam and Ralph Dickhout were important for much of the experiment set up in this project. An acknowledgement is also extended to Dennis Herman for his computer support.

Also, I would like to express my deep gratitude to my son, Daniel Zendehboudi and my mother, Mahsoltan Zendehboudi, for their support and understanding. I am greatly indebted to my parents for educating me with aspects from both life and sciences, and for absolute support. They deserve far more credit than I can ever give them. My heartfelt appreciation goes to my wife, Masoomeh Karimi, for her true love, sacrifice, encouragement, unflagging confidence in me, for listening to my complaints and frustrations, and for inspiring, amazing, and helping me get through the tough and stressful times during my PhD study. I am also thankful to her for carefully reviewing my thesis.

Lastly, I offer my best regards and blessings to all my friends and my colleagues(Nima Rezaei, Saeid Mehdiabadi, Ali Mohsenipour, Reza Gheshlaghi, Keyvan Nowruzi, Ali Shafiei, Hossein Parsaei, Mousa Jafari, Amin Rajabzadeh, Abolfazl Maneshi, Majid Soltani, Shahab Eslami, Rafat Parsaei, Saeideh Naderi, Hengameh Aghamohseni, Lena and Saloumeh Ghasemian) at the University of Waterloo who supported and encouraged me in any respect during the completion of the project.

This thesis is dedicated to my son, Daniel;

may he be inspired to question and learn.

Table of Contents

Appendices

List of Tables

List of Figures

Nomenclature

A_f	Cross sectional area of fracture, (m^2)
A_m	Cross sectional area of matrix, (m^2)
b	Fracture aperture, (m)
C_p	Storage term in Equation (5.11), (m^{-1})
f	Fracture
g	Acceleration due to gravity, (m/s^2)
$H(t)$	Gas/liquid interface position measured from the top of model, (m)
h_c	Entry capillary threshold height, (m)
$h_c^{'}$	Capillary height at the exit face , (m)
K	Intrinsic permeability , (m^2) or (Darcy)
K_g	Gas permeability , (m^2) or (Darcy)
K_o	Oil permeability , (m^2) or (Darcy)
$K_{eff,f}$	Effective permeability of the fracture, (m^2) or (Darcy)
K_m	Permeability of matrix in the model, (m^2) or (Darcy)
k_r	Relative permeability
L	Length of model, (m)
L_f	The length of a vertical fracture, (m)
m	Matrix
nw	Non-wetting phase
Bo	Bond Number
Ca	Capillary Number
Re	Reynolds Number

p	Matrix or fracture pressure, (Pa)
p_c	Capillary pressure, (Pa)
p_g	Gas pressure, (Pa)
p_w	Water pressure or wetting pressure, (Pa)
P_{Vacuum}	Vacuum pressure, (Pa)
P_{th}	Capillary threshold pressure of matrix, (Pa)
PV	Pore volume, (m^3)
q	Flow rate, (m^3/s)
q_{cr}	Critical pumping rate, (m^3/s)
q_{max}	Maximum probable rate, (m^3/s)
RF	Recovery factor
S_e	Effective saturation
S_g	Gas saturation
Sgr	Residual gas saturation
S_o	Oil Saturation , percent of pore volume (PV)
S_{or}	Residual oil saturation
S_{nw}	Non-wetting saturation, percent of pore volume (PV)
S_w	Wetting phase saturation, percent of pore volume (PV)
S_{wr}	Residual wetting Saturation , percent of pore volume (PV)
t	Time, (s)
V_{nw}	Non-wetting velocity, (m/s)
V_w	Wetting velocity, (m/s)
w	Wetting phase

x	x axis
y	y axis
α	Proportionality constant for communication rate
σ	Interfacial tension, (N/m)
σ_{og}	Gas-oil surface tension, (N/m)
θ	Inclination angle
Δ	Difference operator
μ	Dynamic viscosity, (kg.m/s)
μ_g	Viscosity of gas, (kg.m/s)
μ_L	Viscosity of liquid, (kg.m/s)
μ_o	Viscosity of oil, (kg.m/s)
μ_w	Viscosity of water, (kg.m/s)
ϕ_e	Total effective porosity of the model
ϕ_f	Fracture porosity, volume of fracture over the total bulk volume of the model
ϕ_m	Matrix porosity, pore volume of the matrix over the bulk volume of the matrix
ρ_w	Density of oil, (kg/m^3)
ρ_g	Density of gas, (kg/m^3)
$\Delta\rho$	Density difference between the two immiscible fluids
Δp	Pressure gradient, (Pa)
∇p	Pressure gradient vector

Chapter 1

Introduction and Objectives

1.1 Introduction

A large proportion of the world's proven oil reserves have been found in reservoir rocks that are naturally fractured (Waldren and Corrigan, 1985; Nelson, 1985; Aguilera, 1995; Nelson, 2001). The current increasing global oil and gas demand has meant that fractured reservoirs have found an increasingly significant role as global energy source in the Middle East and elsewhere.

Naturally fractured carbonate reservoirs are described as geological formations with a heterogeneous distribution of porosity and permeability. These reservoirs are usually thought to comprise of an interconnected fracture system that provides the main flow paths. Fractures have high permeability and low storage volume about 3-4% of the oil original in place (OOIP) (Aguilera, 1995; Sahimi, 1995). The reservoir rock or matrix acts as the main storage of the hydrocarbon. The matrix regions have low permeability and high storage volume. Hence, the rock matrix contains most of the oil. However the production of oil to the wells is through the high permeability fracture system, implying that it is the matrix-fracture interaction that mainly controls the fluid flow. Production from the matrix-fracture system can be associated with various physical mechanisms including oil expansion upon pressure decline in the reservoir, water imbibition, and gravity drainage by gas injection when using horizontal wells (Saidi, 1987; Nelson, 2001).

From geological point of view, it is plausible to distinguish between various classes of fractured reservoirs (Nelson, 1985; Aguilera, 1995; Nelson, 2001). The most important aspect of a fractured medium to provide an acceptable drainage rate is whether or not the fracture network provides a continuous flow path for acting fluids (Saidi, 1987). In other words, whether it has regions with different fracture geometries or a system consisting of a hierarchy of fractured systems at different scales, i.e. multi-scale fractures (Waldren and Corrigan, 1985; Nelson, 1985). When the fracture network is not continuous in nature, the reservoir can then be split up into two separate flow domains, consisting of fractured and non-fractured media. It is evident that in the fractured domain, the reservoir is heterogeneous, considering the presence of different fracture density, fracture apertures, and permeability anisotropies.

The presence of fractures with permeability values that are orders of magnitude higher than that of the porous matrix gives rise to distinct mechanisms of oil displacement and production from naturally fractured reservoirs (Van Golf, 1996). Notable among them is the gravity drainage mechanism that occurs when the local reservoir pressure drops below the saturation pressure, whereby the evolved gas phase can travel to the upper sections of the reservoir through vertical fractures. A new zone, called the secondary gas cap, or the gas invaded zone is formed when all the fractures are filled with the gas and span the matrix block that contains oil. The lower pressure gradient within the gas phase causes the gas pressure to be higher than that of oil at the same elevation. Therefore, as long as the gas pressure is higher than the threshold capillary pressure of the gas-oil interface in the matrix, the gas enters the matrix and displaces the oil downwards by the action of gravity. (Nelson, 1985; Aguilera, 1995).

Gravity drainage has been reported to increase oil recovery by more than 60% in some reservoirs and recovery can be as high as 90% even for tertiary gravity drainage conditions (Chatzis et al., 1988; Dullien et al., 1990; Dullien, 1992). Several authors have developed theories for the gravity drainage process (Saidi, 1974; Saidi et al., 1979; Chatzis et al., 1988; Kantzas et al., 1988; Dullien et al., 1990). In petroleum engineering, there is a special attention given to gravity drainage, especially for gas injection as a secondary and tertiary recovery method in porous media. However, great efforts are still needed to explore new issues and also find out solutions for unsolved problems in gravity drainage from fractured porous media.

1.2 Motivations and Objectives

The primary motivation of this study is to further the understanding of two-phase fluid transport characteristics through fractured porous media under gravity drainage process conditions.

The study of two phase flow in fractured porous media is an important and challenging problem in petroleum engineering and hydrogeology. A few of researches on this kind of porous systems have concentrated on investigating the communication between matrix and fracture in unsteady state conditions to better account for the capillary, viscous, and gravitational forces present in fractured media. On the other hand, a significant number of studies have been numerical modeling of the fractured porous media without support from experimental data. Furthermore, there is a dilemma. Many of the experimental researchers have commented that some of their results are either contradictory to, or difficult to explain with theoretical concepts of flow in porous media. Part of the problem lies in the lack of information on how the fluids are moving in the matrix and fracture parts of a system during the experiments. By contrast, the work reported here tracks the gas-liquid interfaces and explains the communication rate and production mechanisms for gravity drainage processes in a logical way. It also includes detailed production rate, communication rate, critical rate and maximum rate measurements throughout the experiments.

Generally, the motivations for the current research work to study gravity drainage in fractured porous media are as follows:

1) Fractured petroleum reservoirs contribute almost 35-40% of the world's oil and gas reserves (Sahimi, 1995; Van Golf, 1996). More fundamental understanding is needed.
2) Most fractured reservoirs having primary or secondary gas cap are produced by gas injection or free fall gravity (Saidi, 1987; Van Golf, 1996).
3) Gravity drainage in fractured media is still a controversial subject among the researchers in this field.

To address the aforementioned, this thesis consists of two important parts including: experimental and modeling tasks in order to meet main objectives of the research objectives listed below:

1) To enhance our understanding of gravity drainage process in naturally fractured reservoirs, focusing on the communication between the fracture and matrix as well as the interplay of capillarity and gravity forces by investigation of different aspects of gas gravity drainage in fractured porous media.

2) To visualize gravity drainage in fractured systems using glass beads packed models with fractures and to focus on oil recovery efficiency, residual oil saturation and oil production mechanism for different cases.
3) To focus on the behavior and movement of the macroscopic Gas-Liquid (G-L) interface through matrix and fractures in order to address the velocity distribution in fractured media that have different fractures configurations during the gravity drainage process. To obtain the recovery performance of the employed macroscopic porous media models as a function of liquid withdrawal rate, as well.
4) To simulate the experimental results using COMSOL and then to compare the outputs of simulation runs with the experimental data obtained in this study. This part enables the development of best scenarios for producing oil from fractured media using the gravity drainage as a method of oil recovery.

To achieve the objectives for this PhD research work, the following tasks were done:

- Unconsolidated glass-bead types of experimental prototype were designed. Each model is equipped with a certain pattern of fractures such as vertical and horizontal fractures.
- Free-fall and Controlled gravity drainage experiments were carried out with focus on visualizing pore-scale aspects of the multiphase flow process, as well as fluid flow interaction between the matrix and the fractures.
- Parametric sensitivity analyses were performed considering the effect of different system parameters such as fracture aperture, matrix height, permeability, and fluid viscosity on the liquid drainage rate and gas-liquid interfaces movement. Each series of experiments was initiated with a detailed Design of Experiment (DOE) through which different experimental steps and phases were designed and ranked considering the effects of various independent parameters on the dependent variables.
- Last part of the work presented in this thesis is modeling of experiments using COMSOL as a multiphase flow modeling software and then comparing the outputs from the modeling software to experimental results. It is widely accepted in the petroleum engineering literature that the modeling and reservoirs simulators, which are based on observations from hydrocarbon producing fields and laboratory tests, demonstrate a close link between these and emphasize the need for interdisciplinary approach to improve our current understanding of fractured reservoirs and the predictions of oil and gas production.

1.3 Lay-Out of the Thesis

The characterizations of naturally fractured reservoirs and literature review of previous research works in relation to this study are presented in Chapter 2. The first part of the chapter is a review of general information regarding fractured petroleum media, types of fractured reservoirs and the geologic aspects that describe fractured oil reservoirs, especially those parameters related to experimental works and numerical simulations such as fracture porosity, fracture aperture, matrix porosity, and matrix permeability. The second part is previous research works regarding gravity drainage processes and also the numerical simulation of naturally fractured reservoirs that is composed of three categories: dual porosity models, dual permeability models, and finally common simulation softwares.

The experimental work for free fall gravity drainage (FFGD) in unconsolidated fractured porous media and important results related to the issue are addressed in Chapter 3. Visualization of immiscible displacement of liquid by gas was covered in the chapter. Visualization of the experiments under different conditions was carried out to determine oil production mechanism and gas-liquid interface movement in the fractured porous media during the gravity drainage process.

The experimental study and empirical approach of controlled gravity drainage (CGD) are presented in Chapter 4. The governing equations, sensitivity analysis of various parameters, mechanism of oil production at constant pumping rate from fractured glass beads systems are described in this chapter. The physical model experiments were conducted at room conditions under constant production rate. The experiments were carried out to include the effect of pumping rate on immiscible CGD recovery factor and flow behaviour in the fractured porous media. The last section of chapter 4 summarizes the dimensional analysis work completed for the CGD process to facilitate the identification of the key variables affecting critical pumping rate and recovery factor. The dimensional analysis also can help the scalability of experimental findings to field applications in the range of the dimensionless numbers.

Discretization of the governing equations and simulation of the fractured media by COMSOL are presented in Chapter 5. In the modeling approach, the governing equations were written for each part of the fractured porous media separately and then all reasonable assumptions were mentioned. The last part of Chapter 5 presents the outcomes of the numerical modeling for free fall gravity drainage and controlled gravity drainage processes, and comparison is made between simulation outputs and experimental results. Finally, the main conclusions obtained from this research work and recommendations are presented in the Chapter 6.

Chapter 2

Background and Literature Review

2.1 Naturally Fractured Reservoirs

Naturally-fractured reservoirs are an important component of the global hydrocarbon reserve and production base. In many parts of the world, fractured reservoirs account for the bulk of production. In other areas, such as the Rockies of North America, low permeability formations that were once considered unconventional hydrocarbon resources are now quickly becoming main stream reservoirs (Saidi, 1987).

A naturally fractured reservoir can be defined as a reservoir that contains fractures (planar discontinuities) created by natural processes like diastrophism and volume shrinkage, distributed as a consistent connected network throughout the reservoir. Fractured petroleum reservoirs represent over 27% of the world's oil and gas reserves. However, they are among the most complicated class of reservoirs to produce efficiently. A typical example is the Circle Ridge fractured reservoir located on the Wind River Reservation in Wyoming, USA. This reservoir has been in production for more than 50 years but the total oil recovery until now has been less than15% (Saidi, 1987).

It is undeniable that reservoir characterization, modeling and simulation of naturally fractured reservoirs present unique challenges that differentiate them from conventional, single porosity reservoirs. Not only due to the intrinsic characteristics of the fractures, as well as the matrix, have to be characterized, but the interaction between matrix and fractures must also be modeled accurately. Furthermore, most of the major naturally fractured reservoirs have active aquifers associated with them, or would eventually resort to some kind of secondary recovery process such as waterflooding, implying that it is essential to have a good understanding of the physics of multiphase flow for such reservoirs. This complexity of naturally fractured reservoirs necessitates the need for their accurate representation from a modeling and simulation perspective, such that production and recovery from such reservoirs be maximized (Aguilera, 1995).

Recently, new areas of research are being explored including the origin and development of fracture systems, fracture detection methods, efficient numerical modeling of fluid flow and methodologies to test these models (Robert, 2002). As stated earlier, the fractures are considered as a macroscopic planar discontinuity in rock which is interpreted to be due to deformation or diagenesis. These fractures may be due to compression or dilatant processes and may have a positive or negative impact on fluid flow. Naturally fractured reservoir can be defined as any reservoir in which naturally occurring fractures have, or are predicted to have, a significant effect on flow rates, anisotropy, recovery or storage (Nelson, 2001).

The porous system of any reservoir can usually be divided into two parts (Eshraghi, 1995):

- Primary Porosity (matrix porosity): This porosity is usually inter-granular and is controlled by lithification and deposition. The matrix porosity contributes

- Secondary Porosity (fractures): Post lithification processes cause this porosity. Fractures are highly permeable and hence contribute significantly to the fluid flow but as they are not very porous, their contribution to fluid storage is negligible.

The post-lithification processes that cause secondary porosity are general in the form of solution, recrystallization, dolomotization, and fractures or jointing.

In a naturally fractured reservoir, as explained before the matrix porosity and fracture permeability have different roles in providing fluid storage and fluid flow direction. Therefore, it is important to consider their contributions for oil production performance and recovery rate during EOR method. Hence dual porosity formulation was developed by Warren and Root (1963).

Most of the petroleum reservoirs show a dichotomy of porous space but with varying degree of matrix and fracture presence. A low fractured reservoir is one in which the fracture porosity is not significant. Most natural fractured reservoirs are highly fractured and consist of a significant amount of fracture porosity. Hence this dichotomy for natural fractured reservoirs is justified (Eshraghi, 1995).

The dual porosity concept superimposes the secondary or fracture media on the primary or matrix media and this superimposition is idealized as primary porosity coupled with the secondary porosity, as shown in Figure 2.1.

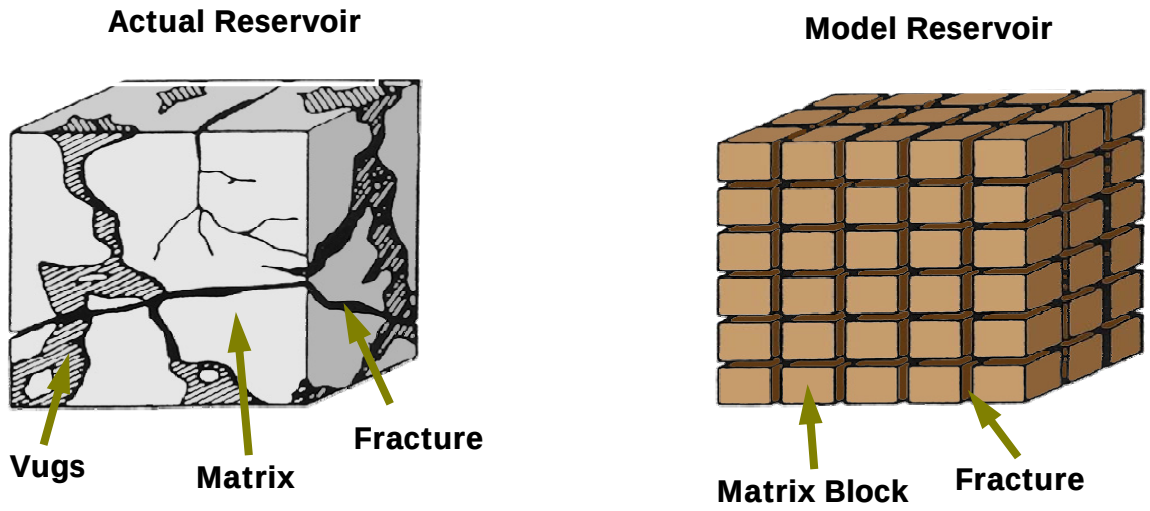

Figure 2.1: Idealization of the dual porosity reservoir (Saidi, 1987)

Naturally fractured reservoirs represent a challenge to the reservoir-modeling world due to their complexities. Substantial research has been accomplished in the area of geo-mechanics, geology and reservoir engineering of fractured reservoirs (Saidi, 1987).

2.2 Petrophysical Properties of Fractured Reservoirs

2.2.1 Porosity: In a fractured reservoir the total porosity (ϕ_t) is the result of the simple addition of the primary and secondary porosities,

$$\phi_t = \phi_1 + \phi_2 \tag{2.1}$$

where ϕ_1 =primary porosity and ϕ_2 = secondary porosity.

From a large number of laboratory measurements on various types of rocks, the fracture porosity was considerably less than the matrix porosity (Nelson, 1985; Eshraghi, 1995). The two porosities are expressed by the conventional definitions,
ϕ_1 = matrix void volume/total bulk volume and ϕ_2 = fracture void volume / total bulk volume.

The two porosities are relative to the total bulk volume (matrix + fractures).
In the correlation of matrix porosity (ϕ_m) and the fracture porosity (ϕ_f), the fact that the matrix porosity refers only to the matrix bulk volume may be taken into consideration:

$$\phi_m = \frac{Volume\ of\ void\ space\ of\ the\ matrix}{Matrix\ bulk\ volume}$$

while the fracture porosity is given by:

$$\phi_2 \approx \phi_f \tag{2.2}$$

In this case the primary porosity, as a function of matrix porosity, is expressed by:

$$\phi_1 = (1-\phi_2)\phi_m \tag{2.3}$$

and the effective primary porosity, containing the oil phase, is:

$$\phi_{1,eff} = (1-\phi_2)\phi_m(1-S_{wi}) \tag{2.4}$$

where S_{wi} is the initial water saturation in fractured oil reservoirs.
Therefore, the equation of double porosity in the fractured systems can be written as follows (Eshraghi, 1995; Van Golf, 1996):

$$\phi_e = \phi_m + \phi_f - \phi_m\phi_f \tag{2.5}$$

2.2.2 Permeability: The basics of permeability established for a conventional reservoir remain valid in the case of a fractured reservoir. But in presence of two systems (matrix and fractures), permeability may be redefined as matrix permeability, fracture permeability and system (fracture-matrix) permeability. The definition of permeability may create some confusion especially for fracture permeability, which may be interpreted either as single

fracture permeability or as fracture network permeability, or sometimes as fracture permeability of fracture- bulk volume. Therefore, the various expressions of permeability will be examined and discussed here in detail (Sahimi, 1995).
The intrinsic fracture permeability is associated to the conductivity measured during the flow of fluid through a single fracture or through a fracture network, independently of the surrounding rock (matrix). It is, in fact, the conductivity of a single channel (fracture) or of a group of channels (fracture network). In this case the flow cross-section is represented only by the fracture void areas excluding the surrounding matrix area. In a simplified case of a block, where the fracture is parallel to the flow direction, by use of the equation of flow rate through the conduit for fracture and the formula based on the Darcy concept, K_f is obtained by (Van Golf, 1996):

$$K_f = \frac{b^2}{12}\cos\alpha \tag{2.6}$$

where b is the fracture aperture and α is the dip angle.

For a fracture system having n fractures of similar orientation, the intrinsic permeability is expressed by the arithmetic average:

$$K_f = \frac{\sum_{i=1}^{n} b_i^2}{12}\cos\alpha \tag{2.7}$$

For a fractured system with fracture porosity ϕ_2, the conventional fracture permeability, K_f is:

$$K_{eff,f} = K_f.\phi_2 \tag{2.8}$$

2.3 Types of Fractured Reservoirs and Oil Recovery

According to the research performed on 100 fields (Van Golf, 1996), fractured reservoirs are divided into four groups:
Type I: This Type of reservoirs has low matrix porosity and permeability. Fractures provide both storage capacity and fluid-flow pathways.

Type II: Type II reservoirs have low material porosity and permeability. Matrix provides some storage capacity and fractures provide the fluid-flow pathways.

Type III: Type III (micro porous) reservoirs have high matrix porosity and low matrix permeability. Matrix provides the storage capacity and fractures provide the fluid-flow pathways.

Type IV: This type of reservoirs has high matrix porosity and permeability. The matrix provides both storage capacity and fluid-flow pathways.

Studies show that majority of reservoirs in the world are of type II and III (Sahimi, 1995; Van Golf, 1996). Therefore, reservoirs of other types are found rarely. Based on the previous studies and also my preliminary experiments, production mechanisms for these two types (II and III) are very similar (Saidi, 1987; Zendehboudi et al, 2008). Moreover, the number of fractured media type III in Iran and US is much more than that of type II and the reservoir characterization and production history of type III are more available and easier to access for implementation of scaling up of experimental results and also EOR screening criteria for type III of fractured reservoir (Sahimi, 1995; Van Golf, 1996). Therefore, we focus on type III of fractured reservoirs in this research.

2.3.1 Fractured reservoirs versus conventional reservoirs: Before discussing type II and type III fractured reservoirs, it is beneficial to compare fractured reservoirs with unfractured reservoirs in order to understand why fracture reservoirs behave differently and need to be treated differently. Although porosity and permeability vary widely in fractured reservoirs, type I, II and III fractured reservoirs have low matrix permeabilities and could not be produced economically without the presence of fractures. High permeability – low porosity fractures in a low permeability – higher porosity matrix provides the mechanism for recovery of hydrocarbons (Sahimi, 1995). However, this dual porosity system adds a measure of complexity that is absent in unfractured reservoirs. The production characteristics of fractured reservoirs differ from those of conventional reservoirs in several fundamental ways:

1) Because of the high transmissivity of the fracture network, the pressure drop around a producing well is very low and pressure gradients do not play a significant role in production. Production is driven instead by complex mechanisms that govern fracture/matrix- block communication and fluid-flow phenomena (Van Golf, 1996; Dastyari et al., 2005).

2) In fractured reservoirs with some matrix permeability, the pressure decline per barrel of oil produced is low compared to conventional reservoirs. This occurs because fluid expansion, gravity drainage, and imbibitions provide a continuous supply of oil from matrix blocks into the fractures during production (Van Golf, 1996; Saidi, 1996).

3) The gas to oil ratio (GOR) in fractured reservoirs normally remains lower compared to homogeneous reservoirs throughout production, if the reservoir is properly managed. This occurs because liberated gas flows preferentially upward through fractures to the top of the reservoir rather than horizontally toward the nearest well bore as in an unfractured reservoir. The liberated gas communicates with the gas cap and expands it. The gas content of produced oil is lowered accordingly in such type of fractured reservoirs with a gas cap (Saidi, 1987; Saidi, 1996).

4) Fractured reservoirs lack transition zones. The oil-water and gas-oil contacts are essentially knife- sharp type of interfaces, both prior to and during production, since the high permeability of the fracture network provides a mechanism for rapid equilibration of fluid contacts (Van Golf, 1996; Saidi, 1996).

5) Water cut in fractured reservoirs is strictly a function of production rate. The petrophysical characteristics of the reservoir rocks and PVT properties of the fluids have insignificant effect on water production (Saidi, 1987; Dastyari et al., 2005).

6) Convective circulation occurs during the production of many fractured reservoirs. As a result, PVT properties are constant throughout a fracture reservoir, compared to a conventional reservoir where bubble point varies as a function of depth within the oil column (Van Golf, 1996; Saidi 1996).

Because of these fundamental differences, mistaking a fractured reservoir for an unfractured reservoir early in the field-development phase can lead to mistakes in exploitation strategy that have profoundly negative effects on reservoir performance. Most wells completed in newly discovered fractured reservoirs produce at high rate initially (Sahimi, 1995; Van Golf 1996). If investment decisions are made, as they sometimes are, by assuming that those high production rates can be maintained over extended periods of time, the field may be economically doomed from the start. When wells in fractured reservoirs are pumped at excessively high rates, the GOR can increase rapidly instead of maintaining low as in a properly managed field (Sahimi, 1995; Van Golf 1996). This eventually leads to a rapid decline in reservoir pressure. Rapid pressure decline can change the delicate balance of recovery mechanisms that feed the matrix oil into the fractures and drastically decrease recovery factor. Finally, if an incorrect secondary recovery technique is chosen, ultimate recovery may be further reduced. The most common example of poor reservoir management is water flooding a fractured reservoir. The inevitable early water breakthrough leaves a large amount of recoverable oil behind by way of bypassing matrix blocks (Eshraghi, 1995; Van Golf, 1996).

2.4 Gravity Drainage in Fractured Reservoirs

Gravity drainage is an important production mechanism in the development of many oil reservoirs with attractive features such as a large dipping angle, significant vertical thickness, and high permeability. It is also important in aquifer water infiltration. This mechanism will be especially promising in the cases in which a gas cap (initial or secondary) is present, in direct contact with the oil zone. Capillary continuity is perhaps the most important parameter affecting the performance of gravity drainage process (Saidi, 1979; Firoozabadi et al., 1992). Oil recovery by gravity drainage in a fractured reservoir strongly depends on the total height of the capillary continuity. When modeling multiphase flow in a fractured porous medium, the capillary forces should be taken into account for both matrix and fracture. Considering matrix blocks to be discontinuous, it is only appropriate if and only if the fracture capillary pressure is assumed to be zero. There is not a reliable assumption to believe that fracture capillary pressure could be zero in value (Fung, 1991; Blunt et al., 2001).

It is reported in the literature that high oil recoveries can be achieved by employing gravity drainage processes in laboratory and in field. For example, Kantzas et al. (1988) reported the results of gravity drainage experiments, using unconsolidated media with maximum oil recovery of 99% of the initial oil in place (IOIP). Da Sle and Guo (1990) reported an ultimate oil recovery of 94% of IOIP in Westpem Nisku D Reef field. Characterizing and

modeling of gravity drainage processes are still of great interest. Several gravity drainage models have been developed, and reported, in the literature (Saidi, 1976; Schechter and Guo, 1996). However, these models simply overlook the communication term between the matrix and fracture, by assuming a constant rate of oil flowing from matrix to fracture during gravity drainage process. Researchers have developed theories for the gravity drainage process in homogeneous media (Chatzis et al., 1988; Kantzas et al., 1988; Dullien et al., 1990). Many other studies have been conducted on the modeling and experimental aspects of gas flooding. For example, experimental studies carried out using micromodels and packed columns have reported that oil recovery as high as 90% of the initial oil in place is attainable, if gas gravity drainage is considered the dominant mechanism in the depletion process (Chatzis et al., 1988; Dullien et al., 1990; Dullien, 1992).

Visual investigation of the immiscible displacement of the oil being displaced by the gas has been the subject of several articles (Chatzis et al., 1988; Oren, 1992; Zhi-An, 1994; Sajjadian et al., 1999; Blunt et al., 2001). Haghighi and Yortsos (1997) studied the drainage process in a horizontal fractured system. They observed and modeled the flow patterns in the matrix and fracture according to the pore-scale phenomena, using percolation theory concepts. Sajjadian et al. (1999) performed a visualization study of the gravity drainage using a glass micromodel with fractures. Furthermore, Zhou and Blunt (1998) studied the effect of wettability on gravity drainage process. Flow visualization of tertiary oil recovery by inert gas injection under gravity drainage in models with macroscopic heterogeneities has also been reported elsewhere (Catalan, 1994). In absence of predictive theoretical models, experimental laboratory studies may be a way to predict the performance of the gravity drainage processes. To properly scale up the experimental data to the field scale, the laboratory physical models should be appropriately scaled to the specific reservoir in geometry, physical and even chemical processes. To build such a system a good understanding of the process (interplays of the different physical forces) is required (Por et al., 1989; Kulkarni et al., 2005).

Understanding of the production mechanisms that contribute to hydrocarbon production from naturally fractured media has been substantially improved during the past few decades. Enormous research and development projects have been commenced with the cooperative aid of academic divisions as well as industrial branches (Chatzis et al., 1988; Oren, 1992; Zhi-An, 1994; Sajjadian et al., 1999; Blunt et al., 2001). However, there are still ambiguous areas, especially among its upstream division, over which further R&D activities are needed. As an example, research topics such as gravity drainage mechanism in fractured porous media, under both free-fall gravity drainage, or controlled gravity drainage and their associated debatable issues such as complex fluid flow communication between matrix and fractures are still in great deal of interest in academic research activities. Efforts have been made to critically address these research topics through a series of relevant publications for the recovery of residual oil (Saidi, 1974; Chatzis, et al., 1988; Kantzas, et al., 1988; Dullien, 1990).

Production from fractured reservoirs under gravity drainage mechanism is dominated by two major interacting forces namely, capillary forces and gravity forces (Dullien, 1992). The viscous force is the only major driving force for production of non-fractured (i.e. homogeneous) reservoirs (Da Sle, 1990; Paul, 2005). Considering the gravity drainage

process in a fractured medium, there are two major parameters affecting the overall system drainage rate, namely, the density difference between interacting gas and liquid, and also the elevation difference between gas-liquid interfaces in matrix and fracture. The latter two parameters are responsible for drainage type of liquid movement through the matrix block. Consider the case of a vertically suited matrix block which is surrounded by two vertical fractures on both sides, and is draining under the influence of controlled gravity (pumping the liquid out of the system) as it is one of the cases for the experimental set up of the current study. Essentially, the oil content of fractures, which is not a considerable volume as a result of their low storage capacity values, would be drained first because of the associated high values of inherent permeability. The resulting void space would then be occupied by invading gas phase, which originally comes from either associated gas cap or from the source of gas injection. It is believed that the original oil held in place in the matrix, which contributes the most to ultimate oil recovery, needs longer time to be transmitted towards fractures, compared to the time associated with fracture drainage (Schechter and Guo, 1994; Zendehboudi et al., 2008). Interaction of gravity and capillarity forces dictates this communication phenomenon (Schechter and Guo, 1994; Zendehboudi et al., 2008). This time delay makes fractures to be filled up with invading gas phase. In other words, the presence of vertical fractures causes the gas-liquid contact inside fractures to move downwards ahead of the corresponding contact in the matrix block by gravity drainage mechanism. The gas phase invades all the way through the fracture until it fills up the whole fracture volume, except the height with respect to threshold capillary pressure, which is indeed negligible. If the matrix block is surrounded by gas, the gravity forces tend to drain the oil out of the matrix while the capillary forces tend to retain the oil inside the tortuous pores (Thomas et al., 1983; Tavassoli et al., 2005).

Free-fall gravity drainage (FFGD) takes place when gravity force is the only acting force on the draining liquid (Dullien, 1992). However, the fluid withdrawal rate under FFGD recovery mechanisms might not compensate the CAPEX and OPEX of recovery process; it is needed to increase the ultimate recovery using different EOR (or, IOR) processes (Thomas et al., 1983; Trivedi and Babadaghli, 2008). In a fractured medium, one can enhance the ultimate recovery factor using techniques which reduce the interfacial tension (i.e. injection of surface active agents) or reduce the entrapment of liquid. In most cases, the matrix height is much greater than its capillary threshold height; otherwise, the liquid content would not drain under free fall gravity drainage mechanism (Dullien, 1992; Sahimi, 1995). In general, the ultimate liquid production is governed by the matrix capillary pressure.

The gravity drainage mechanism of fluid-flow in naturally fractured reservoirs was modeled and validated by solving the available analytical equations (Firoozabadi and Hauge, 1990). The block to block interaction effect was included in this model. It is assumed that the information concerning block dimensions, which are essential to any reservoir characterization, are known and therefore are not discussed here Whereas, the effects of oil relative permeability, threshold height, change in the initial irreducible water saturation while gas is being displaced by spreading (or, not spreading) oil need to be further reviewed (Schechter et al, 1996; Aziz et al, 1993).

Under pure gravity dominated flow, the ultimate recovery would be dictated by a trade -off between the gravity and capillary forces (Saidi, 1987; Dullien, 1992). It should be noted that there are two major flaws in numerical simulators for naturally fractured reservoirs. The first one is the inappropriate governing equations used for the modeling. These equations do not consider some vital modeling parameters; or if they do, there are some doubts regarding defined parameters. For example, most of these governing equations have some problems when they are dealing with the matrix-fracture flow communication (i.e., the defined shape factor for considering the flow communication has not been generalized yet) (Zimmerman, 1991; Saidi, 1997; Mora and Wattenberger, 2009). In addition, the governing equations in gravity dominated flow, either free fall gravity drainage or controlled gravity drainage, have not been clearly defined yet. Aside from that, most of the simulation studies lack some primary reservoir data, especially those related to fractured section such as fracture size, distribution, and orientation.

Most of the early studies focused on the representation of reservoirs by means of single reservoir blocks. Most of the time these studies have relied on sparse experimental data in the literature (Mattax and Kyte, 1962; Kleppe and Morse, 1974; Kazemi and Merrill, 1979) to verify their models. However those experiments provided rough approximations of the recovery obtained in the actual reservoirs. Later, experimental works focused on understanding the mechanisms that control the flow of fluids in porous media (Horie et al. 1988; Firoozabadi and Hauge, 1990; Labastie, 1990; Firoozabadi and Markeset, 1992). Hughes (1995) presents a detailed discussion of the aforementioned experiments. From the most recent experiments, we can see that most of them lack an explicit velocity distribution, saturation distribution and variation of communication rate in fractured porous media, since accurate measurement and considering entire main parameters have been the biggest difficulties in these kinds of studies. Some of the experimental studies focused on the mechanisms dominant in gravity drainage situations and in small block imbibition displacements. Whereas others, have emphasized understanding flow through a single fracture with no transfer from the matrix.

Li et al. (2000) discussed the results of the experimental work on gas gravity drainage on artificially fractured Berea sandstone cores at reservoir conditions (Spraberry Trend Area, West Texas). They concluded that fractures could improve the efficiency of immiscible displacement, but suggested additional experimental investigation for further clarification that our research work shows contradictory finding compared to the idea presented.

Dastyari et al. (2005) investigated the gravity dominated immiscible gas injection in a single-matrix block using 2D glass micromodels, in both free and forced gravity drainage modes. The authors reported that the free gravity drainage is initially a very fast process, but slows down at longer times. This observation appears to be supported by the original gravity drainage theories (Cardwell and Parsons, 1948; Terwilliger et al., 1951) as well as other macroscopic experimentation (Meszaros et al., 1990). However, three other conclusions of Dastyari et al. (2005) appear to contradict the previous observations. Firstly, the authors suggested that the oil recovery in an un-fractured system appears to be higher than that of a fractured system. This observation contradicts the observations of Catalan et al. (1994) and Li et al. (2000) which indicate that the presence of fractures in the direction of flow enhanced the oil production rates. Secondly, the authors stated that the residual oil

saturation increases to more than twice of the natural gravity drainage, which contradicts the observations of Thomas et al. (1990) and Karim et al. (1992). Thirdly, the authors reported that gas injection in both un-fractured and fractured models results in higher residual oil saturations, which appears to contradict almost all the experimental studies summarized in this section, which suggest that gravity stabilized gas injection can result in very low residual oil saturations.

Jones, Wooten, and Kaluza (1988) studied single phase flow through rough-walled fractures, and found that for wide fractures, Whiterspoon's et al. (1980) cubic law equation can be used to calculate absolute permeability and to characterize single-phase flow. Romm (1966) presented two-phase flow experiments in smooth vertical parallel plates. He concluded that fracture relative permeabilities are equal to the phase saturation. Also, he suggested these results cannot be applied to flow in fractured media where a system of interconnected fractures is present.

In general, several authors (Kazemi and Merrill, 1979; Beckner, 1990; Gilman et al., 1994) have assumed that fracture capillary pressures are negligible. Others have shown experimentally that capillary continuity becomes important when gravity provides a driving force (Horie et al., 1988; Firoozabadi and Hauge, 1990; Labastie, 1990; Firoozabadi and Markeset, 1992). Kazemi (1990) concluded that the capillary continuity is prevalent in the vertical direction and has suggested that, in order to reduce the number of equations to solve, the fractured reservoir simulations should use the dual permeability formulation for the z direction and the dual porosity formulation for the x and y directions. However, the uncertainty problem related to shape factor remains unsolved and in all three directions, both methodologies should be applied to get accurate results.

Gravity drainage from a block, under constant pressure, consists of two main parts: first: oil recovery as the gas-oil front in matrix is moving before it reaches the block threshold height (one phase flow period). Second: oil recovery during two-phase flow conditions which takes place from about the time that matrix gas-oil front reaches the threshold height to final recovery. Oil recovery during this second period is dictated by the oil relative permeability, which is affected by the fluid distribution and the shape of capillary pressure curve. The oil relative permeability should be calculated from laboratory measured gravity drainage tests under actual reservoirs conditions (Chatzis et al., 1988; Dullien, 1992). Such a procedure may not be practical in low permeability rocks. In this case, the centrifuge method may be used at best, with the necessary precautions and corrections before calculating relative permeability (Dullien, 1992; Sahimi, 1995).

To calculate the relative permeability from gravity drainage or centrifuge experiments, often the entire oil relative permeability curve cannot be matched with one Corey exponent "n" (Corey model, $k_{ro} = k_o.S_o^n$) (Dullien, 1992). This is particularly the case when the high oil saturation portion of relative permeability corresponds to an $n > 4$ value. In this case the part related to the high oil saturation can be matched with one "n" value and the low oil saturation part (the film flow part) with different "n" value (Dullien, 1992).

Several gravity drainage models have been developed for porous media, especially fractured ones in the literature. In these models, capillary pressure, communication rate between matrix and fracture are usually either neglected or considered inappropriately.

However, these two parameters play important roles in many cases (Zendehboudi et al., 2008; Zendehboudi, et al., 2009).

Almost all the gravity drainage models are complicated. Some of the models don't have analytical solutions and have to be solved numerically. Schechter and Guo (1996) conducted a review on the papers in the field. There are four main models as summarized by Schechter and Guo (1996). These include the Cardwell-Parsons-Dykstra (1985) (CPD) model, Nenniger-Storrow (1987) (NS) model, Pavone-Bruzzi-Verre (1990) (PBV) model and Luan (1993) model. After comparing to experimental data, Schechter (1996) concluded that the accuracy of these models to predict the oil production by gravity drainage is poor. Schechter and Guo (1996) also developed a gravity drainage model which did not improve the accuracy significantly.

Because the analytical models do not work well, an empirical model developed to characterize spontaneous imbibition was proposed to model the gravity drainage process. The model was suggested originally by Aronofsky et al. (1987) to match oil production in naturally fractured reservoirs developed by water flooding. Many applications have been conducted since then. Schechter and Guo (1996) used a similar equation to fit the experimental data of spontaneous water imbibition in oil-saturated rocks by substituting production time with the dimensionless time. Baker et al. (1983) inferred the fracture spacing by matching production data from the Spraberry trend naturally fractured reservoir using the model with dimensionless time. Li and Horne (2000) also applied the imbibition model proposed by Aronofsky et al. (1987) to evaluate water injection in geothermal reservoirs.

Non-linear nature of the fundamental gravity drainage equation (Cardwell and Parsons ,1948) has prompted application of experimental, numerical and empirical techniques to gravity drainage process characterization. No single model to adequately define the gravity drainage process is available.

In this thesis, our study and discussions are limited to free fall gravity drainage and controlled gravity drainage of gas-oil systems. Furthermore, empirical equations were obtained for prediction of recovery factor and production rate of fractured porous media under the gravity drainage processes. The equations were derived with fewer limitations compared to previous empirical modes as it was tried to consider most of the parameters significantly affecting gravity drainage performance.

2.4.1 Description of gas gravity drainage along with a mathematical concept through block to block interaction: The gas phase entering from the top of the block will displace oil that is produced at the bottom of the block in a gas or oil phase. The gas is considered to be the non-wetting phase, and gas compressibility is ignored. In the case of oil saturated block totally surrounded by gas, the initial pressure of the column is considered to be above the threshold pressure. Therefore, gas can enter the block. By assuming suitable initial and boundary conditions, the final equation for gravity drainage is as follows (Zhou et al., 1998; Blunt et al., 2001):

$$q = A\frac{K_o}{\mu_o}\frac{(L - H - h_c + h_c^{'})}{\left(L + (\frac{1}{M} - 1) \times H\right)}\Delta\rho g \qquad (2.9)$$

where M= $(K_o/\mu_o)/ (K_g/\mu_g)$ is the mobility ratio, A is the medium's cross-sectional area and H is the distance of gas-oil interface from top of the matrix. In such displacement, the capillary pressure of the matrix decreases oil production. The oil can be produced to the extent that gravitational forces exceed capillary forces.

In a displacement with a sharp interface, under certain conditions depending on the gas-oil capillary pressure, and the block height, the block saturated with oil can be totally entrapped by gas circumventing the block if h_c>L. On the other hand, to penetrate into the block, the dynamic capillary pressure of gas must exceed the threshold capillary pressure, p_c. In the case of small blocks totally surrounded by gas, it is very unlikely to achieve the static pressure value. The maximum gravity drainage rate at H=0 is:

$$q = A\frac{K_o}{\mu_o}\frac{(L - h_c + h_c^{'})}{L}\Delta\rho g \qquad (2.10)$$

where h_c is the entry capillary threshold height and $h_c^{'}$ is the capillary height at the exit face (bottom of the block) and it is zero when it is at gas oil contact.

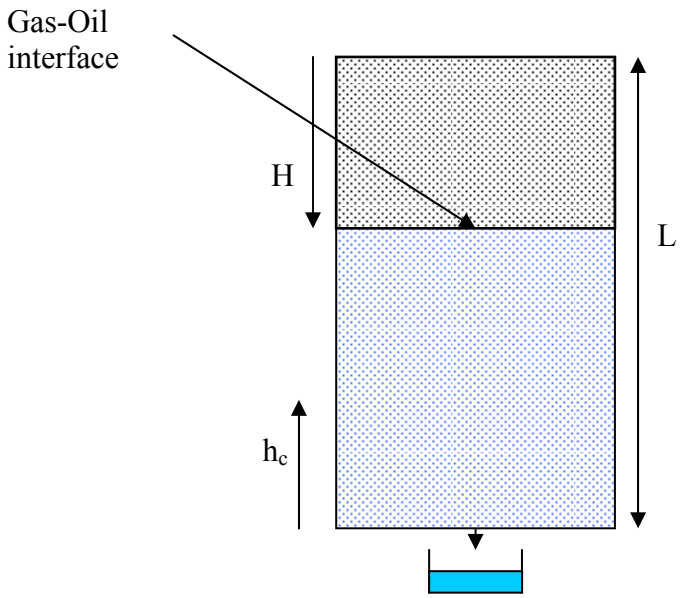

Figure 2.2: Simple schematic of gravity drainage process in a matrix block.

2.5 Contribution of the Thesis in Experimental Work of Gravity Drainage Processes

In the previous experimental studies mentioned earlier in this text there are some significant missing points:

1) No experimental work discussed the effects of fracture aperture on communication between matrix and fracture, gas-liquid interface movement and recovery performance at breakthrough during the gravity drainage process.
2) Velocity distribution in fractured media and effect of various fracture configurations on recovery performance have not seen in the experimental projects.
3) No research work has addressed the production mechanism under controlled gravity drainage process in fractured porous media.
4) Although some researchers (Schechter and Guo, 1996; Blunt et al, 2002) investigated the dimensional and parametric sensitive analysis of gravity drainage but these researches have been done under the gravity drainage conditions in homogeneous porous media and this issue in fractured porous media remains unaddressed. Hence, it is necessary to investigate these important points in order to figure out production mechanism and effective parameters contributing in fractured porous media under gravity drainage with a logical approach.

The current study has addressed all the above-mentioned issues to provide us with a better understanding of the physics of gravity drainage processes.

In general, the original contributions of the experimental work to the existing literature are summarized as:

1) Demonstration of the FFGD and CGD processes through the fractured porous media having different patterns of fractures. This will help to figure out more physics and production mechanism of gravity drainage in fractured porous media using visualization techniques.
2) Experimental demonstration of the capillary continuity and communication between matrix and fracture in the fractured porous system with unconsolidated glass beads matrix part at various conditions.
3) Experimental demonstration of the possibility of gas breakthrough control during controlled gravity drainage by setting appropriate pumping rate.
4) Definition of new concepts of 'Critical Pumping Rate (CPR)' and 'Maximum Possible Withdrawal Rate (MPWR)' for CGD process.
5) A new correction factor was introduced for fluid transferring rate equation proposed by Warren and Root (1963). The correction factor was derived for FFGD in the fractured porous media, which is taken into account as an unsteady state process.
6) The empirical correlations were obtained using regression analogy to relate the dimensionless numbers such as Bond number and ratio of permeabilities to the recovery factor and difference of the gas-liquid interface positions in matrix and fracture during gravity drainage processes with high accuracy. It was concluded that the correlation's regression fit employed is a useful tool for predicting FFGD and CGD oil recoveries.

2.6 Modeling and Simulation of Fractured Porous Media

Successful EOR schemes for oil reservoirs, economical approach for environmental projects and effective removal method for remediation plans are joined with fluid flow in porous media, which require modeling of multiphase-fluid flow and transport in subsurface soil and rock systems (Aziz and Settari, 1979; Blunt and King, 1992; Hoteit and

Firoozabadi, 2008). The mathematical model enables the researchers to predict future behaviors of subsurface media under possible changes such as pumping rate and pressure distribution. However, the capability of such numerical models decreases drastically where sufficient information concerning capillary pressure vs. saturation and relative permeability functions for the various fluid pairs and porous media are missing. Determination of the capillary and permeability functions can be carried out based on measurements or partially inferred from prediction models (Chatzis et al., 1983; Dernond and Roberts, 1987). Equilibrium and steady state experimental methods are usually highly restrictive by their initial and boundary conditions, huge time efforts required, and also they are often difficult to be replicated (Persoff, 1991; Sahimi, 1995). Prediction methods are typically including two general approaches: conceptual/analytical and computational based methods. The analytical methods are generally based on a simplified conceptual pore model for predicting permeability from pore size distribution data. Computational methods cover a wide range of the methods such as numerical modeling and continuum/discontinuous analysis modeling (Kazemi, 1990; Carlson, 2004).

In general, a displacement process is mainly affected by the petrophysical properties of the medium, and also physical properties of the fluids in both homogeneous and heterogeneous porous media (Chatzis et al., 1988; Ayatollahi et al., 2005). In two-phase immiscible flow, interactions between the high permeable medium and low permeable medium and also interactions between porous media and the fluids control the fluid flow pathways. This is because that the fluid flow dynamics depends on a combination of conditions such as heterogeneity and oil content (Zendehboudi et al., 2008; Zendehboudi et al., 2009). A large number of numerical techniques have been developed to model two-phase flow in porous media (Barenblatt and Zheltov, 1960; Saidi, 1979; Dean and Lo, 1988; Blunt and King, 1992; Zhi and Dong, 1994; Blunt et al., 1995). The finite difference and finite volume techniques are conventionally used for numerical simulation of the fluid flow in very large scale problems (Blunt and King, 1992; Blunt et al., 1995). However, it has been proved that the finite difference method is strongly influenced by the mesh quality, mesh size, and mesh orientation, which makes this method unattractive for unstructured gridding (Kazemi and Gilman, 1993; Blunt et al., 1995, Chen et al., 1999). Finite element methods have been employed to model single-phase and two-phase flow in heterogonous permeable media with different capillarity pressures (Mualem et al., 1976; Ghanem et al., 1988; Blunt and King, 1992; Blunt et al., 1995). Up-scaling methods are also being considered by replacing a porous medium containing heterogeneities with an equivalent homogeneous medium (Van Genuchten, 1980; Saidi, 1987; Chen et al., 1995).

Numerical models for naturally fractured reservoirs are generally divided into categories, namely, double-porosity, single permeability (dual porosity) model and double- porosity, double- permeability (dual permeability) model. The difference between the two models is that the second type considers matrix block-to-block flow while the first one neglects this mechanism. Also it is clear that the dual porosity model requires a transfer function calculation between matrix and fracture. Therefore, proper calculation of mass transfer from matrix to fracture plays an important role in generating better simulation results (Li et al., 2000; Tony et al., 2002).

Geomechanical modeling of the subsurface fracture network through use of the sub-critical fracture growth scheme is a powerful first step in an attempt to model naturally fractured

reservoirs. The numerical model described by Olson (2004) can complete this step. The second step is to quantify the influence of fracturing on subsurface fluid flow.

In many porous fractured reservoirs, the long-term production and recovery are controlled by matrix-fracture transfers, which take place in the multiphase conditions resulting from depletion or the implementation of secondary/tertiary methods. Therefore, fractured reservoir simulators have to incorporate reliable formulations and algorithms in order to correctly represent the physics of multiphase transfers between the constitutive media, matrix, fractures, and/or faults. Considered on a general basis, the problem is complex as multiple physical mechanisms can be involved in those transfers, including pressure diffusivity, capillarity, gravity, viscous drive, molecular diffusion, and thermal conduction (Firoozabadi et al., 1994).

Fractures have a big impact on reservoir production; however, they are inherently difficult to quantify. Historically, two approaches have been developed to model fluid flow in natural fractured reservoirs: 1) the continuum approach, and 2) discrete fracture pattern simulation. Both techniques are discussed in the following sections.

2.6.1 Double porosity and double permeability: The most popular and effective technique to model naturally fractured reservoirs has been through a dual porosity approach in which the fracture and matrix are separated into two different continuums, each with its own set of properties. They also interact with each other and the fluid can transfer in between. Most of the existing dual porosity models idealize matrix-fracture interaction by assuming orthogonal fracture systems (or parallelepiped matrix blocks) and pseudo-steady state flow.

The foundation of the dual porosity model was laid down by Barenblatt (1960) and Warren and Root (1963) more than forty years ago. The continuum reservoir simulation is based on the idea that a heterogeneous hydrocarbon reservoir can be represented by an equivalent homogenous medium. Warren and Root (1963) expanded this approach to a naturally fractured reservoir. They proposed to describe the fractured reservoir with two types of porosity: 1) the primary or matrix porosity, and 2) the secondary or fracture porosity. This approach is called the double porosity or dual porosity approach. The two systems are linked through a transfer function, which represents the exchange of fluid between them. These transfer functions depend on the shape and dimensions of the matrix block, transmissibility of the block, relative permeability, capillary pressure, and density differences between phases (Mattax and Dalton, 1990). Warren and Root (1963) acknowledged that a naturally fractured reservoir was inherently heterogeneous. However, if the scale of heterogeneity is small compared to the scale of the reservoir, the reservoir is considered homogeneous (Warren and Root, 1963). Warren and Root (1963) derived the analytical solution for the response of an infinite reservoir based on the following assumptions: 1) the matrix porosity is homogeneous, isotropic, and contained within a systematic array of identical, rectangular parallelepipeds; 2) the fracture system consists of an array of uniform orthogonal fractures, aligned with the principal axes of permeability. 3) Flow can occur between the matrix and the fractures, but flow from matrix to matrix block cannot occur; 4) Quasi-steady state exists in the matrix blocks at all times; and 5) only single phase flow of a slightly compressible liquid is considered. Warren and Root (1963) define the following dimensionless parameters:

$$t_D = \frac{K.t}{(\phi_1 c_m + \phi_2 c_f)\mu_L . r_w^2} \tag{2.11}$$

$$p_D = \frac{2\pi.K.h}{q.\mu_L}(p_0 - p_{(r,t)}) \tag{2.12}$$

and

$$r_D = \frac{r}{r_w} \tag{2.13}$$

where K is the permeability, h is the reservoir thickness; q is the flow rate at the wellbore, μ_L is the viscosity, p_0 is the initial reservoir pressure, $p(r,t)$ is the pressure at radius, r, and time , t, Φ_f and Φ_m are the porosity of the fracture and matrix system respectively, C_f and C_m are the total compressibility of the fracture and matrix system respectively, and r_w is the wellbore radius. With these dimensionless parameters, Warren and Root (1963) derived the following equations for calculating pressure in a reservoir:

$$v_m(\textit{flow flux in matrix}) = \frac{-K_m}{\mu_L}\nabla p_m \tag{2.14}$$

$$v_f(\textit{flow flux in fractures}) = \frac{-K_f}{\mu_L}\nabla p_f \tag{2.15}$$

$$\frac{1}{r_D}\frac{\partial}{\partial r_D}(r_D\frac{\partial p_{2D}}{\partial r_D}) - \omega\frac{\partial p_{2D}}{\partial t_D} - (1-\omega)\frac{\partial p_{2D}}{\partial t_D} = 0 \tag{2.16}$$

$$(1-\omega)\frac{\partial p_{1D}}{\partial t_D} - \lambda(p_{2D} - p_{1D}) = 0 \tag{2.17}$$

where p_D is dimensionless pressure, t_D is dimensionless time and ω is a measure of the fluid capacitance or storage capacity due to the secondary porosity (or fracture) and is determined through:

$$\omega = \frac{\phi_2 c_f}{\phi_1 c_m + \phi_2 c_f} \tag{2.18}$$

The second parameter, λ, is related to the flow capacity of the matrix blocks and the contrast between the matrix and fracture permeability, and is determined through (Warren and Root, 1963):

$$\lambda = \alpha \frac{K_m}{K_f} r_w^2 \tag{2.19}$$

where α is a shape factor (Warren and Root, 1963)

A natural extension of the double porosity approach is to allow for flow between matrix blocks, called the double or dual permeability model. To solve for fluid flow through the matrix block as well as the fracture system one has to solve the Barenblatt-Zheltov equations (1960).

2.7 Contribution of the Study in Numerical Modeling of Fractured Porous Media

Previous attempts were made in modeling gravity drainage processes using several of numerical simulation tools (Blunt, 2001; Zhang, 2002; Hoteit and Firoozabadi, 2008). The most common tool is a very popular commercial reservoir modeling software, CMG. The advantages of such tools are that it is simple to use and is readily available. The disadvantage is the limited access to the governing equations and the algorithm used in the numerical simulation. However, COMSOL software, which is used here in this study, has some advantages over CMG including its flexibility and powerful functionality in conducting complex 2-D and 3-D numerical simulations. The software uses a simple graphic user interface (GUI) to define the control volume of the simulated system. Furthermore, the predefined equations can be combined and modified to suit the needs of the problem analyzed. However, it should be noted that selection of appropriate size for mesh and time intervals are important to impede instability during solution time and meet required criteria for convergence.

At the field scale, flow in fractured reservoirs is simulated by a dual porosity or dual permeability approaches in which the reservoir is composed of two domains: a flowing fraction, which represents the fractures, and a relatively stagnant matrix (Saidi and Tehrani, 1979; Hoteit and Firoozabadi, 2008). The transport of fluids between fracture and matrix is represented by a transfer function (Barenblatt and Zheltov, 1960; Warren and Root, 1963; Saidi and Tehrani, 1979). Our attempt in modeling the gravity drainage process involved separating the matrix part and fracture part into two subdomains. The uncertainties associated with the shape factor for communication rate were eliminated as it was replaced by setting continuity condition in the interface between matrix part and fracture part. This method applies the fluid flow equation to air as the gas phase and to oil as the liquid phase.

In the numerical simulation, the average gas and oil saturations are calculated as time is progressed for each element in matrix, and fracture parts. Oil drainage rate and gas-liquid interface velocity are computed from the knowledge of gas-liquid interface coordination in the two subdomains, and their dependencies on average oil saturations are established. Then the new guesses that are required in the single porosity formulations are calculated.

The goal of this simulation study was to develop a numerical model that describes the gravity drainage process in fractured porous media. A numerical simulation was run based on the conditions of experiment for homogeneous porous medium under free fall gravity drainage (FFGD) and controlled gravity drainage (CGD). Another simulation run was conducted for our constructed fractured porous medium undergoing both FFGD and CGD. The simulated oil production history and the simulation results from COMSOL were compared to the results of the experiments to validate the numerical model. In this study, the effects of fracture, pumping rate, and mesh size using FEMLAB were evaluated using basis of the dynamic modeling in immiscible two-phase flow. This is encouraging for further developments in simulating oil production from heterogeneous porous media as the model may ultimately be matched for utilization by oil industries for fractured petroleum reservoirs with more complexities.

Chapter 3

Free Fall Gravity Drainage in Fractured Porous Media

3.1 Scope

Gravity drainage is a primary recovery method which produces mostly oil and gas using the natural energy reservoir as the driving force to push the fluids into the production well, and is typically applied during the initial production phase of an oil reservoir. This oil production method results in the movement of oil from the upper to the lower parts within a reservoir into the direction of the producing wells driven by gravitational forces (Dullien et al., 1992). Fractured reservoirs are very important contributors to world oil and gas reserves and production. A large number of these reservoirs are being produced by free fall or gas injection type of gravity drainage process (Saidi, 1974).

Gravity drainage experiments were performed to find the initial (characteristic) rate for various systems and to investigate the effects of fracture length and aperture, liquid properties, matrix properties and initial oil saturation effects on the production history and characteristics of gas-liquid interfaces advance. Free fall gravity drainage through fractured models was investigated; the attention was focused on the starting point of gas penetration into the matrix, the recovery rate and oil recovery in various systems. The movement of gas-oil contact was visualized and oil recovery versus time was determined experimentally. These experiments enabled us to capture some aspects of the flow communication between matrix block and fracture during gravity drainage.

This chapter describes the design of experiments, and details the visualization experiments carried out using different fractured porous media under free-fall gravity drainage conditions. The results are presented and discussed for different operating conditions.

3.2 Design of Experiments

Design of Experiment is a descriptive discipline which indeed has very broad applications among all the engineering, natural, and social sciences. The application procedure has been generalized in the form of selecting one or more independent variables, manipulating their effects on one (or some) dependent parameters, and then determining the sensitivity of dependent variable(s) upon changing the independent parameters (Montgomery and Runger, 2006; Montgomery, 2008). Obtaining good results from a standard design of experiments procedure depends upon successful completion of the following steps:

1) Set the objectives,
2) Select various process variables,
3) Select an experimental design,
4) Execute the design,
5) Check that whether the data are consistent with the experimental assumptions or not,
6) Analyze and interpret the results,
7) Use (i.e. present) the results [this phase could lead to perform further experimental runs or consider additional design of experiments or even revise the original one].

3.2.1 Set the objectives: It is the best practice to delineate the general objectives of a set of experiments through a team discussion. All the objectives should be written down, even the "unspoken" ones (Montgomery and Runger, 2006; Montgomery, 2008). The following objectives have been set for the experiments in this study:

1) Understanding the physics of free fall gravity drainage process in fractured media and extending the results to predict the real field case performance, if it is possible.
2) Focusing on the behavior and movement of Gas-Liquid (G-L) interface through matrix and fractures and obtaining the recovery performance of employed models as a function of relevant dimensionless numbers.
3) Defining new concepts for "Characteristic Rate" and then obtaining this parameter for each particular fractured model.
4) Performing parametric sensitivity analysis.

3.2.2 Select the various process variables: This step includes screening the design in order to identify which parameters are affecting the overall system response. According to our understanding of the physics of Free Fall Gravity Drainage process and also following performing some preliminary gravity drainage tests, it was concluded that the following five parameters could be considered to be the main affecting variables influencing the general performance of controlled gravity process (Zendehboudi et al., 2008; Zendehboudi et al., 2009):

- Fracture aperture,
- Matrix height,
- Fracture height,
- Matrix permeability, and
- Fluid properties.

Since the process variables include both inputs and outputs (i.e., factors and responses) the dependent variables are:

- Characteristic (initial) Rate,
- Recovery factor,
- Residual oil saturation, and,
- Vertical elevation difference between the G-L interface positions in matrix and fractures during the gravity drainage processes.

It is wise to critically choose a sound range of variation for experimental input factors just before designing the physical models. This makes it possible to have a reasonable idea about the experimental outputs before performing a particular test relative to other designed experiments.

3.2.3 Selection of an experimental design: Considering the number of important factors evaluated in the current study and the nature of the process, it appears that the most relevant experimental design method is factorial with two levels of design. This type of experimental design is frequently used in experiments involving several independent factors where it is necessary to study the combined effect of the involving parameters on system response. However, as the number of factors in a two level factorial design increases, the number of runs for even a single replicate of the 2^k design becomes very large. Fractional factorial designs can be used in our case to draw valuable conclusions from fewer runs. Therefore, the basic purpose of a fractional factorial design is to economically investigate cause-and-effect relationships of significance in a given experimental setting. There are lots of good reasons on why selecting

only two levels is the most common choice amongst engineers. First and foremost, having two design levels is ideal, simple, and also economical for screening designs (Montgomery and Runger, 2006; Montgomery, 2008). However, it is recommended to conduct the experiment at some centre points between the high level and also the low level of each experimental factor. The standard layout of a 2-level design generally uses “+1” and “-1” notations to denote the "high level" and the "low level" limits of each factor respectively. Table 3.1 demonstrates the series of designed experiments in which 32 trials (i.e., experimental runs) have been planned, considering each factor to be set to its high or low limit during that particular run.

Table 3.1: Design of Experiment data-table for the FFGD experiments

Run No.	Fracture aperture	Matrix height	Fracture height	Matrix permeability	Fluid viscosity	surface tension
1	-1	-1	-1	-1	-1	-1
2	+1	-1	+1	-1	-1	-1
3	-1	+1	-1	-1	-1	-1
4	-1	-1	+1	+1	-1	-1
5	-1	-1	-1	-1	+1	-1
6	-1	-1	+1	-1	-1	+1
7	+1	+1	-1	+1	+1	+1
8	-1	+1	+1	+1	+1	+1
9	+1	-1	-1	+1	+1	+1
10	+1	+1	+1	-1	+1	+1
11	+1	+1	-1	+1	-1	+1
12	+1	+1	+1	+1	+1	-1
13	-1	-1	-1	+1	+1	+1
14	-1	+1	+1	-1	+1	+1
15	-1	+1	-1	+1	-1	+1
16	-1	+1	+1	+1	+1	-1
17	+1	-1	-1	-1	+1	+1
18	+1	-1	+1	+1	-1	+1
19	+1	-1	-1	+1	+1	-1
20	+1	+1	+1	-1	-1	+1
21	+1	+1	-1	-1	+1	-1
22	+1	+1	+1	+1	-1	-1
23	-1	-1	-1	-1	+1	+1
24	-1	-1	+1	+1	-1	+1
25	-1	-1	-1	+1	+1	-1
26	-1	+1	+1	-1	-1	+1
27	-1	+1	-1	-1	+1	-1
28	+1	-1	+1	-1	-1	+1
29	+1	-1	-1	-1	+1	-1
30	+1	+1	+1	-1	-1	-1
31	+1	-1	-1	+1	-1	-1
32	-1	+1	+1	+1	-1	-1

Use of “+1” and “-1” notations for the factor setting is called data coding. This aids in the interpretation of the coefficients fitted to any experimental model. After factor settings are coded properly, all the center points have the value "0". Regarding our study, centre points have been chosen for all the independent variables. Since we were dealing with eight different fractured media, and also 100 replicate runs had been considered in order to examine the repeatability of the experiments, a total of 400 experimental runs were designed to be performed in order to study various effects of all independent variables on the system responses.

3.3 Experimental Setup and Procedures

Figure 3.1 shows the schematic diagram of fractured packed models which were used in gravity drainage experiments. All experiments were conducted at room conditions. There were several peripheral accessory equipments in order to perform these gravity drainage experiments: a vacuum equipment was used to remove dissolved gas from test liquids and also pre-dry the glass beads; two digital balances were used for measuring the cumulative liquid production from both matrix and fractures; and a high resolution camcorder was employed for continuous recording of liquid-air interface movements in both matrix and fractures. Pictures taken at various stages of gravity-stabilized displacement were analyzed by image processing techniques to track the gas-liquid interfaces movement through the matrix and fractures. For improved imaging, we also dyed the oil red by adding a little bit of oil soluble red dye for better color contrast when the test fluid is Varsol oil. The fractures were made using long pieces of Plexiglas with thickness equal to model’s thickness. Slots with different dimensions were made using Plexiglas pieces by milling them in the machine shop to create apertures of 1 mm, 2 mm, 3 mm, 5 mm, and 11 mm, and then placed a mesh over the two sides of the slots to prevent the beads from entering the fracture space. To obtain the same initial condition for each experiment, models were saturated by adding dry glass beads to a known volume of liquid in order to attain the desired matrix packing height.

The fractured models were of rectangular geometry with certain patterns of fractures. A known volume of liquid was filled into the fractured model. Glass beads were loaded from the top of the model while packing continuously. The packing operation must be continuous to prevent the formation of any layering in the fractured medium during the packing process. Glass beads’ loading was stopped when the glass beads in the rectangular model reached 1-2 cm above the target height. After 5 minutes tapping stopped, the glass beads height would continuously drop. More glass beads were then added into the fractured porous medium to achieve the target height. Every time glass beads were added, manual mixing with a stick was needed to ensure packing uniformity. Following the packing, the excess liquid was removed from the porous medium and measured. The volume of liquid that remained in the physical model was the pore volume of porous medium (V_P). The bulk volume of the porous medium (V_B) was the space of the column occupied by liquid and glass beads. Thus the effective porosity of the porous medium was found as:

$$\phi_e = \frac{V_P}{V_B} \tag{3.1}$$

When the experimental run started, the cumulative liquid production from matrix and fractures were separately recorded and measured. As mentioned above, each physical model is equipped with a certain pattern of fractures. Figure 3.1 shows the different configurations of fractures in the porous media used in this study.

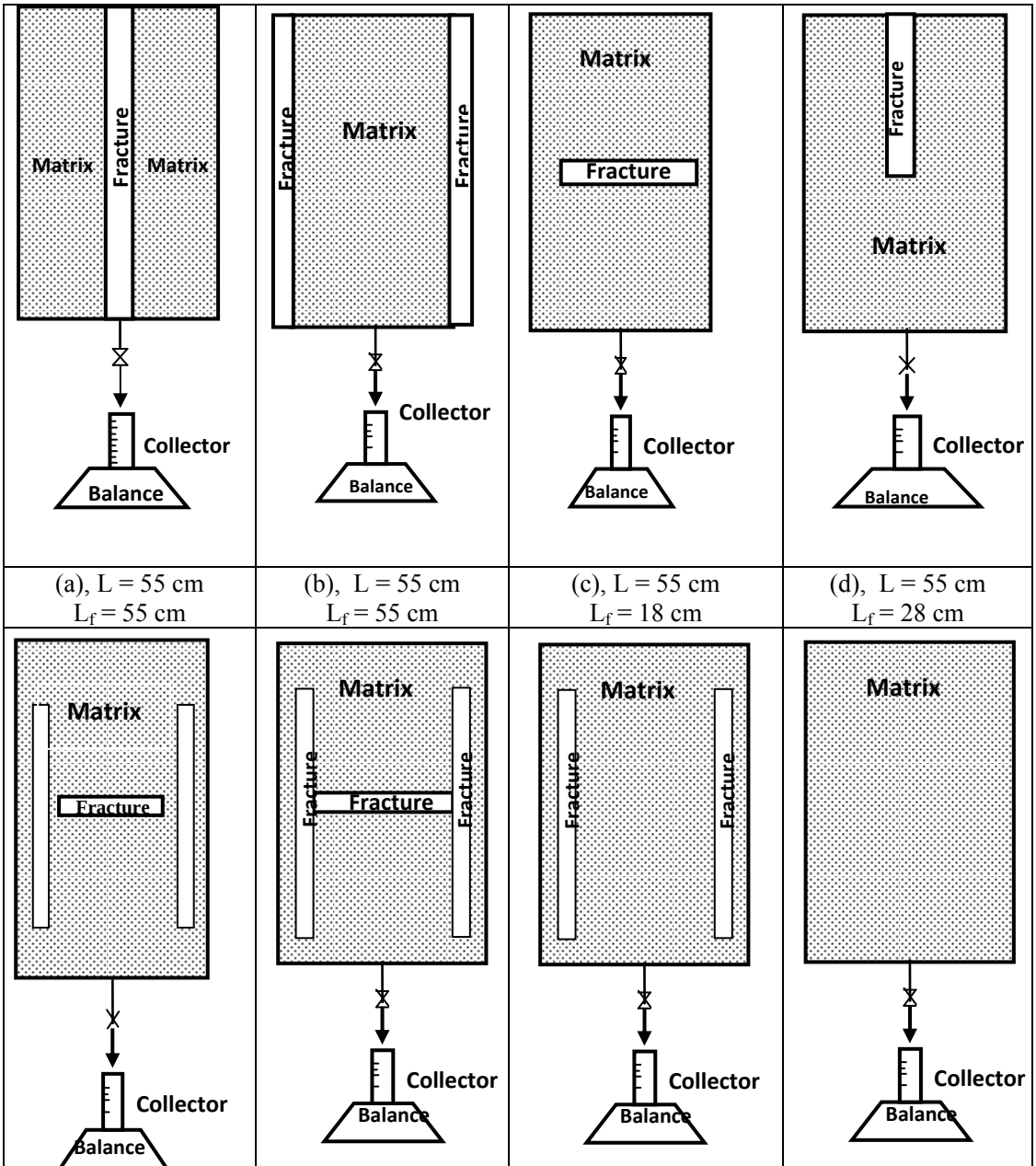

(a), L = 55 cm L_f = 55 cm	(b), L = 55 cm L_f = 55 cm	(c), L = 55 cm L_f = 18 cm	(d), L = 55 cm L_f = 28 cm
(e), L = 55 cm L_f = 45 cm (Vertical) , 18 cm (Horizontal)	(f), L = 55 cm L_f = 45 cm (Vertical) , 18 cm (Horizontal)	(g), L = 55 cm L_f = 45 cm	(h), L= 55 cm

Figure 3.1: Schematic of the apparatus for free fall in porous media with various patterns of fractures.

3.3.1 Test fluids: Gravity drainage tests were performed using laboratory test liquids consisting of de-ionized water, Varsol oil and aqueous solutions of CMC with different concentrations to resemble the oil phase, and air was used to simulate the gas phase. A sodium salt of low viscosity Carboxy Methyl Cellulose, commonly referred to as CMC, was found to be an appropriate polymer which can be mixed with de-ionized water to simulate the oil phase for liquid viscosity (Srivastava et al., 1990). More information regarding CMC is in Appendix A. Water viscosity was increased by adding Carboxy Methyl Cellulose to represent different oil viscosities. Since the CMC powder does not readily dissolve in water, a blender was used to break-up the large aggregates of CMC formed during the dissolution process in order to speed up the dissolution rate and produce a homogeneous solutions. The effect of CMC powder concentration on the viscosity of prepared solutions is shown in Table 3.2. The physical properties of test fluids are also shown in Table 3.3. Methods for viscosity and surface tension measurements are brought in Appendix B.

Table 3.2: The effect of CMC concentration on the mixture viscosity

CMC (wt%) in de-ionized water	Viscosity of CMC solution (mPa.s)
0	1.0 ± 0.2
1	4.8 ± 0.3
2	11.9 ± 0.4

Table 3.3: Physical properties of test fluids

Test Fluid	Density (g/cm^3)	Surface tension (mN/m)	Viscosity (mPa.s)
CMC solution (1%)	1.05	73.2 ± 0.6	4.8 ± 0.3
CMC solution (2%)	1.07	74.1 ± 0.5	11.9 ± 0.4
Varsol oil	0.78	25.0 ± 0.5	1.2 ± 0.3
Water	1.00	72.0 ± 0.4	1.0 ± 0.2
Air	1.2×10^{-3}	N/A	0.018

3.3.2 Model properties: As explained in section 3.3, the porosity of packed models was measured by the saturation method and it was concluded that all the prepared models had similar porosity values because of the random packing procedure. The falling head permeability measurement technique was used to measure the permeability of different physical models used (Dullien, 1990). Tables 3.4 and 3.5 contain properties of glass beads (i.e. particles size distribution) and the physical properties of different packed models used in this study, respectively.

Table 3.4 :Particles size distribution and permeabilities of three types of glass beads employed in the experiments

Type of glass beads	Min diameter (mm)	Max diameter (mm)	Average diameter (mm)	Permeability (Darcy)
BT2	0.84074	1.40971	1.12522	1013 ± 95
BT3	0.59436	0.84074	0.71755	408 ± 67
BT4	0.41912	0.59436	0.50673	204 ± 49

Table 3.5: Properties of employed packed models

Run No.	Model height, L (cm)	Matrix glass beads size	Porosity, %			Permeability ,Darcy		Test fluid	Fracture aperture (b), mm	Fractures pattern
			ϕ_f	ϕ_m	ϕ_e	$K_{eff,f}$	K_m			
1	55	BT2	1.410	38	38.86	15979	1013	CMC(1%)	5	b
2	55	BT2	1.410	38	38.86	15979	1013	CMC(2%)	5	b
3	55	BT2	1.410	38	38.86	15979	1013	CMC(2%)	5	b
4	55	BT2	1.410	38	38.86	15979	1013	CMC(2%)	5	b
5	55	BT2	0.920	38	38.56	3465	1013	CMC(2%)	3	b
6	55	BT2	0.920	38	38.56	3465	1013	CMC(1%)	3	b
7	55	BT3	1.410	38	38.86	15979	408	CMC(1%)	5	b
8	55	BT3	1.410	38	38.86	15979	408	CMC(2%)	5	b
9	28	BT3	1.410	38	38.86	15979	408	CMC(2%)	5	b
10	40	BT3	1.410	38	38.86	15979	408	CMC(2%)	5	b
11	55	BT4	1.410	38	38.86	15979	204	CMC(1%)	5	b
12	55	BT4	1.410	38	38.86	15979	204	CMC(1%)	5	b
13	55	BT4	1.410	38	38.86	15979	204	CMC(1%)	5	b
14	55	BT4	1.410	38	38.86	15979	204	CMC(2%)	5	b
15	55	BT4	0.920	38	38.56	3465	204	CMC(1%)	3	b
16	55	BT4	1.410	38	38.86	15979	204	Water	5	b
17	55	BT2	0.620	38	38.37	1028	1013	CMC(2%)	2	b
18	55	BT2	1.410	38	38.86	15979	1013	Varsol	5	b
19	55	BT3	1.410	38	38.86	15979	408	Varsol	5	b
20	55	BT3	0.920	38	38.56	3465	408	Varsol	3	b
21	55	BT3	3.208	38	40.12	128000	408	Water	11	a
22	55	BT3	1.712	38	39.09	27720	408	Water	11	d
23	55	BT3	3.207	38	40.12	128000	408	Varsol	11	a
24	55	BT3	1.712	38	39.09	64000	408	Varsol	11	d
24	55	BT3	0.920	38	38.56	32000	408	Varsol	11	d
26	55	BT2	0.231	38	38.14	2619	1013	CMC(2%)	5	c
27	55	BT2	0.046	38	38.03	533	1013	CMC(2%)	1	c
28	55	BT2	0.231	38	38.14	2619	1013	Varsol	5	c
29	55	BT3	1.410	38	38.86	15979	408	Varsol	5	e
30	55	BT3	1.531	38	38.86	17120	408	Varsol	5	f
31	55	BT2	N/A	38	38.00	N/A	1013	Varsol	N/A	unfractured
32	55	BT2	0.231	38	38.14	2619	1013	CMC(1%)	5	c
33	55	BT4	1.410	38	38.86	15979	204	CMC(1%)	5	e
34	55	BT4	1.531	38	38.93	17120	204	CMC(1%)	5	f
35	55	BT2	N/A	38	38.00	N/A	1013	CMC(2%)	N/A	unfractured
36	55	BT3	0.702	38	38.43	7989	408	Varsol	5	a
37	55	BT3	0.702	38	38.43	7989	408	Water	5	a
38	55	BT4	1.410	38	38.86	15979	204	CMC(2%)	5	e
39	55	BT2	1.410	38	38.86	15979	1013	Varsol	5	e
40	55	BT2	1.410	38	38.86	15979	1013	CMC1%	5	e
41	55	BT3	1.215	38	38.74	13696	408	Varsol	5	g
42	55	BT4	1.215	38	38.74	13696	204	CMC(1%)	5	g

The effective porosity (ϕ_e) reported in Table 3.5 for each fractured system is defined as:

$$\phi_e = \phi_f + \phi_m - \phi_f.\phi_m \tag{3.2}$$

In the above equation, the fracture porosity (ϕ_f) is defined as the ratio of fracture volume over the total bulk volume of the sample. Matrix porosity (ϕ_m) is also defined as the ratio of matrix pore volume over bulk volume of the matrix.

The effective fracture permeability ($K_{eff,f}$) reported in Table 3.5 can also be correlated with fracture porosity and aperture through the following two equations (Saidi, 1987):

$$K_f = \frac{b^2}{12} \tag{3.3}$$

$$K_{eff,f} = K_f.\phi_f \tag{3.4}$$

If fracture-matrix communication is neglected (the assumption is correct when we are dealing with high viscous oil and very low permeable matrix), the total effective permeability for the whole model with a long vertical fracture would be like two parallel porous media, as follows:

$$K_e = K_f.\phi_f + K_m \frac{W_m}{b + W_m} \tag{3.5}$$

In above equation, K_m is the matrix permeability and W_m represents the width of matrix. If the fracture aperture is negligible compared to the width of matrix, then Equation (3.5) simplifies to Equation (3.4) for calculating the effective permeability of a medium with fractures in parallel flow with that in matrix.

3.4 Oil Recovery Mechanism

During the gas invasion process, it was observed that no gas entered the matrix at the beginning of the experiments. During this period, gas invades into the fractures because of the lower resistance to flow (i.e., higher permeability). During these early stages in which no gas has entered into the matrix side, one can write the following mass balance equation to relate gravity rate to the fracture parameters:

$$q = -(\frac{dH_f}{dt}).A_f = -(\frac{K_f}{\mu_L} A_f)(\Delta\rho.g) \tag{3.6}$$

where μ_L is the liquid viscosity; q is the drainage rate ; $\frac{dH_f}{dt}$ is the recession rate of interface position through the fractures; A_f is fracture cross sectional area perpendicular to the flow direction; $\Delta\rho$ and g are density difference between gas and liquid and gravitational force, respectively.

As the gas invasion process is progressed, the driving force for gas flow into the fracture decreases gradually. At the time at which the liquid level in the fracture is low enough (say at distance h from the top of each model) such that $\Delta\rho.g.h$ for each particular system is equal to the difference between the capillary pressure threshold of matrix and that of the fracture, liquid drainage would start in the matrix domain. The liquid drainage rate in fractures at the start of gas invasion into the matrix is called "characteristic (initial) drainage rate". After this time, liquid drainage occurs both from matrix and from fractures. According to the drainage phenomena observed in our simplified fractured macromodels, it was found that there are two counter-acting driving forces for liquid drainage out of each particular model. Liquid drains mainly from both matrix and fractures based on the effect of gravitational force. However it is evident that there is liquid flow communication between matrix and fractures where by a portion of the liquid which drained from matrix would be transferred from the matrix side to the fracture side. It was observed that some parts of the matrix side in the vicinity of each side fracture are affected more by liquid flow communication rather than the rest of the matrix. These portions of the matrix which are adjacent to the side fractures have more potential for flow communication. Other portions of the matrix which are far away from the fracture are therefore not affected by the presence of fractures. This point is verified by the qualitative analysis of interface movement in matrix, as the liquid-air interface in matrix is relatively flat in regions near the half-way distance of parallel fractures (see Figure 3.2). However, this interface is considerably inclined towards the fracture in the areas adjacent to each fracture. This tilted interface becomes flat as the driving force for the liquid communication between fracture and matrix decreases versus time. This

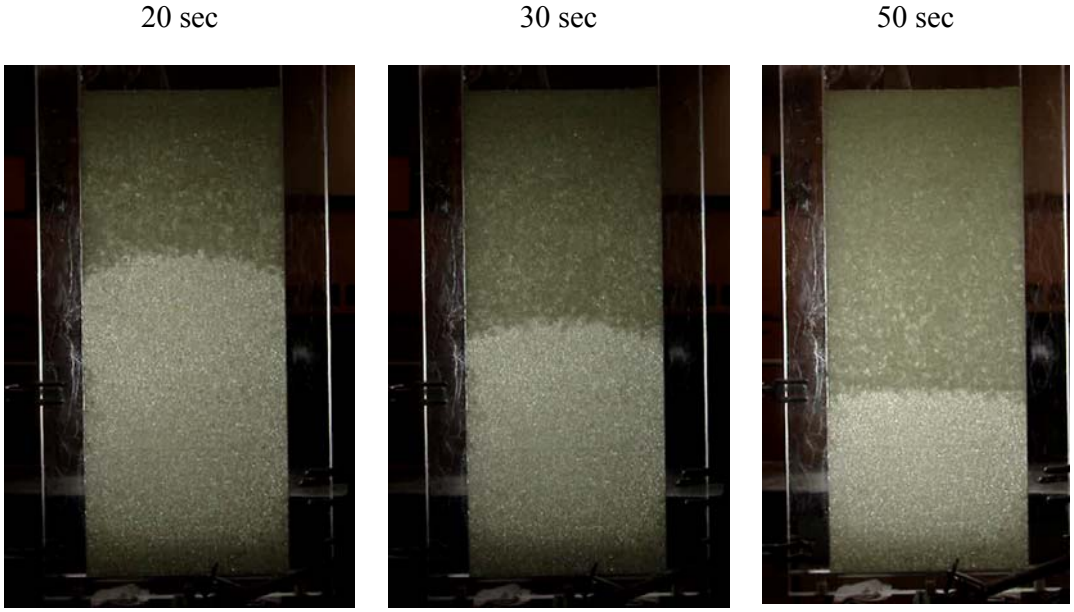

Figure 3.2: Schematic of interface advancement at three different times for the BT2 glass beads model saturated with CMC solution (1%) in fractured model(b) , b=2 mm , L model=55 cm.

communication rate depends on the properties of test fluids, matrix permeability, and vertical distance between the liquid levels in matrix and fractures. Figure 3.2 shows the oil recovery mechanism at various stages and the interface advancement during the gravity drainage experiments.

Determination of fluid flow direction through fracture network and between matrix blocks and fracture is of great importance. When the fractured network model starts to produce by gravity drainage (Figure 3.2), the gas enters in the porous medium. If the top ends of vertical fractures are located at the same level with matrix part will, the vertical fractures would be invaded first by gas. The gas will continue to flow in the fractures and at a certain time when the driving forces for gas invasion in both matrix and fractures parts become the same, the gas will invade the matrix. This is because the conductivity (permeability) of the fractures is greater than that of the matrix. Now assume the fracture height is lower than matrix height as fracture pattern is placed in lower level than matrix is, as such fractured media can be seen in the fractured media with fractures configurations of e, f and g. In these cases, the gas first invades matrix and as soon as the gas-liquid front touches the top part of fractures, the movement of gas-liquid interface stops in matrix and gas starts invading in the vertical fractures. This process proceeds until the driving force for gas invasion equals for both matrix and fracture parts and then we observe gas-liquid interface movement in matrix and fracture domains.

During the gravity drainage process, oil flows from matrix to vertical fractures and also the gas-oil fronts continue moving to reach the horizontal fracture (if placed in the middle of the fractured medium). If a horizontal fracture is placed in the middle, then that is where the upper and lower matrix blocks communicate and can greatly affect the oil recovery from matrix blocks and the total oil recovery. If both vertical fractures have the same dimensions and their apertures are equal or greater than the horizontal fracture, some of oil from the side parts of the horizontal fracture starts flowing to the vertical fractures. The affected regions of the horizontal fracture communicating are adjacent to the side fractures. Also, the upper matrix block drains oil into the middle horizontal fracture and then a fraction of the oil in the horizontal fracture is drained by lower matrix blocks. As mentioned above, remaining liquid flows through the middle horizontal fracture toward the left and the right vertical fractures, which then flows downward to the bottom (Figure 3.3). Therefore, it can be concluded that the horizontal fracture can considerably increases the production rate and ultimately recovery performance during initial period of gravity drainage process.

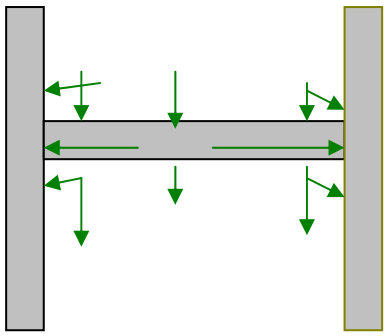

Figure 3.3: A schematic carton to show liquid transferring between different parts of a fractured porous medium containing such fracture configuration.

3.5 Experimental Results and Discussion

Free fall gravity drainage experiments were carried out in various porous media models with different initial conditions. The experiments for each model were repeated two or three times. The average result was used to obtain the production history and gas/liquid interface advance. Comparison between runs for a given system shows very good repeatability of experiments as will be documented later.

Parametric sensitivity analyses were performed in this study in order to investigate the effect of different system parameters on the gravity drainage process performance. In this section, the effects of model length, matrix permeability, fluid pair properties, and fracture aperture on the gravity drainage process performance were investigated. This analysis contains a quantitative approach (analyzing the drainage rates versus time) as well as relevant qualitative analysis (analysis of interface movements in both fractures and matrix using video-recording and digital imaging techniques). Gas-liquid interface position "H(t)" was measured from the top portion of each individual packing all the way down along the model length with respect to time as the gas phase invades the fractures and matrix space respectively. Qualitatively speaking, all the test results for models a, b and d in Figure 3.1 are conveying the message that at the very beginning of the experimental duration, the gas-liquid interface advances faster in the fracture compared to that in the matrix. At each time, the elevation difference of interface positions is defined by the interface position in the fracture minus that of the matrix,

$$\Delta H(t) = [H_f(t) - H_m(t)] \tag{3.7}$$

Table 3.6 provides a summary of main results obtained from these experiments.

Table 3.6: Results of Free fall gravity drainage experiments for 42 sample runs after 5 hrs

Run No.	Model height (L) ,cm	Matrix glass beads size	Fracture Length (L_f), cm	Test fluid	Fracture aperture (b), mm	Fractures pattern	Initial flow rate, cm^3/s	Residual liquid saturation, %	RF, %
1	55	BT2	55	CMC(1%)	5	b	1.90 ± 0.2	6.2 ± 0.3	87.0 ± 0.7
2	55	BT2	55	CMC(2%)	5	b	1.10 ± 0.3	7.1 ± 0.3	86.0 ± 1.1
3	55	BT2	55	CMC(2%)	5	b	1.10 ± 0.2	5.0 ± 0.3	90.0 ± 0.8
4	55	BT2	55	CMC(2%)	5	b	1.10 ± 0.3	5.0 ± 0.3	90.0 ± 0.9
5	55	BT2	55	CMC(2%)	3	b	0.50 ± 0.1	7.2 ± 0.3	86.0 ± 1.0
6	55	BT2	55	CMC(1%)	3	b	0.80 ± 0.1	6.1 ± 0.3	86.0 ± 1.1
7	55	BT3	55	CMC(1%)	5	b	1.90 ± 0.3	7.3 ± 0.3	76.0 ± 0.7
8	55	BT3	55	CMC(2%)	5	b	1.10 ± 0.2	8.2 ± 0.5	75.5 ± 1.1
9	28	BT3	28	CMC(2%)	5	b	1.00 ± 0.2	8.3 ± 0.6	57.0 ± 0.4
10	40	BT3	40	CMC(2%)	5	b	1.10 ± 0.3	8.1 ± 1.1	68.5 ± 0.7
11	55	BT4	55	CMC(1%)	5	b	1.85 ± 0.2	7.0 ± 1.0	70.0 ± 0.9
12	55	BT4	55	CMC(1%)	5	b	1.85 ± 0.3	5.4 ± 0.6	75.0 ± 0.8
13	55	BT4	55	CMC(1%)	5	b	1.85 ± 0.2	5.3 ± 0.7	75.0 ± 0.9
14	55	BT4	55	CMC(2%)	5	b	1.05 ± 0.2	8.6 ± 0.8	70.0 ± 0.7
15	55	BT4	55	CMC(1%)	3	b	0.80 ± 0.1	7.1 ± 0.4	69.5 ± 1.2
16	55	BT4	55	Water	5	b	6.20 ± 0.5	5.2 ± 0.6	71.0 ± 1.1
17	55	BT2	55	CMC(2%)	2	b	0.40 ± 0.1	7.1 ± 0.7	85.0 ± 0.8
18	55	BT2	55	Varsol	5	b	5.30 ± 0.3	13.4 ± 0.9	83.0 ± 0.9
19	55	BT3	55	Varsol	5	b	5.20 ± 0.6	14.1 ± 0.2	79.0 ± 0.7
20	55	BT3	55	Varsol	3	b	2.40 ± 0.2	14.4 ± 0.2	78.0 ± 0.6
21	55	BT3	55	Water	11	a	7.60 ± 0.4	7.4 ± 0.8	77.0 ± 0.5
22	55	BT3	30	Water	11	d	3.40 ± 0.2	7.6 ± 0.3	76.0 ± 0.7
23	55	BT3	55	Varsol	11	a	6.40 ± 0.5	15.1 ± 0.6	80.0 ± 1.7
24	55	BT3	30	Varsol	11	d	3.10 ± 0.4	15.0 ± 0.7	79.0 ± 1.4
24	55	BT3	15	Varsol	11	d	1.30 ± 0.2	14.3 ± 0.3	79.0 ± 1.2
26	55	BT2	18	CMC(2%)	5	c	N/A	8.2 ± 0.4	86.0 ± 0.8
27	55	BT2	18	CMC(2%)	1	c	N/A	7.4 ± 1.3	86.5 ± 0.7
28	55	BT2	18	Varsol	5	c	N/A	13.0 ± 0.9	82.5 ± 0.9
29	55	BT3	46	Varsol	5	e	N/A	14.1 ± 0.8	79.0 ± 1.2
30	55	BT3	46	Varsol	5	f	N/A	14.1 ± 1.0	79.0 ± 1.4
31	55	BT2	N/A	Varsol	N/A	N/A	N/A	15.2 ± 0.7	82.0 ± 1.1
32	55	BT2	18	CMC(1%)	5	c	N/A	7.4 ± 0.5	85.0 ± 1.2
33	55	BT4	46	CMC(1%)	5	e	N/A	8.2 ± 0.9	70.0 ± 1.8
34	55	BT4	46	CMC(1%)	5	f	N/A	8.1 ± 0.7	70.5 ± 1.0
35	55	BT2	N/A	CMC(2%)	N/A	N/A	N/A	6.4 ± 0.8	86.0 ± 1.3
36	55	BT3	55	Varsol	5	a	2.70 ± 0.5	14.1 ± 1.2	79.5 ± 0.9
37	55	BT3	55	Water	5	a	2.70 ± 0.4	7.3 ± 0.6	76.0 ± 1.0
38	55	BT4	46	CMC(2%)	5	e	N/A	8.1 ± 0.5	70.0 ± 1.1
39	55	BT2	46	Varsol	5	e	N/A	14.1 ± 0.4	83.0 ± 0.8
40	55	BT2	46	CMC(1%)	5	e	N/A	6.1 ± 0.3	86.0 ± 0.7
41	55	BT3	46	Varsol	5	g	N/A	15.1 ± 0.4	79.0 ± 0.8
42	55	BT4	46	CMC(1%)	5	g	N/A	8.2 ± 0.3	69.0 ± 0.6

3.5.1 Effect of matrix permeability: Three different types of unconsolidated packed models were employed in terms of the size of packing materials. Figure 3.4 shows the effect of matrix permeability on the cumulative liquid production performance versus time in fractured porous medium (b). This Figure represents the experimental data related to the run numbers 1, 7, and 11 according to Table 3.6. In all of these experimental runs, models were packed to the ultimate height of 55cm, and two vertical fractures with 5mm aperture were also made along each side of these models. These models were saturated with 1 wt% aqueous CMC solution prior to the free-fall gravity drainage tests.

Qualitative analysis of the recorded events has shown that gas-liquid interface in the matrix was not stable during the early stages of the tests. The interface was tilted towards the side fractures in the areas adjacent to these fractures. However as time went by, the gas-liquid interface became more horizontally flat, which indicates that the displacement became more gravitationally stable. This gravity-dominated process is very fast during the early experimental duration when higher permeability matrices were employed. According to the experimental results for the test with BT2 glass beads as the matrix, almost 50% of the initial liquid in place was drained within the first 75 seconds of the run time. However this cumulative drainage was reduced to almost 19% of the initial saturation within the same time interval for the models with BT3 glass beads as the matrix (Figure 3.4). As it is summarized in Table 3.6, a system with higher matrix permeability (i.e. lower capillary threshold height) has higher ultimate cumulative production (87% for Run #1, 76% for Run #7, and 70% for Run #11).

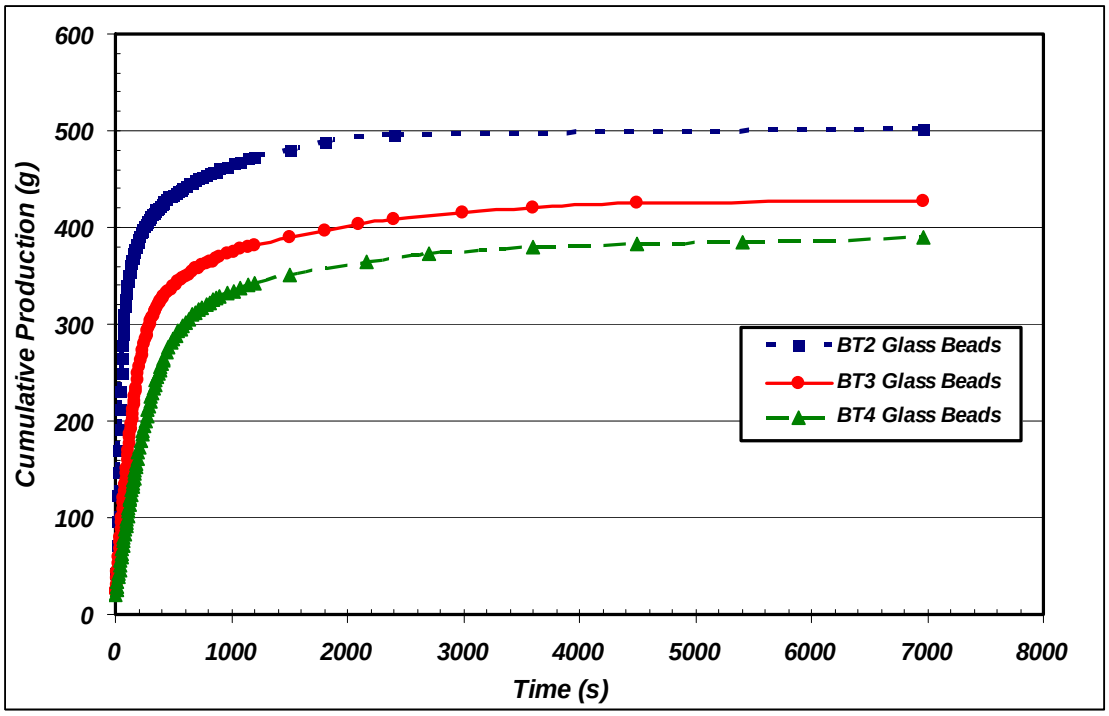

Figure 3.4 : Comparison of production history using models made with BT2, BT3 and BT4 glass beads and model length = 55 cm , fluid pair: CMC solution (1%)-Air , b = 5 mm.

Figure 3.5 shows the variations of liquid height difference in fractures and matrix versus time for different matrix permeabilities. At the beginning of gravity drainage process, the effect of matrix

permeability on liquid height difference is negligible because of the fact that flow is mainly due to the fracture drainage. This height difference reaches a local maximum at which liquid drainage from matrix started. The time to reach this local maximum is delayed as the matrix permeability decreases. Beyond this point, the difference between the gas-liquid contact locations in fractures and matrix tends to decrease significantly with time as the interface location in the matrix drops while the interface position in the fractures remain relatively unchanged as it almost reaches to its threshold value. Remember that all the interface heights in fractures and matrix were measured from the top of the packed model towards the production end in the downward direction. During this period, models with higher permeability have lower (H_f - H_m) values.

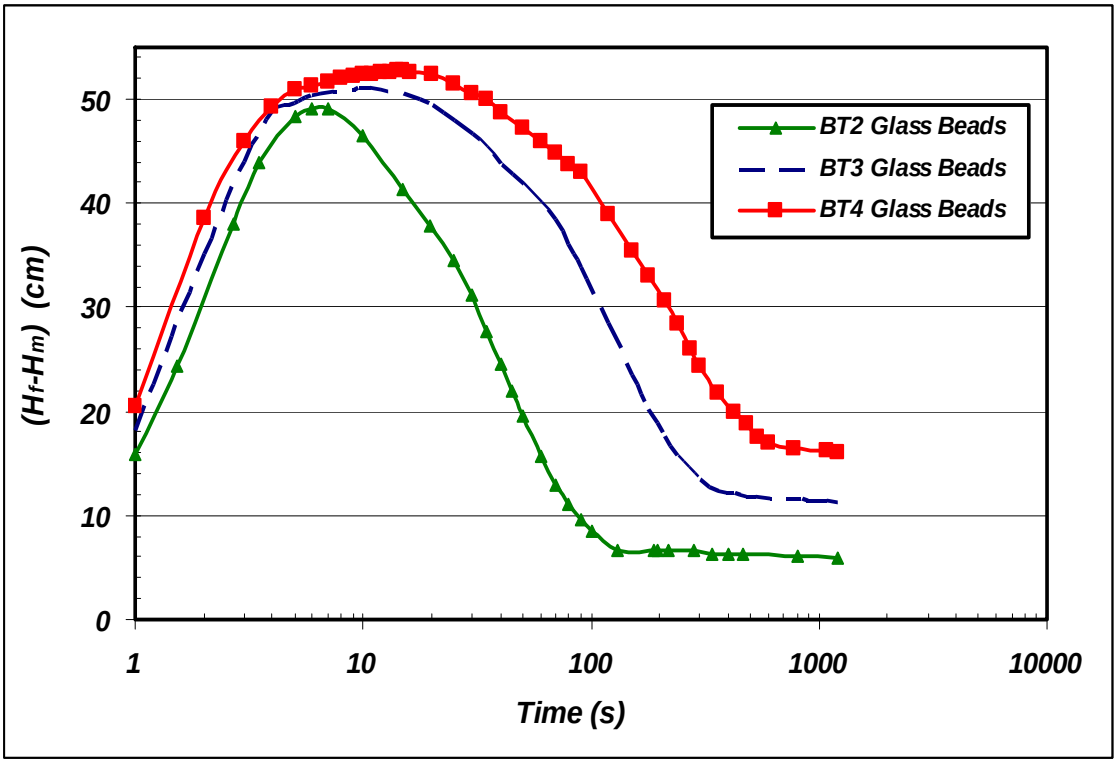

Figure 3.5 :Difference between the gas-liquid contact locations in fracture and matrix using data obtained with the media made with BT2 , BT3 and BT4 glass beads and model length = 55 cm , fluid pair: CMC solution (1%)-Air , b=5 mm.

Figure 3.6 shows the effect of matrix permeability on the liquid communication rate between matrix and fractures. It is clear that during the gravity drainage process in such systems, there are two separate driving forces which affect the liquid communication rate between fracture and matrix: 1) the matrix permeability, and 2) the difference between gas-liquid interface positions in fracture and matrix. According to Figure 3.5, during the early stages of the process the effect of matrix permeability is more pronounced on the communication rate. As time goes on, it is evident that the contribution of interface height difference (H_f - H_m) will dominate the rate of liquid communication. For example, the models with higher interface height difference (i.e. those with lower matrix permeabilities) have higher liquid communication rate.

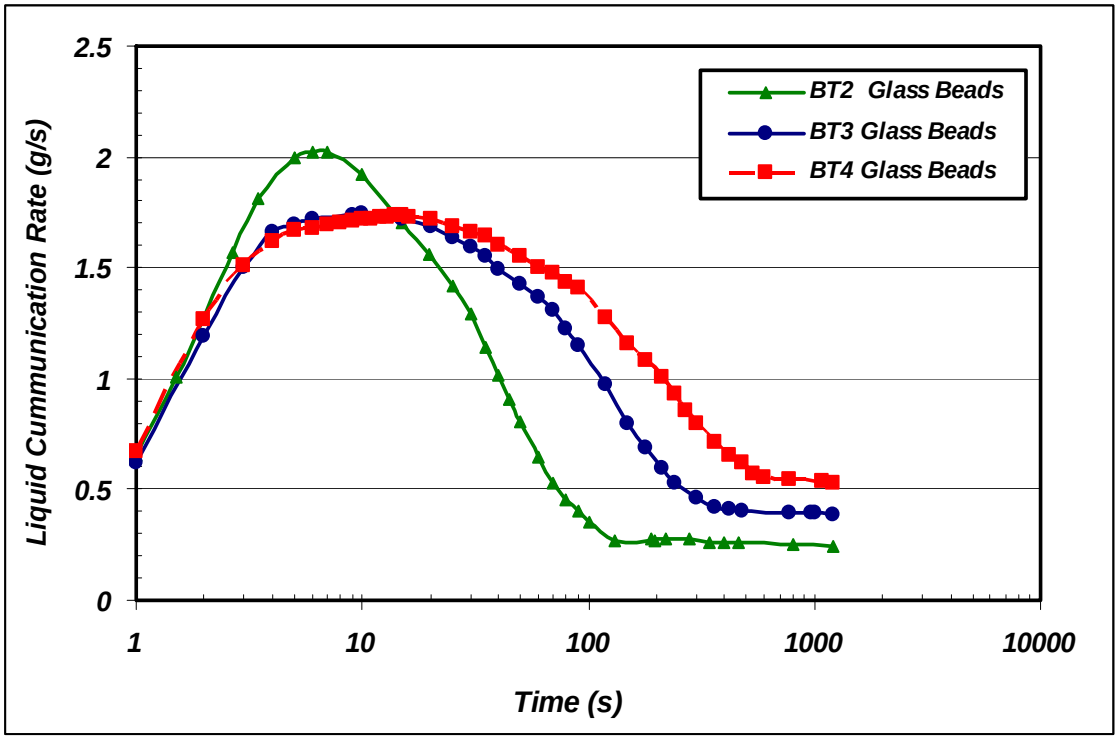

Figure 3.6: Liquid communication rate from matrix to the fractures in three different matrix permeability models versus time. [model length = 55 cm, fluid pair: CMC solution (1%)-Air , b = 5 mm].

3.5.2 Effect of liquid viscosity: In order to investigate the effect of liquid viscosity on the gravity drainage process performance, different aqueous solutions of CMC were used, with viscosities higher than that of de-ionized water. Free-fall gravity drainage tests were performed on the same type of glass bead packed models having the same length (55 cm) and the same fracture aperture (5 mm), but different fluid pairs (Table 3.6, Run numbers 11, 14, and 16). The experimental results of cumulative production were plotted versus time in Figure 3.7. As it is depicted in Figure 3.7, it is concluded that in models with similar physical and dimensional properties under free-fall gravity drainage, the less-viscous the liquid is, the higher would be the cumulative liquid drainage. It is also concluded that in experiments with lower viscosity liquids, the drainage rate was also higher than those with higher viscosity liquids during the early stages of the process. However, all the three models produced approximately the same ultimate amount of cumulative liquid, which means they all had a similar recovery factor. It is also evident that as the viscosity of the liquid increases, the amount of the characteristic drainage rate from the fracture and also the maximum production rate from the system decreases accordingly. However, the residual liquid saturation increases with increased liquid viscosity (Table 3.6).

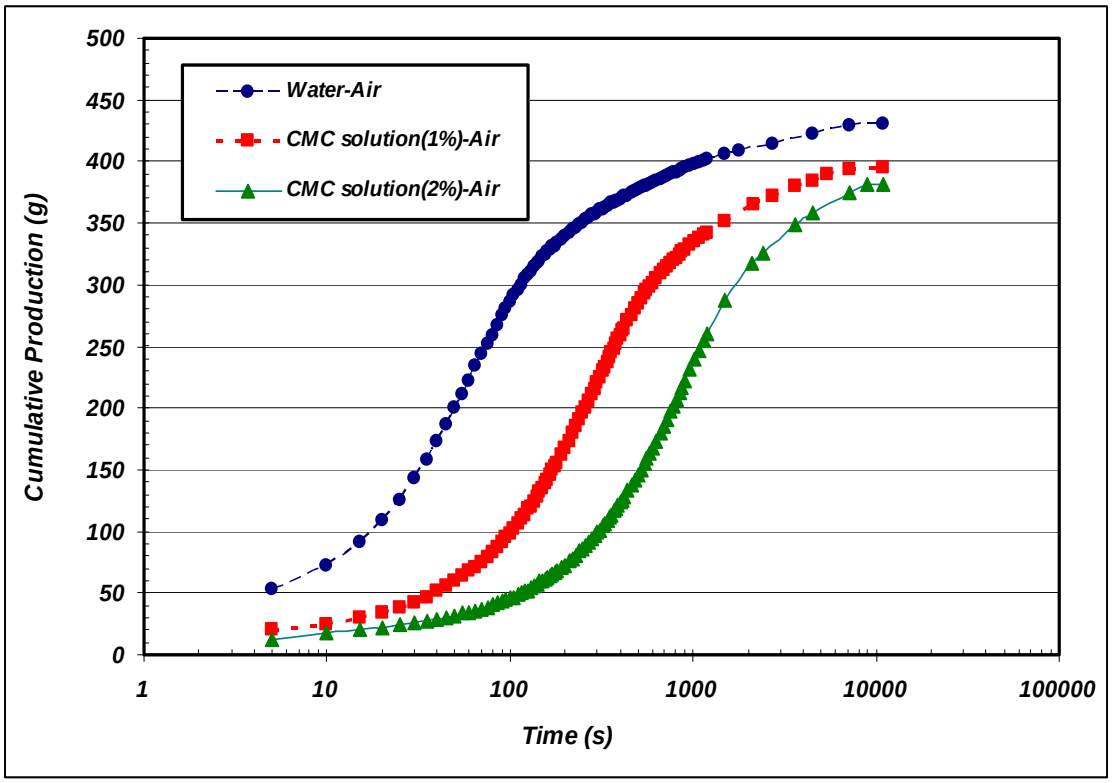

Figure 3.7: Cumulative amount of liquid recovered versus time for models with BT4 glass beads for variable liquid viscosity [Length of model = 55 cm, fracture aperture (b) = 5 mm].

Figures 3.8 and 3.9 show the effect of different liquid viscosities on the height difference of interface locations in matrix and fractures $\Delta H(t)$ and also the liquid communication rate between fractures and matrix respectively. As indicated in Figure 3.8, the measured $\Delta H(t)$ values were higher for Run #16 (water as the test liquid) compared to the other two cases before reaching the local maximum at which gas invasion into the matrix started. This point can be justified according to the lower viscosity values of de-ionized water compared to the CMC aqueous solutions with higher viscosities. When gas invasion into the matrix has commenced, the air-liquid interface in the matrix moves downwards faster in systems with lower liquid viscosity compared to those with higher viscosities. Therefore, the measured $\Delta H(t)$ values decrease more during this period for systems with lower viscosity liquids compared to higher ones. It is worthwhile to note that during this stage of the drainage process, the liquid level in fractures reached its threshold height and the velocity of interface drop in matrix depends mainly on the liquid viscosity. The higher the viscosity value is, the lower is the interface drop within the matrix, hence the higher would be the measured $\Delta H(t)$ value.

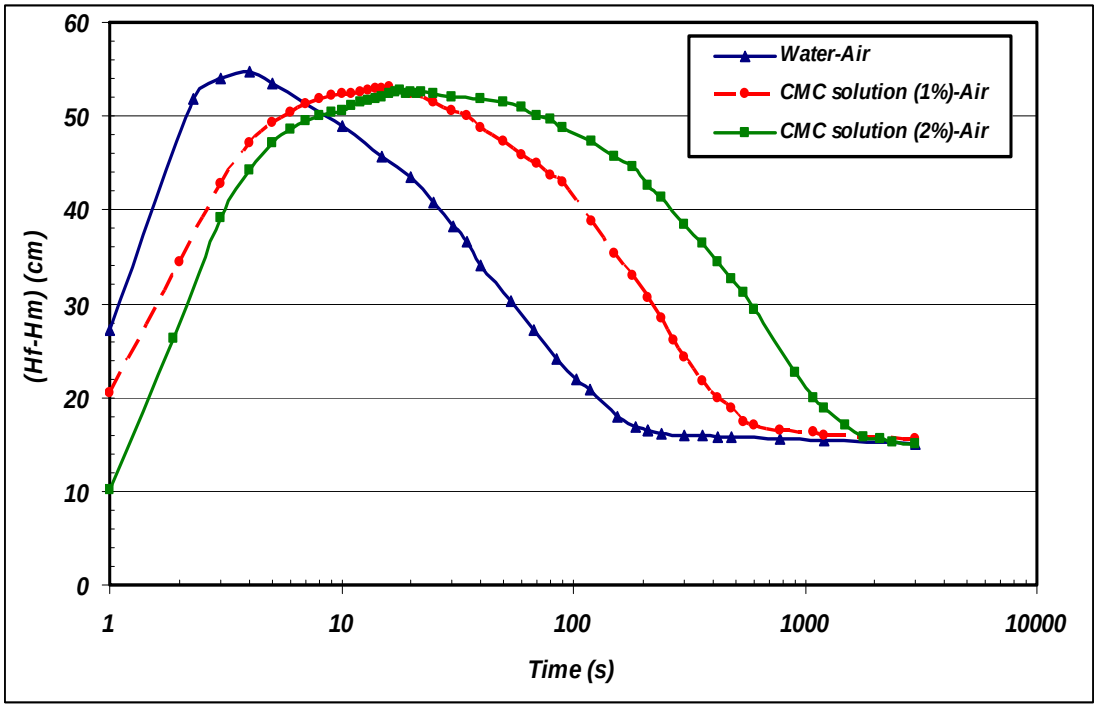

Figure 3.8: Comparison of difference between the gas-liquid contact locations in fracture and matrix using data obtained with the BT4 model for different viscosities.

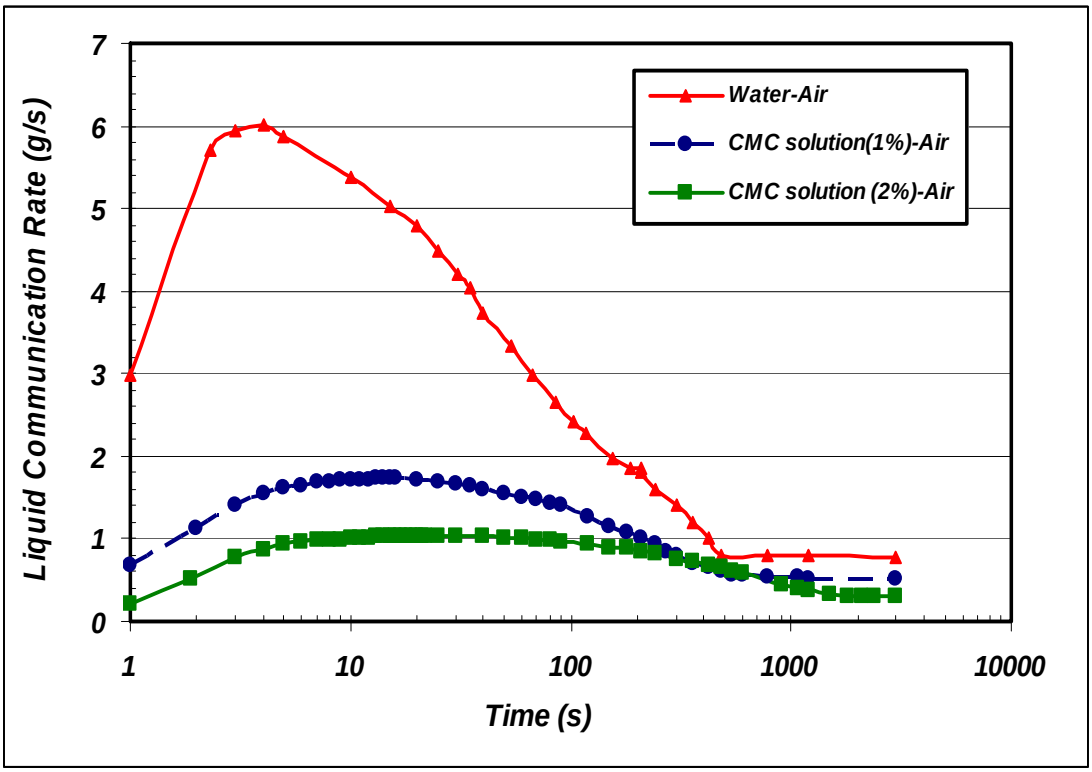

Figure 3.9: Effect of liquid viscosity on the rate of liquid communication between matrix and fracture in the models filled with BT4 glass beads [L = 55 cm, b = 5 mm].

Figure 3.9 shows the effect of liquid viscosity on liquid communication rate between fractures and matrix. According to the results shown in this figure, it is concluded that systems with lower liquid viscosities have higher liquid communication rate; as liquid viscosity decreases, the height difference between local positions of liquid interfaces within fractures and matrix decreases (Figure 3.8, after the local maximum point). The condition of low viscosity and also $\Delta H(t)$ values would result in lowering the driving forces available for liquid communication towards the fractures. Experimental results show that upon increasing the liquid viscosity to about 20 mPa.s, the amount of liquid communication between the matrix and the fractures in all of our experimental prototypes diminished to nearly zero.

3.5.3 Effect of interfacial tension: Gas–oil gravity drainage at low interfacial tension was found to be very effective in oil recovery from fractured media in both secondary and tertiary injection (Saidi, 1995).The capillary threshold height and also entrapment of hydrocarbon during enhanced oil recovery (EOR) methods depend on the balance between capillary and gravitational forces represented by the Bond number as oils with lower interfacial tension have shorter capillary threshold height and more overall recovery if other properties of porous media and test liquids were unchanged during the free fall gravity drainage. Normally, when the gas–oil interfacial tension decreases, which in turn causes reduction of capillary pressure between the phases; it would increase the oil recovery considerably if the porous medium has the same wettability for both test liquids. In order to investigate the effect of surface tension, first the fractured medium (e) was filled with water. In the model there were two vertical fractures and a horizontal fracture between them with a small gap created between side fractures and horizontal one. Under gravity drainage conditions, approximately 66 percent of the original liquid in place was produced during 90 seconds. The measured over time, the gas-liquid interfaces in fracture and matrix parts were also tracked. When the system was saturated with Varsol oil, the surface tension reduced from 72 mN/m to 25 mN/m. The oil production was about 66 % of original oil in place during 90 seconds. Since viscosities of these two test fluids were a little different (1.2 mPa.s for Varsol compared to 1 mPa.s for Water) and all other properties except interfacial tension had the same values for both cases, therefore the bulk flow rates of both systems were identical. The fractured porous medium saturated with water had a recovery factor almost as much as that for the medium saturated with Varsol oil during the initial period of free fall gravity drainage.

Variation of recovery factor with time is given in Figure 3.10. Although the capillary threshold height is shorter for the fractured porous medium filled with Varsol compared to the model saturated with water, the final recovery stays the same and equals to 77% after 5 hrs for the two fractured systems. The reason for the same recovery is that the film flow is more dominant in liquid recovery from waterwet glass beads, while in the second case, Varsol is not able to form a effective continuous film flow like water does, therefore we have more residual Varsol saturation in the drained part which is about 18% in comparison with 13% for the fractured medium filled with water. It should be noted that if the glass bead was oil wet, low value of interfacial tension for Varsol oil would increase the overall recovery performance significantly because film flow phenomenon plays important role in decreasing residual oil and finally it significantly affects the final oil recovery.

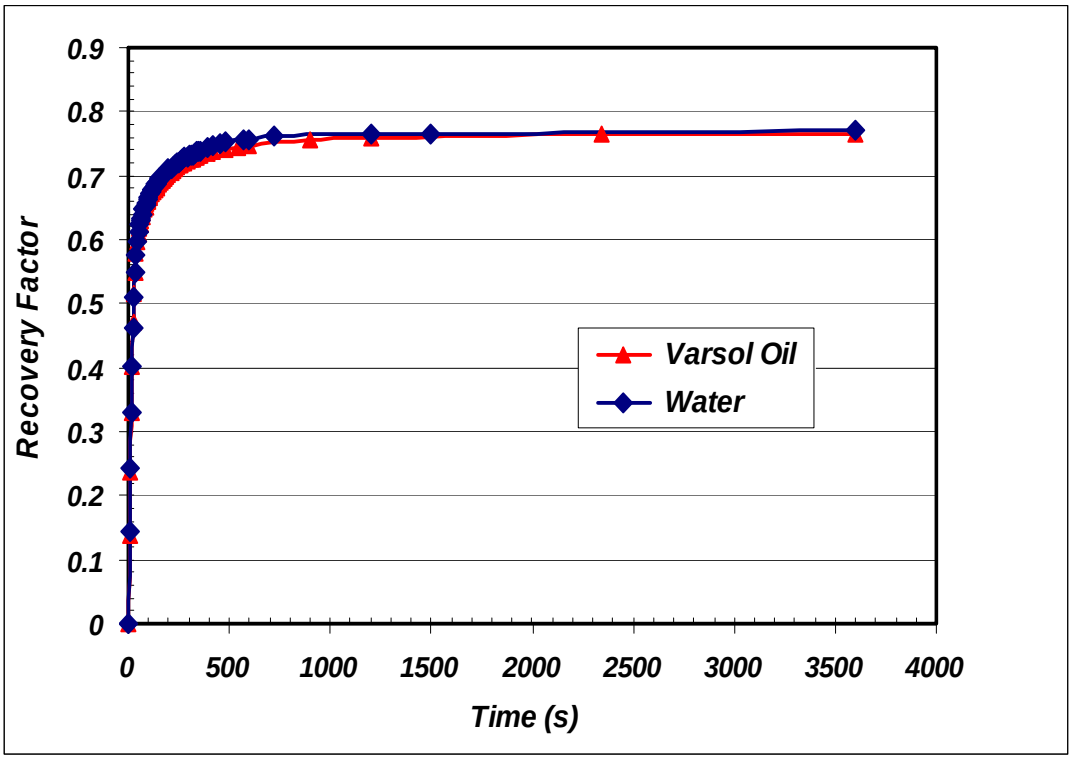

Figure 3.10: Recovery factor versus time for the porous media saturated with Varsol oil and water [BT2 glass beads fractured medium, model length = 55 cm, b = 5 mm, fracture configuration (e)].

Experimental results show that capillary pressure drainage height does not affect the recession rate of the liquid level in the fractures and both cases have the same rate for gas-liquid movement in the fractures. The equality of the recession rate for liquid level in matrix part of both fractured porous media is also established during initial time of the process, however, as time passes, capillary pressure has a stronger effect on movement of gas-liquid interface in matrix. Consequently, the recession rate of liquid level has higher magnitude for the physical model saturated with lower interfacial tension liquid (Figure 3.11). The same experiment was done on fractured porous medium of configuration (b). The model contained BT3 glass beads which were saturated with Varsol oil and water and the experimental result (see Figure 3.12) confirm the theoretical concept explained for the previous scenario as both curves follow almost the same trend and value for oil recovery.

As mentioned above, the maximum flow rate which occurs during the initial stage of the free fall gravity drainage depends on dimensions of porous medium, petrophysical properties of fracture and matrix parts, and viscosity of liquid. Therefore, the maximum flow rate for both cases explained here is approximately the same.

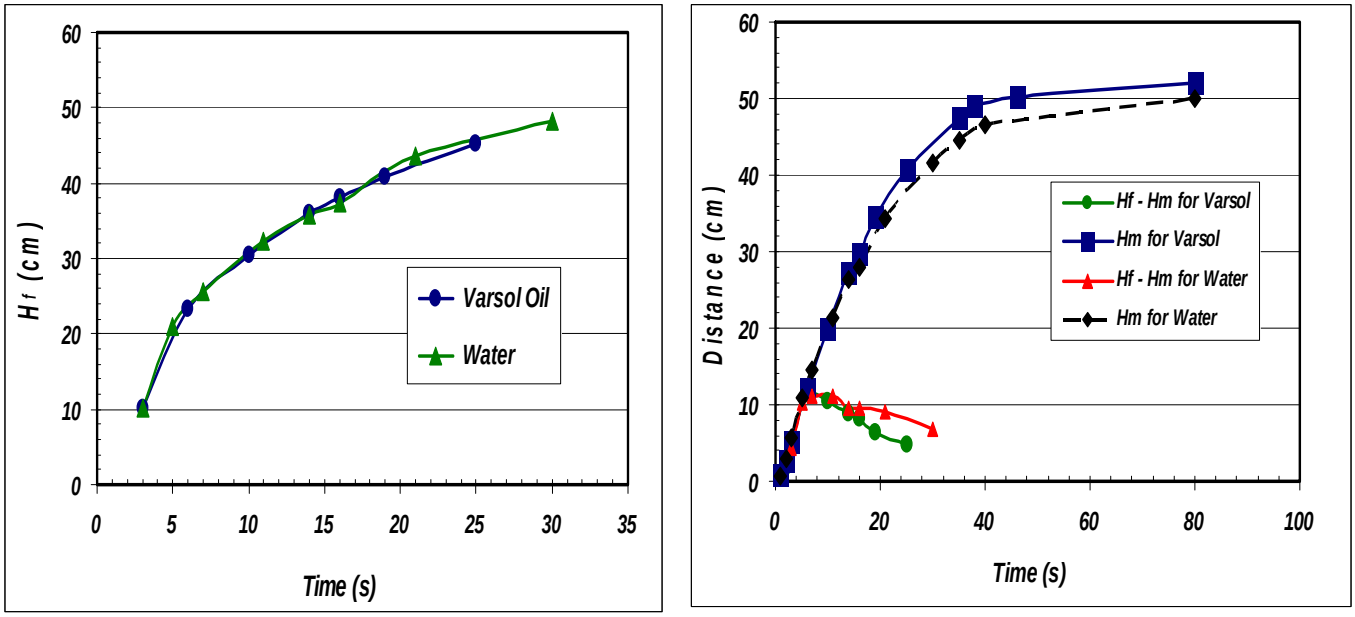

(a) (b)

Figure 3.11: a) Gas–liquid interface position in fracture versus time, b) Difference between the gas-liquid contact locations in fracture and matrix (H_f-H_m), and gas-liquid interface in matrix (H_m) using experimental data obtained from the media made with BT2 glass beads but different test fluids named Varsol and water [model length = 55 cm, b = 5 mm, fractures configuration (e)].

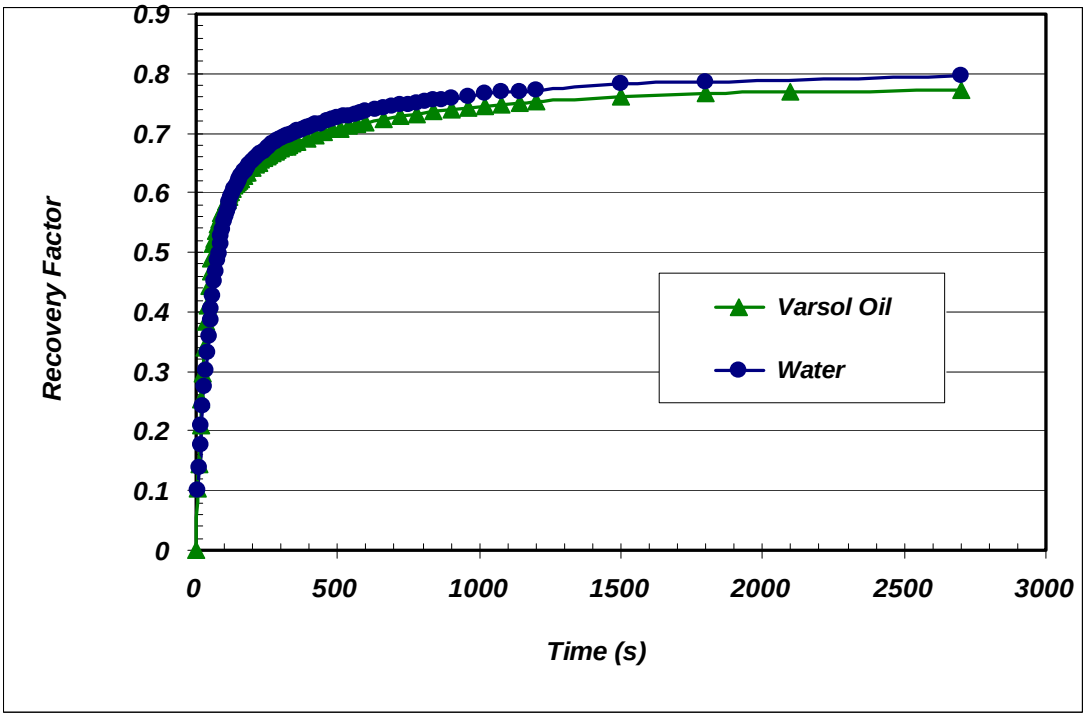

Figure 3.12: Comparison of recovery performance for two models filled with water and Varsol at various times [media made of BT3 Glass Beads, b = 3 mm, fracture configuration (b), L = 55 cm].

3.5.4 Effect of fracture aperture: Comparing the experimental results for runs number 2, 5, and 17 (Table 3.6) gives an idea about the effect of fracture aperture on the gravity drainage process performance. In these runs, BT2 type of glass beads was used as the main matrix with the total height of 55cm, 2 wt% aqueous solution of CMC was used as the test liquid, and three different sizes of fracture apertures (2, 3, and 5 mm) were tried. Figures 3.13 and 3.14 show the effect of fracture aperture on the cumulative liquid drainage and also liquid production rate respectively. It is clear that increasing the magnitude of fracture aperture results in higher liquid production rates just during the initial period of the process, but it does not have any significant effect on the liquid ultimate recovery. Figure 3.16 shows that at the initial times of the process during which the communication rate keeps on increasing, the amount of liquid drainage rate from the fracture decreases. The plots reveal that at the start of communication between the fracture and matrix, we have the highest production rate; however, the production rate is decreasing with time as the reservoir is depleting, and the behavior of fractured model approaches that of homogeneous medium, when the fracture is totally drained.

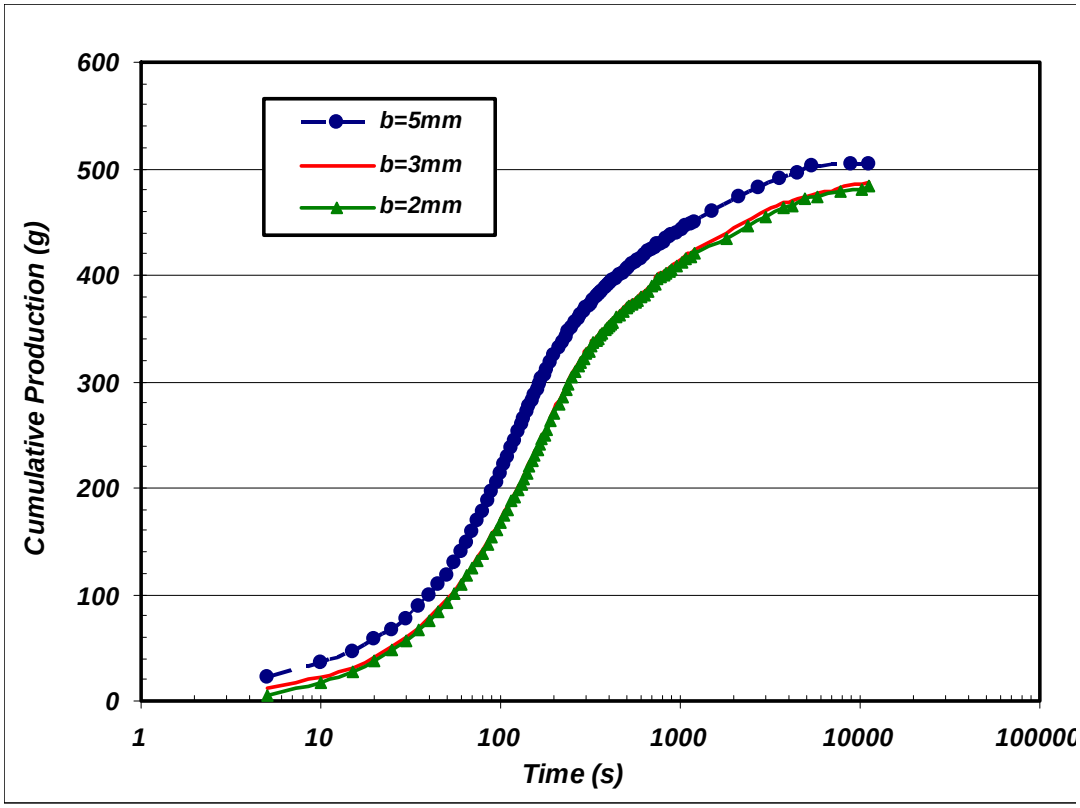

Figure 3.13: Cumulative production versus time for runs # 2, 5 and 17.

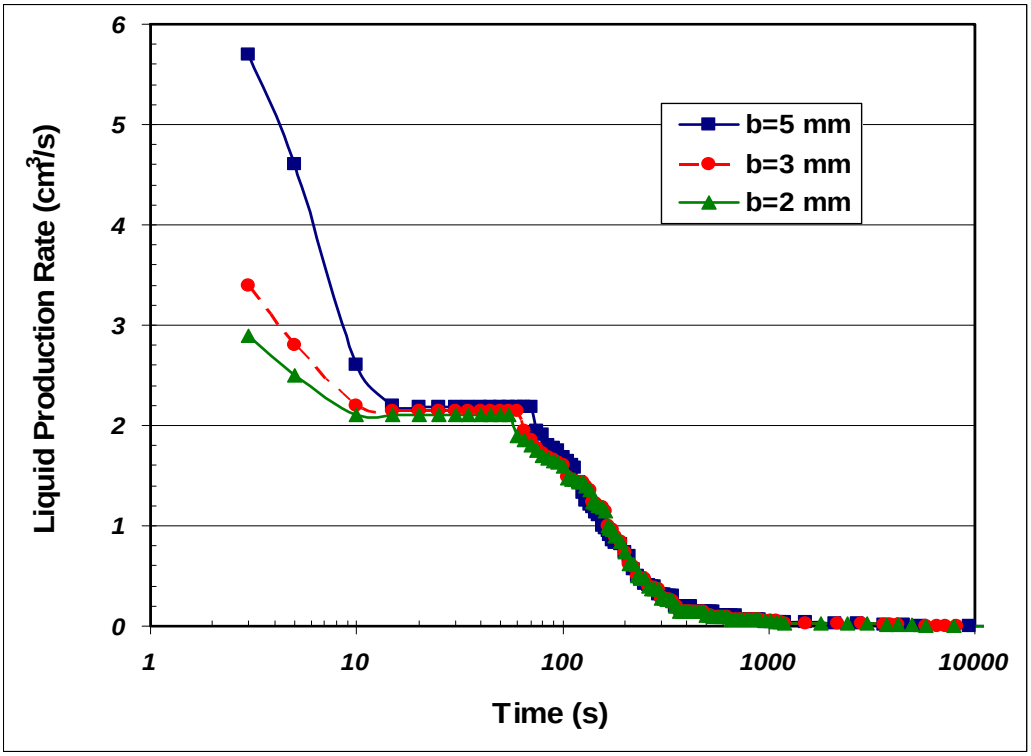

Figure 3.14: Liquid production rate versus time for runs # 2, 5 and 17 with BT2 glass beads.

Figure 3.15 shows the effect of the fracture aperture size on the difference between the gas-liquid contact locations in fracture and matrix. The employed models have the same physical and dimensional properties at stated above regarding Figures 3.13 and 3.14. In addition, Figure 3.16 depicts the liquid communication rate versus time for different fracture aperture sizes. According to the results mentioned in these two figures, it is concluded that as the fracture aperture size increases, the values of height difference between interface locations in matrix and fractures and also liquid transfer rate increases accordingly. It is also clear that as the aperture size increases, the value of characteristic rate from the fracture also increases. Maximum production rate is also higher in the case of models with higher fracture aperture; however, the amount of residual liquid saturation is almost the same for all of these runs as this is mainly a function of the matrix permeability and threshold capillary height, which are the same among these three runs (Tables 3.6 and 3.10).

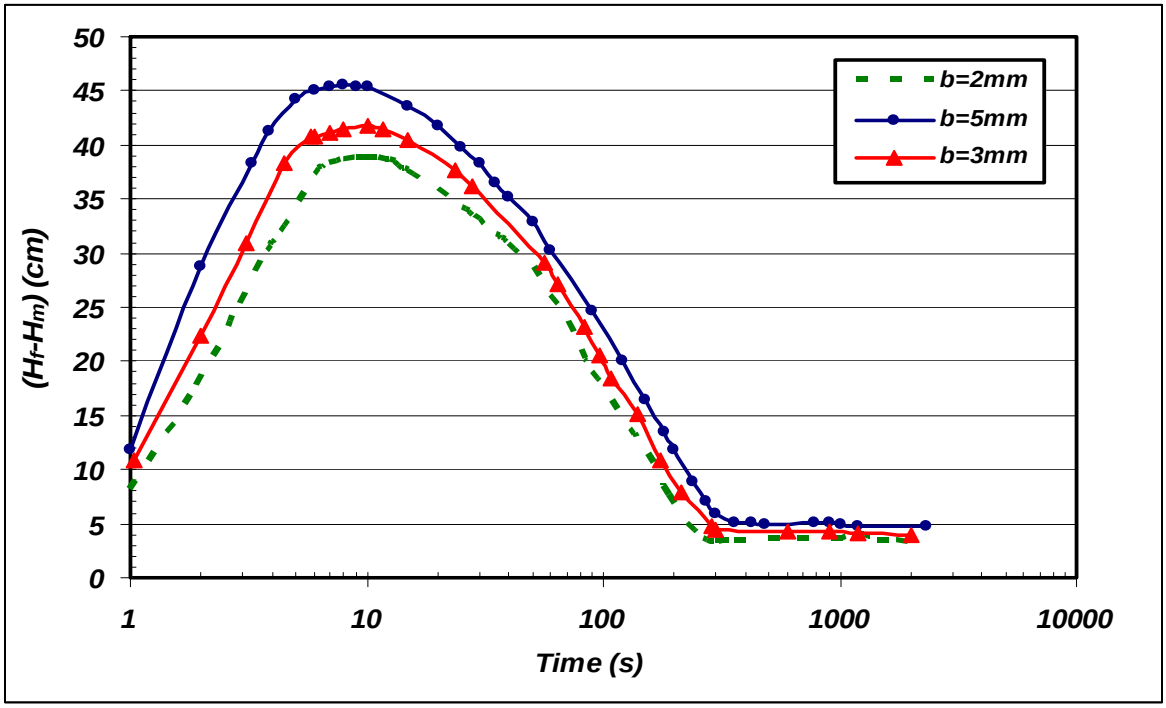

Figure 3.15: Effect of magnitude of the fracture aperture on difference between the gas-liquid contact locations in fracture and matrix in the models filled with BT2 glass beads and CMC solution (2%).

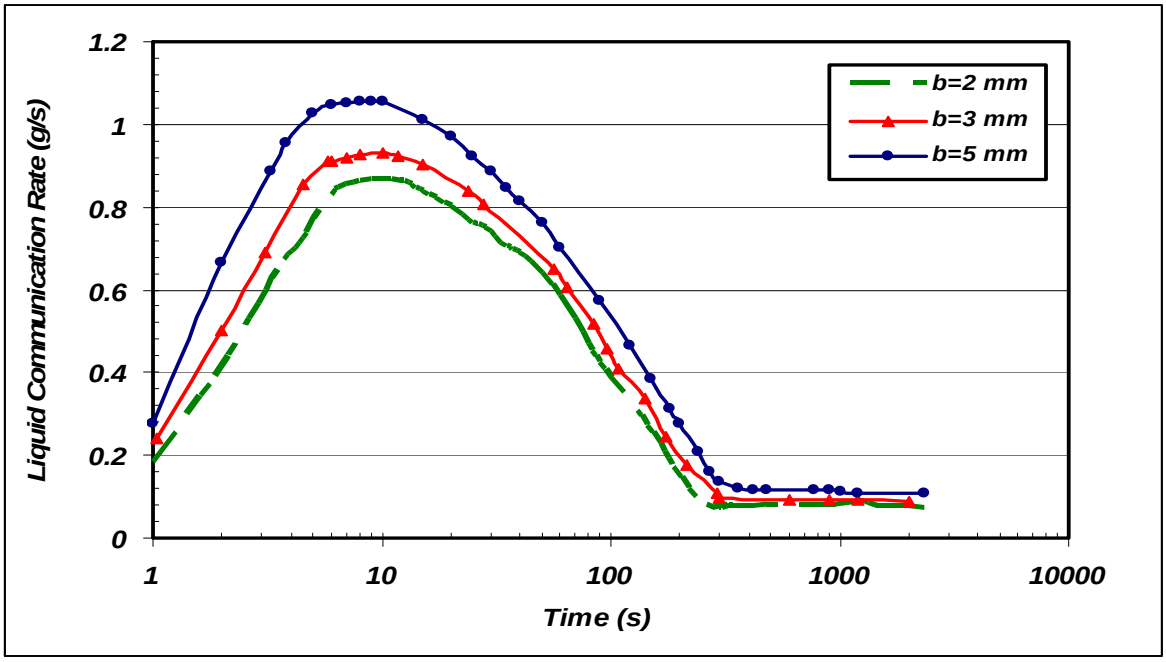

Figure 3.16: Liquid communication rate versus time for different fracture apertures in BT2 glass beads cases.

3.5.5 Effect of model length: Table 3.6 contains results of three experimental runs (Run # 8, 9, and 10) that deal with the effect of model length on the gravity drainage process performance. In these runs, BT3 type of glass beads was used as the packing material for the matrix which was attached to two 5 mm-aperture vertical fractures on both sides, and 2 wt% aqueous CMC solution was used as the test liquid. Figures 3.17, 3.18, and 3.19 show the effect of length of model (28, 40, and 55cm) on the cumulative liquid recovery, elevation difference between interface positions in matrix and fractures, and liquid transfer rate. According to Figure 3.17, models with larger length have higher cumulative liquid drainage. This is because models with larger length have higher ratio of the model length to the drainage capillary height. However, the amount of characteristic drainage rate is almost the same for these models, as this is mainly a function of the fracture and matrix permeability. The maximum production rate is also higher in the models with larger length; however the residual liquid saturation is almost the same for all of these cases as it is mainly a function of the threshold capillary height of the matrix (Table 3.6).

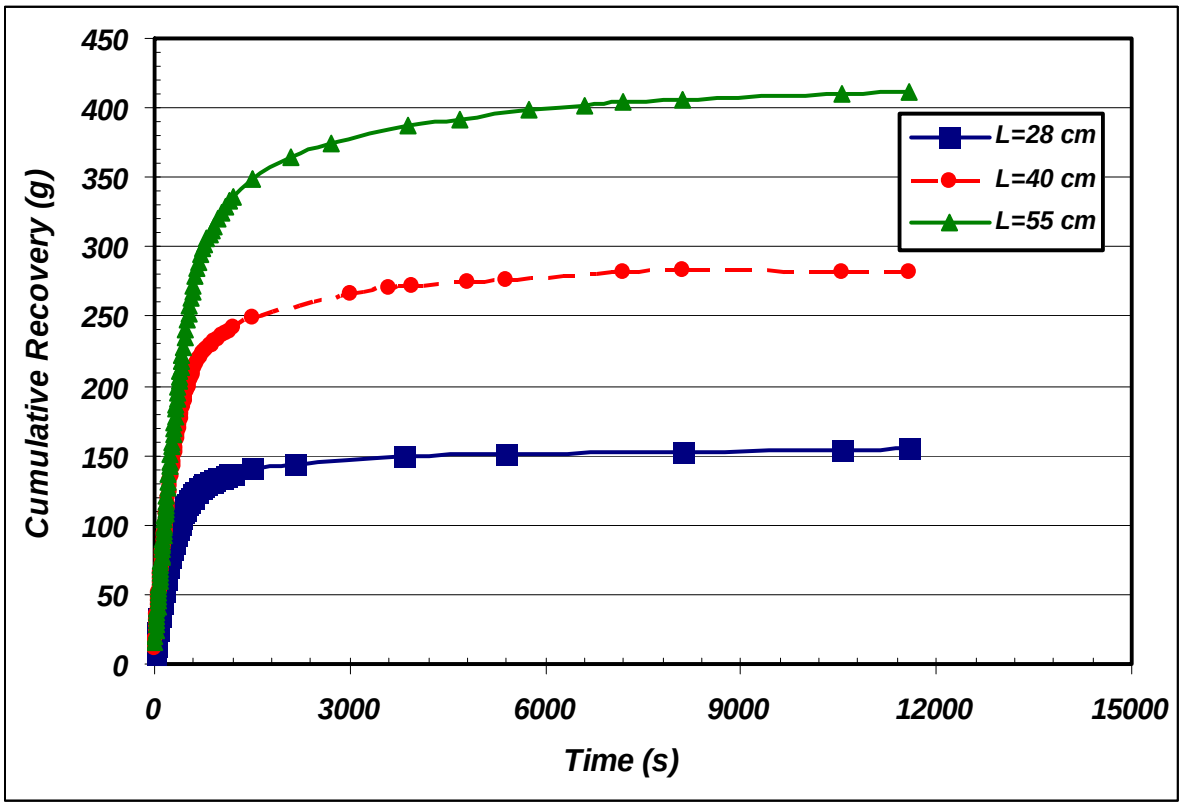

Figure 3.17 : Effect of model length on production curve during free-fall gravity drainage in BT3 glass beads models filled with CMC solution (2%), and b = 5 mm.

Figures 3.18 and 3.19 show the effect of model length on the hydrostatic pressure difference between fracture and matrix and also on liquid communication rate. It is evident that the longer the model is, the higher would be the $(H_f - H_m)$ value. It is also concluded that models with the larger length have higher rate of liquid transfer between matrix and fractures at any particular time.

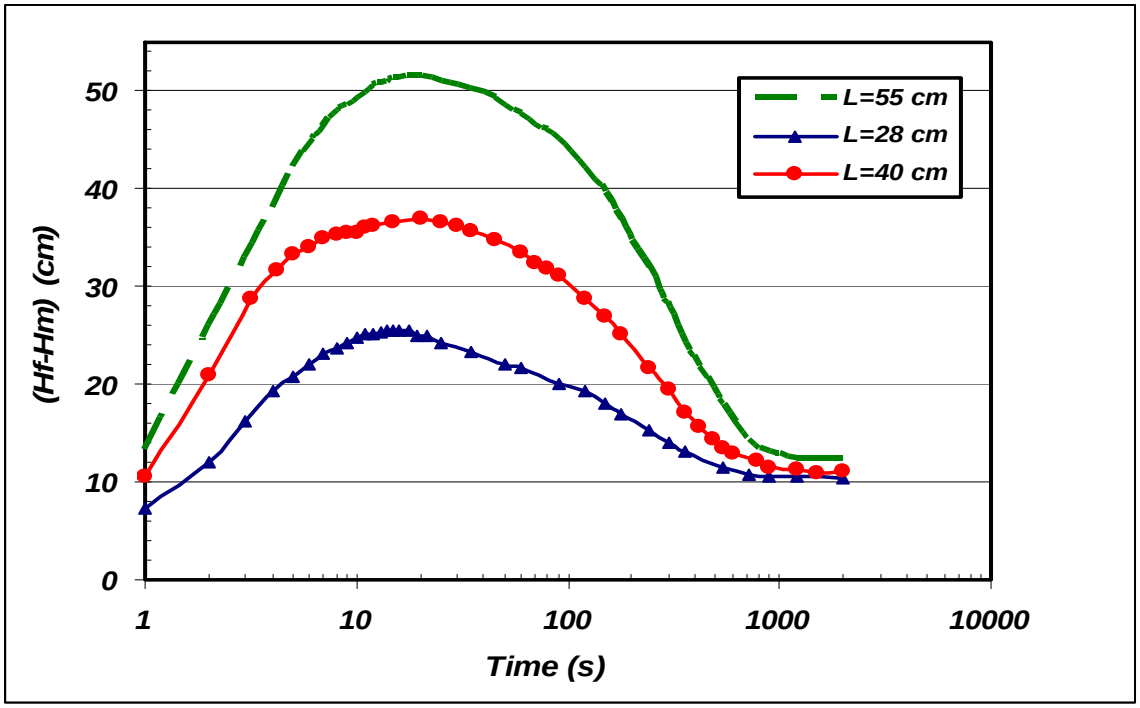

Figure 3.18: Gas-liquid interface height difference between matrix and fracture versus time for the BT3 models having different length.

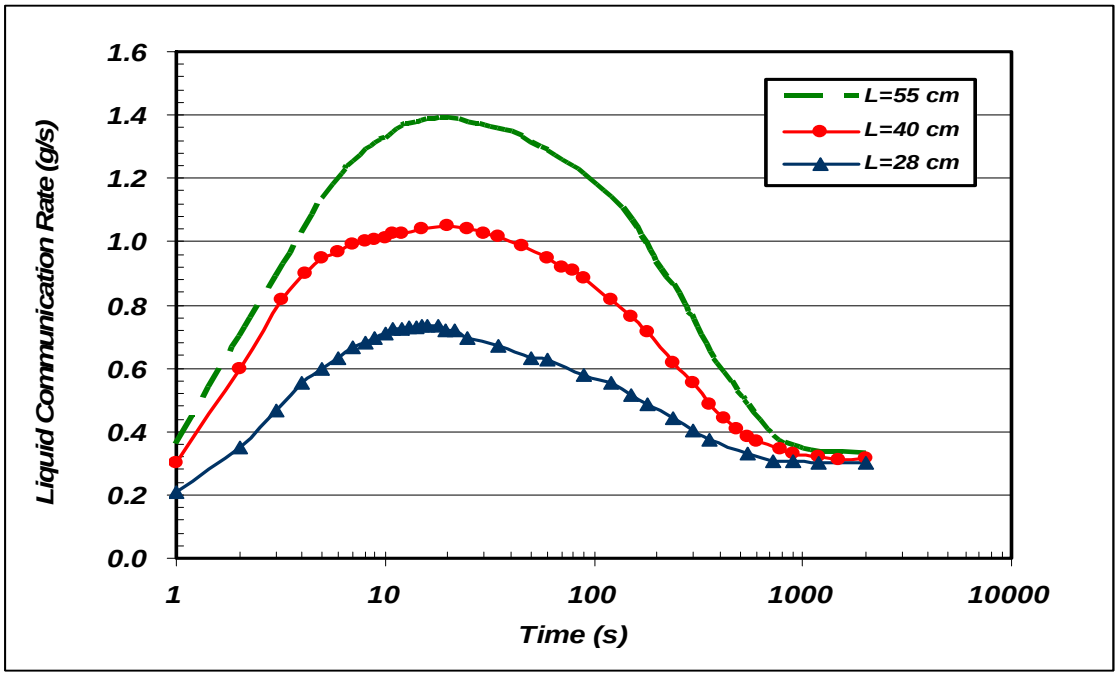

Figure 3.19: Influence of model length on liquid rate flowing from matrix to fracture for runs # 8, 9 and 10.

3.5.6 Effect of fracture length and fluid properties in a model with single fracture: In this configuration, a fracture was placed in the middle of the rectangular box all the way down along the model height as two matrix parts with the same properties were located on either side (see figure 3.1a). In order to investigate the effect of fracture length on important parameters contributing in free fall gravity drainage process, a set of experiments with free fall gravity drainage was carried out using unconsolidated glass beads for the matrix, and a vertical fracture of 55cm length inserted in the middle of it. For other fracture lengths, the fracture was placed as desired and the bottom tip of fracture was away from the production well. Model (a) with BT3 type of glass beads was saturated with de-ionized water prior to the free-fall gravity drainage test. Experimental results indicate that gas invades the fracture space first and after the driving force for further gas invasion in the fracture and matrix respectively become the same, the gas can invade the matrix as well. At that point we define the initial flow rate for fluid flow in fracture from production data and performed image analysis of interface advancement. Visualization study of the process has shown that initially the gas-liquid interface in the matrix was not stable and tended to dip lower at locations close to the fracture. However, as the drainage process of drainage is progressed the gas-liquid interface became flat, indicative of stable displacements. The free fall gravity drainage is initially fast. 50% of the water was drained from the system within the first 2 minutes of the experiment (see Figure 3.20). The same experiment was repeated in models BT3 glass beads using the water-air fluid pair with a smaller fracture length (L_f = 30 cm). The same phenomenon was observed regarding the downward interface movement, however, less recovery was attained (46% in the first 2 minutes), though the final recovery for the case of L_f =30 cm was about the same as that on the model with longer fracture. It is apparent from Figure 3.20 that the longer the fracture, the higher is the recovery rate in free-fall gravity drainage.

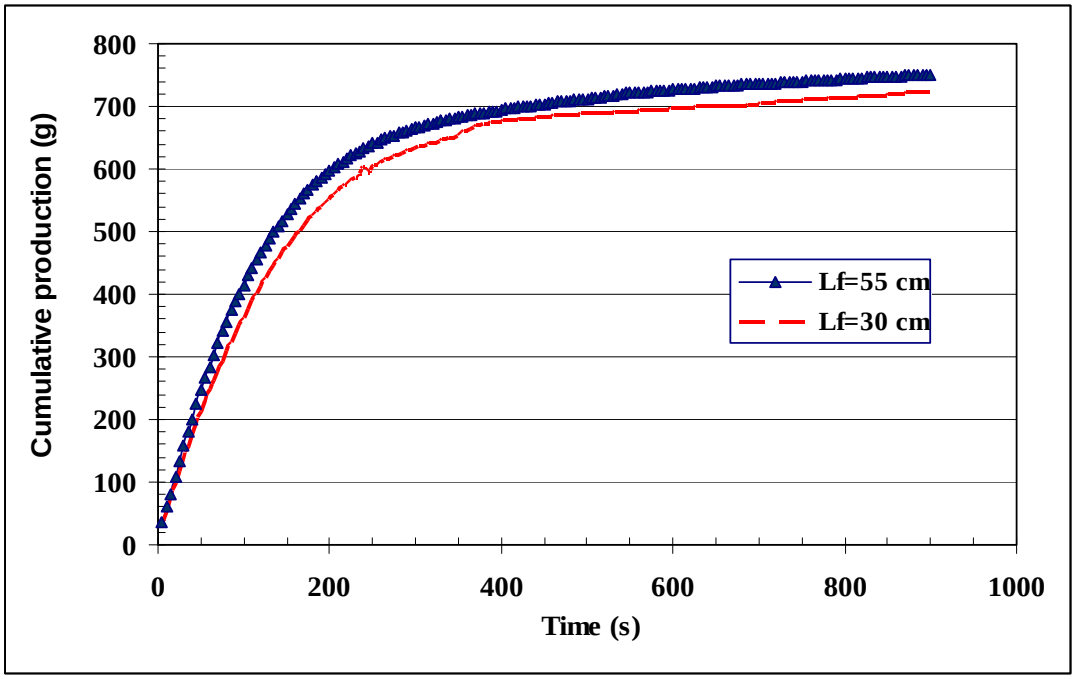

Figure 3.20: Cumulative production of water recovered versus time for models with BT3 glass beads with variable fracture length.

To investigate the effect of liquid viscosity and surface tension, Varsol oil was used as a test fluid, having a little higher viscosity than water and a much lower surface tension. Free-fall gravity drainage tests were performed on the same type of glass bead model for three different fracture lengths, namely 55, 30 and 15 cm respectively (Figure 3.21). Based on the results shown in Figures 3.20 and 3.21, it can be concluded that if we have two systems with the same physical and dimensional properties under free gravity drainage, the system filled with the water produced at higher rate at the start of production compared to models containing the more viscous oil. The lower surface tension value of Varsol oil compared to that of water results in slightly higher final oil recovery factor. For the same fracture length of 30 cm, it was found that the oil recovery after 8 hours were 79% and 80% for BT3 glass bead models with water and Varsol oil respectively. The ultimate recovery for the cases with Varsol oil was a bit higher compared to water due to capillary pressure end effects. Based on the results given in Table 3.6, it is seen that the initial oil rate decreases as fracture length decreases. The residual oil saturation attained in the total length of model is lower when Varsol oil was used compared to water. This reduction can be explained by the capillary end-effects due to water's higher surface tension compared to Varsol oil. Packed columns with water produce higher wetting phase saturation value for a given location above the production-end compared to another liquid of much lower surface tension, as this is well known (Dullien, 1992).

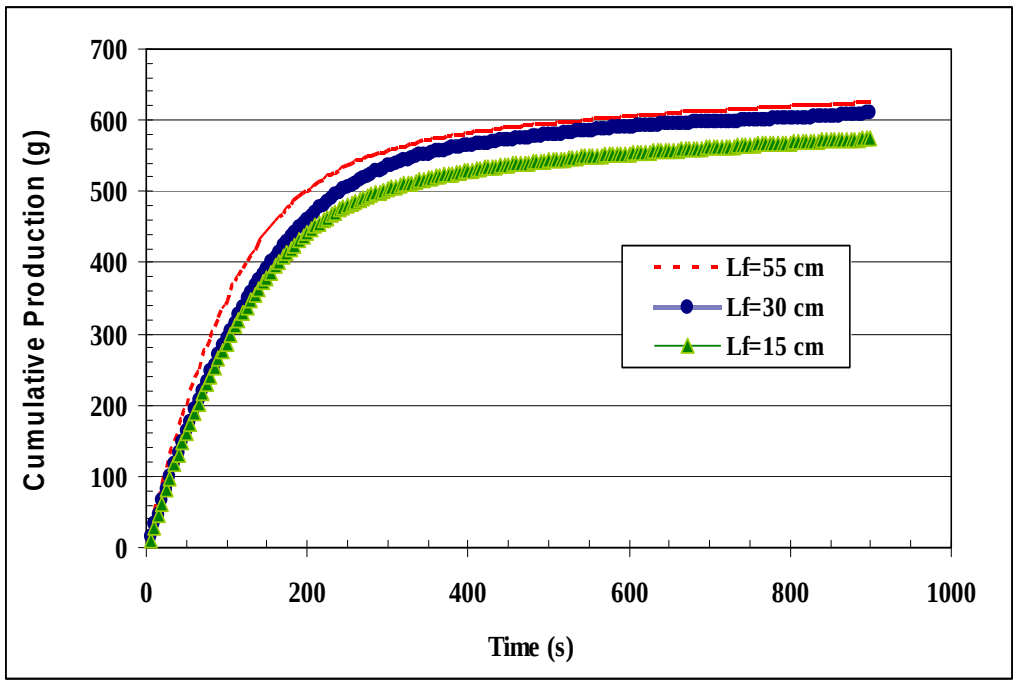

Figure 3.21: Cumulative production of oil recovered versus time for models with BT3 glass beads with variable fracture length.

3.5.7 Effect of fractures configuration: We conducted laboratory experiments to investigate the effect of fractures pattern on the oil flow rate during free fall gravity drainage. Water wet glass beads were used as matrix part and three different fractures patterns were placed in the rectangular porous medium to simulate fractures network in fractured porous media. The experiments were performed in the 55 cm long rectangular models saturated with 2% CMC solution, which were filled with BT3 glass beads. In the first case, there was no horizontal

fracture. The maximum flow rate was adjusted at 1.3 cm^3/s. When a horizontal fracture was placed between two vertical fractures, but not crossing them, this caused an increase of around 9-10% in initial flow rate. It means that the horizontal fracture increases the overall permeability in the models and also plays an important role in transferring liquid to vertical fractures. When a fractured porous medium with fractures configuration (f) was employed, during the gravity drainage process, it was observed that this configuration produced oil with higher rate during initial periods compared with the first fractured model which did not have horizontal fracture as the magnitude of its initial volumetric rate was 1.5 cm^3/s (15% more than the flow rate for the model with just two vertical fractures on both sides). Also it is evident that the homogeneous porous media have the lowest production rate during initial period of the experiment which was 0.7 cm^3/s.

Table 3.7 shows the maximum flow rate for the porous media with various fracture patterns under free fall gravity drainage. The properties of models are the same as written in the first paragraph of this section; just the employed liquid was changed from CMC solution (2%) to Varsol oil. The magnitude of production rate reveals the role of liquid communication between matrix and fractures and also liquid transferring from a fracture to another fracture as it causes that the liquid flow rate in the media with fracture network increases. The table below supports this discussion regarding the effect of fracture network configuration on the maximum production rate or recovery rate for initial times during production.

Table 3.7: Maximum flow for variable fracture configuration of porous medium saturated with Varsol

Case No.	Fracture pattern	Maximum flow rate, cm^3/s
1	Model (h): Homogeneous	4.4 ± 0.4
2	Model(g): Has two vertical fractures	4.8 ± 0.3
3	Model(e): Has two vertical fractures and one horizontal fracture between them, but not touching the vertical ones	5.1 ± 0.5
4	Model(f): Is the same as model(e), except the horizontal fracture is connected to vertical fractures from both sides	5.3 ± 0.4

Regarding recovery factor, if a horizontal fracture placed in the middle of the porous medium, it can build an effective capillary continuity according to the fracture aperture size; all four experimental models have almost the same ultimate production performance, otherwise the upper matrix part and lower matrix part act as separate porous media. Due to discontinuity of flow, there is some oil left above the horizontal fracture which equals 1.5% of oil in place. Therefore this type of fractures decreases the ultimate recovery. The highest recovery is achievable in the model with two parallel fractures on both sides and then for the homogeneous medium.

It can be understood from Figure 3.22 that the model with fracture configuration (f) produces liquid with greater recovery rate compared to other models. This is due to the presence of vertical fractures and connection between horizontal fracture and vertical fractures, while the porous medium pattern (h) has lower production rate among other experimental models at the start of free fall gravity drainage process.

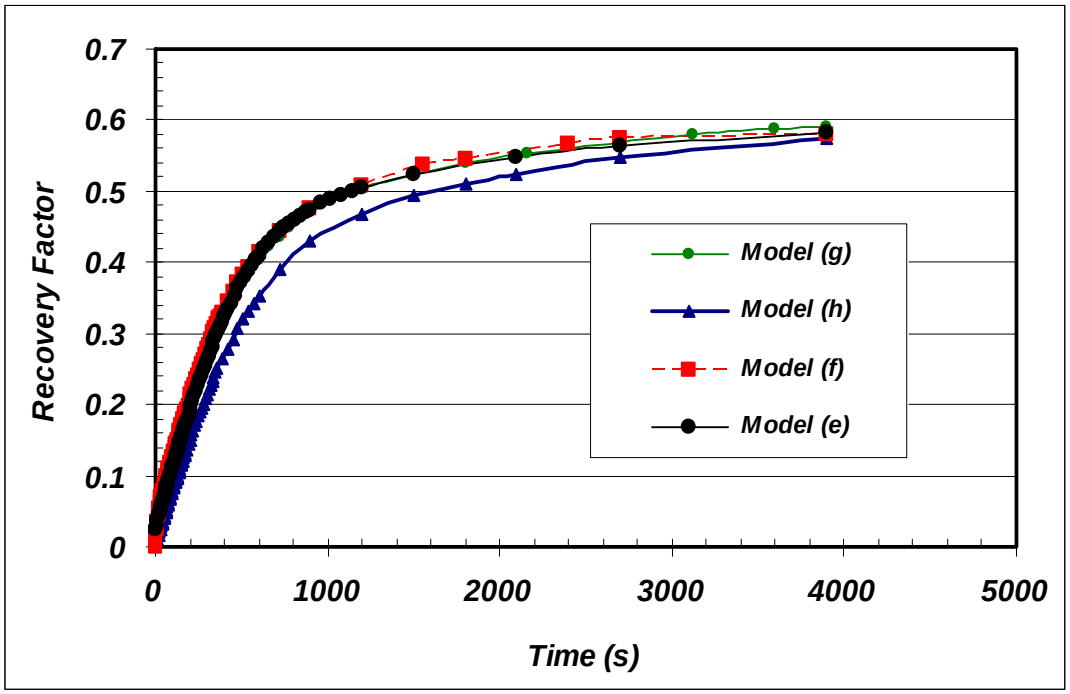

Figure 3.22: Comparison of recovery factor for various fractured model to figure out effect of fracture network (BT3 Glass beads, b= 5 mm, fluid pair: CMC (2%)-Air, L = 55 cm).

The gas-liquid interface movement in fracture and matrix parts is also presented for the fractured porous media. Figure 3.23 shows the difference between the gas liquid positions in matrix and fracture against time for the physical models with fractures patterns e, f, and g. The plot shows fractured medium (f) has the lowest difference (H_f-H_m) due to having higher effective permeability, because gas-liquid interface in the matrix advances with the higher rate, and also more communication exists between vertical fractures and other parts of the model. Therefore, there is lower rate of gas-liquid interface movement downward in the vertical fracture.

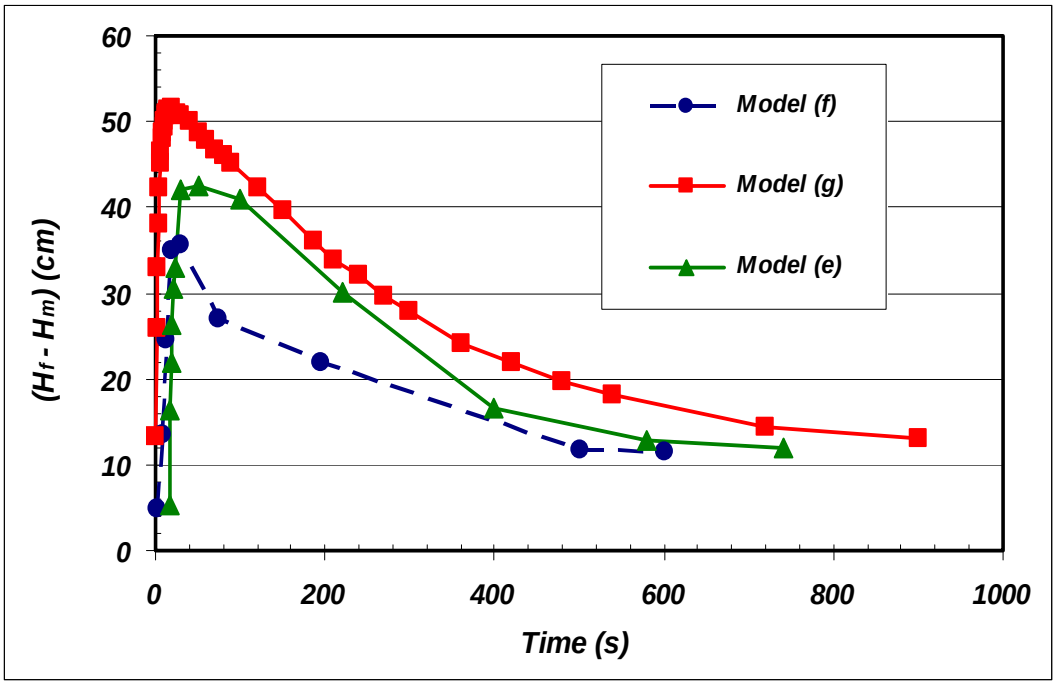

Figure 3.23: Effect of fractures configuration on difference between the gas-liquid contact locations in fracture and matrix in the models filled with BT3 glass beads and CMC solution (2%).

3.5.8 Effect of horizontal fracture and capillary continuity: The interaction of fluid flow between matrix blocks and the role of fracture in gravity drainage have imposed a real challenge to researchers during the last thirty years. The main issue in understanding the flow behavior in fractured porous media is the block-to-block interaction. In this experimental research, some phenomena about the block-to-block interaction, i.e. capillary continuity are detailed.

When a fractured medium contains horizontal fractures, capillary continuity may exist in a weak or strong form. The capillary continuity phenomenon is an important contributor to oil recovery in fractured reservoirs. Capillary continuity, as a recovery mechanism, may provide fluid communication between partially or completely isolated matrix blocks, thus increasing the recovery rate by gravity drainage or viscous displacement. Capillary continuity increases the height of the continuous fluid column in a reservoir and thereby the recovery of oil, since the gravity drainage efficiency is dictated by the height of the fluid column. Capillary pressure continuity in vertically stacked matrix blocks has been studied extensively, e.g. by Horie et al. (1990), Labastie (1990) and Stones et al. (1992). They investigated the properties of materials present in the fracture, the effect of the overburden pressure and the permeability, and how this affected capillary continuity. An important aspect is the critical fracture aperture, defined as the aperture below which liquid drops may form stable liquid bridges across the fracture. A formula for critical aperture was suggested by Sajadian and Danesh (1998), but it is not clear if this was consistent with the experimental results presented (Ringen et al., 2005).

Consider a stack of two matrix blocks separated by a horizontal fracture under free fall gravity. Assume that a hanging drop touches the bottom surface of the upper block almost at one point like the case shown in Figure 3.24.

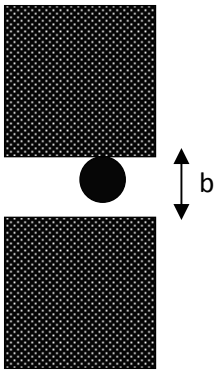

Figure 3.24: Schematic of formed droplet between blocks.

In this situation, there are two cases for drainage:

1) In some points between two blocks, oil drainage is by formation and detachment of droplets, resulting in a discontinuous flow. This means that the diameters of formed droplets are smaller than the fracture aperture at those points. The following equation shows the capillary pressure associated with a drop of radius r.

$$P_{cf} = \frac{2\sigma}{r} = \Delta\rho.g.b \qquad (3.8)$$

where r is the radius of droplet , b is the fracture aperture at a certain point, σ is the interfacial tension and Δρ is the density difference. However, it should be noted that the radius of drops is dictated by the surface tension of liquid/gas fluid pair, as well as density difference between them.

2) In other contact points of the matrix blocks/fracture space, we have a continuous flow between blocks. The drained oil is transferred through a liquid bridge/or multiple bridges from block to block. This means the diameters of droplets are equal or bigger than the fracture aperture.

A laboratory flow apparatus was built to obtain data on water-air and oil-air drainage displacements in models with a horizontal fractured. For this purpose, three configurations have been used: a porous medium which a fracture with aperture of 5 mm is located in the middle (model (c)), a porous medium with a 1 mm fracture aperture located in the middle, and a porous system with no fracture (model (h)). In this study, a medium containing fracture pattern (e) was used to investigate the effect of fracture aperture and surface tension on capillary continuity.

Experimental results showed that for the BT4 glass beads as matrix and a fracture of 5 mm were saturated with CMC 2%, the presence of fracture causes a flow discontinuity in vertical direction. Some portion of matrix above the horizontal fractures is not invaded by air, therefore air bypassed the liquid in that area above the fracture and flow around the fracture to push the liquid toward production well (see Figure 3.25). Consequently there is some liquid left in the matrix part above the fracture and this phenomenon decreases the final liquid recovery and increases the residual liquid saturation. If we change the fracture aperture from 5 mm to 1 mm, the effective flow continuity exists between upper matrix and lower matrix and liquid drops build some bridges to keep capillary continuity. The recovery factor and residual liquid saturation for

latter case have equal values with those for a homogeneous porous medium with the same dimensions and petrophysical properties. In order to consider the effect of interfacial tension, the test fluid was changed to Varsol oil. It was observed that a reasonable capillary continuity was established during gravity drainage even for fracture aperture equal to 5 mm and no significant amount of oil remained above the fracture because smaller the interfacial tension (IFT) is, the smaller will be the capillary pressure which needs to be overcome by the weight of the droplet. The main results are presented in Table 3.8 to show the effect of fracture aperture size on capillary continuity.

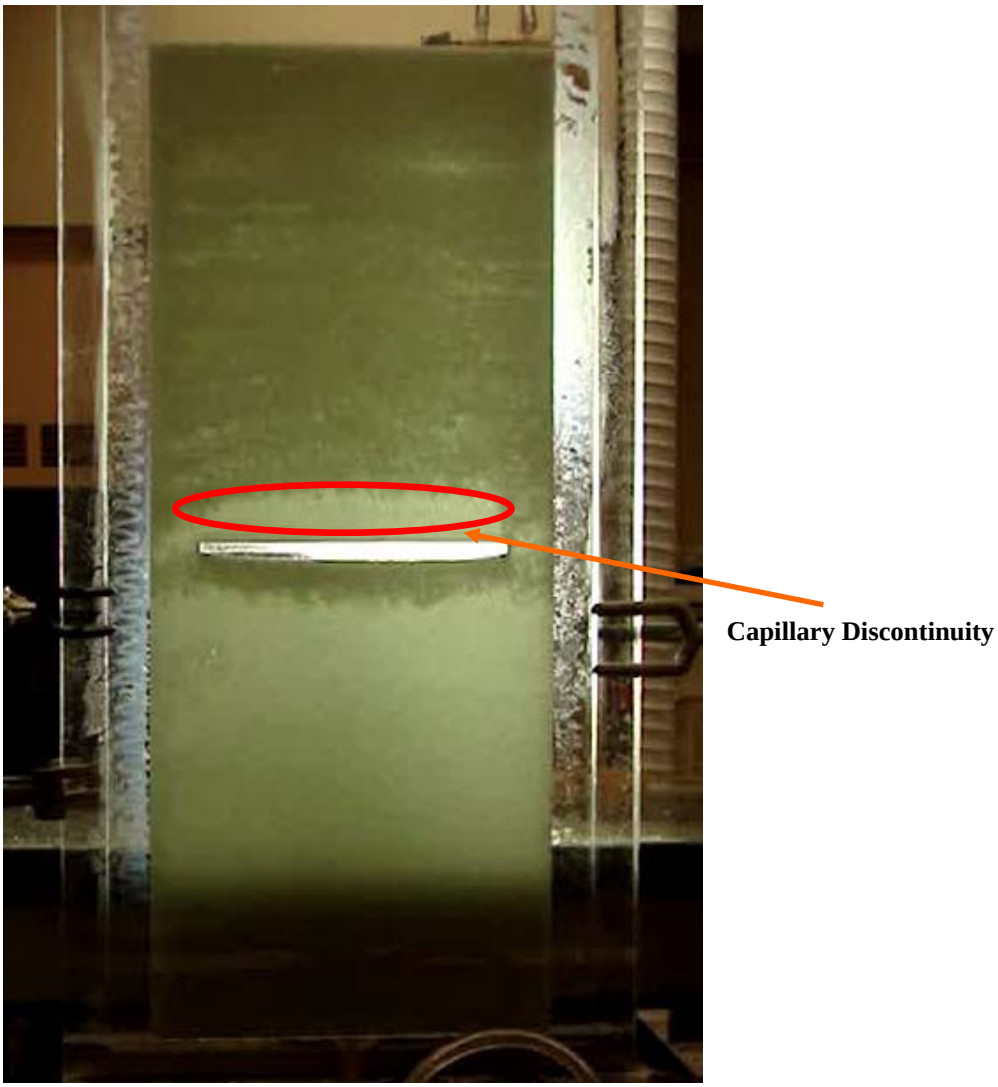

Figure 3.25: A view of liquid displacement in a fractured medium in whose the horizontal fracture exhibits a capillary discontinuity [BT4 Glass beads; b= 5 mm , fluid pair: CMC solution (2%)-Air].

In the case of water-air drainage, the thin fracture system showed a more stable front than the wide fracture system. However, the final water saturation was higher in the areas near the wide fracture, thus showing that capillary pressure in the narrow fracture has more effect. Also during oil-air drainage, the final oil saturations were higher in the blocks near the wide fracture, again showing the weak effect of fracture capillary pressure when having wide fractures. When the

fracture aperture is thick, the oil will drain mainly by film flow process. The film flow process over the fracture walls cannot provide adequate liquid transmissibility for flow across the fracture between the matrix blocks. The oil transmissibility by film flow is so small that production of oil from the bypassed region of the upper block will take an extremely long time. Since the drainage flow rate by film flow is very small, this kind of capillary continuity is recommended to be considered as non-effective or discontinuity. For the case of non-capillary contact between blocks (thick fracture) the total amount of recovery will be equal to the number of blocks times the recovery of one of blocks if all blocks' properties are exactly the same. But for the full capillary continuity between the blocks, the performance of a stack block is like that of a single block with the same height.

This work showed that the thin fracture systems had a more stable front and delayed the gas breakthrough compared to wide fracture systems, and that capillary pressure plays an important role when the fracture is narrow. We observed that neither the capillary pressure nor the relative permeability curves in the fracture affected the results for the narrow fracture system. This leads us to the conclusion that when the fracture is 1 mm thin, there is almost perfect capillary continuity.

The results of capillary continuity experiments indicated that although different degrees of capillary continuity have the same effect on ultimate recovery point of view, their transmissibilities are not the same. At the best conditions (narrow fracture aperture), due to a larger number of liquid bridges, the transmissibility of a stack blocks is such that the flow rate is close to that of a single block with the same height.

Table 3.8: Properties of employed packed models along with obtained results for capillary continuity investigation

Model length (L), cm	Matrix glass beads size	Porosity (φ_e), %	Pattern of fractures	Fluid	Fracture aperture (b), mm	Maximum Flow rate, cm^3/s	residual Oil saturation, %	Recovery factor,%
55	BT2	38.0	N/A	CMC (2%)	Homogeneous media, No fractures	1.6 ± 0.3	12.1 ± 0.4	79.0 ± 1.3
55	BT2	38.0	(c)	CMC (2%)	5	1.6 ± 0.2	13.5 ± 0.3	77.5 ± 1.1
55	BT2	38.0	(c)	CMC (2%)	1	1.6 ± 0.2	12.2 ± 0.3	79.1 ± 0.9
55	BT2	38.0	(c)	Varsol Oil	5	6.5 ± 0.4	15.1 ± 0.4	78.2 ± 1.2

3.5.9 Effects of initial liquid saturation on recovery history: Free-fall gravity drainage experiments were performed with BT4 glass bead models using the CMC solution (1 wt%)–air system to investigate the production characteristics of media that are fully saturated with liquid and compare them to that of media with same initial gas saturation. First, gravity drainage was performed in a fully saturated model. To establish initial gas saturation for the next run, the liquid was injected back into a drained packed model from the bottom. This results in the trapping of gas as a residual phase in the matrix with about 15% PV gas saturation. The presence of initial gas saturation reduces the matrix permeability by about 30% in bead-pack type of porous media (Chatzis et al., 1983). Now having this condition established, we performed the

free-fall gravity drainage test and monitored the production history as before. The results obtained with BT4 beads in runs 11, 12 and 13 are shown in Figure 3.26. It is evident that the amount of liquid recovered from a fully saturated model with a fracture is greater than that obtained from the same system with residual gas present in the matrix. When the cumulative amount of liquid up to a particular time is normalized by dividing it with the maximum amount of recoverable liquid, we obtain the fraction of recoverable liquid as a function of time. Therefore, we can compare the production history of two systems by plotting the fraction of recoverable liquid remaining in the system as a function of dimensionless time. This comparison is made in the plot shown in Figure 3.26.

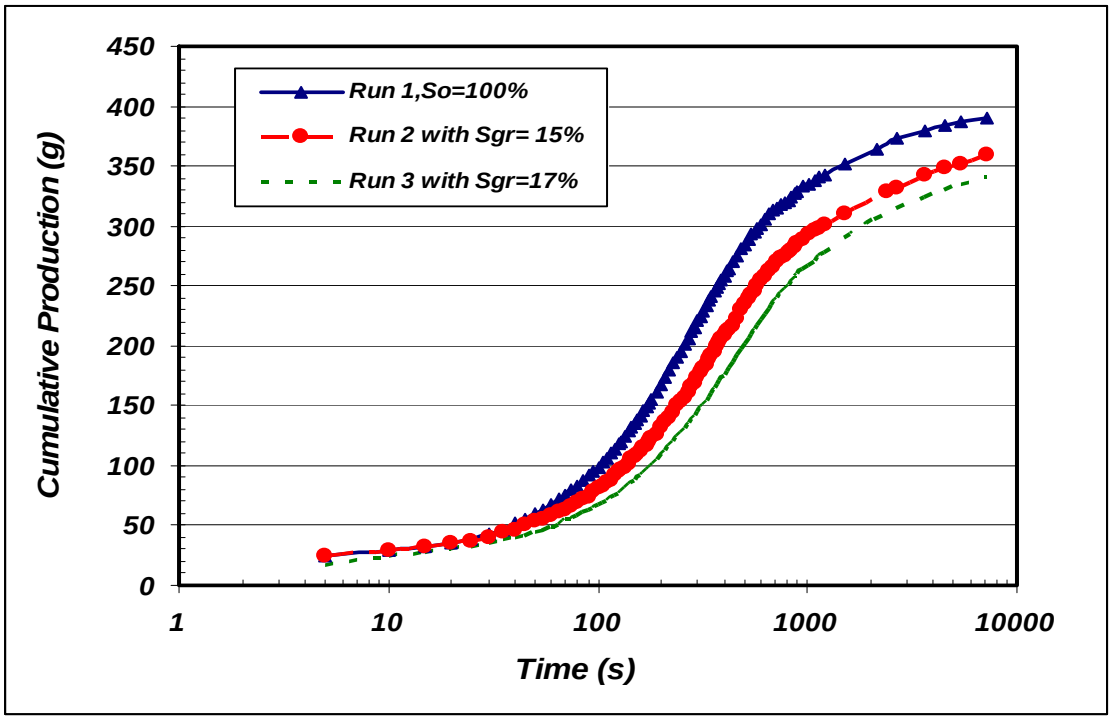

Figure 3.26: Comparison of cumulative production in the BT4 glass bead model with different initial liquid saturation conditions, fluid pair: CMC solution (1%)-air.

For gravity drainage conditions, the characteristic time is the length of system divided by the free-fall Darcy velocity in that system. Using the matrix permeability, actual time t, fluid and model properties, the dimensionless time can be defined as:

$$t_D = \frac{tK_m \Delta\rho g}{\mu_L . L} \qquad (3.9)$$

It can be seen that the production history presented in the form shown in Figure 3.27 is described extremely well by the same characteristic function. This observation permits us to describe the production history from a partially saturated system by utilizing the supposedly known fractional recovery curve of a fully liquid saturated model or system. Also, from Figure 3.26, we can see that the liquid production rate at early times of gravity drainage is almost equal for all three systems with different initial gas saturation. It should be mentioned that the initial gas saturation is not uniformly distributed through the model. The top portions of the matrix and also the areas

of matrix close to the fractures have lower saturation of trapped gas. Therefore, the communication between matrix and fracture is not much affected by the presence of initial gas saturation, implying that the initial production rates are not affected much because, as mentioned before, the area close to the fracture has the highest contribution on the communication between matrix and fracture. Based on our experimental results, it is obvious that the cumulative production in the presence of initial gas saturation decreases.

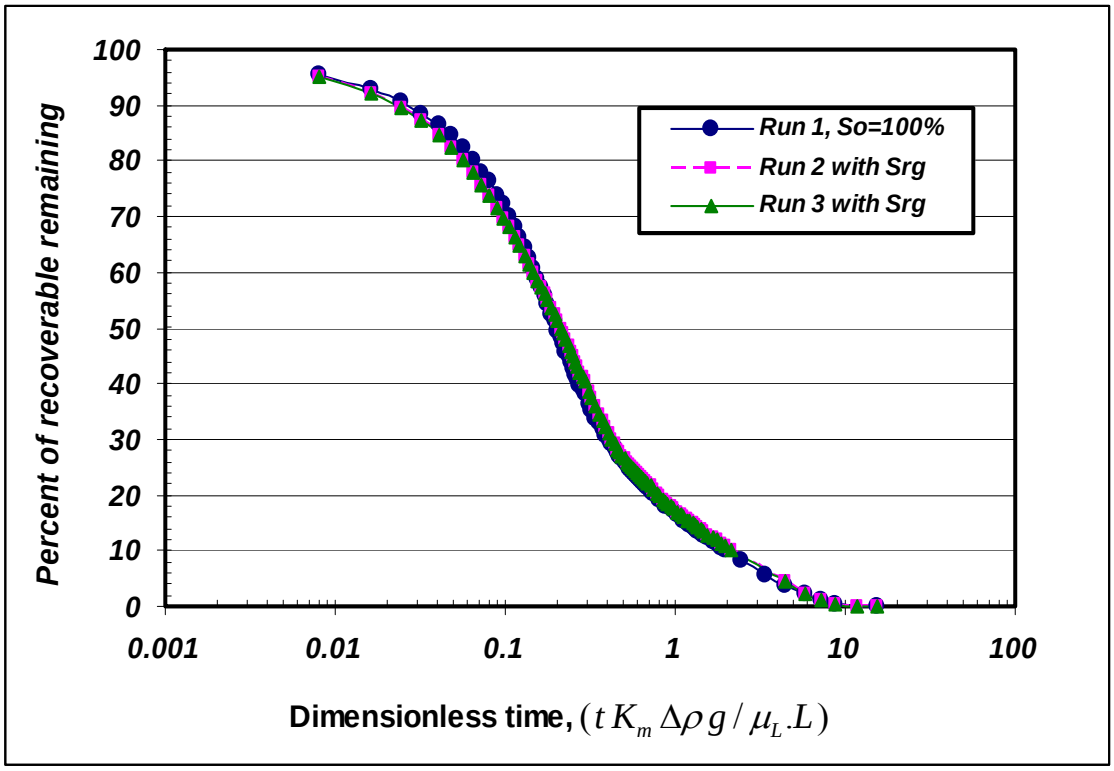

Figure 3.27: Comparison of production history in model No.11 with BT4 beads starting at different initial liquid saturation conditions.

3.5.10 Comparison of production history: In this section, a comparison is made for model pattern (a) with fracture aperture of 1.1 cm under free fall gravity and different matrix permeability. The oil recovery rate is a strong function of matrix properties during free fall gravity drainage. The larger the permeability is, the larger will be the cumulative production at a given time, as shown by the results in Figure 3.28. Given enough time, the ultimate recovery in a given system with fracture and in another one without a fracture is the same, simply because the microscopic recovery efficiency of the matrix dominates in pore volume. Upon comparison to the production history of a homogeneous model with the same matrix permeability at a given time, the results clearly show that porous media with fractures produce more oil compared to porous media that have no fractures.

The effect of matrix permeability, for the same fracture aperture and fracture orientation, is best illustrated when the production history is presented in the form shown in Figure 3.29. The plots of oil recovery history shown in Figure 3.29 indicate that on a relative basis of time, the effect of

fracture on oil recovery is stronger for media with low matrix permeability. The presence of fractures is more pronounced at low matrix permeability compared to media of much higher matrix permeability.

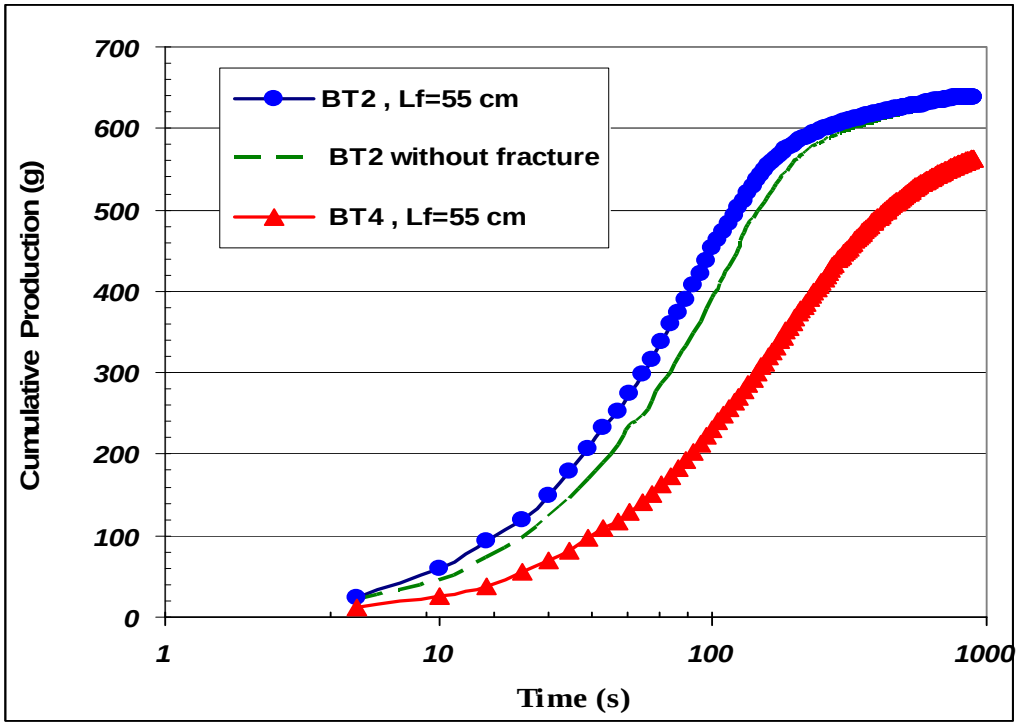

Figure 3.28: Comparison of production history using models made with BT2 and BT4 glass beads and fracture length = 55 cm. Production history of a homogeneous model with BT2 glass beads is also shown for comparison to that with the fracture.

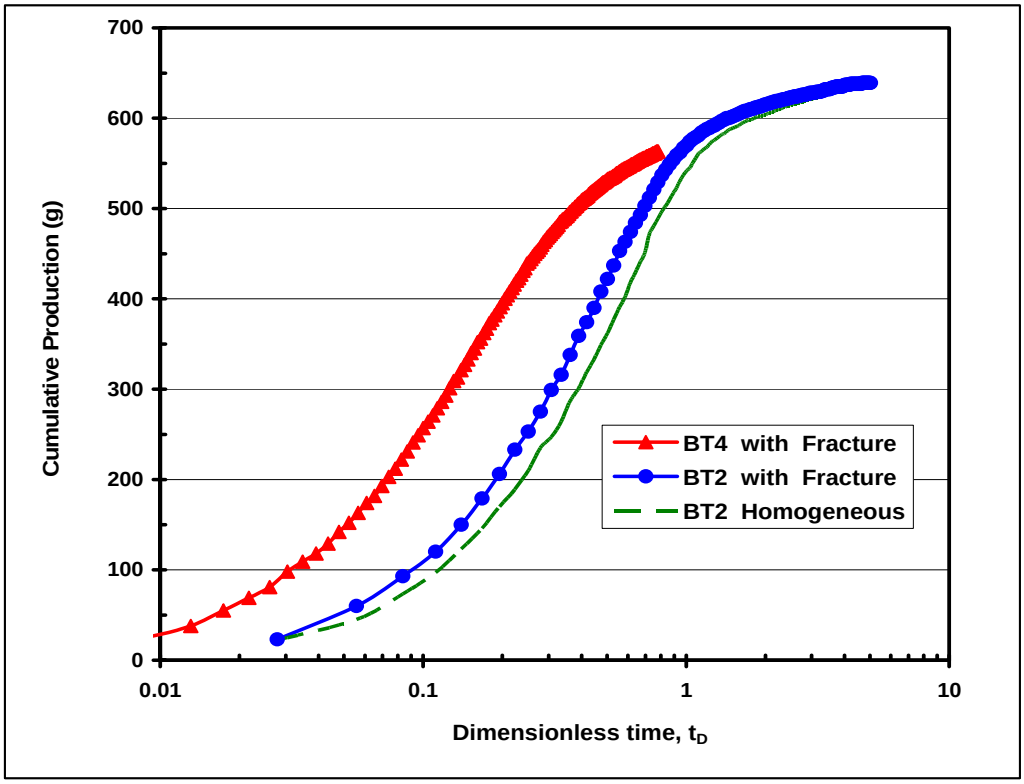

Figure 3.29: Production history of models made with BT2 and BT4 glass beads and fracture length = 55 cm using dimensionless time. Comparison of the production history of a homogeneous model with BT2 glass beads versus dimensionless time can be made to that of fracture systems.

3.5.11 Effect of the term defined by $\frac{K_m.\Delta\rho.(H_f - H_m).g}{\mu_L}$:

In this part, an accurate communication flow equation incorporating a time dependent shape factor is derived and verified for improving the dual-porosity, dual-permeability modeling during free fall gravity drainage in fracture porous media. The equation expresses the transfer rate in terms of the liquid phase pressure gradient in the matrix, surface area of fracture, liquid permeability, liquid viscosity and a variable matrix-fracture shape factor.

The single phase approach of Darcy's equation can be extended to be used for multiphase flow in order to compute the flow rate transferring from matrix to fracture by the following equation:

$$q_{com} = -AK_m \frac{K_{ro}}{\mu_L} \frac{\partial p_L}{\partial x} \qquad (3.10)$$

where, K_m is the average absolute permeability in the matrix block, μ_L is the liquid viscosity, p_L is the pressure of the liquid phase in the matrix, A is the total fracture surface area, which is calculated from the fracture geometry and x is the direction perpendicular to the vertical axis. A finite difference approximation of equation (3.10) may be written in the following form:

$$q_{com} = -AK_m \frac{K_{ro}}{\mu_L} \frac{\Delta p_L}{\Delta x} \tag{3.11}$$

It is further assumed that the pressure drop, Δp_L , responsible for the communication flow rate, q_{com} , may be calculated as the difference between the average liquid-phase pressure computed in the matrix and fracture, and these two average values of pressure are separated by a distance equal to half the fracture spacing. A flow correction, F_{com}, is introduced to take care of the deviations due to the assumption made here. Consequently, equation (3.11) can be written in the following form:

$$q_{com} = -F_{com} AK_m \frac{K_{ro}}{\mu_L} \frac{(p_m - p_f)}{W/2} \tag{3.12}$$

On the other hand, the pressure difference between matrix and fracture can be interpreted as the difference of interface positions in the fracture and the matrix during free gravity drainage at each specific time:

$$p_m - p_f = \Delta\rho.g.(H_f - H_m) \tag{3.13}$$

The fracture surface area contributing in liquid communication is defined as the below formula:

$$A=L.W \tag{3.14}$$

L and W are model height and model thickness, respectively.

The proposed communication rate equation can be implemented in a fractured reservoir simulation during unsteady state processes. Current numerical simulators determine the transfer flow rate from the following expression (Warren and Root, 1963):

$$q_{com} = \alpha \frac{K_m}{\mu_L}.(p_m - p_f) \tag{3.15}$$

where α is the constant shape factor. Equation (3.15) is valid just when dealing with steady state conditions as the surface area subject to liquid transferring from matrix to fracture stays constant. However, during an unsteady state process such as gravity drainage, the fracture surface area which is responsible for the communication is variable with time and a variable constant shape factor was used in this case. Modification of equation (3.15) includes the substitution of the shape factor by the flow correction factor that was obtained by combining the experimental approach and statistical regression.

$$F_{com} = \frac{a}{t_D^{1/2}} \tag{3.16}$$

Figure 3.30 indicates that equation (3.16) can predict the value of dimensionless correlation, F_{com}, to calculate communication rate from matrix to fracture with a high accuracy.

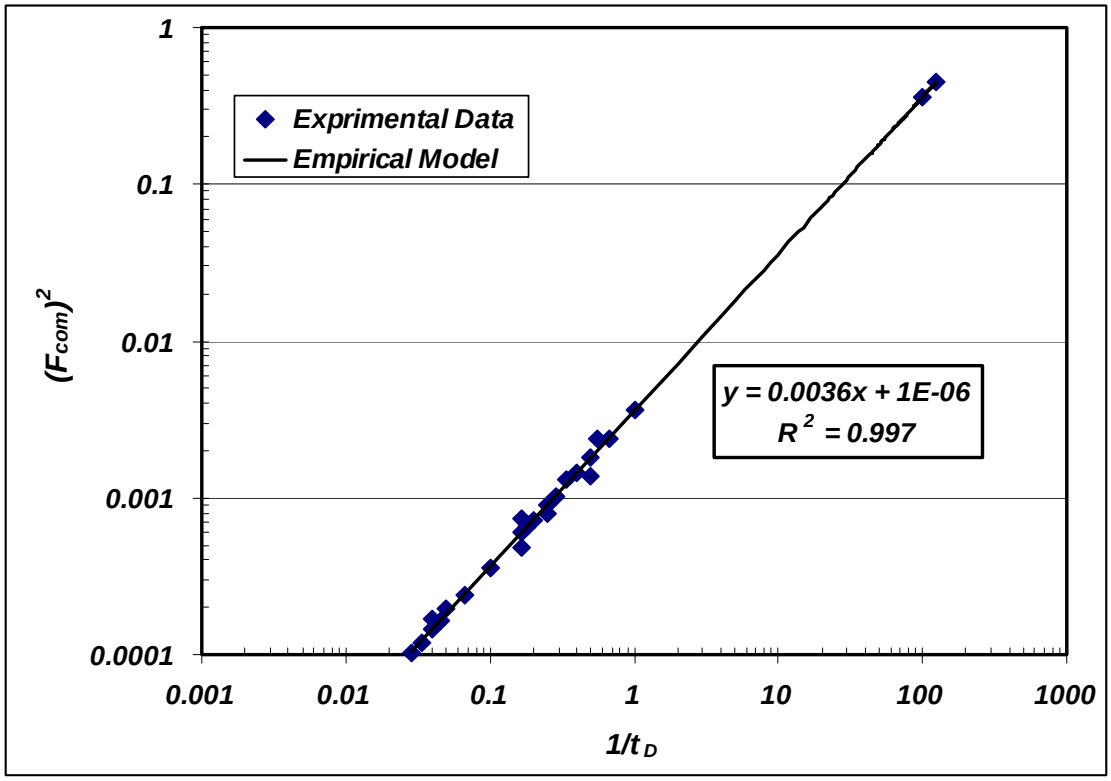

Figure 3.30: Regression analysis for data points corresponding to correlation factor for communication flow rate at various times for employed different fractured media with fractures pattern (b).

Based on data shown in figure 3.30, the value of the coefficient 'a' for equation (3.16) is 0.06 and the equation can be used for transfer flow rate in fractured media with fracture configuration 'b'.

Figure 3.31 shows the effect of driving force for communication between matrix and fracture on the liquid rate flowing from matrix to the fracture. It is clear that as this term increases, the communication rate increases assuming other parameters remain constant. As shown in the graph, the communication Darcy velocity changes linearly with the term namely, $\frac{K_m.\Delta\rho.(H_f - H_m).g}{\mu_L}$ and communication Darcy velocity in the system with lower permeability changes sharper with driving force compared to that for more permeable system. However, the model with the higher permeability has a higher communication velocity and consequently, higher liquid communication rate up to 1.4 g/s.

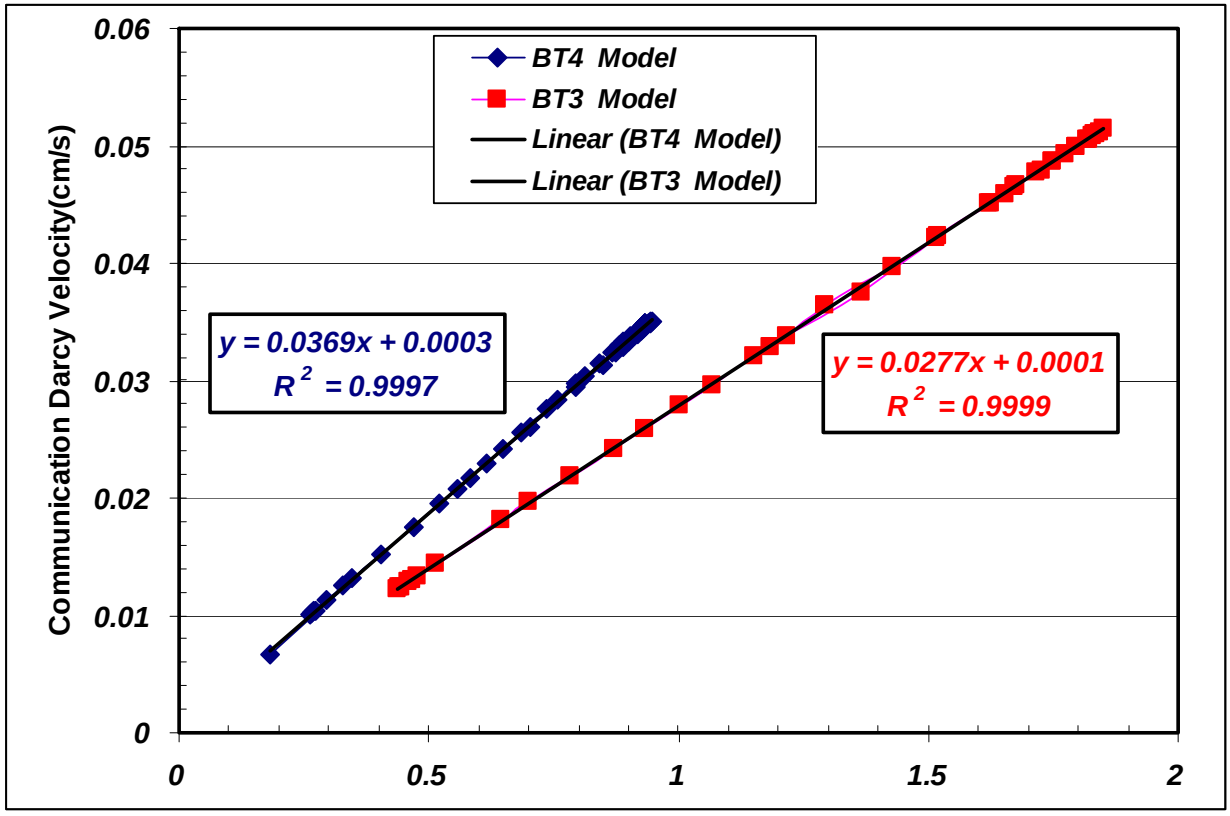

Figure 3.31: Liquid communication Darcy velocity as a function of $\frac{K_m.\Delta\rho.(H_f - H_m).g}{\mu_L}$ for two different models (both models were saturated with CMC solution (2%) and had L = 55 cm, b =5 mm).

3.5.12 Effective permeability in fractured media: During free fall gravity drainage in fractured porous medium of type b (having two vertical fractures on both sides), there are three stages during oil production (though those steps exist for porous media a and d, as well):

1) First, gas invades the fractures and no oil is produced from matrix part; only fractures contribute to oil production, therefore, the effective permeability is equal to the effective permeability for fracture:

$$K_e = K_{eff,f} \qquad (3.17)$$

2) After gas invasion starts in the matrix porous medium, both fractures and matrix contribute to oil production and each part has a share in the magnitude of total effective permeability of the porous medium. Since this kind of flow is neither pure in parallel nor pure in series, it would be difficult to define an effective permeability during this short period because the effective permeability is a function of several parameters such as communication rate which is variable with time during free fall gravity drainage process.

3) When the gas-liquid interface reaches the bottom of fracture and there is no more oil in the fracture. It should be noted that because of the small volume of fluid in the fractures, the

initial period (first two steps mentioned above) may be very short (it makes impractical to measure important parameters in some cases). Therefore, the pressure equalization between matrix and the fracture happens soon. The reservoir (or fractured medium) then responds like an unfractured porous medium with a permeability equal to K_e which is greater than matrix permeability and we cannot take into account the matrix permeability as effective permeability for the model in this stage; although, there is no fluid left in the fracture. A good estimate for calculating the magnitude of effective permeability is to use a cumulative rate plot versus time and then obtain volumetric flow rates, and finally applying Darcy's equation to find effective permeability. The calculations show difference between that value and matrix permeability well.

The experimental results show that this effective permeability may be expressed as follows:

$$K_e = K_m + c.K_{eff,f} \tag{3.18}$$

where, c is a constant which depends on the particle size. The effective permeability for fracture media can also be obtained by pressure decline curve analysis. The above equation also shows that during film flow along the fracture length which is parallel with the flow in matrix, therefore, effective permeability for this case can be calculated by the formula which is valid for parallel porous layers.

The following table summarizes the magnitude of permeability for homogeneous and fractured media:

Table 3.9: Effective permeability for the fractured porous media (b) under FFGD

Run no.	Type of glass beads	Type of reservoir	Fracture aperture	Effective permeability
1	BT2	Unfractured	N/A	K_m for BT2
2	BT2	fractured	5 mm	1.2 K_m for BT2
3	BT2	fractured	3 mm	1.1 K_m for BT2
4	BT3	Unfractured	N/A	K_m for BT3
5	BT3	fractured	5 mm	1.5 K_m for BT3
6	BT4	Unfractured	N/A	K_m for BT4
7	BT4	fractured	5 mm	1.95 K_m for BT4

The experimental results in Table 3.9 show that the effect of fracture on effective permeability is more significant in the porous media with lower matrix permeability.

3.5.13 Production flow rate: Usually, a maximum flow rate is observed in vertical fracture reservoirs when communication between matrix and fracture starts simultaneously and therefore, the drainage flow comes from both matrix and fracture domains. However, when dealing with homogeneous porous media, the maximum flow rate occurs at the beginning of gravity drainage process. Table 3.10 lists the values of maximum production rate for the experimental porous media under gravity drainage process.

According to the dynamics of fluid flow in porous media, if the porous medium is unfractured and flow regime is Darcian, one can use the following equation to find the maximum flow rate during free fall gravity drainage:

$$q_{\max} = A.\frac{K}{\mu_L}.\frac{\Delta\rho.g.(L-h_c)}{L} \qquad (3.19)$$

where, q_{max} is the maximum production rate; K is total effective permeability; μ_L is the viscosity; L is the length; ρ is the density, and g the gravitational force , and h_c is capillary threshold height for the porous media used in our experiments.

The experimental results show that the presence of fractures increases the maximum flow rate compared to that for the porous media without fractures. If we use effective permeability, which is combination of matrix and fracture permeabilities in the above formula, it gives a good estimate regarding the maximum production rate in fractured porous media. Noteworthy that the maximum oil production rate in gravity drainage tests is estimated by using the plot of the oil production rate (or cumulative production) versus time. There is an abrupt change in oil production rate when the gas-oil surface touches the top of the core sample because of the effect of the entry capillary pressure. This approach in the estimation of initial oil production rate is not accurate. In order to obtain an empirical approach for liquid production rate, q/qmax was plotted versus a new dimensionless time which is defined as follows:

$$t_D = \left[\sqrt{\frac{K_m}{\phi}}\left(\frac{\sigma}{\mu_L.L^2}\right)\right]t \qquad (3.20)$$

where σ is the surface tension of test liquid and other parameters were defined in previous parts. The results show that $Ln(q/q_{max})$ is a linear function of natural logarithm of the dimensionless time with a reasonable accuracy for all our fractured porous media saturated with various liquids. Equation (3.19) presents this relationship between these dimensionless numbers.

$$Ln\left(\frac{q(t)}{q_{\max}}\right) = a.Ln(t_D) + b \qquad (3.21)$$

The coefficients a and b of the above equation depend on petrophysical properties of fractured medium and test fluid. The History matching can provide the values of these constants if the oil production data are available.

Figures 3.32 and 3.33 indicate the relationship between production rate and dimensionless time for two different fractured porous media.

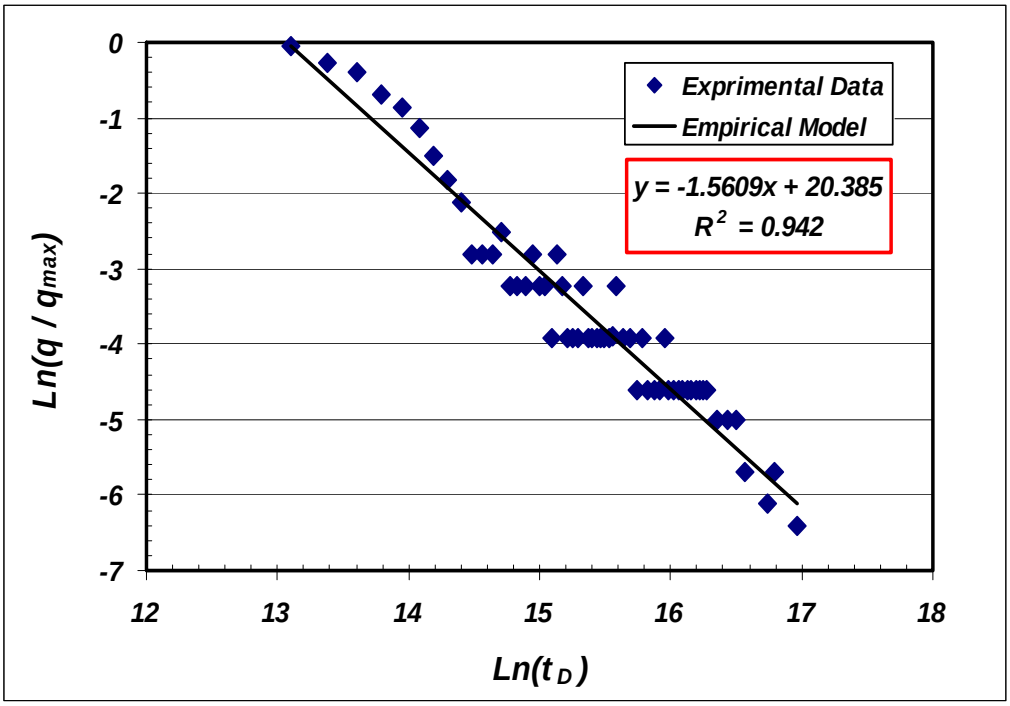

Figure 3.32: Ln (q/q_{max}) versus Ln(t_D) for model(e) saturated with Varsol oil [BT2 glass beads, L = 55 cm].

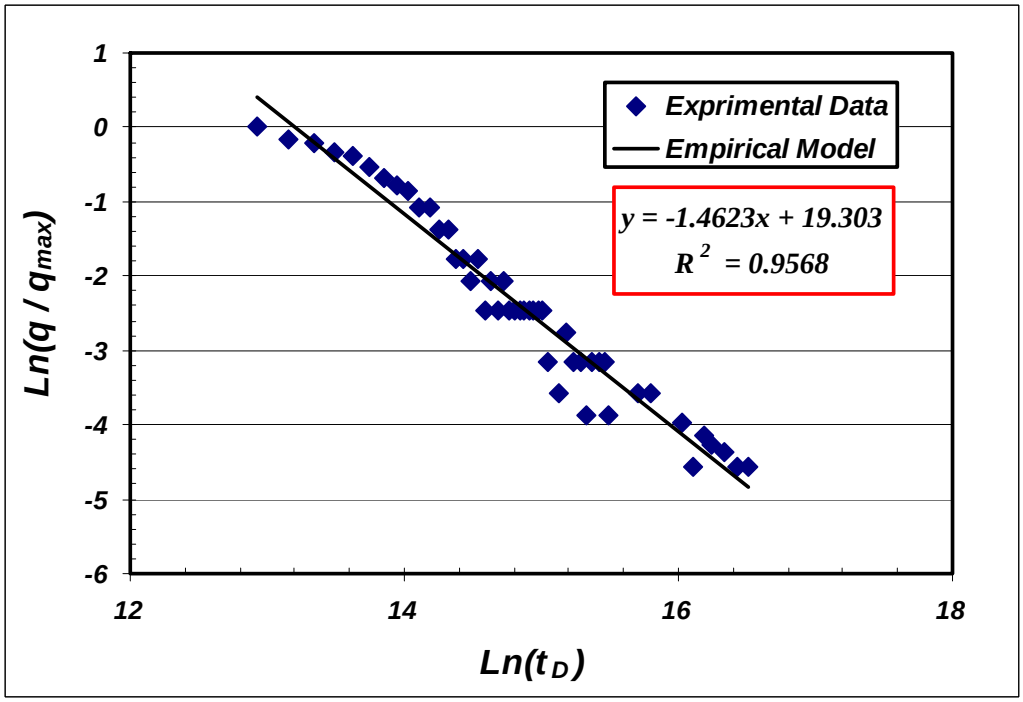

Figure 3.33: Relationship between liquid production rate and dimensionless time for fractured porous medium (a) with a vertical fracture in the middle [BT3 glass beads, b = 5 mm, L = 55 cm, fluid pair: Air-Varsol].

Table 3.10: Maximum flow rate of free fall gravity drainage experiments for 42 sample runs

Run No.	Model height, L (cm)	Matrix glass beads size	Fracture Length ,L_f (cm)	Test fluid	Fracture aperture (b),mm	Fractures pattern	Maximum flow rate, cc/s
1	55	BT2	55	CMC(1%)	5	b	5.30 ± 0.6
2	55	BT2	55	CMC(2%)	5	b	2.60 ± 0.2
3	55	BT2	55	Water	5	b	14.40 ± 0.9
4	55	BT4	18	Water	5	c	2.10 ± 0.3
5	55	BT2	55	CMC(2%)	3	b	1.95 ± 0.2
6	55	BT2	55	CMC(1%)	3	b	4.70 ± 0.3
7	55	BT3	55	CMC(1%)	5	b	1.60 ± 0.2
8	55	BT3	55	CMC(2%)	5	b	1.10 ± 0.2
9	28	BT3	28	CMC(2%)	5	b	0.75 ± 0.1
10	40	BT3	40	CMC(2%)	5	b	1.00 ± 0.2
11	55	BT4	55	CMC(1%)	5	b	1.30 ± 0.1
12	55	BT4	55	Water	5	a	3.30 ± 0.4
13	55	BT4	55	CMC(2%)	5	c	0.30 ± 0.1
14	55	BT4	55	CMC(2%)	5	b	0.95 ± 0.1
15	55	BT4	55	CMC(1%)	3	b	1.00 ± 0.1
16	55	BT4	55	Water	5	b	3.20 ± 0.3
17	55	BT2	55	CMC(2%)	2	b	2.10 ± 0.2
18	55	BT2	55	Varsol	5	b	9.80 ± 0.3
19	55	BT3	55	Varsol	5	b	5.60 ± 0.3
20	55	BT3	55	Varsol	3	b	4.80 ± 0.3
21	55	BT3	55	Water	11	a	6.00 ± 0.4
22	55	BT3	30	Water	11	d	5.20 ± 0.2
23	55	BT3	55	Varsol	11	a	5.80 ± 0.3
24	55	BT3	30	Varsol	11	d	4.30 ± 0.2
25	55	BT3	15	Varsol	11	d	3.20 ± 0.3
26	55	BT2	18	CMC(2%)	5	c	1.60 ± 0.2
27	55	BT2	18	CMC(2%)	1	c	1.40 ± 0.1
28	55	BT2	18	Varsol	5	c	11.60 ± 0.6
29	55	BT3	46	Varsol	5	e	5.10 ± 0.4
30	55	BT3	46	Varsol	5	f	5.30 ± 0.3
31	55	BT2	N/A	Varsol	N/A	N/A	12.00 ± 0.5
32	55	BT2	18	CMC(1%)	5	c	3.90 ± 0.3
33	55	BT4	46	CMC(1%)	5	e	1.70 ± 0.2
34	55	BT4	46	CMC(1%)	5	f	2.00 ± 0.2
35	55	BT2	N/A	CMC(2%)	N/A	N/A	1.50 ± 0.1
36	55	BT3	55	Varsol	5	a	4.75 ± 0.3
37	55	BT3	55	Water	5	a	3.60 ± 0.2
38	55	BT4	46	CMC(2%)	5	e	0.65 ± 0.1
39	55	BT2	46	Varsol	5	e	10.00 ± 0.9
40	55	BT2	46	CMC(1%)	5	e	7.20 ± 0.5
41	55	BT3	46	Varsol	5	g	4.80 ± 0.2
42	55	BT4	46	CMC(1%)	5	g	1.92 ± 0.3

3.6 Dimensionless Groups

In this section, the relevant dimensionless numbers which play important roles in the up-scaling procedure of the experimental results are discussed accordingly.

3.6.1 Bond number: According to the definition provided in the concepts of fluid flow in porous media, Bond number, "Bo", is a dimensionless number which expresses the importance of body forces (i.e. gravitational forces) compared to either surface or interfacial forces (Dullien, 1990):

$$Bo = \frac{\Delta\rho.g.K_m}{\sigma} \tag{3.22}$$

where "Δρ" is the density difference between acting fluids flowing in porous medium, "g" is the gravitational acceleration associated with the body force, "K_m" is the matrix permeability, and "σ" is the surface tension across the interface.
According to the definition, a high value of Bond number for fluid flow inside a particular matrix indicates that the fluid flow inside the matrix is relatively unaffected by the surface tension forces. However, a low value for Bond number (i.e. typically less than unity) reveals the relative importance of capillary forces against gravitational forces. Intermediate numerical values associated with this dimensionless number indicate a non-trivial balance between these two forces. Since understanding of the Bond number value is essential for investigating different aspects of gravity drainage process it is wise to consider it as one of the reference dimensionless groups. This makes it possible to realize its physical importance on the different aspects of FFGD process defined previously in section 3.2, including recovery factor and elevation difference between G/L interface positions in matrix and fractures.

3.6.2 Reynolds number: For fluid flow in porous media, Reynolds number is defined as follows (Dullien, 1990):

$$\mathrm{Re}_p = \frac{\rho.v.D_p}{\mu_L} \tag{3.23}$$

where "ρ" is the liquid density, "*v*" could be defined as either pore velocity or specific discharge (i.e. withdrawal rate in the case of flow influenced by only gravitational force in gravity drainage process), "D_p" is a representative grain diameter for the porous medium which is often taken as the 30% passing size of grains from a grain size analysis using sieves, and "μ_L" is the liquid dynamic viscosity.

According to the dynamics of fluid flow in porous media, one can differentiate between laminar (i.e. Darcy) and turbulent (i.e. non-Darcy) regimes of liquid flow based on the magnitude of Reynolds Number for each particular flow system. The threshold value of unity ($Re_p = 1$) has been considered for the critical Reynolds Number above which the liquid flow through a particular porous material would be no longer follow Darcy's flow regime. According to the literature, experimental results have shown that flow regimes with values of Reynolds number up to 10 may still be Darcian flow (Dullien, 1990). For each particular porous medium with definite pore size distribution in which a known liquid is flowing down gradient under the action of gravity force only, the magnitude of the discharge rate (or the associated value of Darcy velocity)

is the parameter by which one could differentiate between the type of flow regime, whether it is laminar or turbulent. To be consistent with the majority of open literature cases where this dimensionless number has been defined, the macroscopic discharge velocity (i.e. withdrawal rate in case of flow under gravity drainage process) was used in analogy regarding dimensionless analysis of FFGD process. Table 3.11 shows the withdrawal velocity criteria upon which the liquid drainage rate out of the matrix domain with definite properties would remain within the range of Darcian flow regime:

Table 3.11: Reynolds number as a function of drainage velocity for the employed fractured porous media and the drainage rate criteria for laminar flow regime

Type of glass beads	Reynolds number (Re_p) and production rate (q) criteria for laminar flow			
	Water	Varsol Oil	CMC 1%	CMC 2%
BT2/D_P=1125 μm	$Re_p=11.25v$, $q \le 2.70\ cm^3/s$	$Re_p=7.32v$, $q \le 4.15\ cm^3/s$	$Re_p=2.34v$, $q \le 12.82\ cm^3/s$	$Re_p=0.95v$, $q \le 31.60\ cm^3/s$
BT3/D_P=710 μm	$Re_p=7.10v$, $q \le 4.21\ cm^3/s$	$Re_p=4.62v$, $q \le 6.45\ cm^3/s$	$Re_p=1.48v$, $q \le 20.22\ cm^3/s$	$Re_p=0.61v$, $q \le 50.03\ cm^3/s$
BT4/D_P=506 μm	$Re_p=5.06v$, $q \le 5.92\ cm^3/s$	$Re_p=3.29v$, $q \le 9.06\ cm^3/s$	$Re_p=1.05v$, $q \le 28.60\ cm^3/s$	$Re_p=0.43v$, $q \le 69.70\ cm^3/s$

3.6.3 Porosity ratio, ($\frac{\phi_f}{\phi_e}$): In order to fulfill the sufficient numbers of dimensionless groups required for the dimensionless analysis, the dimensionless porosity has been defined as the ratio of the magnitude of fracture porosity, "ϕ_f", to the magnitude of effective porosity, "ϕ_e", in each particular fractured medium. The parameter indicates what fraction of total oil in place occupies the fracture.

3.7 Recovery Factor for Free Fall Gravity Drainage

Since free-fall gravity drainage is a gravity-dominated process, and the only resistance is the capillary pressure force, the oil production depends significantly on the properties of the porous media, fluids used, and their interactions. These include permeability and relative permeability of the porous media, pore structure, matrix sizes, fluid viscosities, initial water saturation, the wettability of the rock-fluid systems, and the interfacial tension. It is difficult to include all these important parameters in an analytical model. This may be why the existing analytical models do not work well in characterizing and modeling the gravity drainage process, as described previously. Mathematical models developed to predict oil production accurately by gravity drainage from fractured gravity have been few. An empirical oil recovery model was proposed accordingly to match and predict oil production during free fall gravity drainage. The model was

tested with experimental and field data of oil production under free-fall gravity drainage. The results demonstrated that the oil recovery model could satisfactorily work in the oil-gas drainage system. Initial oil production rate can be estimated using the oil recovery model. The empirical model suggested by Zendehboudi et al. (2009) in this study to match the oil production by gravity is expressed as follows:

$$R.F(t) = 1 - At^{B} \tag{3.24}$$

A and B are constant values for each specific case, which depend on petrophysical properties of rock and physical properties of oil existing in the reservoir. The values of these constants can be obtained by a history match technique once the oil production data are available. Then it would be possible to predict the future production performance of the known fractured reservoir and it can assist to select the best scenario for oil production from the case under study.

Figure 3.34 shows recovery factor versus time for two fractured porous mediums that there is a good agreement between experimental data and the empirical equation proposed above.

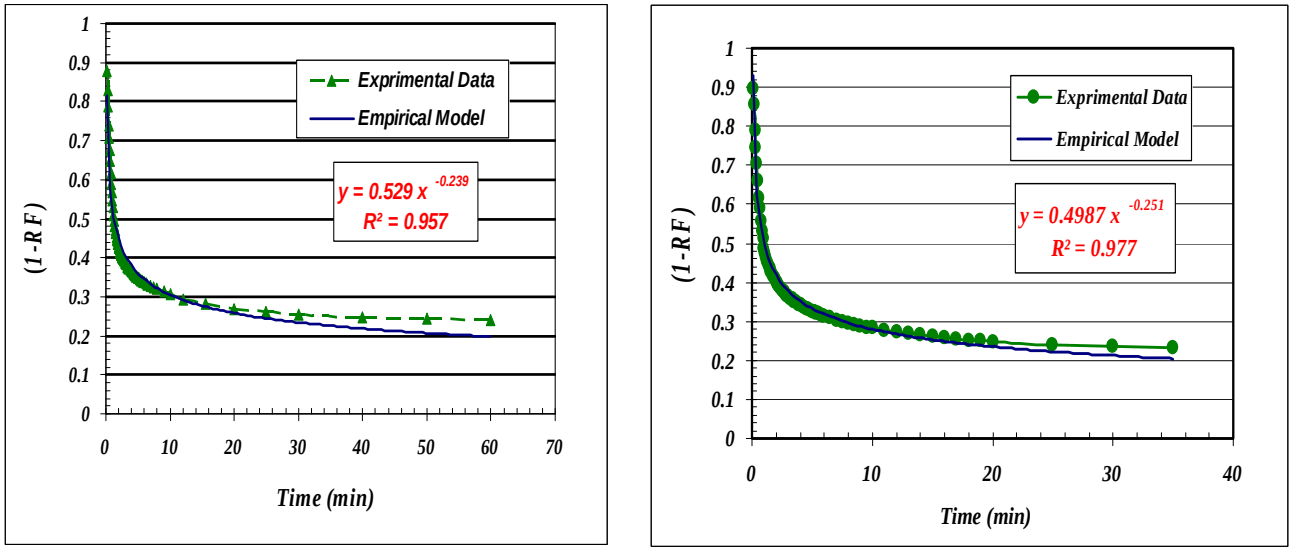

(a) (b)

Figure 3.34: Variation of (1-RF) during free fall gravity drainage for a) BT2 glass beads model (g) saturated with CMC solution (1%). b) fractured porous medium (b) [fluid pair: Varsol oil-Air, BT3 glass beads].

It is well understood that the residual wetting phase saturation for systems of different permeability in the absence of capillary end-effects is independent of matrix permeability. The results of residual liquid saturation shown in Table 3.6 support this statement, as the measured residual liquid saturation varied in the range of 5-10% P.V. However, for finite in height porous media, the residual liquid saturation increases as the permeability and height of packing decreases.

The experimental runs were conducted to investigate the effect of Bond number and capillary end ($L_{effective}/L$) on liquid recovery. The variations in the Bond number were obtained by varying the physical properties of the test fluids and also the specification of the porous medium.

The following empirical model was developed by fitting the production data versus three variables, namely: the Bond number, the ratio of the effective length over the length of porous medium and the ratio of fracture porosity over effective porosity.

$$RF = 1.12\, B_O^{-0.0616} . (\frac{L_{effective}}{L})^{1.12} + \frac{\phi_f}{\phi_e} \quad , \qquad \text{If } L_{effective} > 0 \qquad (3.25)$$

$$RF = \frac{\phi_f}{\phi_e} \qquad \text{If } L_{effective} \leq 0 \qquad (3.26)$$

The effective length is defined as:

$$L_{effective} = L - h_c \qquad (3.27)$$

In equation (3.27), h_c is the capillary threshold height for the porous media used in our experiments.

3.8 Conclusions

The experimental work of free fall gravity drainage in the fractured porous media led to the following conclusions:

- The experimental results have shown that the free-fall gravity drainage rate increases in the presence of fractures. The models with a longer fracture produced higher oil recovery rate compared to models without fracture.
- The models with larger matrix permeability produced more oil during the production process when compared at the same time. In addition, free-fall gravity drainage appears to be stable and piston-like displacement, even for media with fractures.
- For a given fracture-matrix system and for different initial oil saturation conditions, it was found that the production history can be correlated by plotting the fraction of recoverable oil remaining versus time.
- The characteristic rate did not depend on petrophysical properties of the matrix part of a system.
- The model length, fracture permeability and fracture aperture were important parameters that significantly affect production characteristics. The effect of a fracture on liquid recovery was greater in systems of low matrix permeability compared to the effect a fracture has in porous media with matrix of much higher permeability.
- The fractures patterns in a fractured medium significantly affected the magnitudes of recovery rate and effective permeability.
- The extent of capillary contact between matrix blocks controls fluid saturation development and influences the gravity drainage oil recovery in fractured porous media.
- The rate of liquid transferring from matrix to the fractures depends on properties of test fluid, matrix permeability, and difference of liquid levels in matrix and fractures.
- Final liquid recovery can be correlated to the Bond Number through an equation fitted to the data.

Chapter 4

Controlled Gravity Drainage in Fractured Porous Media

4.1 Scope

Oil production from a fractured reservoir, composed of a gas cap and an oil zone, is usually taking place using surface or submersible pumps. The pumping usually is operated under constant withdrawal rate until gas breakthrough, at which time the pumping rate would be influenced by the presence of gas at the production well. It is evident that pumping rate dictates both pressure and fluid flow regimes in the volume which is under the drainage influence of the pump. The main focus of this chapter is on the gas-liquid (G-L) interface behavior and recovery performance of employed models as a function of liquid withdrawal rate. A series of flow visualization experiments were performed using unconsolidated packed models of rectangular geometry with various configurations of fractures. Parametric sensitivity analyses were performed considering the effect of different system parameters such as fracture aperture, matrix height and permeability, well spacing and fluid viscosity on the Critical Production Rate (CPR), Maximum Possible Withdrawal Rate (MPWR) and G-L interfaces in both matrix and fractures.

Experimental results have shown that higher pumping rates cause higher difference between liquid levels in fracture and in the matrix, thus the gas breakthrough happens sooner. Moreover, it was determined that as long as the porous medium is drained with a constant liquid withdrawal rate less than critical, the height difference between G-L interfaces in matrix and fracture remains constant. In this chapter, a new concept of "Critical Pumping Rate" (CPR) was defined at which each particular porous medium has a recovery factor equal to the recovery factor for higher rates just before gas enters into the production well at the bottom, and also the difference between liquid levels in fracture and matrix remains unchanged at rates higher than this specific rate. Known this particular withdrawal rate, there are two main advantages, namely: 1) choosing a pumping rate lower than it to drain the reservoir without getting gas breakthrough; and 2) understanding the physics of pumping behavior from fractured media and extending the concept to the real cases. In addition, the maximum liquid pumping rate from each physical model has also been studied and it was found that this rate depends strongly on the storage capacity of the fractures, petrophysical properties of each model as well as physical properties of test fluids.

The key objective of this chapter is to advance our understanding of controlled gravity drainage in naturally fractured reservoirs, as well as to find out the interaction between capillary and gravity forces in the mentioned process. To achieve these objectives, unconsolidated glass-bead types of experimental prototype have been designed, each model is surrounded vertically by one vertical fracture at each side. Controlled gravity drainage experiments have been performed with focus on visualizing pore-scale aspects of the multiphase flow process, as well as fluid flow interaction between matrix and fractures. This study was undertaken with a detailed Design of Experiment (DOE) phase through which different experimental steps and phases have been designed and ranked considering the effects of various independent parameters on dependent variables. This step is described in detail after this introductory section. The methodological plan of this study is first to perform a parametric sensitivity analysis in order to determine the effects of various system parameters on overall system production performance. In particular,

experimental results were analyzed in order to delineate the effect of fracture aperture, matrix height and permeability, well spacing and fluid properties on the magnitude of newly defined "Critical Pumping Rate" and also "Maximum Possible Withdrawal Rate".

4.2 Design of Experiments (DOE)

Design of Experiment (DOE) is a structured, organized method that is used to determine the relationship between the different factors (Xs) affecting a process and the output of that process (Y). This method was first developed in the 1920s and 1930, by Sir Ronald A. Fisher, the renowned mathematician and geneticist. Experimental design is a strategy to gather empirical knowledge, i.e. knowledge based on the analysis of experimental data and not on theoretical models. It can be applied whenever you intend to investigate a phenomenon in order to gain understanding or improve performance. Building a design means, carefully choosing a small number of experiments that are to be performed under controlled conditions (Montgomery and Runger, 2006; Montgomery, 2008). There are four interrelated steps in building a design:

1) Define objectives to the investigation, e.g. better understand or sort out important variables or find optimum.
2) Define the variables that will be controlled during the experiment (design variables), and their levels or ranges of variation.
3) Define the variables that will be measured to describe the outcome of the experimental runs (response variables), and examine their precision.
4) Among the available standard designs, choose the one that is compatible with the objective, number of design variables and precision of measurements, and has a reasonable cost

4.2.1 Set the objectives: The first decision before designing an experiment is "what is the objective, or purpose, of this study?" The focus of the study may be to screen out the factors that are not critical to the process, or it may be to optimize a few critical factors. A well-defined objective leads the experimenter to the correct DOE (Montgomery and Runger, 2006; Montgomery, 2008). The following objectives have been finalized for the experiments regarding the current study:

1) Investigate the physics of controlled gravity drainage process in a fractured medium; and extending the results to predict the real field case performance, if it is possible.
2) Focus on the behavior and movement of Gas-Liquid (G-L) interface through matrix and fractures, and obtaining the recovery performance of employed physical models as a function of liquid withdrawal rate.
3) Define new concepts of "Critical Pumping Rate" and also "Maximum Possible Withdrawal Rate", and then obtaining these two parameters for each particular fractured model.
4) Perform parametric sensitivity analysis.

4.2.2 Select various process variables: This step includes screening the design in order to identify which parameters are affecting the overall system response. According to our understanding of the physics of Free Fall Gravity Drainage Process (Zendehboudi et al., 2008; Zendehboudi et al., 2009), and also following some preliminary controlled gravity drainage tests, it was concluded that the following 6(six) parameters could be considered to be the main

affecting variables that influence the general performance of controlled gravity process. This includes:

1) Fracture aperture, 2) Matrix height, 3) Matrix permeability, 4) Interfacial tension, 5) Well spacing, and 6) Fluid viscosity.

Since the process variables include both inputs and outputs, i.e. factors and responses, the dependent variables are namely: 1) Critical pumping rate, 2) Maximum possible withdrawal (i.e. pumping) rate, 3) Recovery factor, and 4) Vertical elevation difference between the G-L interface positions in matrix and fractures during the controlled gravity drainage processes.

It is wise to critically choose a sound range of variation for experimental input factors just before designing the models. This makes it possible to have a reasonable clue about the experimental outputs before performing each particular test relative to the other designed experiments.

4.2.3 Select an experimental design: Considering the number of factors evaluated in the current study (total of 6) and the nature of the process, it appears that the most relevant experimental design method is factorial with two levels of design (Montgomery and Runger, 2006; Montgomery, 2008). This type of experimental design is frequently used in experiments involving several independent factors where it is necessary to study the combined effect of the involving parameters on system response. However, as the number of factors in a two level factorial design increases, the number of runs for even a single replicate of the 2^k design becomes very large. Fractional factorial designs can be used in our case to draw out valuable conclusions from fewer runs. Therefore, the basic purpose of a fractional factorial design is to economically investigate cause-and-effect relationships of significance in a given experimental setting. There are lots of good reasons on why to select only two levels is the most common choice amongst engineers. First and foremost, having two design levels is ideal, simple, and also economical for screening designs (Montgomery and Runger, 2006; Montgomery, 2008). However, it is recommended to have some centre points between the high level and also the low level of each experimental factor. The standard layout of a 2-level design generally uses “+1” and “-1” notations to denote the "high level" and the "low level" limits of each factor respectively. Table 4.1 demonstrates the series of designed experiments in which 32 trials (i.e. experimental runs) have been planned, considering each factor to be set to its high or low limit during that particular run.

Use of “+1” and “-1” notations for the factor setting is called data coding. This aids in the interpretation of the coefficients fitted to any experimental model. After factor settings are coded properly, all the center points have the value "0". Regarding our study, centre points have been chosen for all the independent variables except the well spacing. So, the appropriate experimental design for our controlled gravity drainage experiments is half fractional factorial design including 2^{6-1} trial runs. Since we were dealing with seven different withdrawal rates, and 80 replicate runs have been considered in order to examine the repeatability of the experiments, a total of 350 experimental runs have been designed to be performed in order to study various effects of all independent variables on the system responses

Table 4.1: Design of Experiment data-table for the CGD experiments

Run no.	Fracture aperture	Matrix height	Matrix permeability	Fluid viscosity	Well spacing	Fluid interfacial tension
1	-1	-1	-1	-1	-1	-1
2	+1	-1	-1	-1	-1	+1
3	-1	+1	-1	-1	-1	+1
4	+1	+1	-1	-1	-1	-1
5	-1	-1	+1	-1	-1	+1
6	+1	-1	+1	-1	-1	-1
7	-1	+1	+1	-1	-1	-1
8	+1	+1	+1	-1	-1	+1
9	-1	-1	-1	+1	-1	+1
10	+1	-1	-1	+1	-1	-1
11	-1	+1	-1	+1	-1	-1
12	+1	+1	-1	+1	-1	+1
13	-1	-1	+1	+1	-1	-1
14	+1	-1	+1	+1	-1	+1
15	-1	+1	+1	+1	-1	+1
16	+1	+1	+1	+1	-1	-1
17	-1	-1	-1	-1	+1	+1
18	+1	-1	-1	-1	+1	-1
19	-1	+1	-1	-1	+1	-1
20	+1	+1	-1	-1	+1	+1
21	-1	-1	+1	-1	+1	-1
22	+1	-1	+1	-1	+1	+1
23	-1	+1	+1	-1	+1	+1
24	+1	+1	+1	-1	+1	-1
25	-1	-1	-1	+1	+1	-1
26	+1	-1	-1	+1	+1	+1
27	-1	+1	-1	+1	+1	+1
28	+1	+1	-1	+1	+1	-1
29	-1	-1	+1	+1	+1	+1
30	+1	-1	+1	+1	+1	-1
31	-1	+1	+1	+1	+1	-1
32	+1	+1	+1	+1	+1	+1

4.3 Experimental Work

In this section, details of the experimental set up, test fluids, and experimental procedures are presented and discussed accordingly.

4.3.1 Experimental setup: Figure 4.1 shows the schematic diagrams of the experimental setups used in the current study. The experimental setups comprised of the following components:
a) A rectangular porous medium,
b) A particular pattern of fractures,

c) High definition video-recording and high-resolution digital imaging facilities: The G-L interface movement through both matrix and fractures were recorded continuously during the experiments,
d) Peristaltic pump with variable discharge rates,
e) Digital balance to weigh the withdrawn liquid,
f) Vacuum equipment to remove dissolved gas from test liquids.

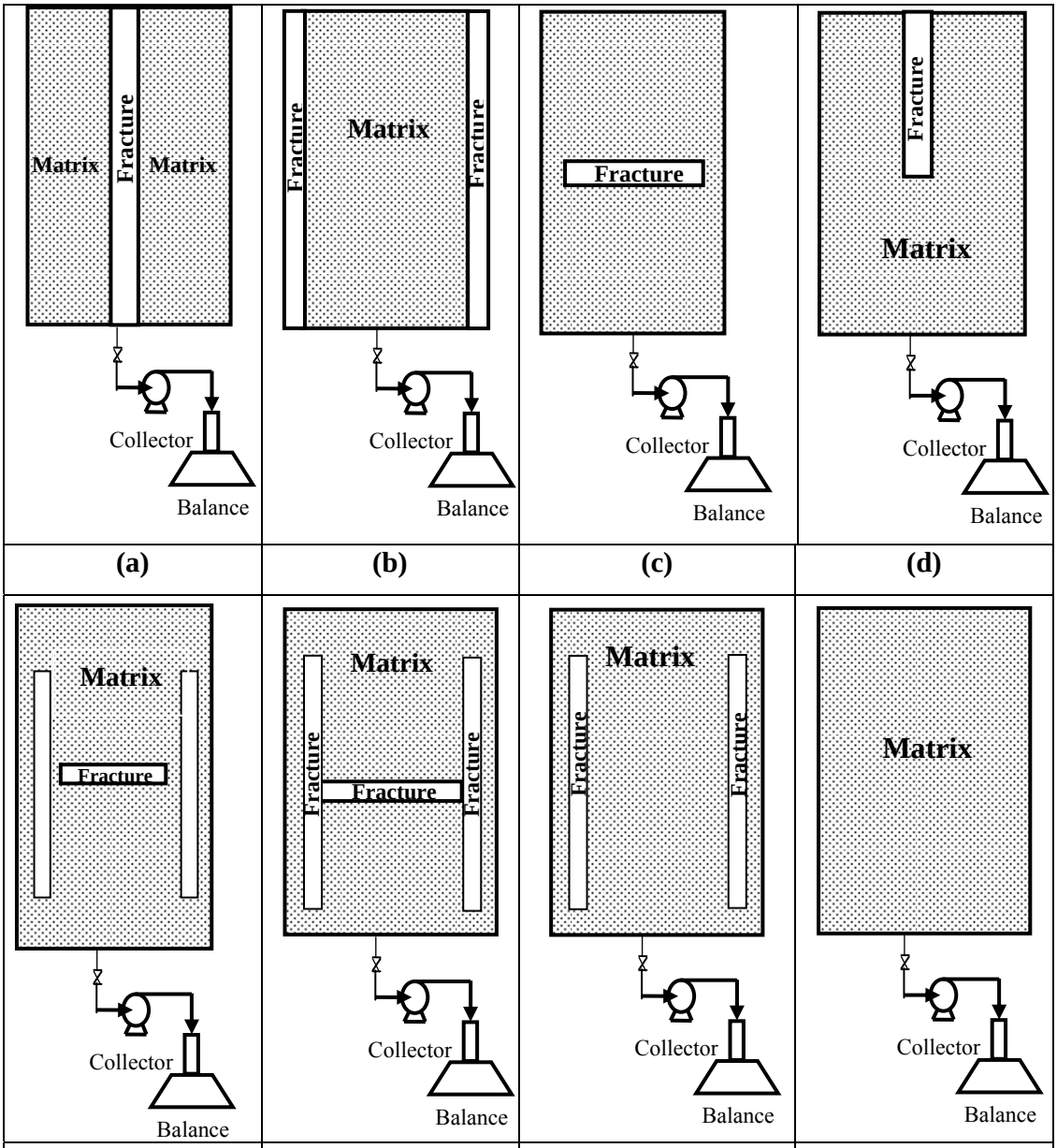

Figure 4.1: Schematic of the apparatus for controlled gravity drainage in porous media with various patterns of fractures.

Controlled gravity drainage experiments were conducted at room conditions. Pictures and movies taken at various stages of controlled gravity drainage experiments were analyzed using image processing techniques to track the gas-liquid interface movement through the matrix and fractures. To resume the same initial condition for each experiment, models were saturated by adding dry glass beads to a known volume of liquid in order to attain the desired matrix packing height. The Peristaltic pump was connected to each model's bottom part for producing liquid at various fixed discharge rates. A wide range of high and low pumping rates was then applied to each particular fractured medium.

4.3.2 Test fluids: Varsol oil, de-ionized water and aqueous solutions of Carboxy Methyl Cellulose (CMC) with different concentrations were employed as common laboratory liquids for investigating the oil recovery history and gas-liquid interfaces movement by controlled gravity drainage, primarily in fully saturated porous media models. Water viscosity was increased by adding Carboxy Methyl Cellulose (CMC) to represent different oil viscosities. The effect of CMC powder concentration on the viscosity of prepared solutions was brought in Chapter 3 (Table 3.2). The physical properties of fluids were mentioned in the previous chapter (Table 3.3).

4.3.3 Experimental procedure and data analysis approach: Controlled gravity drainage experiments were carried out in various models with different initial conditions. Some of the experiments have been repeated two or three times in order to make sure from their accuracies. For each particular experimental run, the average results were used to obtain both the production history and also G-L interface advancement in matrix and fractures. Looking at the replicate runs preformed in this study shows clearly that almost all of the performed experiments were conducted as accurately as possible, i.e. a high degree of repeatability has been achieved. A summary of model characteristics is presented in Table 4.2. Experimental results related to nineteen sample experiments are presented in Table 4.3.

As was stated before, parametric sensitivity analyses were performed in this study in order to investigate the effect of different system parameters on some aspects of the controlled gravity drainage process such as newly defined concept of "Critical Pumping Rate", and also "Maximum Possible Withdrawal Rate". The effects of model length, matrix permeability, fluid pair properties, well spacing, and fracture aperture on the controlled gravity drainage process performance were investigated. This analysis contains quantitative approach (such as analyzing the drainage rates and also cumulative production versus time and also investigating CPR and MPWR at different conditions) as well as relevant qualitative approach (analysis of interface movements in both fractures and matrix using video-recording and digital imaging techniques). Gas-liquid interface positions in both matrix and fractures "H(t)" were measured from the top portion of each individual packing all the way down along the model's height with respect to time as the gas phase invaded the fractures and matrix space respectively.

Table 4.2: Properties of employed packed models

Run No.	Fracture length, L_f (cm)	Matrix glass beads type	Porosity, %			Permeability Darcy		Viscosity (mPa.s)	Fracture aperture "b", (mm)	Fracture pattern	Well location
			ϕ_f	ϕ_m	ϕ_e	$K_{eff,f}$	K_m				
1	55	BT2	1.41	38	38.86	15979	1013	4.8 ± 0.3	5	b	Center
2	55	BT2	1.41	38	38.86	15979	1013	11.9 ± 0.4	5	b	Center
3	55	BT2	1.41	38	38.86	15979	1013	11.9 ± 0.4	5	b	Corner
4	55	BT2	1.41	38	38.86	15979	1013	1.0 ± 0.2	5	b	Center
5	55	BT2	0.92	38	38.56	3465	1013	11.9 ± 0.4	3	b	Center
6	55	BT2	0.92	38	38.56	3465	1013	4.8 ± 0.3	3	b	Center
7	55	BT3	1.41	38	38.86	15979	408	4.8 ± 0.3	5	b	Center
8	55	BT3	1.41	38	38.86	15979	408	11.9 ± 0.4	5	b	Center
9	55	BT3	1.41	38	38.86	15979	408	11.9 ± 0.4	5	b	Corner
10	28	BT3	1.41	38	38.86	15979	408	11.9 ± 0.4	5	b	Center
11	40	BT3	1.41	38	38.86	15979	408	11.9 ± 0.4	5	b	Center
12	55	BT4	1.41	38	38.86	15979	204	4.8 ± 0.3	5	b	Center
13	55	BT3	1.41	38	38.86	15979	408	1.0 ± 0.2	5	b	Center
14	55	BT4	1.41	38	38.86	15979	204	11.9 ± 0.4	5	b	Center
15	55	BT4	1.41	38	38.86	15979	204	11.9 ± 0.4	5	b	Corner
16	55	BT4	0.92	38	38.56	3465	204	4.8 ± 0.3	3	b	Center
17	55	BT4	1.41	38	38.86	15979	204	1.0 ± 0.2	5	b	Center
18	55	BT2	0.62	38	38.37	1028	1013	11.9 ± 0.4	2	b	Center
19	55	BT2	0.62	38	38.37	1028	1013	11.9 ± 0.4	2	b	Corner
20	55	BT3	1.41	38	38.86	15979	408	1.2 ± 0.3	5	b	Center
21	55	BT3	0.70	38	38.43	7989	408	1.2 ± 0.3	5	a	Center
22	55	BT3	0.23	38	38.14	2619	408	1.2 ± 0.3	5	c	Center
23	55	BT3	0.35	38	38.23	4000	408	1.2 ± 0.3	5	d	Center
24	55	BT3	1.41	38	38.86	15979	408	1.2 ± 0.3	5	e	Center
25	55	BT3	1.53	38	38.86	17120	408	1.2 ± 0.3	5	f	Center
26	55	BT3	1.21	38	38.74	13696	408	1.2 ± 0.3	5	g	Center
27	55	BT3	N/A	38	38.00	N/A	408	1.2 ± 0.3	5	h	Center

Table 4.3: Results of controlled gravity drainage experiments for 27 sample runs

Run No.	Model length L (cm)	Matrix glass beads	Fracture aperture "b" (mm)	Viscosity "μ_L" (mPa.s))	Recovery factor (%PV)	Fracture pattern	S_{or} (%PV)	CPR* "Q_{cr}", (cm^3/s)	MPWR** Q_{max}, (cm^3/s)
1	55	BT2	5	4.8 ± 0.3	85.2 ± 0.5	b	16.1 ± 0.5	8.6 ± 0.1	8.9 ± 0.2
2	55	BT2	5	11.9 ± 0.4	85.2 ± 0.3	b	16.2 ± 0.3	4.3 ± 0.3	7.1 ± 0.3
3	55	BT2	5	11.9 ± 0.4	85.1 ± 0.4	b	16.1 ± 0.2	3.8 ± 0.2	4.9 ± 0.2
4	55	BT2	5	1.0 ± 0.2	85.2 ± 0.2	b	16.2 ± 0.1	9.4 ± 0.2	11.4 ± 0.1
5	55	BT2	3	11.9 ± 0.4	85.3 ± 0.4	b	16.3 ± 0.1	4.0 ± 0.3	5.9 ± 0.2
6	55	BT2	3	4.8 ± 0.3	85.0 ± 0.3	b	16.1 ± 0.4	7.5 ± 0.1	7.8 ± 0.2
7	55	BT3	5	4.8 ± 0.3	83.0 ± 0.4	b	18.2 ± 0.3	3.1 ± 0.2	6.1 ± 0.1
8	55	BT3	5	11.9 ± 0.4	83.2 ± 0.5	b	18.3 ± 0.2	1.5 ± 0.3	5.4 ± 0.3
9	55	BT3	5	11.9 ± 0.4	83.1 ± 0.2	b	18.1 ± 0.3	1.3 ± 0.2	4.4 ± 0.1
10	28	BT3	5	11.9 ± 0.4	83.0 ± 0.4	b	18.2 ± 0.2	0.8 ± 0.1	3.8 ± 0.3
11	40	BT3	5	11.9 ± 0.4	83.1 ± 0.4	b	18.1 ± 0.3	1.1 ± 0.3	4.4 ± 0.3
12	55	BT4	5	4.8 ± 0.3	81.2 ± 0.2	b	20.2 ± 0.1	1.4 ± 0.2	5.1 ± 0.2
13	55	BT3	5	1.0 ± 0.2	83.1 ± 0.5	b	18.1 ± 0.2	6.6 ± 0.2	7.5 ± 0.2
14	55	BT4	5	11.9 ± 0.4	81.2 ± 0.3	b	20.0 ± 0.3	0.7 ± 0.3	4.8 ± 0.1
15	55	BT4	5	11.9 ± 0.4	81.2 ± 0.1	b	20.1 ± 0.2	0.5 ± 0.2	4.0 ± 0.1
16	55	BT4	3	4.8 ± 0.3	81.3 ± 0.3	b	20.2 ± 0.2	1.2 ± 0.3	4.3 ± 0.1
17	55	BT4	5	1.0 ± 0.2	81.2 ± 0.4	b	20.1 ± 0.1	3.3 ± 0.1	5.7 ± 0.2
18	55	BT2	2	11.9 ± 0.4	85.3 ± 0.4	b	16.0 ± 0.3	3.4 ± 0.1	4.9 ± 0.2
19	55	BT2	2	11.9 ± 0.4	85.2 ± 0.3	b	16.2 ± 0.2	3.1 ± 0.2	4.1 ± 0.3
20	55	BT3	5	1.2 ± 0.3	84.3 ± 0.4	b	17.1 ± 0.5	6.4 ± 0.3	7.3 ± 0.2
21	55	BT3	5	1.2 ± 0.3	84.2 ± 0.1	a	17.2 ± 0.4	6.2 ± 0.3	7.0 ± 0.1
22	55	BT3	5	1.2 ± 0.3	84.5 ± 0.3	c	17.2 ± 0.3	N/A	5.2 ± 0.3
23	55	BT3	5	1.2 ± 0.3	84.4 ± 0.5	d	17.0 ± 0.3	4.9 ± 0.3	5.9 ± 0.3
24	55	BT3	5	1.2 ± 0.3	84.2 ± 0.4	e	17.3 ± 0.1	7.0 ± 0.1	8.2 ± 0.2
25	55	BT3	5	1.2 ± 0.3	84.1 ± 0.3	f	17.1 ± 0.2	7.2 ± 0.2	8.4 ± 0.1
26	55	BT3	5	1.2 ± 0.3	84.2 ± 0.2	g	17.2 ± 0.1	6.2 ± 0.3	7.1 ± 0.2
27	55	BT3	5	1.2 ± 0.3	84.1 ± 0.4	h	17.1 ± 0.1	N/A	5.0 ± 0.3

*: Critical Pumping Rate

**: Maximum Possible Withdrawal Rate

4.4 Experimental Results and Discussion

In this section, experimental results are presented along with detailed relevant discussions. Table 4.3 presents a summary of the main results obtained from twenty seven (27) experimental runs which are the reference runs upon which most of the conclusions have been derived. In the first section, some qualitative conclusions have been made which are mainly based on critical judgment. These results are suitably supported by related mathematical relations as well as observations derived from visualization studies. In the second section, results obtained from a parametric sensitivity analysis of the process performance have been presented. This section includes a detailed quantitative approach by which one can realize the effects of various system parameters on the production performance of employed fractured media under controlled gravity drainage process.

4.4.1 Qualitative Approach: In this section, some of the experimental results are presented mainly based on the qualitative approach of process analysis. The principal sources of this analysis are visualization techniques and simple mathematical approach, as well as some related experimental data.

4.4.1.1 Liquid production mechanism for controlled gravity drainage experiments: Since pumping of liquid out of the system generates a pressure difference between the top and bottom of the model (top side is open to atmospheric pressure while suction vacuum pressure applies to the bottom side), liquid withdrawal out of the system is a combined effect of capillarity, gravity, and viscous forces. It is noted that the pumping rate could be lower or higher than the free fall gravity drainage rate, i.e. a vast domain of withdrawal rates from below to above the FFGD rate has been examined in the current study. Therefore the magnitude of pumping rate as well as gravity and capillarity forces control both pressure and fluid flow regimes in the volume which is under the drainage influence of pump.

According to the experimental results, it is observed that when the pump is set on a specific flow rate (i.e. constant withdrawal rate), there is no gas invasion through the matrix side during the early stages of the process. During this stage, gas invades into the fractures because of their lower resistance to flow (i.e. higher permeability). During these early stages in which no gas has entered into the matrix, one can write the following mass balance equation to relate withdrawal rate into the fracture parameters:

$$q = -\left(\frac{K_{eff,f}}{\mu_L} A_f\right)\left(\frac{dp}{dL}\right) \qquad (4.1)$$

The effective fracture permeability is defined as:

$$K_{f,eff} = K_f \, \phi_f \qquad (4.2)$$

where "μ_L" is the liquid viscosity , "q" is the constant pumping rate, "K_f" is the intrinsic fracture permeability, "ϕ_f" is effective fracture porosity which is fracture volume divided by total system bulk volume, and (dp/dL) is the pressure gradient along the fracture.

As time proceeds, the driving force for gas and liquid flow into the fracture decreases gradually as the driving force for liquid drainage out of the fracture also decreases accordingly. This is because of the fact that the liquid head inside the fractures decreases versus time. Unlike the starting stage of the experiment at which the invading gas phase couldn't enter into the matrix because of limiting capillary forces, it is now feasible for the gas phase to invade through both fractures and matrix simultaneously. In other words, the gas flow potential through fracture declines versus time as the liquid head within this medium gradually decreases. At a particular time, the gas invasion driving force (i.e. pressure difference) through both matrix and fractures would be equalized to each other, and from then on, the liquid drainage from the matrix side would commence. After reaching this specific point, the liquid will drain simultaneously out of both matrix and fractures. The mathematical representation of this driving force equality at the time at which gas invasion begins into the matrix is described by Equation (4.3):

$$p_f = p_m - p_{th} \tag{4.3}$$

where "p_f" is the fracture pressure, "p_m" is the matrix pressure, and "p_{th}" is the capillarity threshold pressure of the matrix.

According to the drainage phenomena observed in our simplified prototypes of fracture media, it is concluded that there are two counter-acting drainage flow paths for the liquid inside each particular system, the liquid would drain vertically downwards through both matrix and fractures based on the combined effect of gravity, capillarity, and viscous forces. Gravity forces as well as viscous forces (applied pressure driven force along both matrix and fractures) are in favor of the drainage, but capillarity forces slow down the process. At this point, another important aspect would be brought into consideration, which is the liquid communication from matrix side into the fractured space. This concept is described in detail in section 4.4.1.3. The above explanation is valid for the fractured media a, b and d as the top end of fractures is at the same level as the top end of matrix. Consider we are dealing with the models **e**, **f** and **g** in Figure 4.1. As observed in the videos recorded from gas-liquid displacement, liquid drainage starts from top part of the medium which is a region belonging to matrix part. Consequently the following equation can be written to relate pumping rate to pressure difference and other properties of fractured medium:

$$q = -\left(\frac{K_{eff}}{\mu_L} A_m\right)\left(\frac{dp}{dL}\right) \tag{4.4}$$

where K_{eff} is effective permeability for the porous medium which is a function of fracture permeability and matrix permeability, and A_m is the cross-sectional area of matrix. The above formula is applicable during controlled gravity drainage as long as the gas-liquid interface has not reached the top point of fracture network existing in the model. When the gas touched the fracture, the gas-liquid interface movement would be stopped in the porous matrix with lower permeability compared to higher permeability for the fractures and the interface starts moving in the fracture. At a specific time, the driving force for gas invasion in both matrix and fracture parts gets equal, again gas-liquid interface keep moving in the matrix and we have drainage and gas invasion through both parts of the fractured medium. The mathematical formula (4.3) indicates equalization of driving forces for invading porous matrix and fracture parts, therefore

this is valid for all fractured media under controlled gravity drainage at the time which liquid flow starts in the matrix part and gas-liquid interface movement is observed in both parts of the fractured porous media during the oil recovery method. Since we have just production from the fractures prior to gas entry into the matrix, Equation (4.1) can be used to calculate pressure difference along the fracture.

4.4.1.2 Elevation difference between G-L interface positions within matrix and fractures: The experimental data show that as long as the pumping rate is constant, the elevation difference between G-L interface positions in both matrix and fracture mediums remains unchanged during each particular controlled gravity drainage experiment. The same result has been found for the case of experimental results in free fall gravity drainage (FFGD) process (Zendehboudi et al., 2008; Zendehboudi et al., 2009). One can relate these two cases by considering the same experimental prototypes: suppose the matrix length (and as a result total height of the system) is too high by which one can neglect the threshold capillary height of the matrix compared to its length. If such a system goes under free fall gravity drainage, both the drainage rate and also elevation difference between G-L interface positions within matrix and fractures remain constant during the drainage process. Now consider the same experimental protocol, with similar fluid pairs and petrophysical properties as well as fractured system, when performing controlled gravity drainage at a liquid withdrawal rate equal to the drainage rate of FFGD process. It is predicted that these two systems behave similarly as for the production performance as well as the elevation difference between G-L interface positions within fractures and matrix.

The elevation difference between G-L interface positions in matrix and fractures strongly depends on the petrophysical properties of the porous medium, fracture properties, physical properties of the liquid-in-place, and liquid withdrawal rate. For instance, a higher pumping rate and also a smaller fracture aperture cause higher elevation distance between the G-L interfaces in fracture and matrix. This is because of the fact that the liquid communication from matrix to fracture plays an important role in establishing equilibrium between G-L interface positions and also their downward movement in both fractures and matrix. If one considers no liquid communication from matrix to fractures during the course of controlled gravity drainage experiment, the fracture would be drained quickly as it acts like an independent thin slit with negligible capillarity pressure for gas invasion. In this case, the recession rate of G-L interface within the fracture is a function of fracture properties only as well as withdrawal rate. However, the experimental results show that rate of G-L interface movement downwards through the fracture is slower than the rate by which it would move if there would be no communication between matrix and fracture. In addition, it is found that the rate of elevation recession for G-L interface within fractures and matrix are similar to each other as soon as communication starts between these two domains. In other words, elevation difference between G-L interface positions within matrix and fractures remains constant as long as one can maintain constant liquid withdrawal rate out of the system. This finding also supports the idea presented in section 4.4.1.3, i.e., the liquid communication rate is constant during controlled gravity drainage process as long as the pumping rate remains unchanged.

The above concluding remark can be supported by relevant mathematical representation of the process performance. Visualization study proved that the gas-liquid interface moves faster in fractures compared to matrix at the initial stage of the process during which the liquid has not been drained out of the matrix. Considering the downward vertical axis to be positive direction

of flow movement, one can write the following equality between the elevation difference of G-L interface positions through matrix and fractures [ΔH(t)] and interface position within matrix [$H_m(t)$] and fractures [$H_f(t)$] respectively:

$$\Delta H(t) = [H_f(t) - H_m(t)] \tag{4.5}$$

Figures 4.2, 4.3, and 4.4 represent the G-L interface position within matrix, fractures, and also their elevation difference for three selected experimental runs. As it is evident in these three figures, both "$H_f(t)$" and "$H_m(t)$" increase linearly versus time, and the amount of "ΔH(t)" is fairly constant for each of these selected experimental runs. In addition, it is evident that when liquid withdrawal rate is increased, considering all other system parameters to remain unchanged, the rate of G-L interface recession in both matrix and fractures increases as well. This increase in the recession rate of G-L interface also increases the elevation difference between the G-L interface positions within matrix and fractures. Differentiating Equation (4.5) with respect to time; one can see that the rate of elevation change for G-L interface inside matrix is the same as that of fracture.

After initiation of gas invasion through matrix, one can conduct a mass balance through a control volume perpendicular to the flow streamlines so long the withdrawal rate remains constant under the action of pump suction. This mass balance relates the constant total drainage rate to the recession rate of interface position through both matrix and fractures according to the following mathematical representation:

$$q = 2A_f\left(\frac{dH_f}{dt}\right) + \left(A_m \phi_m (1 - \bar{S}_{Lr})\right)\left(\frac{dH_m}{dt}\right) \tag{4.6}$$

in which "q" is the constant withdrawal rate, "A_f" and "A_m" are fracture and matrix cross sectional area perpendicular to the flow direction respectively, "ϕ_m" is the matrix porosity, and $\bar{S}_{Lr}$ is the average residual liquid saturation in the selected element. Since [$H_f - H_m$] is constant during the course of controlled gravity drainage under constant withdrawal rate, one can isolate the rate of change of G-L interface elevation, within the fracture or matrix, according to the following equation:

$$\begin{aligned} q &= \frac{dH_f}{dt}\{2A_f + A_m \phi_m (1 - \bar{S}_{Lr})\} = \frac{dH_m}{dt}\{2A_f + A_m \phi_m (1 - \bar{S}_{Lr})\} \\ &= \frac{dH}{dt}\{2A_f + A_m \phi_m (1 - \bar{S}_{Lr})\} \end{aligned} \tag{4.7}$$

where (dH/dt) is the recession rate of G-L elevation within matrix or fractures. Equation 4.7 states that at constant withdrawal rate for a controlled gravity drainage process with experimental conditions similar to the current study, the recession rate of G-L interface within either fracture or matrix is only a function of matrix and fracture cross sectional area, matrix porosity, and average residual liquid saturation within the model at a particular time. As a result, other parameters such as fluid viscosity and also matrix permeability would not have appreciable

effects on the magnitude of (dH/dt). In other words, one can use this conclusion to predict some experimental results. Consider the controlled gravity drainage process, with constant withdrawal rate, conducting in two dimensionally similar models in which all other parameters are different. According to Figures 4.2 and 4.3, it is concluded that although both matrix permeability and liquid viscosity have been changed, the rate of G-L interface movement through both matrix and fractures remains almost constant. It is worthwhile to note that changing matrix permeability does have an influence on the average residual liquid saturation within the matrix, but according to the experimental results (i.e. slopes of the linear correlations presented in Figures 4.2 and 4.3) this change is not significant at all.

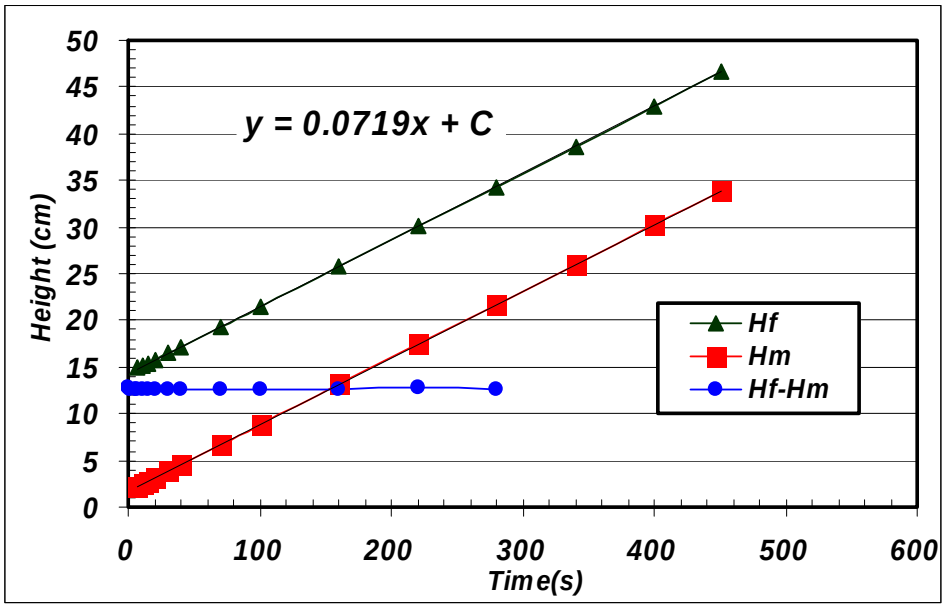

Figure 4.2: G-L interface positions in matrix and fractures versus time; matrix filled with BT3 glass beads, withdrawal rate of q = 0.75 cm^3/s, [b= 5 mm, L= 55 cm, fluid pair: Air-Water].

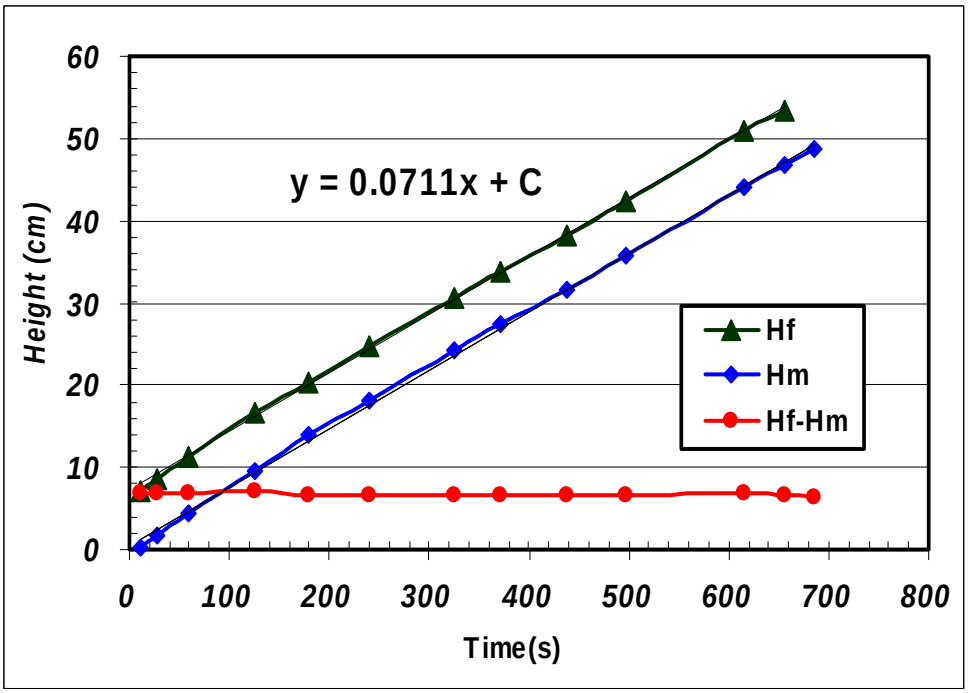

Figure 4.3: G-L interface positions in matrix and fractures versus time; matrix filled with BT2 glass beads, withdrawal rate of q=0.75cm^3/s, [b= 5 mm, L= 55 cm, fluid pair: Air-CMC solution (1%)].

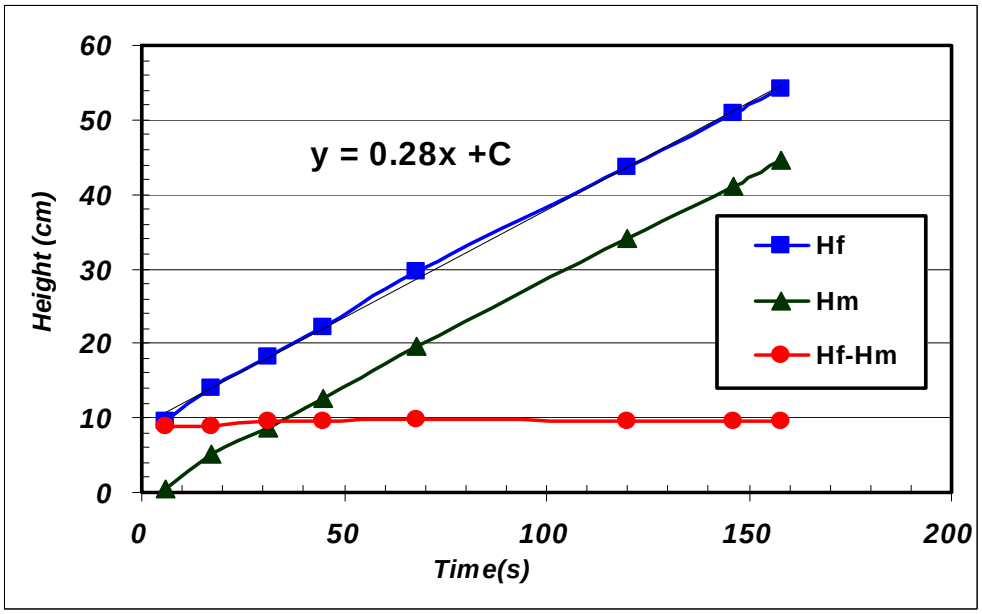

Figure 4.4: G-L interface positions in matrix and fractures versus time; matrix filled with BT2 glass beads, withdrawal rate of 2.8 cm^3/s, [L= 55 cm, b= 5 mm, fluid pair: Air- CMC solution (1%)].

Table 4.4 provides the comparison between experimentally-obtained recession rate for G-L position and the corresponding values obtained using Equation (4.7). As it is indicated in Table 4.4, these two corresponding values are in good agreement with each other. According to the

data presented in Table 4.4 and also Equation (4.1), consider two identical experimental models except their fracture aperture, which are undergoing a constant withdrawal rate. The fracture cross sectional area perpendicular to the flow direction would be lower for the model with smaller fracture aperture. As a result, the pressure gradient along the model height inside the fracture, which is a constant value for each particular model before gas entry into the matrix, would be increased by decreasing the fracture aperture. Refer to Equation 4.7, it is evident that all the contributing parameters remain unchanged except (dH_f/dt) and "A_f", so the recession rate of G-L elevation position inside fracture (as well as that of matrix) would be increased by decreasing "A_f".

Table 4.4: Experimental and predicted values of recession rate for G-L interface position inside either matrix or fractures for 12 different conditions

Withdrawal rate, (cm^3/s)	(A_m=28.2 cm^2 , Φ_m=0.38)					
	Interface velocities dH/dt, (cm/s)					
	Fracture aperture (b) = 5mm		Fracture aperture (b) = 3 mm		Fracture aperture (b) = 2 mm	
	Experimental	Predicted	Experimental	Predicted	Experimental	Predicted
0.4	0.0421 ± 0.0004	0.0386	0.0416 ± 0.0003	0.0412	0.0428 ± 0.0004	0.0425
0.8	0.0792 ± 0.0005	0.0762	0.0828 ± 0.0006	0.0824	0.0853 ± 0.0003	0.0851
2.8	0.2630 ± 0.0005	0.2661	0.2851 ± 0.0004	0.2883	0.2942 ± 0.0006	0.2980
4.6	0.4342 ± 0.0003	0.4380	0.4702 ± 0.0005	0.4742	0.4831 ± 0.0005	0.4890

4.4.1.3 System-specific drainage rates: According to the studies performed on the G-L interface positions within fractures and matrix and also their downward movement rate, a new concept of "Critical pumping rate" has been defined. The CPR is the withdrawal rate at which the height difference between G-L interfaces within matrix and fractures remains constant even if the withdrawal rate would be increased further. This concept is schematically illustrated in Figures 4.5 and 4.6. In most of the experiments conducted in the current study, this elevation difference is close to the total height of the matrix. As a result, the total matrix height dictates this defined critical pumping rate. In addition, ultimate recovery factor, just before gas breakthrough into the production side, would be unchanged at the pumping rates higher than this specific critical pumping rate. Detailed sensitivity analysis of parameters affecting CPR will be presented in the "Quantitative approach" section. Here, a qualitative analysis of the effect of fracture spacing on CPR is presented accordingly.

Another newly defined parameter which is investigated thoroughly in this chapter is the maximum possible withdrawal rate (MPWR). This rate has been defined as the maximum withdrawal rate that each particular system can maintain in a stable manner during the course of controlled gravity drainage (CGD) process. In other words, after reaching this system-specific rate, it is not possible to increase the withdrawal rate any further. This rate depends strongly on the petrophysical properties of matrix and fractures, model dimensions and fluid-pair properties.
According to Equations 4.1 and 4.2, if the fracture spacing decreases, keeping all other parameters constant, the effective fracture porosity would increase, and so does the effective fracture permeability. Considering the withdrawal rate to be constant over time, the pressure gradient along the fracture height would decrease up to the point at which gas invades into the matrix. As the gas phase invades through the matrix, Equation 4.7 governs the relationship between (dH/dt) and withdrawal rate. Decreasing fracture spacing would decrease matrix cross

sectional area; so considering all other parameters to be unchanged in Equation 4.7, the rate of G-L interface's downward movement would increase as long as a constant withdrawal rate would is established. It means, a model with lower fracture spacing experiences smaller G-L interface distance from the topside of the medium at exactly the time when the gas invades through the matrix, compared to the model with higher fracture spacing. The above mentioned analysis is valid only if the withdrawal rate from both models is identical. As a result, model with lower fracture spacing allows us to drain it at higher withdrawal rates without experiencing full drainage of the fractures, i.e. the time at which gas breakthrough occurs at the production side. Consequently, this model could tolerate higher critical pumping rate based on the CPR definition.

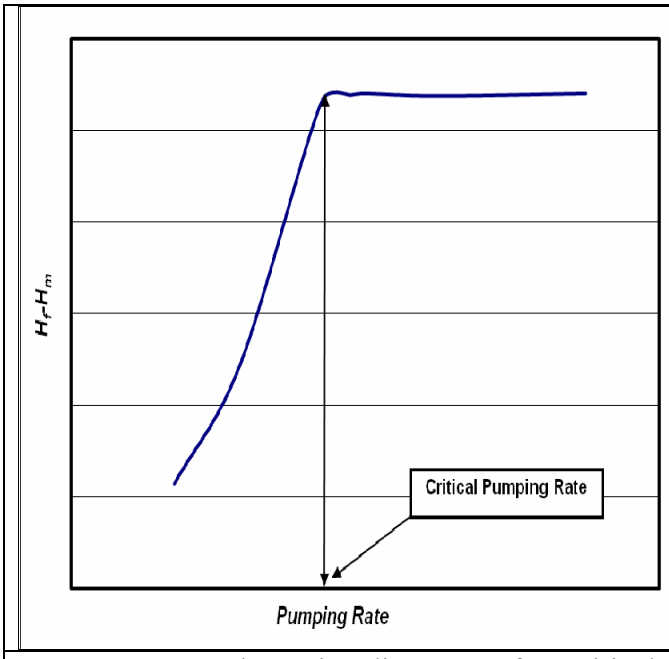

Figure 4.5: Schematic diagram of "Critical Pumping Rate" (CPR) and its relation to the height difference between the G-L interface positions within fractures and matrix.

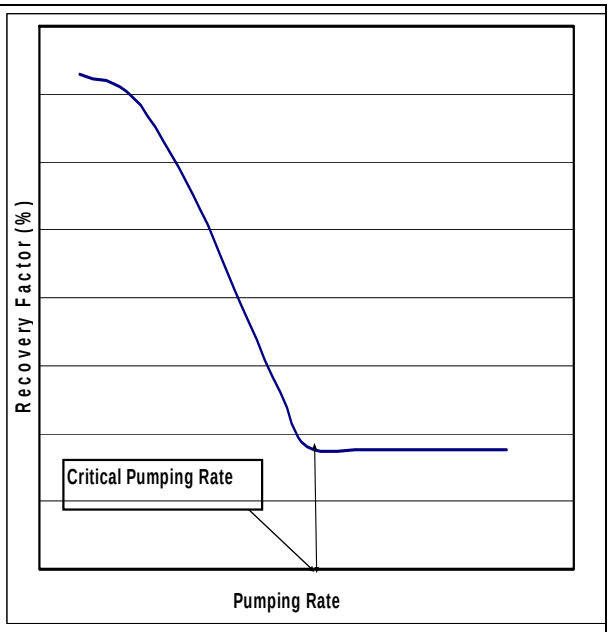

Figure 4.6: Schematic diagram representing the CPR and its relation to the recovery factor just before gas breakthrough during the controlled gravity drainage (CGD) process.

4.4.1.4 Liquid communication between matrix and fractures in CGD: Following material presented in section 4.4.1.1, it is evident that a portion of the liquid which was drained out of the matrix, has been communicating from the matrix side into the fracture sides as soon as gas invades through the matrix. It is observed that some parts of the matrix side, in the vicinity of each side fracture, are affected considerably by matrix to fracture liquid communication rather than the rest of the matrix. These portions of the matrix which are adjacent to the side fractures have higher potential for liquid flow communication. The rest of the matrix, which is far away from each fracture, is therefore not affected by the presence of fractures. Figure 4.7 shows a snap shot of the area affected by the liquid communication phenomena between matrix and fractures during the course of CGD experiment. This finding is also verified by the qualitative analysis of G-L interface movement in matrix, as the liquid-air interface in matrix is relatively flat in regions near the half-way distance of parallel fractures. However, this interface is considerably inclined towards the fractures in the area close to the side fractures.

It is believed that as long as a constant withdrawal rate would be maintained from the system, liquid communication rate between matrix and fracture remains constant as well during controlled gravity drainage process. The logic behind this qualitative observation comes from the fact that according to the experimental results and the materials presented in section 4.4.1.2, rate of G-L interface downward movement within either matrix or fracture remains constant for each particular model under constant withdrawal rate. In addition, the elevation difference between G-L interface positions within matrix and fractures also remains constant after gas invasion occurs within matrix. As a result, in order to have simultaneous liquid drainage from both fractures and matrix sides, it is necessary that the drainage driving forces within these two parts of the system should be the same. In addition, decreasing rate of these two drainage driving forces (i.e. pressure differences) should also be the same unless there wouldn't be any liquid production from the matrix side. Based on the above, one can define the communication rate to be of the form:

$$q_{com} = \alpha \frac{K_m}{\mu_L}.(p_m - p_f) \qquad (4.8)$$

where "q_{com}" is the liquid communication rate between matrix and fracture, "α" is a proportionality constant (Warren and Root, 1963; Mora and Wattenberger, 2009) which is a function of each particular model's properties (such as fracture dimensions), "K_m" is the matrix permeability, "μ_L" is the liquid viscosity, and "p_m" and "p_f" are matrix and fracture pressures respectively. If one differentiates both sides of Equation 4.8 with respect to time, considering the fact that all the parameters in the right hand side except pressures are constant for each particular fractured system, the rate of change of communication rate would be proportional to the difference between the rate of change of pressures in matrix and fractures respectively. Knowing that rate of change of matrix pressure is equal to that of fracture pressure, it is concluded that liquid communication rate remains constant during the course of controlled gravity drainage process under constant withdrawal rate.

Using the analogy between "Free-Fall Gravity Drainage" (FFGD) experiments and "Controlled Gravity Drainage" (CGD) experiments, one can also verify that the liquid communication rate would be constant for each particular system as long as the withdrawal rate remains unchanged. As it was stated before, one can consider the CGD experiments to be absolutely similar to the FFGD experiments in which height of the model is so large that the threshold capillary height within fracture is negligible compared to its height. According to the analysis performed for FFGD experiments regarding the magnitude of communication rate (Zendehboudi et al., 2008), it was found that when the rate of liquid communication reaches a constant value, (corresponding to a constant rate of drainage under free fall conditions), it remains constant as long as the drainage rate remains unchanged. As the withdrawal rate is absolutely constant for each experimental run of CGD process, it results in the communication rate to be a constant value during each CGD experimental runtime.

According to the visualizations performed in this study, the liquid communication occurs through a small portion of fracture height close to the G-L interface position within fracture. One can support the idea of liquid communication rate to be a constant value based on the fact that the difference between matrix and fracture pressures is proportional to the elevation difference between G-L interface positions within matrix and fractures measured from the top side of the

model [$\Delta H = [H_f(t) - H_m(t)]$. As the "$\Delta H$" value is constant as soon as gas invades into the matrix side, the noted pressure difference remains constant during the course of CGD process, and so does the amount of liquid communication rate. For a particular fractured system, considering all other parameters remain unchanged except an increase in the value of withdrawal rate, this could cause higher "ΔH" values and as a result, communication rate would also be increased. Therefore, this communication rate along with the withdrawal rate would affect fluid flow behavior both in fractures and in matrix.

Figure 4.7: Snap shot of G-L interface advancement [matrix filled with BT2 glass beads, Fluid pairs: Air-CMC solution (1%), b = 5 mm, Model height = 55 cm, liquid pumping rate:1.8 cm^3/s].

4.4.1.5 Viscous fingering in CGD process: The displacement of one fluid in a porous medium by another fluid depends both on heterogeneities and on the interaction of several forces. Viscous fingering in porous media is a phenomenon which results when a less viscous fluid is displacing a more viscous one. As time proceeds the interface develops a highly complex fingered pattern. In the oil industry this can lead to a poor recovery of hydrocarbon as the displacing fluid bypasses the oil. In fractured porous media, interactions between immiscible fluid phases within the fractures play a critical role on system's behavior. The presence of heterogeneities such as fractures inevitably influences the formation of viscous fingers. This phenomenon closely relates to the enhanced oil recovery for fractured porous media. The interacting between displacement process and reservoir heterogeneity is one of the most interesting topics recently. However, the boundary conditions and the interface of oil and gas are much complicated when dealing with the modeling of viscous fingering in a fractured porous medium (Gary, 2008).

The displacement conditions in the physical model used can be of two types:

1) Displacement is stable. Therefore, the gas-liquid interface is almost flat and no viscous fingering occurs.
2) Displacement is unstable and the recovery at gas-breakthrough decreases significantly because viscous fingering happens and reduces the volume swept.

There are various factors that affect immiscible displacement during controlled gravity draining and may cause viscous fingering. In what follows, the effect of some of these factors on fingering phenomena is described:

1- Pumping rate: In immiscible displacements at high flow rates smaller and more numerous fingers are formed than at low rates. To control the stability of an immiscible displacement it can be a reasonable step to control the pumping rate, therefore it is possible to obtain a stable displacement by using a rate less than a critical rate which is defined by $\frac{K_{eff}.\Delta\rho.g}{\Delta\mu}$. However in most practical situations this would imply using a rate which would not be economical.
2- Heterogeneity properties: One factor that plays a fundamental role in viscous and capillary finger formation is the heterogeneity of the porous medium. Permeability variations have been found to play an important role in finger initiation and growth (Stalkup, 1983)
3- Mobility Ratio: The effect of the mobility ratio on this process is important. If the mobility ratio (M) is less than 1, then the displacement process is very simple and efficient. The displaced fluids move ahead of the displacing fluid, and the displacement front is stable. Since typically M > 1, the front is unstable and many fingers of the mixture of the gas and the displaced fluid develop, leaving behind large amounts of oil (Sahimi, 1995).

Gravity drainage mechanisms and capillary pressure concepts suggest that for gas-liquid flow in a fracture, the fractures will be invaded by gas (the nonwetting phase) first, and then the gas can enter in the matrix space if the entry capillary pressure is exceeded. If the pump is set on a certain flow rate which is greater than the free fall gravity drainage rate, viscous fingering would be seen during controlled gravity drainage (see Figure 4.38). This phenomenon happens when the ratio of displaced fluid's viscosity to displacing fluid viscosity exhibits a high value. In our cases, the fracture presence accelerates fingers growing and their density as it was observed once the fractures gets invaded by gas, the gas penetrates into the matrix from various points and creates more fingers compared to the case when the porous medium is homogeneous.

4.4.2. Quantitative Approach: In this section, experimental results are presented for a parametric sensitivity analysis. The effects of the variation in different system parameters such as matrix properties (permeability, total height, and initial liquid saturation), fracture properties (fracture aperture and fracture configuration), fluid properties (liquid viscosity and surface tension), and well position on the recovery performance of Controlled Gravity Drainage (CGD) process have been extensively investigated.

4.4.2.1 Effect of Model height: For determining the effect of total model height on the production performance of CGD process, three different runs have been performed (Table 4.3, Run numbers 8, 10, and 11) with the same model and fluid properties but different model height.

In all of the noted cases, BT3 glass beads were used to pack the models, CMC (2%) solution-Air were used as the pair fluid and two fractures were attached to both sides of the vertically standing matrix. The only manipulated variable was the matrix height which was set at 55, 40, and 28 cm respectively. In order to determine the critical pumping rate (CPR) and Maximum possible withdrawal rate (MPWR) for each of these three different systems, each of them was drained under a series of different withdrawal rates. The effect of matrix height on production performance, the recession rate of G-L interface within matrix and fractures, the critical pumping rate, and also the maximum possible withdrawal rate were studied accordingly.

Figure 4.8 shows the effect of model height on the cumulative liquid produced under CGD process. As it is evident in this figure, the model with larger height provides higher ultimate cumulative liquid production. In addition, taller models could keep the assigned withdrawal rate for longer duration of time; hence the gas breakthrough into the production side happens far later than the shorter models. The time at which each particular graph deviates from the straight line trend is the time at which fractures have been emptied as a result of controlled liquid withdrawal. This point is a good indication for the gas breakthrough time into the production side for each particular model. It is clear that as the model height increases, this time is longer as well. Before reaching the gas breakthrough point, all the models have the same production rate controlled by the peristaltic pump. As gas breakthrough happens for each particular model, the cumulative liquid produced afterwards remains almost constant for the cases at which the constant withdrawal rate has been set to low values (like the case in Figure 4.8). On the other hands, if the withdrawal rate is high enough, the cumulative liquid production after gas breakthrough keeps on increasing until reaching its final steady value. This is due to the fact that operating the CGD process at low withdrawal rate, most of the liquid within matrix has already been drained out of the system when liquid level in fracture reaches the bottom, so the cumulative liquid production wouldn't change significantly afterwards. However, in CGD experiments with higher drainage rates, there are still lots of liquid held in matrix when gas breakthrough happens from the fracture side, i.e. cumulative liquid produced would change appreciably afterwards as matrix could still support enough liquid for drainage. For example, for the model with total height of 28cm under withdrawal rate of 0.6 cm^3/s, 212 grams of liquid were produced at the point at which gas entered into the production side (420 seconds), compared to the ultimate cumulative liquid production which is 223 grams after 1800 seconds. Taller models have higher ultimate cumulative liquid recovery as their storage capacity is higher than that of shorter models.

Figure 4.9 presents the effect of withdrawal rate on the difference between G-L interface positions within fractures and matrix during the course of controlled gravity drainage process. It was noted previously that the magnitude of "ΔH" is constant over time if the withdrawal rate remains unchanged. Figures 4.9 shows this elevation difference keeps on increasing as the withdrawal rate increases up until reaching the critical pumping rate for each particular model. This is because of the fact that increasing the withdrawal rate causes a substantial increase in the amount of applied pressure difference (i.e. driving force for drainage) over the total system. This increase in the driving force would result in a jump in the elevation difference between G-L interface positions within matrix and fractures. After reaching the CPR for each particular model, the value of "ΔH" remains constant, i.e. maintaining higher constant values of withdrawal rate compared to associated CPR wouldn't change the magnitude of "ΔH" for each particular model. As a consequence, all the height difference values reported in Figure 4.9 were up to the CPR.

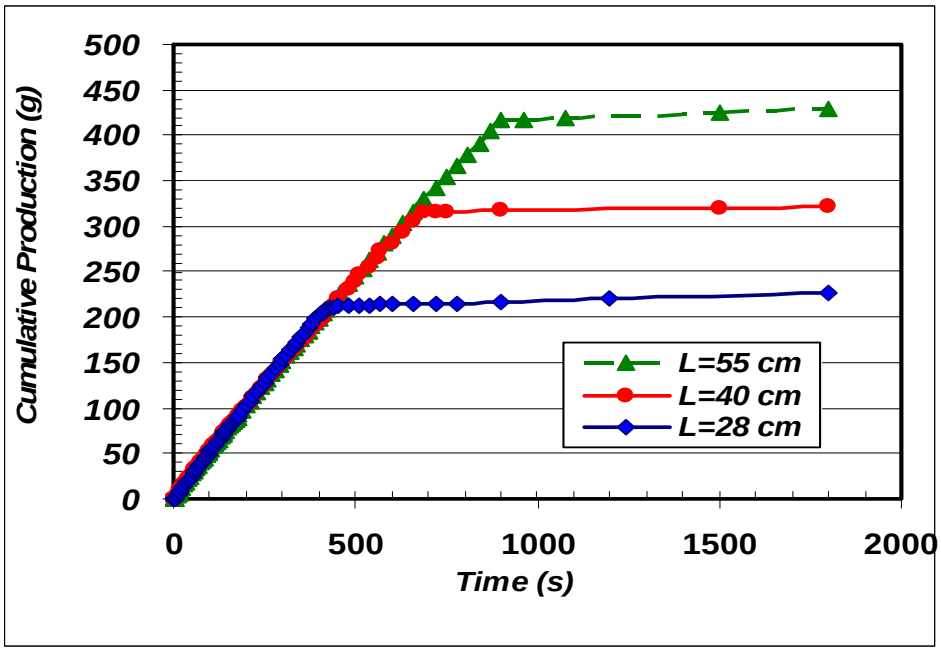

Figure 4.8: Effect of model height on the cumulative production performance during CGD process [Withdrawal rate: 0.6 cm^3/s, matrix filled with BT3 glass beads, Fluid pair: Air - CMC solution (2%), and fracture aperture (b) = 5 mm], Run No. 8, 10, and 11.

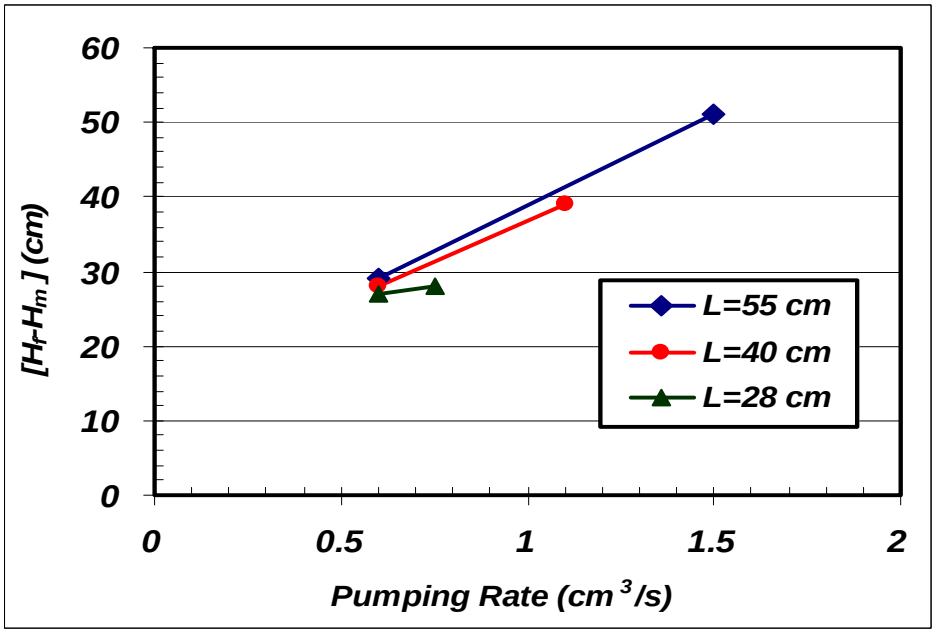

Figure 4.9: Effect of model height on the difference between G-L interface positions within matrix and fractures during CGD process [withdrawal rate: 0.6 cm^3/s, matrix filled with BT3 glass beads, fluid pair: Air - CMC solution (2%), and fracture aperture (b) = 5 mm], Run No. 8, 10, and 11.

Figure 4.10 shows that as the withdrawal rate increases up until reaching the CPR associated with each model (1.5, 1.1, and 0.8 cm^3/s for model heights of 55, 40, and 28 cm respectively), the amount of recovery factor at the point of gas breakthrough at the production side (i.e. the point at which G-L interface through fractures recedes down to the bottom of the fractures) would be decreased accordingly. After reaching the CPR for each particular model, recovery factor doesn't change appreciably when the drainage rate increases (as it is mentioned as one of the criteria for defining CPR). It is because of the fact that when each particular model is operating at a drainage rate higher than the CPR, gas breakthrough occurs very soon at the production side. Following gas breakthrough, most of the fluid withdrawing from the model is the gas phase rather than the liquid phase because of the high mobility of gas phase as well as the presence of two high flow-potential pathways (i.e. fractures) at both sides of the matrix. As a result, recovery at the gas breakthrough time for each particular model operating at high drainage rates does not change significantly compared to the value when the model was operated at its CPR. Another conclusion that could be derived from Figure 4.10 is that as the model height increases, the associated recovery factor at the gas breakthrough time also increases as long as the operating withdrawal rate remains at a similar constant value. It can be justified in the way that the longer the model is, the higher is its storage capacity. Hence at each particular fixed drainage rate, taller model have the ability to maintain that particular withdrawal rate for a longer duration of time, which leads into higher recovery factor. In other words, the taller models can maintain higher constant pumping rates without gas breakthrough for longer time period.

If a particular model would be drained at low enough withdrawal rate, the drainage process is almost like a piston-like displacement. During the drainage process, the cumulative produced liquid is a combination of liquid which was drained as the bulk liquid flow (i.e. bulk liquid withdrawal) and also the portion which comes from the film flow drainage of liquid. From fluid flow connectivity point of view, it is possible at low enough withdrawal rates that the slowly-draining liquid under the film-flow drainage type of process have enough time to communicate with the liquid which is draining ahead of the G-L interface under the influence of bulk drainage type of process within the time limitation of the CGD process. As a result, the final recovery factor, having low enough withdrawal rate, would be appreciably greater. On the other hand, when the system is draining under high constant withdrawal rate, the liquid drained under the influence of bulk-drainage type of process moves faster ahead of the liquid which is draining under the film flow type of drainage. It was experienced that at some high withdrawal rates, there might be some times during which the flow connectivity has been lost. As a result, one cannot reach the high recovery factor values under high withdrawal rates compared to those which are achievable under lower constant withdrawal rates. In most of the systems under high withdrawal rates, maximum "ΔH" cannot be maintained long enough compared to the systems operated at lower drainage rates. That is why such a system results in lower recovery efficiency.

The aforementioned discussion could also be made using the macroscopic point of view. Generally, when the drainage process is performed under high pumping rates, the liquid inside the fractures would be drained much faster than the case at which the pumping rate is low. Therefore, the possibility of liquid communication from the matrix into the fracture would be decreased. As a result, the obtained value of recovery factor just before the gas breakthrough time would be lower than the case in which liquid has enough time to communicate from the matrix to the fracture (i.e. at lower drainage rates). In addition, draining a system under low withdrawal rates results in a small "ΔH_{low}" value, and this elevation difference between interface

positions remains fairly constant until the fracture is emptied. Comparing this "ΔH_{low}" with the "ΔH_{high}" value associated with higher withdrawal rates shows that larger portions of matrix has been drained in the case where the withdrawal rate is lower (i.e. recovery factor associated with "ΔH_{low}" under lower drainage rate would be higher than that of "ΔH_{high}" under higher drainage rate.

Figure 4.11 presents the effect of model height on the "Critical Pumping Rate" (CPR) as well as on the "Maximum Possible Withdrawal Rate" (MPWR). As it is evident in this Figure, the taller the model is, the higher would be its associated CPR and MPWR. Consider the CGD experiment in one of these models up until reaching the point at which drainage occurs from the matrix side. At constant drainage rate, the rate of change of G-L interface position within fracture remains proportional to the withdrawal rate as long as no gas invasion occurs in the matrix. As a result, operating at a particular constant drainage rate, the shorter the model is, the sooner this G-L interface reaches the fracture's bottom. This implies that models with taller height could operate at higher drainage rates (i.e. higher CPR's) without having gas breakthrough at the production well. In addition, the maximum withdrawal rate that a system can sustain is proportional to its storage capacity; the taller the model is, the larger would be its associated storage capacity. It is also concluded that both of these system-specific-rates vary almost linearly with the model height if other parameters remain unchanged.

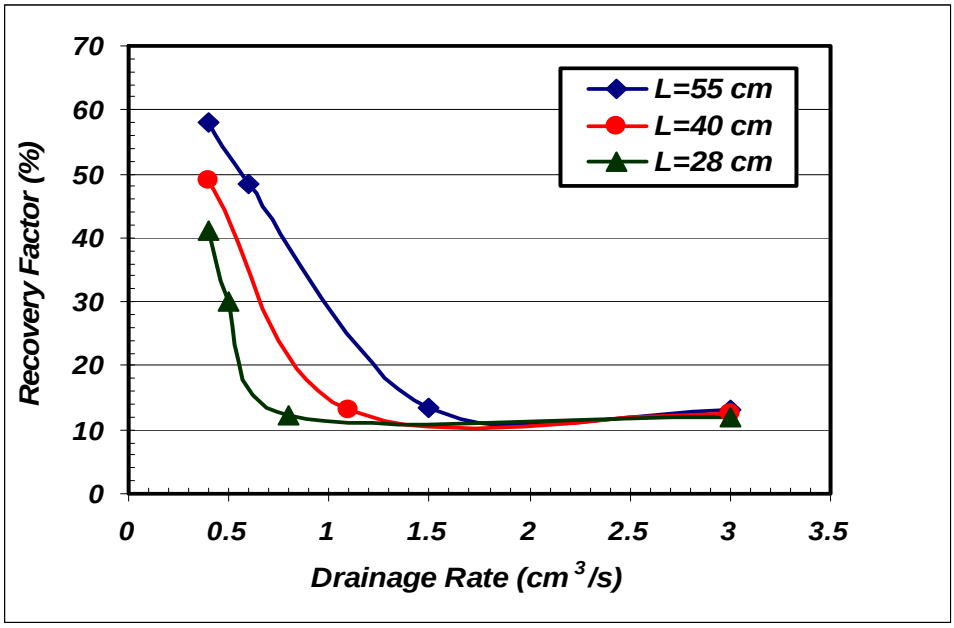

Figure 4.10: Variation of ultimate recovery factor with change in withdrawal rate for different model heights during CGD process [matrix filled with BT3 glass beads, fluid pair: Air – CMC solution (2%), and fracture aperture (b)=5 mm] , Run No. 8, 10, and 11.

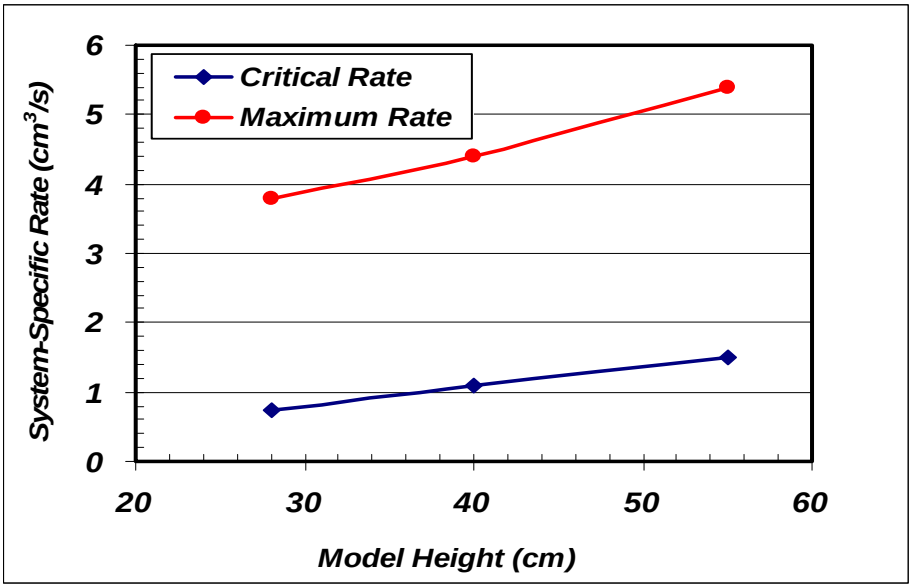

Figure 4.11: Effect of model height on the Critical Pumping Rate and also Maximum Possible Withdrawal Rate during CGD process [matrix filled with BT3 glass beads, fluid pair: Air – CMC solution (2%), and fracture aperture (b) = 5 mm], Run No. 8, 10, and 11.

4.4.2.2 Effect of fracture aperture: In the current study, the fracture aperture has been chosen as an independent parameter to be analyzed in the context of parametric sensitivity analysis. According to Table 4.3, three experimental trials (run numbers 2, 5, and 18) were selected to figure out how fracture aperture variations could affect the CGD process performance. In all of these runs, unconsolidated matrix with the total height of 55cm was prepared by packing of BT2 glass beads, and air – CMC solution (2 wt%) was used as the fluid pair. Run numbers 2, 5, and 18 represents models with fracture apertures of 5, 3, and 2 mm respectively. Figures 4.12 to 4.14 show the effect of fracture aperture on different aspects of CGD process performance.

Figure 4.12 shows the effect of fracture aperture value on the elevation difference between G-L interface positions within fractures and matrix. It is evident that at each particular withdrawal rate, the lower the value of fracture aperture is, the higher would be the associated "ΔH" magnitude. There are two reasons to support this experimental result. First of all, as the fracture aperture increases, the associated value of fracture permeability increases as well. As a result, there is smaller flow resistance against the liquid adjacent to the side of fracture to communicate into the fractures, i.e. the liquid communication rate would be increased as well. In addition, as the fracture aperture size increases, the associated fracture volume increases as well. This increase in the fracture storage capacity would avoid the G-L interface elevation within fracture to drop appreciably compared to the cases with smaller fracture apertures while both of the systems undergo the same withdrawal rate. Both of these mechanisms are in favor of keeping the "ΔH" value to be higher for the smaller magnitude of fracture aperture. It is also worthwhile to note that at very low values of withdrawal rates, it is evident that the values of "ΔH" for these three models are in the same order. It seems that operating the CGD experiments at these lower drainage rates, the above mentioned two mechanisms can support the head recession values, manipulated with the pumping action, to be approximately the same for all of these three models.

As a result, the magnitude of fracture aperture seems to have no effect on the "ΔH" value when withdrawal rate is below a certain rate (in this case 1.5 cm^3/s). Increasing the withdrawal rate above this value, one can appreciate the effect of higher fracture aperture on maintaining lower head recession value, and as a consequence, reaching higher recovery factor and CPR values.

Another conclusion, which can be derived from the results in Figure 4.12, is that for each particular model, the higher the withdrawal rate is, the higher would be the associated "ΔH" value. It is because of the increased pressure difference value along the model as the drainage rate increases. The increase in the pressure difference value causes an increase in the magnitude of "ΔH" for each particular model. The values of "ΔH" for each particular model were shown in Figure 4.12 up until reaching the "ΔH" values associated with each model's corresponding critical pumping rate (CPR's of 4.3, 4, and 3.4 cm^3/s for models with 5, 3, and 2 mm fracture aperture respectively). According to the definition of CPR, all the "ΔH" values associated with withdrawal rates higher than CPR would remain the same as the value at the CPR.

Figure 4.13 shows the effect of fracture aperture on the recovery factor, just before gas breakthrough into the production side, associated with the CGD process under different withdrawal rates up until reaching the CPR associated with each particular model. As it is evident in this figure, the recovery factor for each particular model at the time of gas breakthrough decreases as the withdrawal rate increases up until the CPR value is attained, above which the value of recovery factor remains almost constant based on the definition of CPR. The reason was discussed previously in section 4.4.2.1; increasing the drainage rate would result in an increase in the value of associated "ΔH", which in turn leave much more liquid behind in the matrix part at the time at which gas breakthrough happens from the emptied fracture. As a result, the recovery factor would be decreased during conditions of higher drainage rates. Furthermore, according to the conceptual definition of different fluid flow patterns within the matrix part of each model (bulk drainage type of flow and film-flow type of drainage), it is evident that at lower withdrawal rates, the combined effect of these two flow patterns leads to the substantial increase in the recovery factor of each particular model. On the other hand, the film-flow type of drainage cannot help the bulk-flow drainage process to be more effective in the cases with higher withdrawal rates, resulting in lower values of recovery factor at the point of gas breakthrough. According to Figure 4.13, it is also evident that models with larger fracture aperture show slightly higher recovery factor values at constant withdrawal rates compared to that of models with lower values of fracture aperture. As models with larger fracture aperture have higher fracture storage capacity, therefore, under similar circumstances of CGD type of process they should have higher recovery factor values. However due to the small differences between the fracture storativity of models with fracture apertures of 5, 3, and 2 mm, the recovery factor enhancement as a result of increased fracture aperture value wouldn't be substantial in our lab-scale cases tested.

Figure 4.14 presents the effect of fracture aperture on the values of system-specified drainage rates, namely CPR and MPWR. It is clear that models with larger fracture aperture shows higher CPR and MPWR values. Since a model with higher fracture aperture has larger storage capacity, it's MPWR would be higher as well, compared to the model with smaller fracture aperture (4.9, 5.9, and 7.1 cm^3/s for models with 2, 3, and 5 mm fracture aperture size respectively). As models with higher fracture aperture and correspondingly higher fracture permeability have lower liquid flow resistance in the fracture side, it can be concluded that they also show low flow resistance

for liquid communicating from the matrix into the fracture side when all other parameters remain unchanged. As a result, the liquid communication appears to be higher in the cases with larger fracture aperture. This could be another possible reason behind for obtaining higher values of MPWR for models with larger fracture aperture.

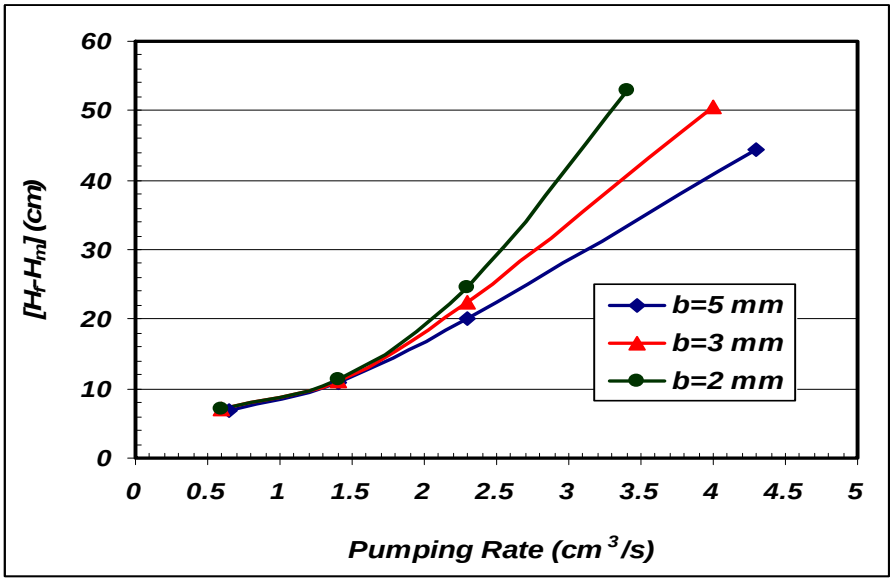

Figure 4.12: Effect of magnitude of fracture aperture on the elevation difference between G-L interface positions in matrix and fractures during CGD process under different constant-withdrawal-rates [matrix filled with BT2 glass beads, fluid pair: Air - CMC solution (2%)].

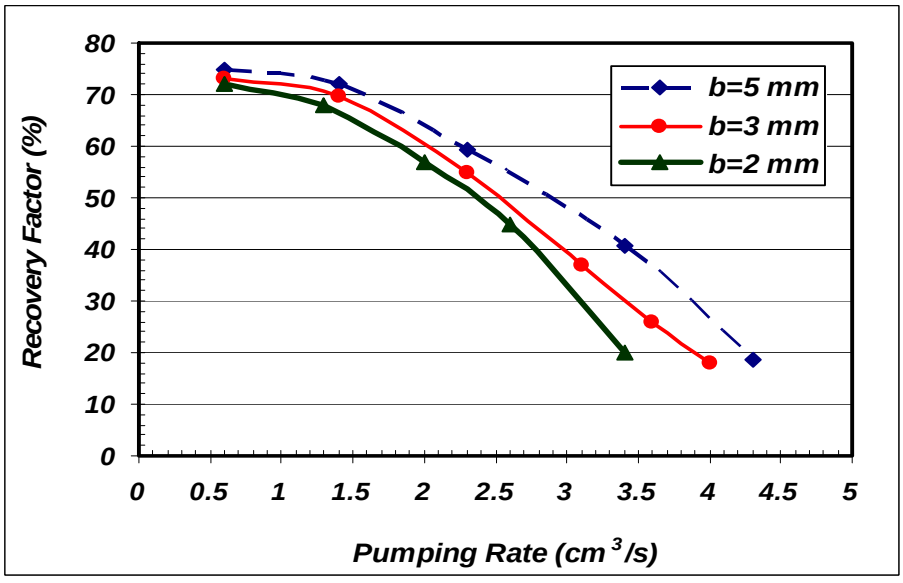

Figure 4.13: Recovery factor at the time of gas breakthrough as a function of withdrawal rate for different magnitudes of fracture aperture during the course of CGD process (matrix filled with BT2 glass beads, fluid pair: Air - CMC solution (2%)].

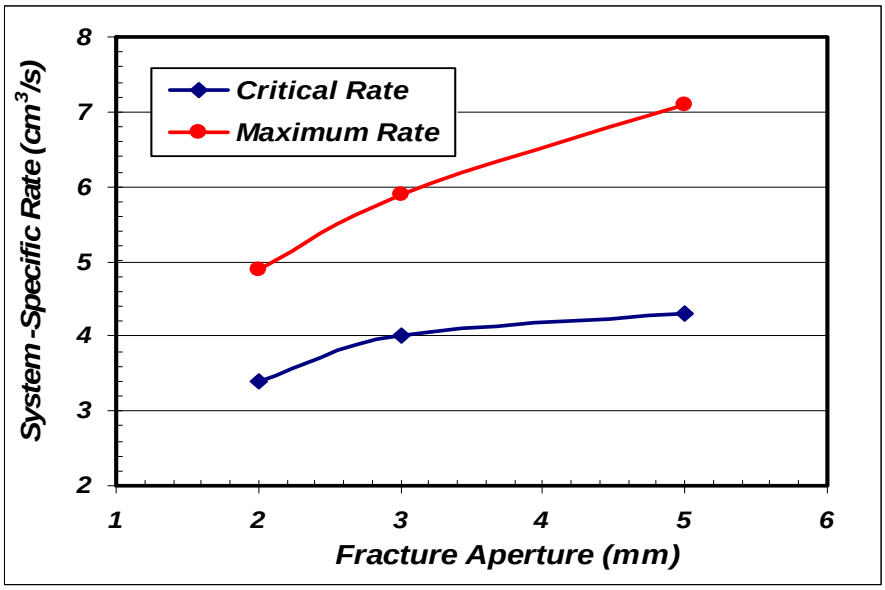

Figure 4.14: Effect of fracture aperture size on the magnitude of CPR as well as MPWR during the course of CGD process (matrix filled with BT2 glass beads, fluid pair: Air - CMC solution (2%)].

4.4.2.3 Effect of matrix permeability: In this section, the various impacts of matrix permeability (i.e. size of the glass beads packed as the matrix medium) on the production performance of controlled gravity drainage process are discussed in detail referring to Figures 4.15 to 4.19. Three different types of unconsolidated models were employed in terms of the size of packing materials. The aforementioned Figures represent the experimental data related to the run numbers 1, 7, and 12 according to Table 4.3. In all of these experimental runs, models were packed to the ultimate height of 55cm, and one vertical fracture with 5 mm aperture size was also attached along each side of the models. All these models were saturated with 1wt% aqueous solution of CMC prior to the CGD experiments.

Figures 4.15 and 4.16 represent the production history of fractured models with different matrix permeability values under two different withdrawal rates (0.6 and 6 cm^3/s respectively). Considering Figure 4.12, it is evident that at the beginning stages of the CGD experiment, all models show similar production behaviour. It seems that this behaviour continues up until passing around 130 seconds of the process duration at which these three curves start to branch off. This might be because of the fact that during this stage, most of the produced liquid has been fed from the fractures into the production side. As the fracture properties are the same, the production history within this period remains similar to each other. Thereafter, when matrix starts to influence more significantly the drainage process, these three curves begin to deviate from each other as the matrix properties (i.e. permeability) differs from one model to the other. The same phenomena can be observed in Figure 4.16, but for a limited time extent. This is because of the fact that when the CGD experiment was performed at higher drainage rates (6 cm^3/s compared to 0.6 cm^3/s), fractures have limited time to compensate for the withdrawal rate. In other words, low storage value associated with each fracture could only handle the higher withdrawal rate (6 cm^3/s, Figure 4.16) for a shorter period of time compared to the case with

lower drainage rate (0.6 cm^3/s, Figure 4.15). It is clear that the higher the matrix permeability value is, the higher would be the associated cumulative production as well as the recovery factor. Since models in which the matrix side comprised of coarser grain size have larger permeability, the liquid can drain easier than in cases with tighter matrix component. This point is verified by both graphs presented in Figures 4.15 and 4.16. In addition, it is clear that after the separation point (i.e. the point at which these three graphs have been branched off in which the acting drainage rate wouldn't be the same as the nominal one) happened in both of these figures, each of these models produced at a different constant withdrawal rate although a constant predetermined drainage rate has been set for all of them. Only the most permeable one could maintain the drainage process at that particular nominal rate. The other two tighter models failed to sustain the rate, i.e. gas breakthrough happened earlier through their emptied fracture space. This separation point happened to be created sooner when all three models were initially operating under higher nominal drainage rate (i.e. 6 cm^3/s). According to Figure 4.15, as the nominal drainage rate is far below the MPWR (Figure 4.19) associated with all three models, it could be maintained for a longer period of time. Even after the separation point, the difference between the nominal and actual withdrawal rates for each of these three models is not an appreciable amount. However, a slightly different conclusion could be made based on Figure 4.16, in which the nominal drainage rate is almost equal to the MPWR of model with BT3 as the matrix continuum, slightly higher than that of model with BT4-type of matrix, and still well below that of model with BT2-type matrix. According to this Figure, the separation point happens sooner as BT3 and BT4 model couldn't even sustain the nominal drainage rate for an appreciable duration of time. The more permeable matrix (with BT2 glass bead size as the matrix continuum) can only be drained at the nominal drainage rate for less than 100 seconds. In addition, the difference between the nominal and actual drainage rates for each of these three models is significant.

Another observation that can be made based on these two plots is that all the production history curves become flat after some time associated with each particular model and drainage rate. It is clear that the higher the withdrawal rate is, the sooner a particular model would be drained (i.e. the sooner will be the gas breakthrough time into the production side), and as a result, the level-off point happens sooner as well. Consequently, the final recovery factor for the model containing the most permeable matrix is just over 85% of the Initial Liquid in Place (ILIP) during 1800 seconds of experimental runtime, while almost similar recovery factor values are attained for the models with BT3 and BT4 as the matrix (83% and 81% of ILIP respectively) after 4500 seconds of experimental time. However, if all of these experiments would be continued for an appreciable longer time (more than 10,000 seconds according to our experimental time durations), the ultimate residual liquid saturation in all models would be reached the nominal values of residual liquid saturation in unconsolidated porous media (7-10% of ILIP), depending on the matrix properties (Kantzas et al, 1988; Zendehboudi et al, 2008).

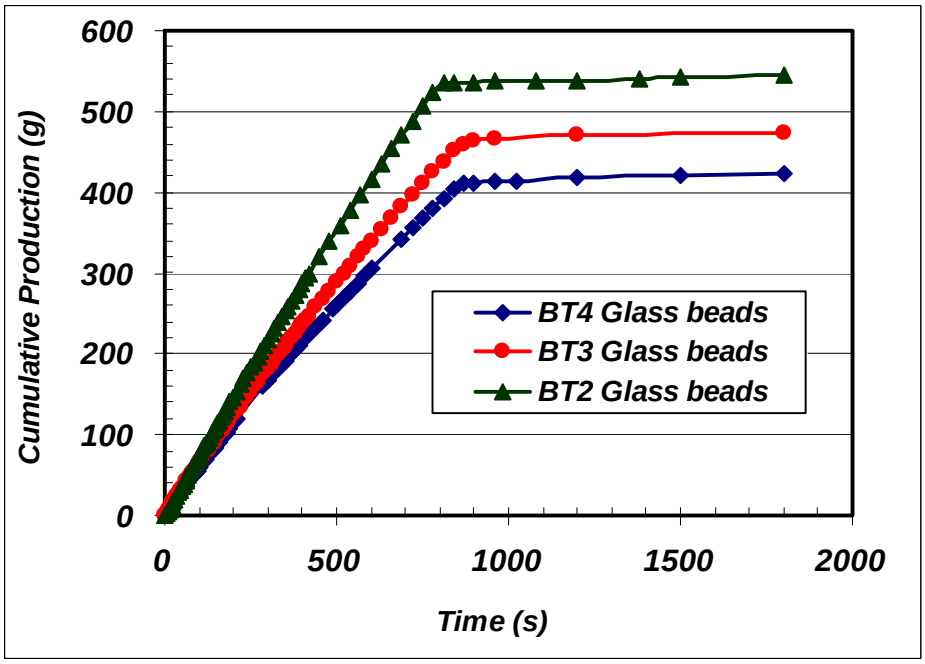

Figure 4.15: Effect of matrix permeability on the production history of fractured prototypes during the CGD process withdrawal rate of q = 0.6 cm^3/s [b= 5 mm, Model height = 55 cm, fluid pair: CMC solution (1wt%)-Air].

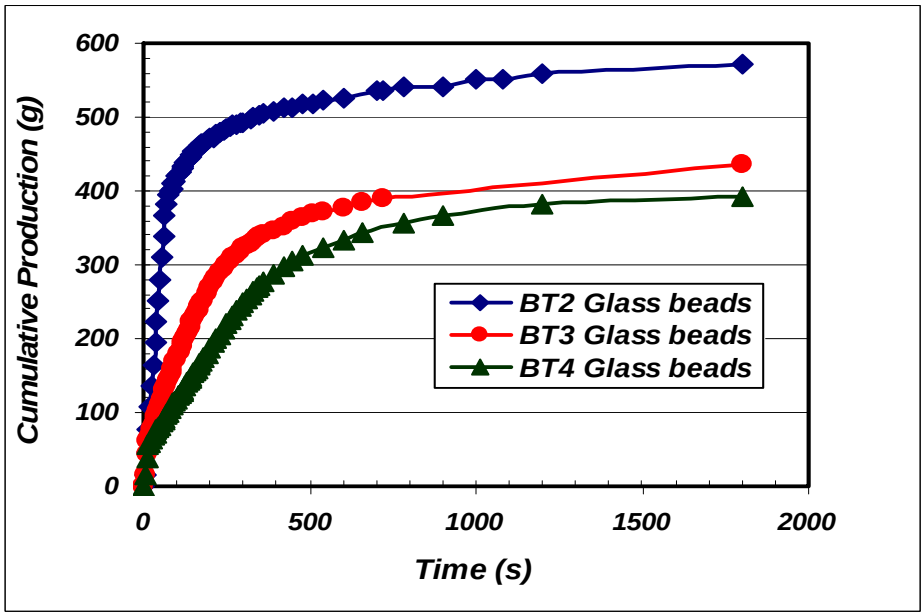

Figure 4.16: Effect of matrix permeability (glass bead sizes of BT2, BT3, and BT4) on the production history of fractured prototypes during the CGD process for withdrawal rate of q = 6 cm^3/s [b= 5 mm, model height = 55 cm, fluid pair: CMC solution (1wt%)-Air].

Figure 4.17 shows the effect of matrix permeability on the elevation difference between G-L interface positions within matrix and fractures. It appears that even at low constant drainage rates, this elevation difference is high for models with tighter matrix; so the more permeable the matrix is, the lower would be the associated value of "ΔH" when controlled gravity drainage experiments was done with constant withdrawal rate. As the matrix permeability significantly affects the rate of liquid communication, this rate would be lower for the case of tighter matrices. As a result, the associated values of "ΔH" would be higher than that of a matrix with higher permeability. In such a model with high values of "ΔH", gas breakthrough at the production face happens sooner than the case with higher matrix permeability. In addition, when the matrix permeability is low, the drainage of liquid is smaller compared to the cases in which the matrix has a higher permeability value. As a consequence, fractures play more important role in providing liquid to be drained out of the system in the case of matrix having low permeability value. As the fracture properties (i.e. fracture length and aperture) are the same for all these models, the liquid level within each fracture recedes more in the downwards direction compared to the cases with higher matrix permeability. This would result in higher "ΔH" values associated with lower matrix permeabilities. Another conclusion which could be pointed out here is that for each particular model (i.e. constant matrix permeability), the value of "ΔH" keeps on increasing when the nominal drainage rate increases. When withdrawing liquid from a particular model having constant matrix properties at higher nominal rates, a higher pressure gradient across the model height develops and this increases the pressure drop in the form of increased "ΔH" value.

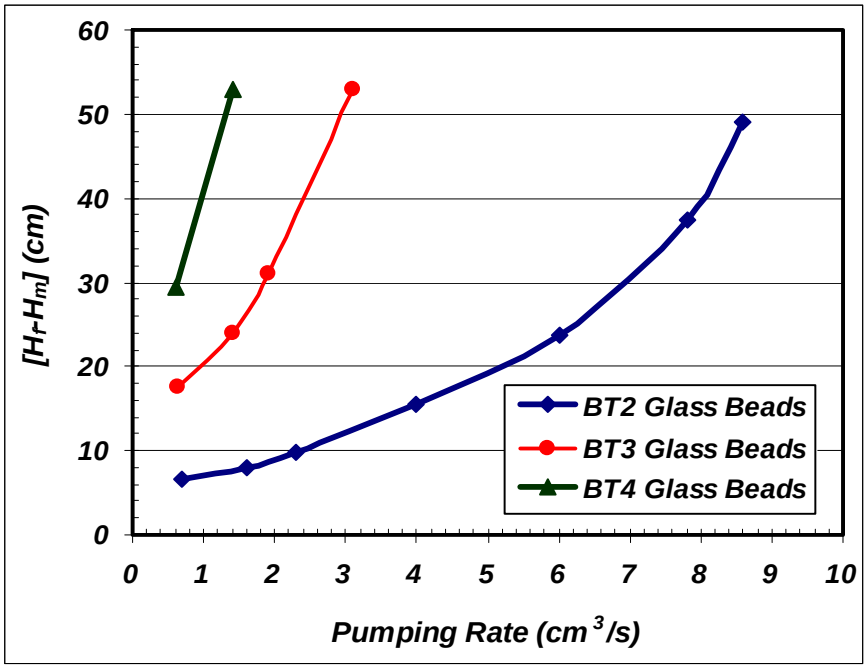

Figure 4.17: Effect of matrix permeability on the height difference between G-L interface positions within matrix and fractures during the CGD process at different levels of withdrawal rate [b= 5 mm, model height = 55 cm, fluid pair: CMC solution (1wt%)-Air].

According to the physics of CGD process and the experimental results presented in Figure 4.17, it is expected that models with low matrix permeability values should show a high value of "ΔH"

even at very low flow rates. This has been verified based on the data points presented in Figure 4.17, as the model with low values of "K_m" (i.e. matrix composed of BT4 glass bead) shows a "ΔH" equivalent to 30 cm even at the withdrawal rate of 0.6 cm^3/s. This high "ΔH" value can be achieved for models with matrices composed of BT3 and BT2 even if the associated withdrawal rates reach 1.8 and 7 cm^3/s respectively. As a result, the CPR value would be higher for the models in which their matrix is of higher permeability (Figure 4.19).

Following the discussion presented regarding results shown in Figures 4.15 and 4.16, one can compare the recovery factor values of these three models in order to examine the effect of matrix permeability on the CGD production performance. Figure 4.17 presents this parametric sensitivity analysis, in which one can appreciate the negative effect of matrix permeability reduction on the recovery factor (just before gas breakthrough into the production face) at each particular constant withdrawal rate. As the matrix is the main storage of liquid within each fractured system, its role in providing liquid for the drainage process would be reduced so long its permeability has been reduced accordingly. This could result in lower recovery factor of such a system with reduced matrix permeability. Aside from that, it is also evident that for each particular model with constant matrix permeability, an increase in the withdrawal rate of CGD process would results in a decrease in the associated recovery factor values. This recovery factor decrease is substantial for the cases in which the matrix permeability is lower in value (BT3 and BT4 respectively). It seems that the sensitivity of recovery factor to withdrawal rate for each particular medium is much more severe whenever the matrix permeability is lower. This point can also be supported using the logic presented previously about the combined effect of two different drainage fluid flow patterns within the matrix.

The magnitude of matrix permeability has also a profound effect on the system-specific withdrawal rates, namely CPR and MPWR. As demonstrated in Figure 4.19, both of these system-specific drainage rates, CPR and MPWR, increase almost linearly when the matrix permeability increases. As matrix permeability increases, liquid transmissibility from matrix to fracture increases as well, so a porous medium with fractures is capable of providing higher drainage rates without gas breakthrough at the production side (i.e. higher values of CPR). In addition, such a model has also higher drainage capacity (even in case of gas breakthrough, i.e. MPWR) than models with lower matrix permeabilities. This is due to the higher liquid communication rate from matrix to fractures as well as lower liquid flow resistance as a result of the high matrix permeability. It is expected that if the matrix permeability increases beyond that of BT2 beads, these two graphs would coincide as a single graph (i.e. with the same increasing rate behavior). This is due to the fact that liquid communication rate increases accordingly as the matrix permeability value increases. It is also clear that as the matrix permeability approaches that of fracture, these two media behave as a homogeneous medium, i.e. both of these specific rates would be the same.

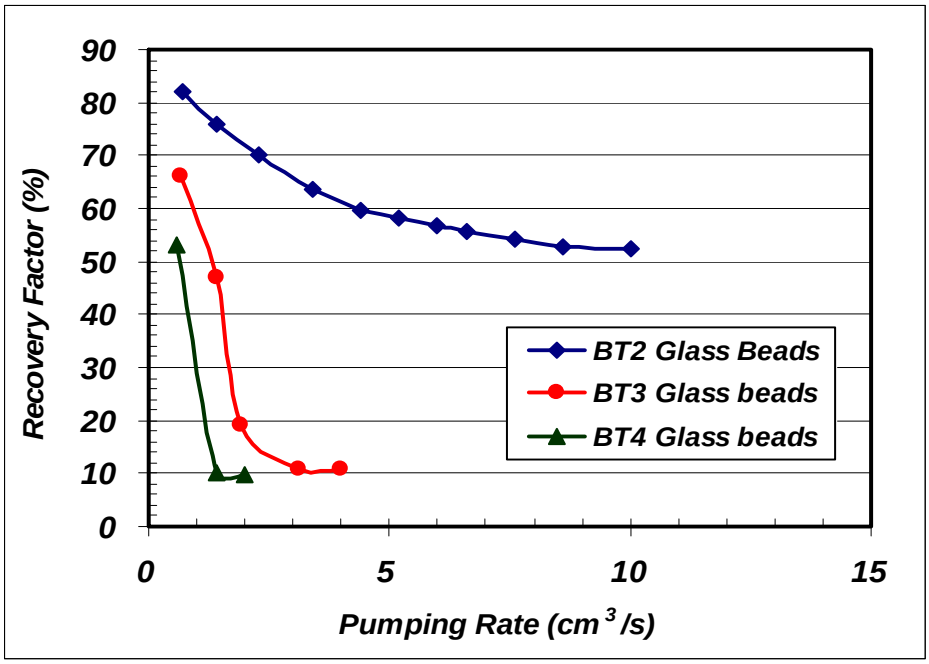

Figure 4.18: Effect of matrix permeability on the recovery factor values before gas breakthrough into the production side during the CGD process at different levels of withdrawal rate [b= 5 mm, model height = 55 cm, fluid pair: CMC solution (1wt%)-Air].

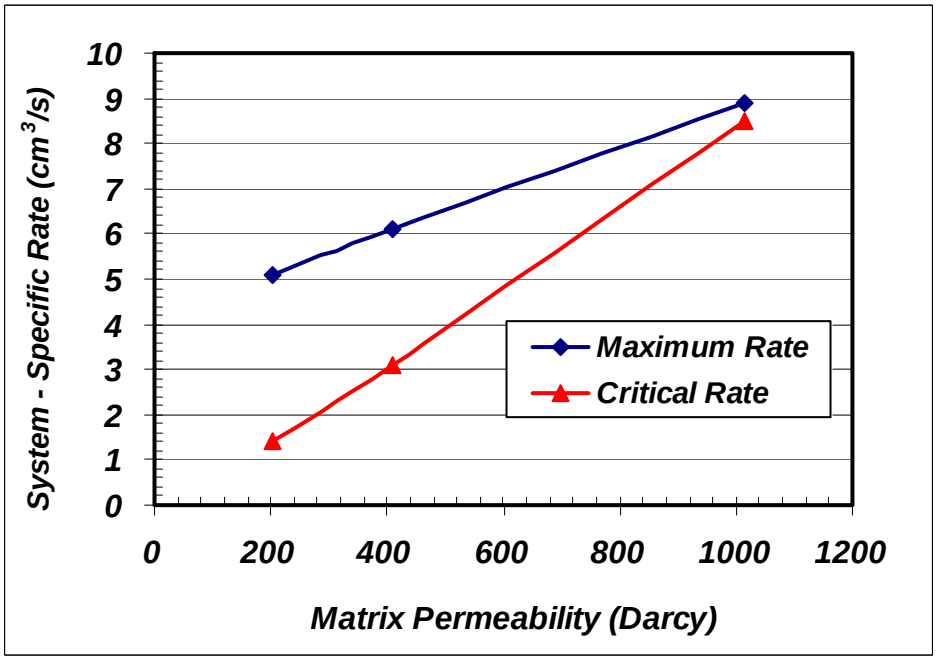

Figure 4.19: Effect of matrix permeability on the magnitude of CPR as well as MPWR during the CGD process [b= 5 mm, model height = 55 cm, fluid pair: CMC solution (1wt%)-Air].

4.4.2.4 Effect of liquid viscosity: An important factor which has a significant impact on the CGD process performance is the liquid viscosity. To achieve different liquid viscosities in our CGD experiments, aqueous solutions of CMC with different concentrations were used as the test liquid, focusing on cases that have higher viscosities than that of water. Controlled gravity drainage tests were performed using models with similar matrix permeability values (BT4 as the packing agent), same model height (i.e. 55 cm), and the same fracture aperture magnitude (5 mm), but different test-liquid properties (i.e. viscosities). This information is summarized in Table 4.2 as run numbers 12, 14, and 17.

Figure 4.20 shows the impact of liquid viscosity on the magnitude of elevation difference between the G-L interface positions within matrix and fractures. The "ΔH" values have been documented up until the values corresponding to the CPR were reached, and from then on, this height difference remained almost unchanged for each particular model. From this Figure, it is evident that the liquid level in the fracture drops faster in the downwards direction (i.e. magnitude of "ΔH" increases with a steeper slope) when the liquid viscosity is higher than water. The reason is that at higher liquid viscosities, the liquid communication rate between matrix and fractures would decrease and as a result, there is no liquid flow support from the matrix side to avoid excessive recession of the G-L interface within the fractures compared to that of matrix. As a consequence, the rate of change of this elevation difference with respect to the drainage rate (i.e. $\frac{d(\Delta H_{F-M})}{dq}$) would be higher for the cases in which the liquid viscosity is higher as well.

Figure 4.20 presents the effect of liquid viscosity on the magnitude of recovery factor just before gas breakthrough into the production side. It is evident that for each particular liquid viscosity, the recovery factor values decrease as the nominal drainage rate increases. As the increased value of liquid viscosity results in a substantial decrease in the liquid communication from matrix to fracture, the recovery performance of such a system also decrease as well. In addition, at a constant withdrawal rate, it is clear that the higher the liquid viscosity is, the lower would be its associated recovery factor. Furthermore, one can see that all these three curves have been leveled off after reaching their CPR level (3.3, 1.4, and 0.7 cm^3/s as the viscosity level increases accordingly), which is compatible with the original definition of critical pumping rate for each particular porous medium with fractures. It is also worthwhile to consider the relative slope of each particular curve just before leveling-off point, i.e. the relative effect of withdrawal rate on the recovery performance of each particular system. It is evident that the higher the liquid viscosity is, the more affected would be the system recovery performance based on an increase in the withdrawal rate. This point is proven based on the increasingly steeping slope of each particular curve just before the leveling-off point. This point was also supported by the data points of Figure 4.20, in which systems with higher liquid viscosity has sharper rate of change of "ΔH" in response to an increase in the drainage rate, hence the recovery performance also would be decreased rapidly for such a system as a result of withdrawal rate increase.

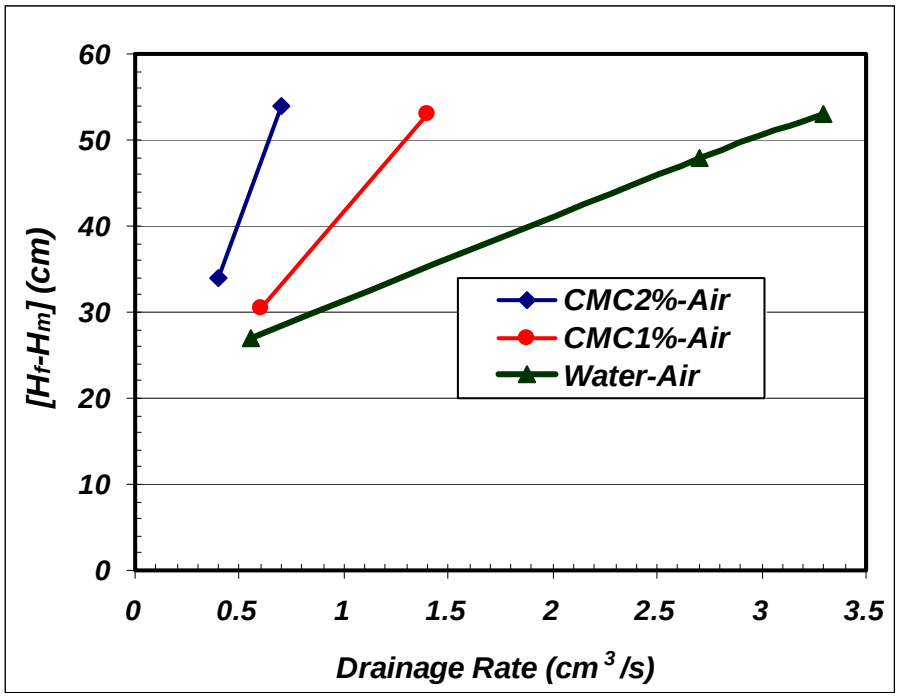

Figure 4.20: Effect of liquid viscosity on the elevation difference between G-L interface positions within matrix and fractures during the CGD process [matrix filled with BT4 glass beads, model height = 55 cm, b = 5 mm].

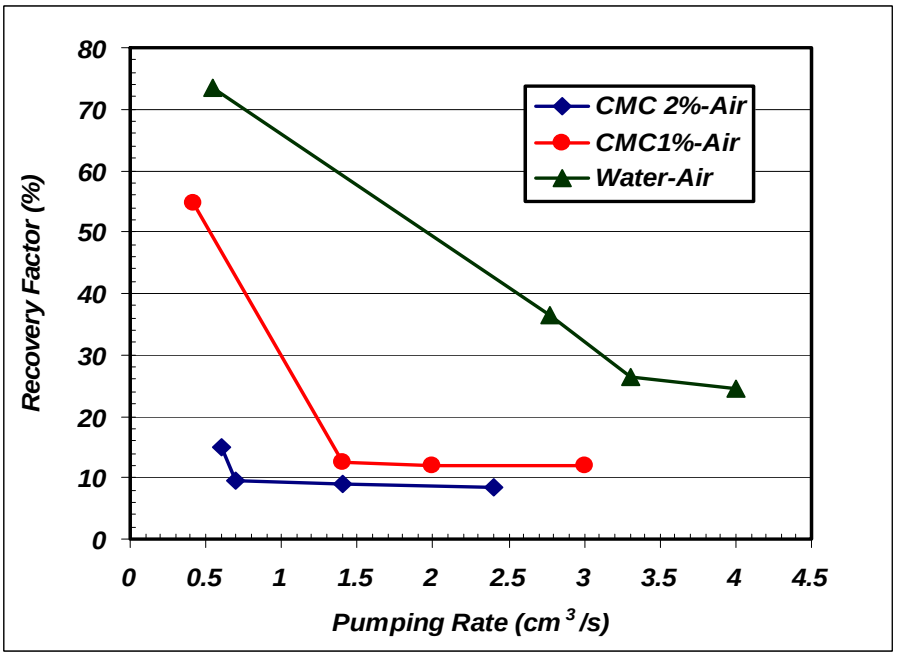

Figure 4.21: Effect of test liquid viscosity on the recovery factor at the gas breakthrough time during the CGD process [matrix filled with BT4 glass beads, model height = 55 cm, b = 5 mm].

Liquid viscosity also affects the two previously defined system-specific rates, CPR and MPWR. According to Figure 4.22, both of these rates are decreasing as a result of an increase in the liquid viscosity. It is expected that the CPR curve would be flattened off after reaching a limiting liquid viscosity point. As the magnitude of CPR is significantly affected by the liquid communication rate, it is expected that at a particular viscosity value, this communication rate would be ceased. In addition, the maximum withdrawal rate that a system can sustain is also affected by the viscosity value of the liquid. It is evident that the higher the liquid viscosity is, the lower would be the magnitude of MPWR.

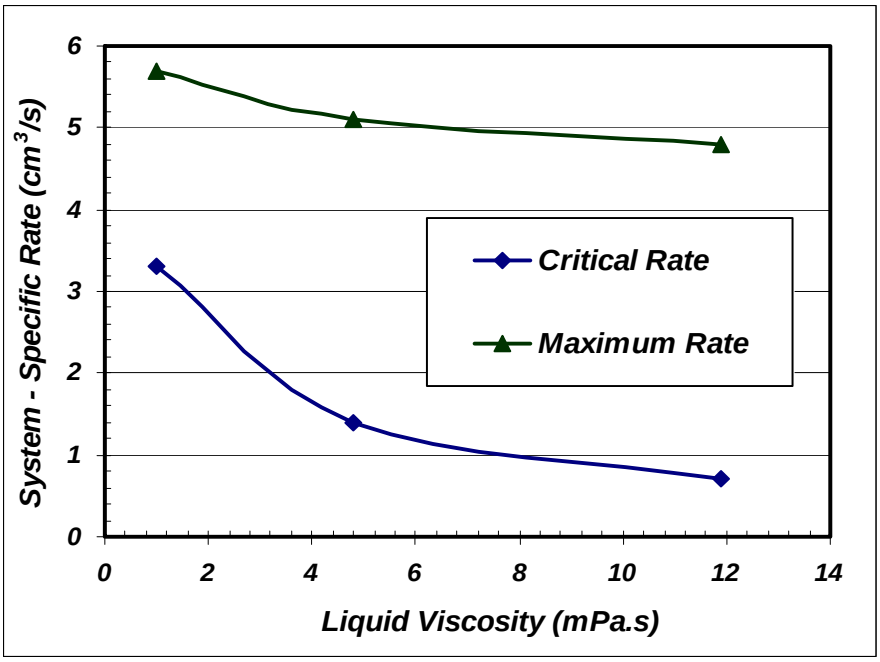

Figure 4.22: Effect of liquid viscosity on the system specific drainage rates during the CGD process [matrix filled with BT4 glass beads, model height = 55 cm, b = 5 mm].

4.4.2.5 Effect of liquid interfacial tension: In order to investigate effect of interfacial tension on the recovery performance and interface positions in matrix and fracture, we saturated the BT3 glass beads porous media using Varsol oil in one case and water in another case and then performed controlled gravity drainage at different pumping rates. Figure 4.23 and 4.24 present the effect of liquid type on the values of system-specified drainage rates, namely CPR and MPWR. These two system specific rates have higher values for the model which was saturated with water (6.6 and 7.5 cm^3/s, correspondingly) compared to the model in which the Varsol oil is test fluid (6.4 and 7.3 cm^3/s, correspondingly) however as seen the difference between those specific rates is small in the two models under controlled gravity drainage and this difference is due to small difference between viscosities of those test liquids.

Figure 4.23 shows the influence of liquid type on the magnitude of elevation difference between the G-L interface positions within matrix and fractures. The "ΔH" values has been demonstrated up until reaching the values corresponding to the CPR, and from then on, this height difference remains almost unchanged for each particular model. Another conclusion can be drawn that the rate of change of this elevation difference with respect to the drainage rate would be higher for the cases in which liquid viscosity is higher as well. The reason for that issue is being lower communication between matrix and fracture in the medium saturated with Varsol. Also if we have two identical fractured porous media which are saturated with two test fluids with the same viscosity, but different interfacial tension under controlled gravity drainage. The experimental results show that if they produce with the same rate, recession rate of G-L elevation within either matrix or fractures would be identical for both systems, however (H_f-H_m) for the model saturated with higher interfacial tension is higher and the difference between the (H_f-H_m) is (h_{c1}-h_{c2}). Figure 4.23 shows this, as the gas-liquid interface position in fracture for the model saturated with water always is almost 6 cm lower compared to that for the medium saturated with Varsol every time, when the model produce liquid with a constant withdrawal rate during CGD.
The theoretical concept related to flow in porous media and experimental results infers that interfacial tension doesn't affect magnitude of MPWR if other liquid properties and model properties remain unchanged, and but it does affect (H_f-H_m) and consequently this changes the amount of critical pumping rate .Reduction of IFT can play a significant role in improving the final recovery, due to increased gravity effects, which in turn, change the process from capillary counter-current flow to gravity driven co-current flow, though it does not change considerably the recovery performance at gas breakthrough during controlled gravity drainage process.

Figure 4.24 shows the recovery factor at gas breakthrough versus pumping rate for water and Varsol air.

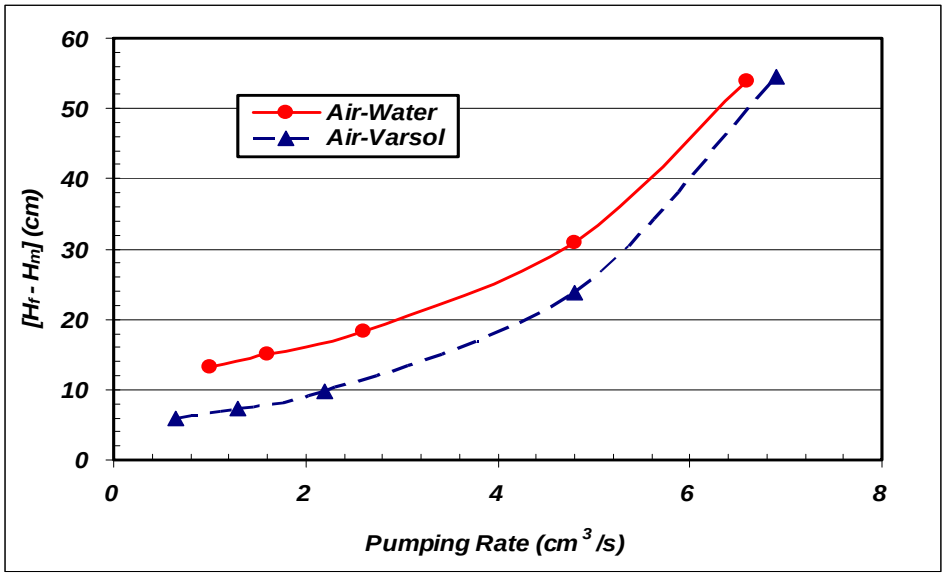

Figure 4.23: Effect of interfacial tension on the elevation difference between G-L interface positions in matrix and fractures during CGD for different withdrawal-rates [matrix with BT3 glass beads, fracture aperture b= 5 mm].

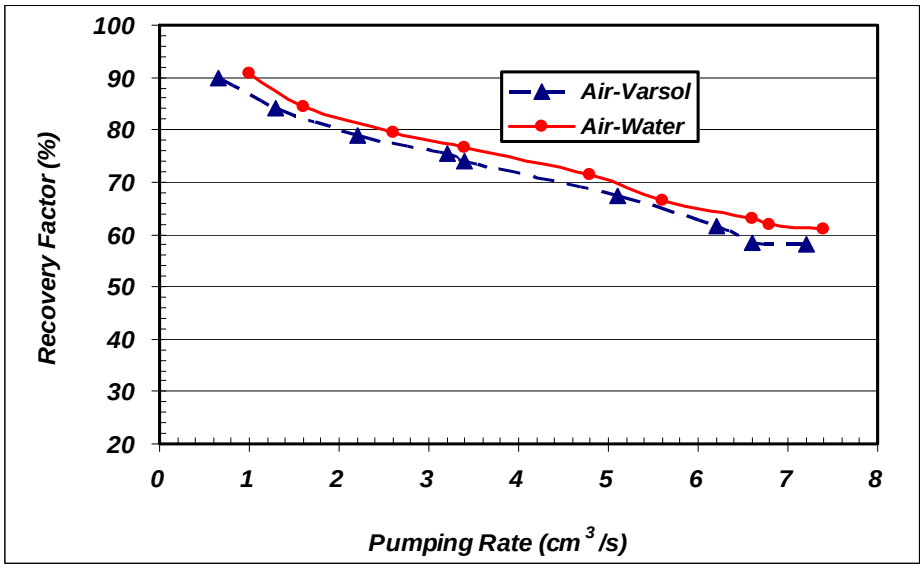

Figure 4.24: Effect of test fluid on recovery factor at gas-breakthrough at various pumping rates in fractured model (b) [BT3 Glass beads, b= 5 mm].

Results presented in Figure 4.24 confirm that during controlled gravity drainage, as long as the bulk flow is responsible for recovery, the interfacial tension of oil doesn't affect recovery factor. The recovery process takes longer time when film flow is active. The porous medium containing oil with lower interfacial tension produces more oil. It should be noted that Varsol oil and water exhibit a small difference in recovery factor due to having slightly viscosity difference.

4.4.2.6 Effect of well location: The position of production well from which liquid was drained and its relative distance from each side fracture affects the CGD process performance as well. In the current study, two different production well locations were considered in order to pump the liquid out of the fractured system, one at the centre of the bottom part of each model, and the other one at the corner side of each system, right below one of the side fractures. Each of controlled gravity drainage tests was conducted by liquid drainage with different constant withdrawal rates. In this section, two distinct experimental runs (run numbers 2 and 3, Table 4.2) were selected in order to determine the impact of production well placement on recovery performance of the CGD process. In both of these experimental runs, a 55 cm long matrix filled with BT2 glass beads was surrounded by one vertical fracture at each side. The air - CMC (2 wt%) fluid pair was employed to saturate both matrix and the two fractures, having 5mm aperture size.

Figures 4.25 to 4.27 show the results of the G-L interface positions in matrix and fractures at different withdrawal rates when the production well is located just below one of the fractures, namely f2 fracture. As depicted in Figure 4.25, when the withdrawal rate is very low (i.e. 0.7 cm^3/s), there is no difference between the behavior of liquid recession rate in both fractures, namely f1 and f2, so that the difference (H_{f2}- H_{f1}) is zero during the experimental runtime. As a result, one can conclude that the system's fluid flow behavior is similar to the case when the production well is located at the center of the model's bottom. This can also be verified by the experimental results presented in Figure 4.28 where the elevation differences between G-L

interface positions within matrix and fractures are the same at the lowest examined withdrawal rate (i.e. 0.7 cm^3/s). As a result, the recovery factor of these two systems at gas breakthrough would also be close to each other at the lowest operating withdrawal rate according to the first data point shown in Figure 4.29.

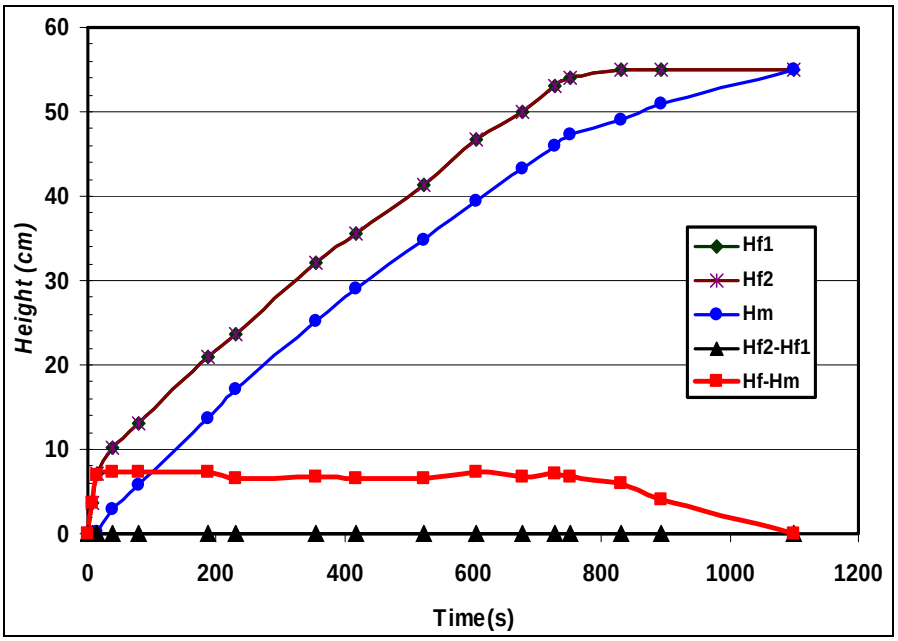

Figure 4.25: Rate of change of G-L interface positions in matrix and fractures when production well is located at the corner [matrix filled with BT2 glass beads, q = 0.7 cm^3/s, L= 55 cm, b= 5 mm, fluid pair: Air- CMC solution (2%)].

As it is evident in Figures 4.26 and 4.27, the flow behavior of the fractured system having a corner production well changes dramatically if the withdrawal rate increases. Depending on the magnitude of the withdrawal rate, an elevation difference occurs between the liquid level in the two fractures, namely f1 and f2. It is clear that "H_{f2}" curve (the liquid head position inside the fracture below which the drainage sink is operating) has a steeper slope in the case with higher withdrawal rate (Figure 4.27) compared to that of Figure 4.26. This is also evident in the magnitude of (H_{f2}- H_{f1}), i.e. this expression has higher numerical values in the experiment with higher drainage rate (Figure 4.27), especially during the early runtime. Based on these two Figures, one can define two different forms of elevation difference between the G-L interface positions within matrix and each of the acting fractures, namely as (H_{f2}- H_m) and (H_{f1}- H_m), in which the first defined elevation difference is higher than the latter one. Consequently, the flow behavior of fractured systems whose liquid level behavior is presented in Figures 4.26 and 4.27 deviate totally from that of the system at which the drainage well is located at the center.

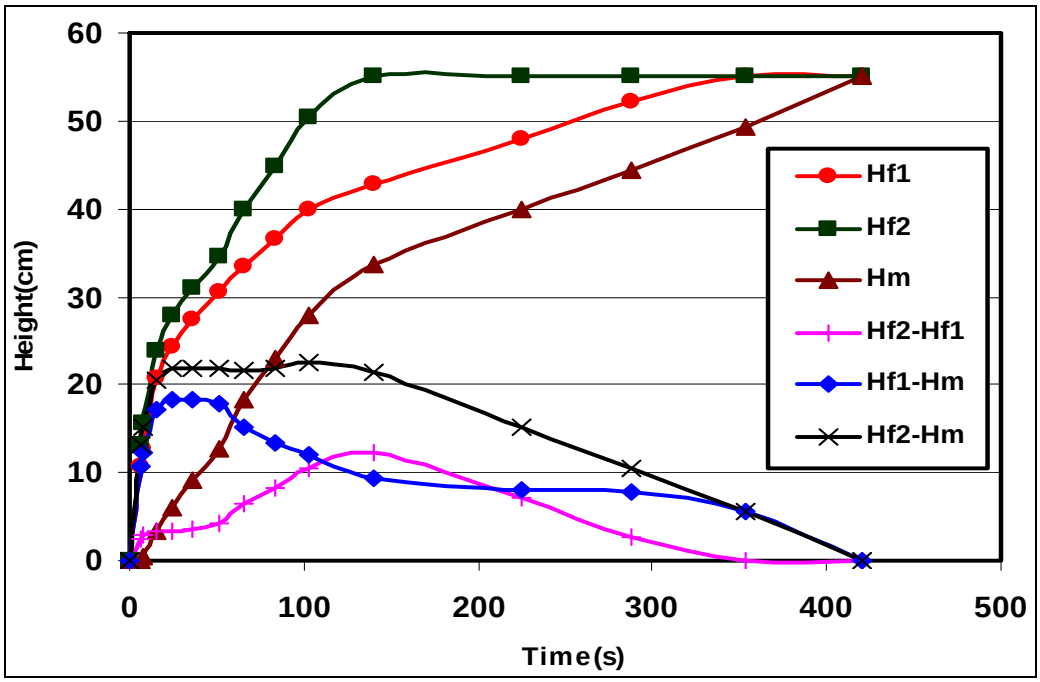

Figure 4.26: G-L interface positions in matrix and fractures versus time when production well is located at the corner [matrix filled with BT2 glass beads, q = 1.8 cm^3/s, L= 55 cm, b= 5 mm, fluid pair: Air- CMC solution (2%)].

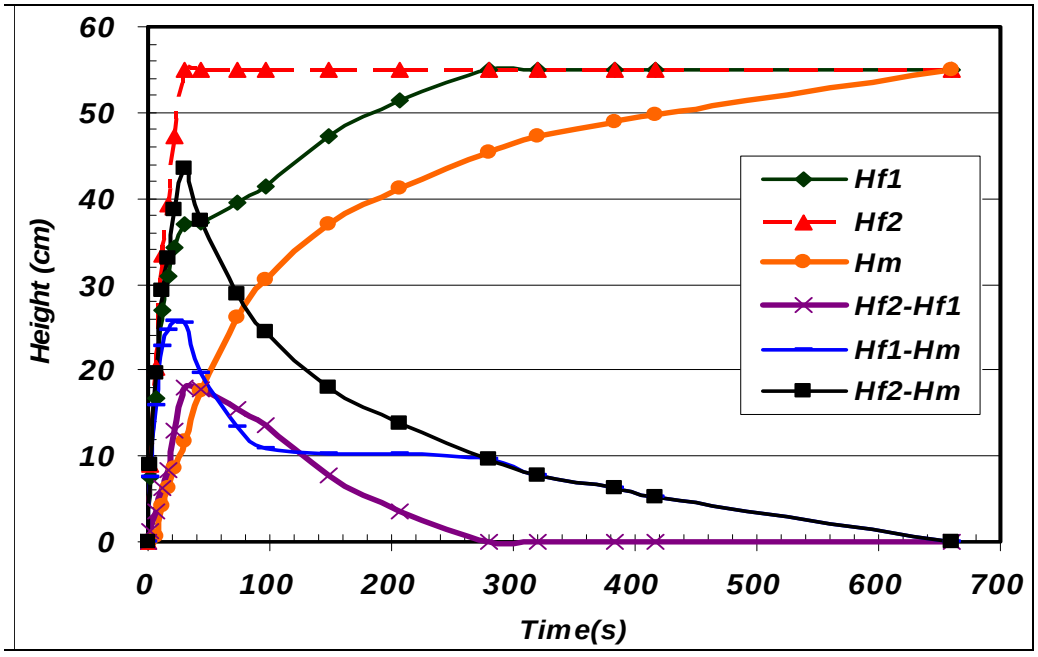

Figure 4.27: G-L interface positions in matrix and fractures versus time when production well is located at the corner [matrix filled with BT2 glass beads, q = 2.8 cm^3/s, L= 55 cm, b= 5 mm, fluid pair: Air- CMC solution (2%)].

By placing the drainage well below one of the fractures, it does not change the physics of controlled gravity drainage process. One can still define a reference elevation difference between G-L interface positions within matrix and fracture in which the acting fracture is the one below which the drainage well is operating, i.e. (H_{f2}- H_m). As long as the withdrawal rate is low enough and there is still liquid inside this reference fracture (f2), this reference elevation difference could be maintained constant as a result of constant low drainage rates (Figure 4.26). However, as the drainage rate increases, it is not possible to keep the difference (H_{f2}- H_m) constant anymore, even for a short period of time (Figure 4.27). It is also evident that the increasing slope of "H_{f2}" is higher when the withdrawal rate is higher (2.8 cm^3/s compared to 1.8 cm^3/s accordingly).

According to Figure 4.26, the fractured system is operating with constant "H_{f2}- H_m" (i.e. nearly 22cm) within the time interval of 20-140 seconds. At t = 140 seconds, this elevation difference starts to decrease when the fracture "f2" is emptied. As a result, the elevation difference would follow the curve of (H_{f1}- H_m) which is held constant at this time (nearly 8 cm from t = 140 seconds up to the t = 300 seconds). During this time interval, this curve governs the actual drainage rate of the system. It is important to note that this actual drainage rate is indeed lower than the nominal withdrawal rate which has been set originally on the peristaltic pump. As time goes on, the elevation difference curve for (H_{f1}- H_m) would meet that of (H_{f2}- H_m) at t = 350 seconds. At this time, f1 was out of liquid. One can conclude that it is not wise to have the production well connected to even a single fracture, or in the worst case, connected to an interconnected fracture network. This may cause early drainage of fracture(s) that have been touched by the drainage well. As a result, early gas breakthrough could happen with reduced value of recovery factor at gas breakthrough. In addition, having the production well intersecting even a single fracture, the drainage rates would be lower than the expected values of withdrawal rate.

Figure 4.28 presents the effect of production well position on the elevation difference between G-L interface locations within matrix and fractures. It is clear that at lower withdrawal rates, both of these graphs show the same trend, i.e. the effect of production well location on the process performance is somehow negligible for low withdrawal rates. However, as the drainage rate increases, this difference increases as well. This is due to the fact that systems with a production well right below one of the side fractures would have the gas breakthrough stage sooner than the system at which the production well is placed at the middle of the model's bottom, especially when CGD experiments are operated at high drainage rates. This results in higher values of "ΔH" associated with rapid drop of the liquid level inside the fracture, which causes gas breakthrough into the production well. These two graphs correspond up to reaching the associated values of CPR (3.8 and 4.3 cm^3/s for producer at corner and centre of the model respectively). In addition, it is evident that for each particular system, the magnitude of "ΔH" increases as the drainage rate increases.

Following the above discussion, one could logically discuss the effect of producer location on the recovery factor of the fractured system. As depicted in Figure 4.29, CGD experiment when the liquid has been withdrawn out of the centre has higher recovery factor values than that when the production well is right below the side fracture at each constant drainage rate. As discussed before, having the production port right below a side fracture causes gas breakthrough sooner than the case at which the liquid is pumped out from the centre. It is important to note that the recovery factor values reported in Figure 4.29 are the values obtained just before gas

breakthrough into the production well. In addition, for both of these two production well positions, it is evident that the recovery factor at gas breakthrough decreases as the drainage rate increases. As discussed previously, lower drainage rates result in lower values of "ΔH" regardless of the position of the production port, so, most of the matrix part has been drained

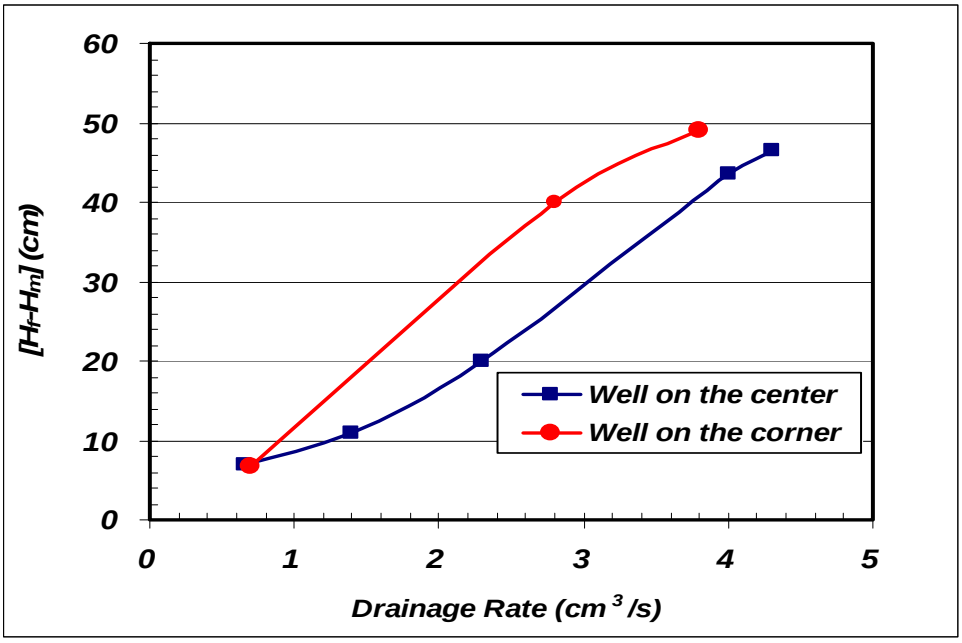

Figure 4.28: Effect of production well placement position on the elevation difference between G-L interface levels within matrix and fractures [matrix filled with BT2 glass beads, fluid pair: CMC solution (2 %) – air, model length: 55 cm, b = 5 mm].

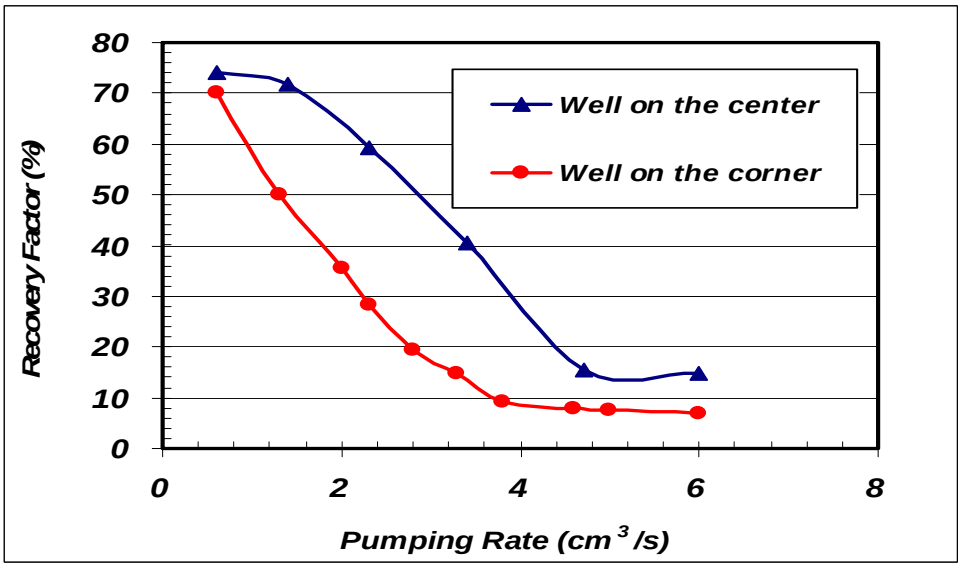

Figure 4.29: Effect of well placement position on the recovery factor just before gas breakthrough time [matrix filled with BT2 glass beads, fluid pair: CMC solution (2 %) – air, model length= 55 cm, b = 5 mm].

successfully at the point where the liquid level within fracture touches the bottom (i.e. just before gas breakthrough). In addition, lower drainage rates guarantee the cooperative effect of film-flow and bulk-flow type of drainage processes in matrix to be responsible for higher recovery factor values just before gas breakthrough.

The location of the production well also affects the corresponding values of CPR as well as MPWR. These two system specific rates have higher values for the model whose drainage well is located at the centre (4.3 and 7.1 cm^3/s correspondingly) compared to the model in which the production well is just below one of the fractures (3.8 and 4.9 cm^3/s correspondingly). This can be described in terms of the length of the flow path that each liquid unit (especially those within the matrix as it has the major source of liquid storativity) should be drained along until reaching the production well. The shorter the flow path length is, the lower would be the flow resistance for the draining liquid, and as a result, the higher would be the volume of liquid capable of being drained along these flow paths. Consequently, the rate of liquid capable of draining towards the production well is higher for the case where the liquid flow-path length is shorter, i.e. when production well is located at the centre of the model compared to the position at the corner below a side fracture.

4.4.2.7 Effects of initial liquid saturation: Analysis of production history was addressed so far for CGD experiments having common initial condition of 100% liquid saturation as the starting point. There could be possibility of presence of limited initial gas saturation within the fractured media upon which the production history could be affected significantly. In order to establish the initial gas saturation condition, liquid could be re-injected at very low volumetric rates (close to the rate at which imbibition occurs) into the packed model which had been already drained out of liquid. This could result in trapping of the gaseous phase (i.e. air) as a residual phase with saturation of almost 20% of the total pore volume. Sensitivity analysis of the effect of residual gas on the production performance was performed using a fractured model with 55 cm long matrix filled with BT4 glass beads (Run number 14, Table 4.2, as the reference model). Qualitatively speaking, similar experimental results have been obtained as those which were discussed previously regarding free-fall gravity drainage experiments (Zendehboudi et al., 2008).

Figures 4.30 and 4.31 show the experimental results of the effect of the presence of residual gas on the CGD experiments for the reference model. As depicted in Figure 4.30, liquid production rate and also cumulative liquid produced could be equal during the early stages of CGD experiment for reference run number 14 and the trial in which all the system parameters are the same as those of reference, except it had 20% PV residual gas saturation (i.e. 80% ILIP to begin with). This could be due to the fact that most of the liquid produced during the early stages of the CGD process comes from the limited storage capacity of side fractures. As the storativity of fractures wouldn't be affected by the presence of residual gas, these two systems could have similar early production performance. According to the visualization results, it is concluded that matrix top portions, and also the area within the matrix adjacent to each side fracture hold lower residual gas saturation compared to the other parts of the matrix when each particular model was saturated under low enough injection rates. It is expected that the liquid communication rate from matrix into the fractures wouldn't change significantly as a result of the presence of the residual gas inside the matrix. The matrix area adjacent to each side fracture is mainly responsible for the liquid communication process. The effective permeability to water in the

presence of residual gas is about 65% of the absolute permeability of the matrix (Chatzis et al., 1983). In addition, the cumulative production decreases as the residual gas saturation increases.

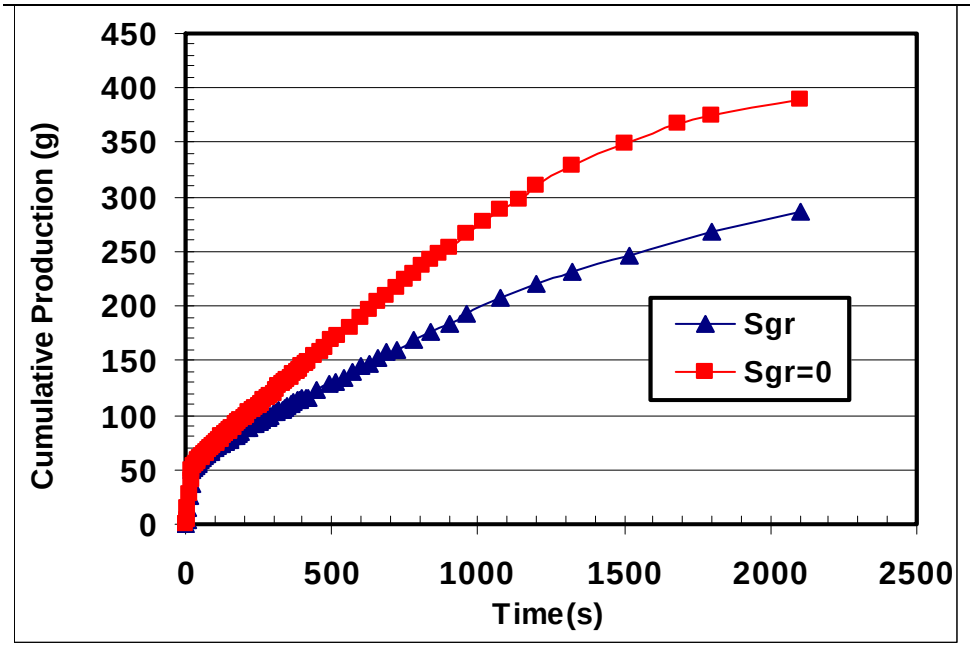

Figure 4.30: Effect of residual gas saturation on the production history of model undergoing CGD experiment [matrix filled with BT4 glass beads, fluid pair: CMC solution (2 wt%) – Air, b = 5 mm, L = 55 cm, q= 2.4 cm^3/s].

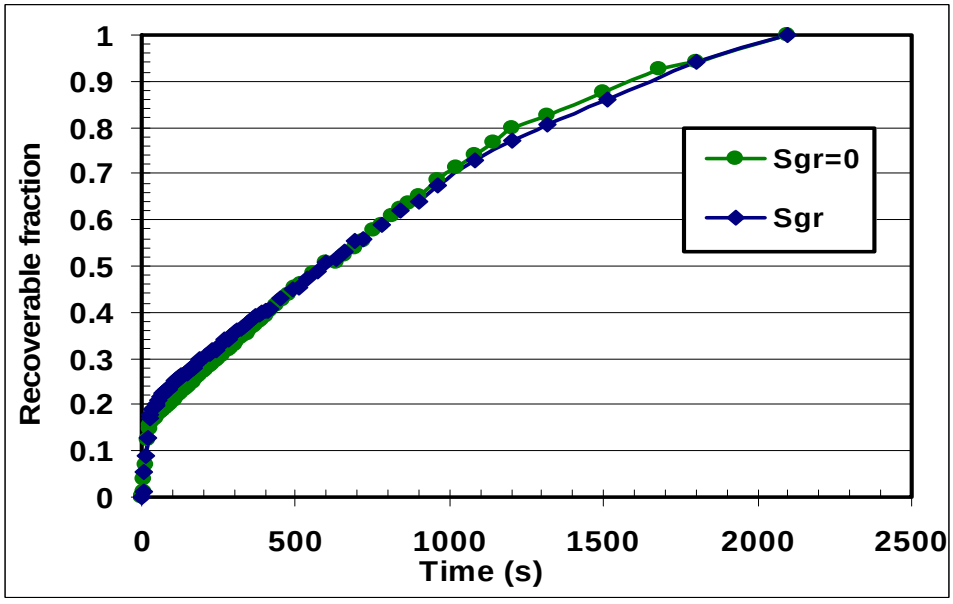

Figure 4.31: Effect of residual gas saturation on the recoverable fraction in a model undergoing CGD experiment [matrix filled with BT4 glass beads, fluid pair: CMC solution (2 wt%) – Air, b = 5 mm, L = 55 cm, q= 2.4 cm^3/s].

When the cumulative amount of liquid up to a particular time is normalized by dividing it with the maximum recoverable amount of liquid, one could obtain the fraction of recoverable liquid as a function of time. Therefore, it is possible to compare the production history of these two systems by plotting the fraction of recoverable liquid remaining in the system as a function of dimensionless time. This comparison is made in the plot shown in Figure 4.31 for the reference model itself, and also when it is saturated partially with residual gas. This observation permits to describe the production history from a partially saturated system by utilizing the supposedly known fractional recovery curve of a fully liquid-saturated system.
As it is discussed above, since the area close to the fractures contains a little volume of air, and also considering the fact that this area has the main responsibility to contribute to liquid communication between matrix and fracture, the presence of residual gas won't affect significantly the values of system specific rates as well as the elevation difference between G-L interface locations within matrix and fractures. This point can be verified by comparing the experimental results of CPR (0.65 cm^3/s with residual gas compared to 0.7 cm^3/s with 100% initial liquid saturation) as well as those of MPWR (4.7 cm^3/s with residual gas compared to 4.8 cm^3/s with 100% initial liquid saturation).

4.4.2.8 Effect of fracture orientation: A series of experiments on controlled gravity drainage was performed in the fractured porous medium which has a vertical fracture with aperture size of 11mm. We first considered this case in which the gravitational force is parallel to the flow in the fracture. This kind of experiment was done for several pumping rate in the physical model and the difference between gas-liquid interfaces in matrix and fracture was plotted versus pumping drainage rate. Like previous experiments as the flow rate coming from the fractured porous medium goes up, the elevation difference increases. Figure 4.32 depicts this behavior. The same experiments were repeated in two fractured macromodels at which the fractures were inclined at 15 and 30 degrees relative to the direction of gravity. Compared to the case in which the flow in the fracture and gravity were parallel, the displacement process in the fracture is slower under free fall gravity drainage as expected. However, the process is similar to the vertical one. For each known pumping rate, both cases have the same gas liquid interface velocity and it was observed that the displacement process in vertical fracture and inclined fracture had identical rate of dH/dt. Therefore, vertical elevation difference between gas-liquid interface positions in matrix and fracture parts for the case with inclined fracture is smaller than that in the model containing the vertical fracture. According to Figure 4.32, the following relationship is established between (H_F-H_m) of first case and that of the fracture media with inclined fracture orientation.

$$(H_F-H_m)_{Vertical}= (H_F-H_m)_{Inclined}/\cos\beta \qquad (4.9)$$

where β is the inclination angle of the fracture. The validity of the above equation can be confirmed by using the analogy that constant pumping rate is proportional to liquid level recession rate in matrix and fracture part as shown in Equation (4.7). From Equation (4.9) it can be concluded that the system with vertical fracture experiences earlier gas breakthrough. Therefore, this phenomenon causes lower recovery factor at breakthrough for the fractured medium with vertical fracture compared to the model with inclined fracture during a controlled gravity drainage test for any pumping rate.

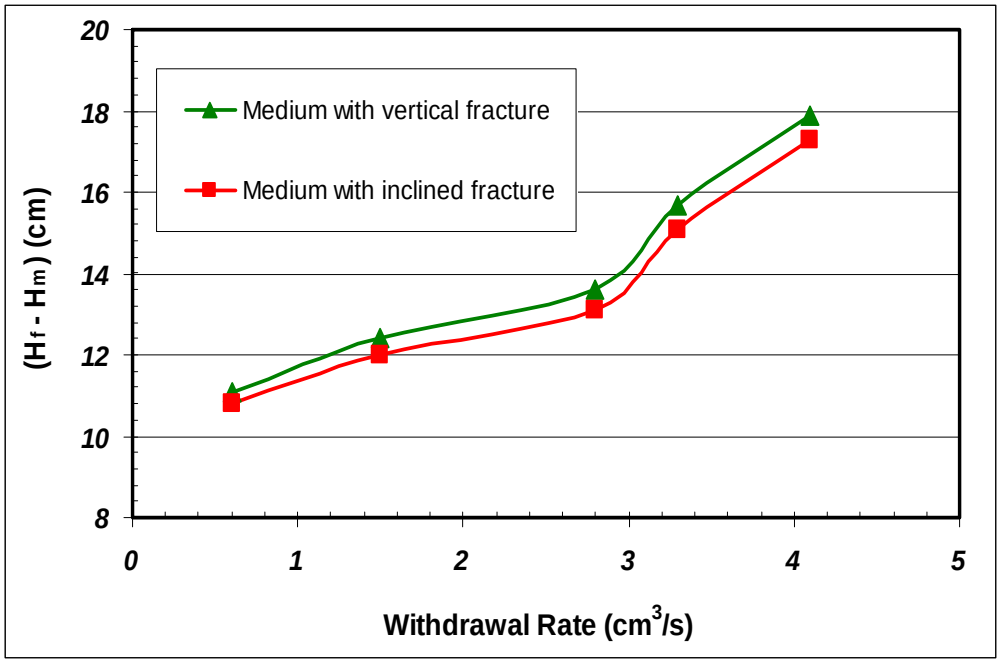

Figure 4.32: Effect of inclination angle of fracture on the difference between G-L interface positions within matrix and fractures during CGD process [matrix filled with BT3 glass beads, fluid pair: Air - Water, fracture aperture (b) = 11 mm, and β= 15^{o}], Model (a) which has a vertical fractured in the middle.

Additionally, the experimental runs performed to show effect of inclination angle, confirmed that as long as the withdrawal rate is constant, the elevation difference between G-L interface positions in both matrix and fracture domain remains unchanged during a particular controlled gravity drainage experiment, no matter whether the fracture is vertical or inclined.

The inclination angle of a fracture affects the values of the two system-specific rates, CPR and MPWR. According to Figure 4.33, both of these rates are increasing as a result of an increase in the inclination angle of fracture. Based on the experimental results it is expected that the associated values of "ΔH" would be higher for the fractured porous medium containing the fracture with the lower inclination angle. In such a model with high values of "ΔH", gas breakthrough into the production well happens sooner than the case with lower inclination angle. As a result, the CPR value would be higher for the models with the inclined fracture. In addition, the maximum withdrawal rate that a system can sustain is also affected by inclination angle of fracture. If the fractures are oriented through the porous medium, it is evident that the higher the inclination angle is, the higher would be the magnitude of MPWR because the fractures have more storativity when they are inclined.

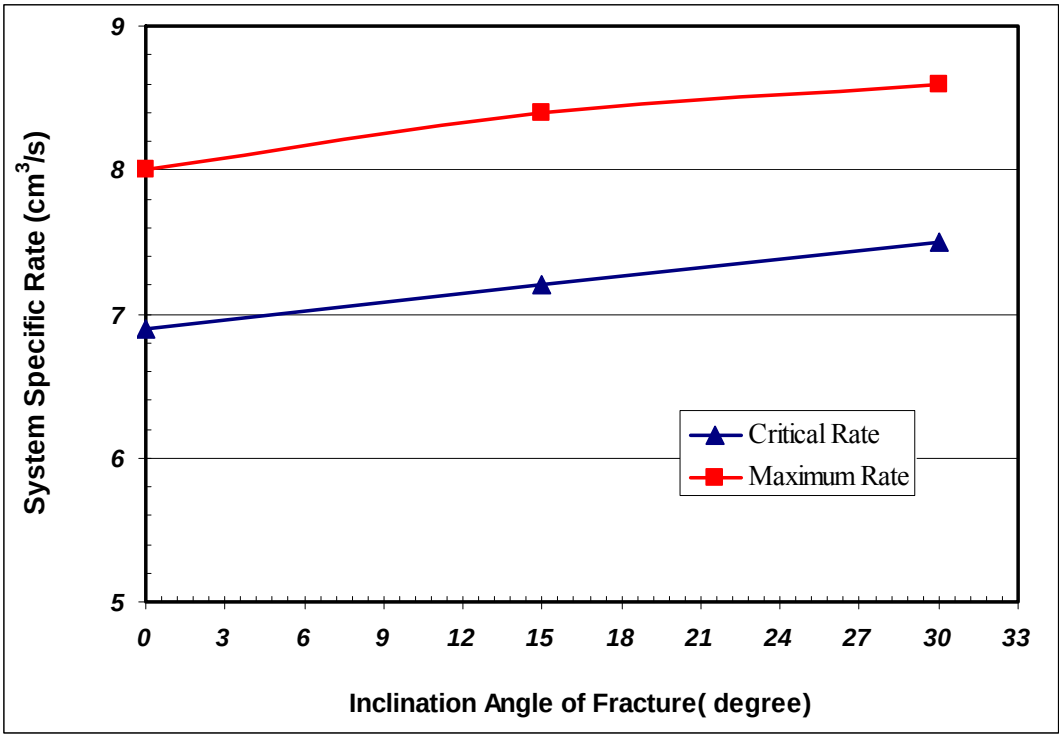

Figure 4.33: Effect of fracture inclination angle on the magnitude of CPR as well as MPWR during the course of CGD process in porous medium (a) [matrix filled with BT3 glass beads, b=11 mm, fluid pair: Air -Water].

4.4.2.9 Effect of fractures pattern: In this part, we investigate the effect of fractures pattern on system specific rates, the difference between G-L interface positions within matrix and fractures, and the recovery factor at gas breakthrough. For this, BT3 and BT2 glass beads were used to make the matrix parts for the fractured models. The test fluids including CMC solution (1% wt) and Varsol oil were employed to simulate the oil phase. It was found that in the models b, e, f, and g shown in Figure 4.1 as long as a withdrawal rate was set on a constant rate and equal for all physical models, the recession rate for gas-liquid interface is the same for all of them if petrophysical properties of matrix and fracture are identical. Therefore, the results show that the fracture pattern does not affect the gas liquid interfaces movement in a controlled gravity drainage process. However, the presence of horizontal fracture in the fracture pattern increases the communication rate as well as the recovery factor at breakthrough if the aperture size of horizontal fracture is small enough in order to establish effective capillary continuity. Experimental results also revealed that the fractured porous medium model (f) has the highest critical rate among the fractured models that we have used in the research.

On the other hand it can exhibit the maximum value of MPWR. The main reason for keeping high magnitudes of CPR and MPWR is important role of connected fracture network in physical model (f) as it causes easily flow transferring from matrix to fracture and vice versa. Additionally, if the intensity of fracture is high in the fracture network, it would have more storage capacity in fractured model and this would enable to recover more oil at any withdrawal rate before gas breakthrough compared to the models whose fractures have lower intensity and could not make a fracture network to maintain a continuous flow path to production well.

Table 4.5 indicates the effect of four fracture patterns used in this study on the magnitude of system specific rates. In addition, the difference between gas-liquid interface position in matrix and fracture, as well as the gas-liquid interface position in fracture could be seen in Figures 4.34 and 4.35 versus time for various fractured porous media at two different pumping rates (0.8 cm^3/s and 1.3 cm^3/s) during controlled gravity drainage. Important point to note here is that the gas-liquid interface advancement in the fracture is almost the same for all kinds of fracture configurations at each particular withdrawal rate before touching the horizontal fracture , but it moves slower when the interface reaches the intersection of horizontal and vertical fracture because some amount of liquid would be provided from horizontal fracture while communication between horizontal fracture and vertical ones to maintain that constant pumping rate set on the pump. Therefore, the fluid transferring by communication lowers the recession rate of gas-liquid interface in vertical fractures. Also when the horizontal fracture is invaded by gas, the same condition is established for gas-liquid interface downward movement velocity. Therefore, as seen in Figure 4.34, no difference exists between the porous media with various fractures patterns with respect to gas-liquid interface positions in matrix and fractures, especially for low pumping rates. As the withdrawal flow rate increases, this difference becomes bigger (see Figure 4.35) due to complex nature of communication between different parts of fractured media.

Table 4.5: Specific flow rates for variable fractures configurations of the BT3 porous media saturated with Varsol

Case No.	Fracture patterns (see Figure 4.1)	Critical pumping flow rate (CPR), cm^3/s	Maximum pumping flow rate (MPWR), cm^3/s
1	Model (h) : Homogeneous	NA	5.0 ± 0.1
2	Model(g): Has two vertical fractures	6.2 ± 0.2	7.1 ± 0.1
3	Model(e) : Has two vertical fractures and one horizontal fracture between them, but not touching the vertical ones	7.0 ± 0.1	8.2 ± 0.2
4	Model(f): Is the same as model(e), except the horizontal fracture is connected to vertical fractures from both sides	7.2 ± 0.3	8.4 ± 0.2

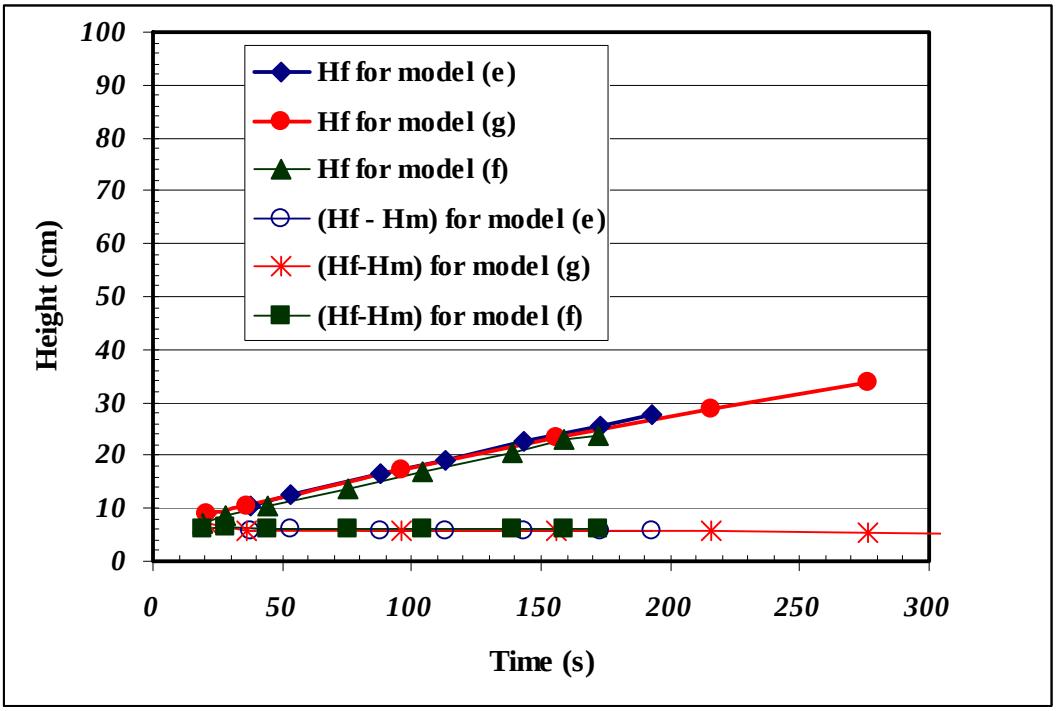

Figure 4.34 G-L interface position in fractures, and the difference between gas-liquid interface position in matrix and fracture versus time; matrix filled with BT3 glass beads, withdrawal rate(q)= 0.8 cm^3/s, [b= 5 mm, L= 55 cm, fluid pair: Air-Varsol].

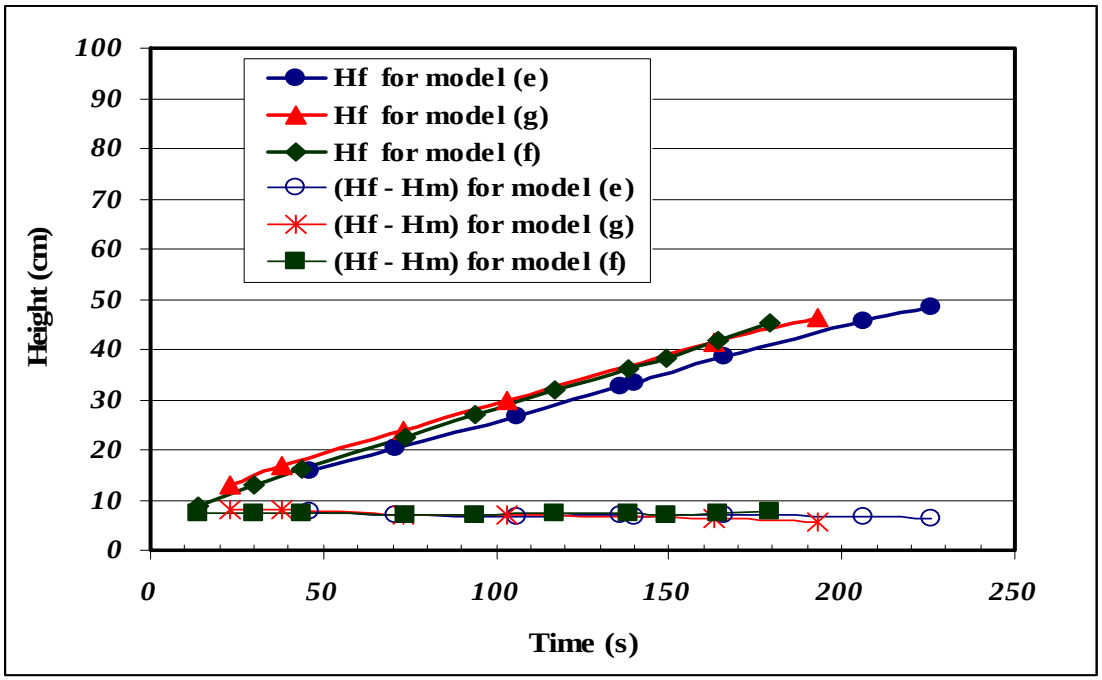

Figure 4.35: G-L interface position in matrix, and difference (H_f-H_m) versus time; matrix filled with BT3 glass beads, withdrawal rate(q)=1.3 cm^3/s, [b= 5 mm, L= 55 cm, fluid pair: Air-Varsol].

4.4.2.10 Effect of physical model properties and production rate on viscous fingering phenomenon: The experiments were conducted on fractured 2D glass bead media in rectangular Plexiglas models with the height of 55 cm and then the physical model was filled with one of common test fluids and kept saturated and finally the fractured porous medium was drained by several pumping rates during controlled gravity drainage. Depending on the permeability of glass beads, liquid viscosity and pumping rate, viscous fingering happens under some conditions. This experimental study examines the influences of the pumping rate, test fluid viscosity, matrix permeability and fracture configuration on the flow pattern in the fractured media. For this purpose, systems with a set of vertical and horizontal fractures were constructed as fractured porous media. After placing the samples on a glass stand, controlled gravity drainage studies were performed by pumping out the liquid by constant withdrawal rates from the production point under the models. Note that the samples were vertically placed and production direction was vertical which is parallel with the gravitational force. During the constant rate flow experiments, gas-liquid interface movement was visualized to identify at which conditions viscous fingering occurs. Figure 4.36 shows viscous fingering in the fractured porous media made of BT3 glass beads. In this case when production rate is very low (e.g., 0.7 cm^3/s) the gas advancement is piston-like, however by increasing rate, finger growth started in porous medium during controlled gravity drainage process. The interesting observation in this study was that when we have the same liquids and the same matrix in a different fractured media which has a vertical in the middle, there was no viscous fingering in that rate (Figure 4.37). The main reason for lack of viscous fingering is as in the second porous medium, air had the chance to move towards production well easily and it prevents occurrence of unfavourable viscous fingering phenomenon. However, it causes early gas breakthrough, resulting in low recovery factor for the second case.

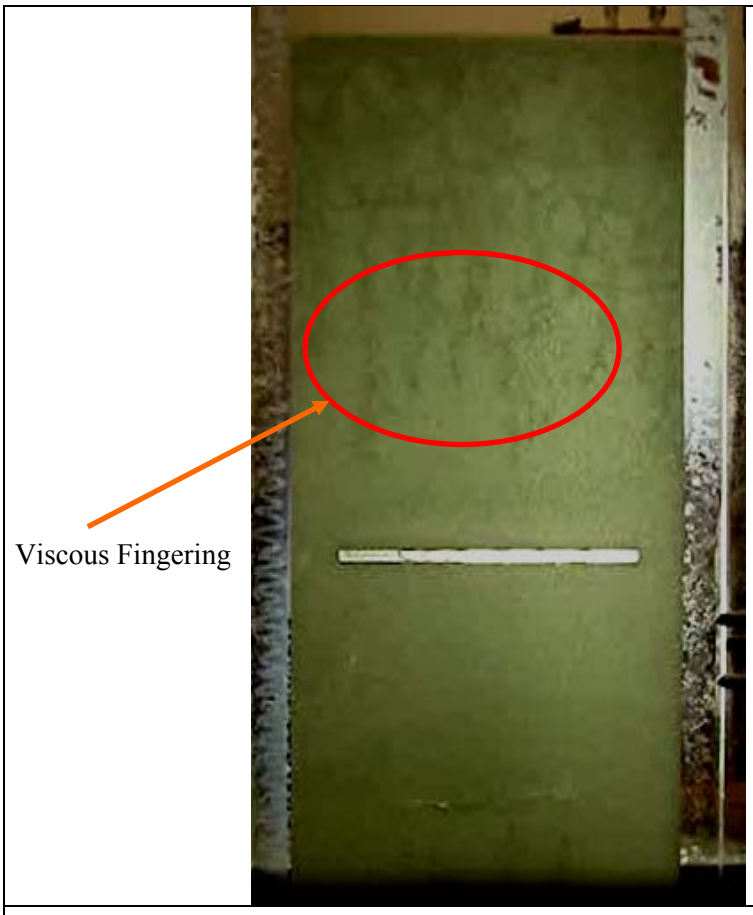

Figure 4.36: Schematic of viscous fingering phenomenon in the fractured porous medium[b= 5 mm , fluid pair=CMC solution (2%)-Air , BT3 glass beads, q = 1.4 cm^3/s]

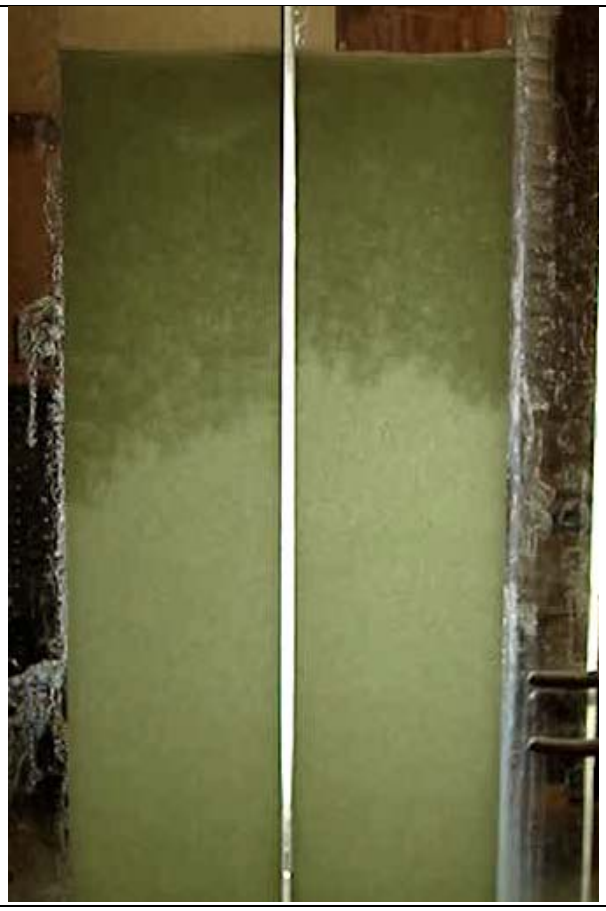

Figure 4.37: Liquid displacement in the fracture medium saturated with CMC solution (2%) [L= 55 cm, b= 5 mm and the matrix part is BT3 glass beads , q= 1.4 cm^3/s]

4.5 Multi-Variable Regression Analysis – Dimensional Analysis

According to the physics of controlled gravity drainage (CGD) process and also experimental findings, a detailed dimensionless analysis has been conducted in which the dimensionless distance between the G-L interface positions within matrix and fractures, critical pumping rate (CPR), maximum possible withdraw rate (MPWR), and recovery factor at gas breakthrough have been correlated as a function of defined dimensionless numbers and dimensionless groups.
The statistical approach presented for this study is summarised in the following sections and with more details in Appendix C.

4.5.1 Multiple linear regression analysis for Critical Capillary Number: Figures 4.38 to 4.40 present the effects of different dimensionless groups (namely as K_f/K_m, Bond number, and critical Reynolds number) on the critical Capillary number. According to the procedure mentioned above for the multiple linear regression analysis, the critical Capillary number should be expressed linearly based on the defined dependent dimensionless variables according to the following relationship:

$$Ca_{Cr.} = \frac{v_{Critical} \cdot \mu_L}{\sigma} = f_1(Bo, \mathrm{Re}_{Cr.}, \frac{K_f}{K_m}, Combination\ of\ these\ \ numbers)$$
$$and \quad \mathrm{Re}_{Cr.} = \frac{\rho . v_{Critical} . D_P}{\mu_L} \tag{4.10}$$

in which "$v_{Critical}$" is the critical pumping velocity for each particular CGD experimental run.

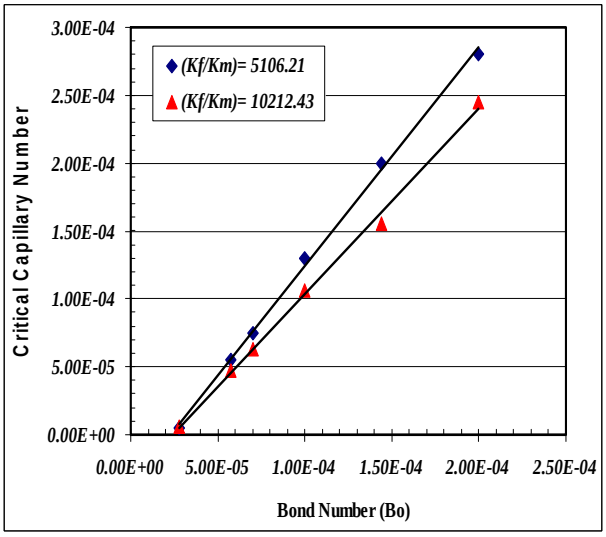

Figure 4.38: Effect of Bond Number (Bo) on critical Capillary number during controlled gravity draining at various conditions.

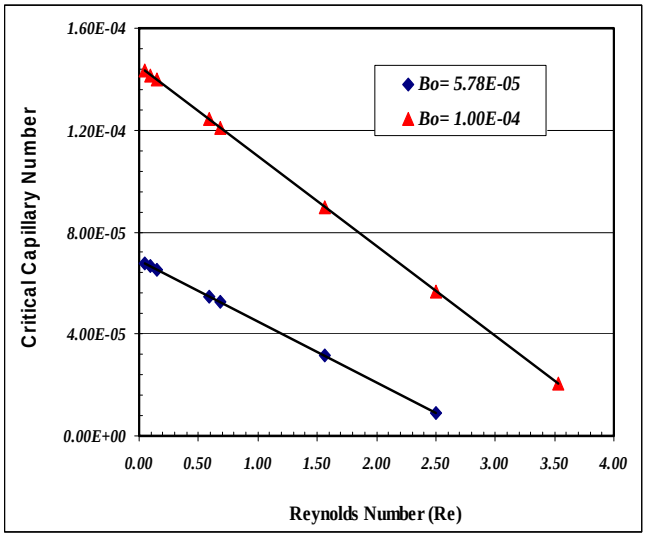

Figure 4.39: Linear function of critical Capillary number with respect to Reynolds number while the fractured porous media are under CGD.

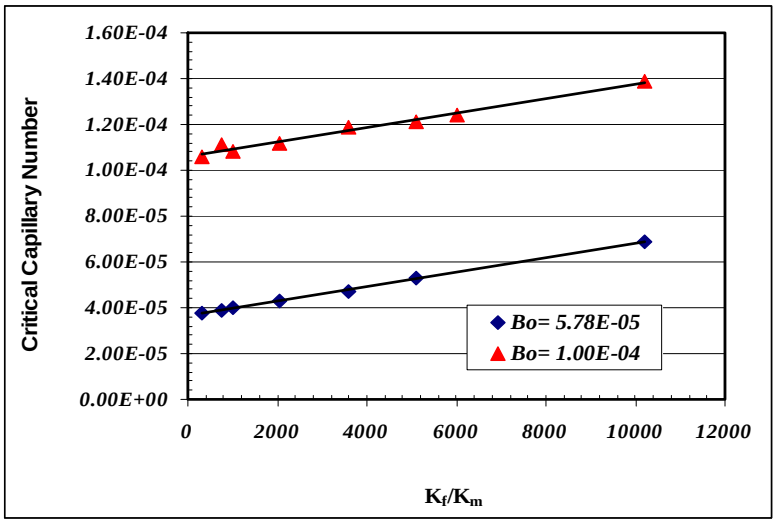

Figure 4.40: Influence of K_f/K_m on critical Capillary number for two different values of Bond number.

According to the Figures 4.38 to 4.40, the critical Capillary number increases linearly with increasing dimensionless both Bond number and K_f/K_m; however it would be decreased linearly with increasing critical Reynolds number. As the liquid viscosity increases, the CPR would be decreased as well. In addition, as the fracture permeability (i.e. fracture aperture) increases (or "K_f/K_m" increases), the fractured system would be capable of handling higher magnitudes of liquid withdrawal velocity (i.e. higher associated CPR's). The last term in Equation 4.10 represents the interaction effect of dependant dimensionless groups on the magnitude of dimensionless CPR. Figures 4.38 to 4.40 clearly show that this interaction term consists of two dimensionless groups, namely as Bond number and critical Reynolds number, so Equation 4.10 could be written as:

$$Ca_{Cr.} = \frac{v_{Critical} \cdot \mu_L}{\sigma} = a + b.Bo + c.\,\mathrm{Re}_{Cr.} + d.\frac{K_f}{K_m} + e.\{Bo.\mathrm{Re}_{Cr.}\} \qquad (4.11)$$

Table 4.6 provides the information regarding the correlation coefficients of Equation 4.11, standard errors, and lower limits as well as upper limits of the coefficients:

Table 4.6: Information table for linear regression model of critical Capillary number

Coefficients	Numerical value	Standard Error	Lower 95%	Upper 95%
a	-5.15397E-05	1.2871E-05	-8.0218E-05	-2.28614E-05
b	1.806883653	0.09123571	1.603597823	2.010169484
c	-8.43132E-06	9.1564E-06	-2.88331E-05	-1.19705E-06
d	3.1254E-09	1.2626E-09	3.12108E-10	5.93868E-09
e	-0.269152134	0.07235542	-0.430370049	-0.107934219

It is clear that the critical withdrawal velocity (which is associated with CPR) appears at both sides of Equation 4.11. As a result, in order to obtain the CPR for any particular fractured set up, one needs to perform a trial and error procedure using Equation 4.11. As an initial guess for the iterative procedure, considering critical Reynolds number to be equal to unity would be a reasonable trial. The critical withdrawal velocity associated with $\mathrm{Re}_{Cr.} = 1.0$ guarantees a Darcian flow by which the iterative procedure could be initiated. Knowing the initial guess for "$v_{Critical,\ guessed}$", the right hand side of Equation 4.11 could be solved as all the parameters are known based on the information provided for each particular CGD experiment. Consequently, the first calculated critical Capillary number would be obtained and as a result, the associated "$v_{Critical,\ calculated}$" could be obtained. If the calculated critical withdrawal velocity wouldn't be similar to its guessed value (i.e. its associated relative error wouldn't be within a reasonable domain) the "$v_{\mathrm{Critical,\ calculated}}$" would be considered as the second guessed value and the iterative procedure would be repeated accordingly until a reasonable match between calculated and guessed values of critical withdrawal velocity would be obtained.

4.5.2 Multiple linear regression analysis for Maximum Capillary Number: From experimental investigation of CGR process, it was concluded that there is a maximum withdrawal rate (i.e. maximum macroscopic drainage velocity) for each particular fractured media under the CGD process below which a constant withdrawal rate could be maintained for a reasonable duration of time. Practically, it is viable to drain a fractured system at a rate below the

maximum withdrawal rate associated with that particular porous medium. As a result, determining the maximum drainage rate for each particular fractured porous medium undergoing a CGD process would be a necessity in order to evaluate the performance of this recovery technique.

The multiple linear regression analysis could be implemented in order to figure out what parameters (i.e. dimensionless groups) are affecting the maximum withdrawal rate associated with each fractured system. The dimensionless objective function containing maximum withdrawal rate (or maximum drainage velocity) is called maximum Capillary number ($Ca_{Max.}$). Following the procedure presented in section 4.5.1 and Appendix C, the individual effect of each dimensionless parameter on the maximum capillary number has been presented through figures 4.41 to 4.43.

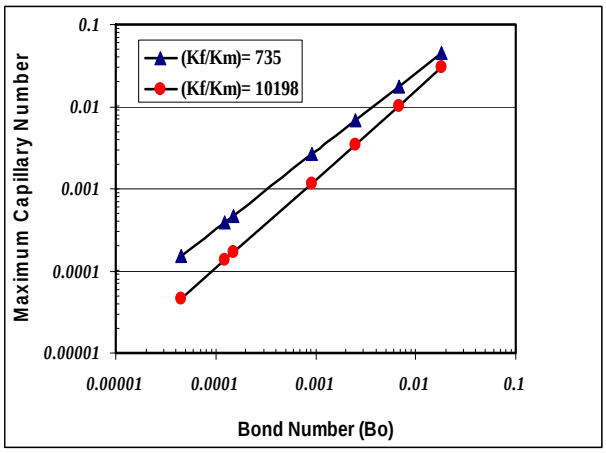

Figure 4.41: Effect of Bond number on maximum Capillary number for two different values of K_f/K_m.

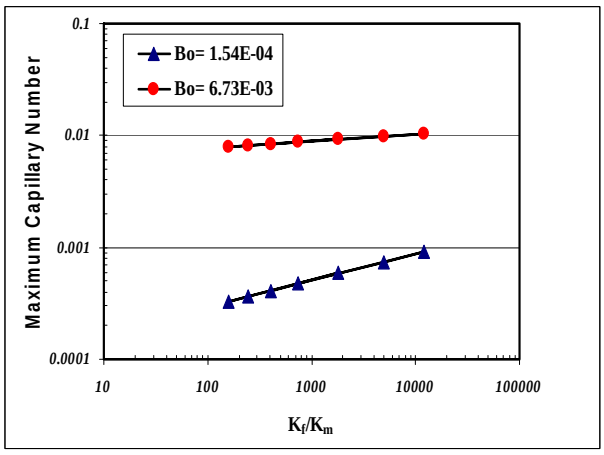

Figure 4.42: Maximum Capillary number versus permeability ratio in logarithmic plot.

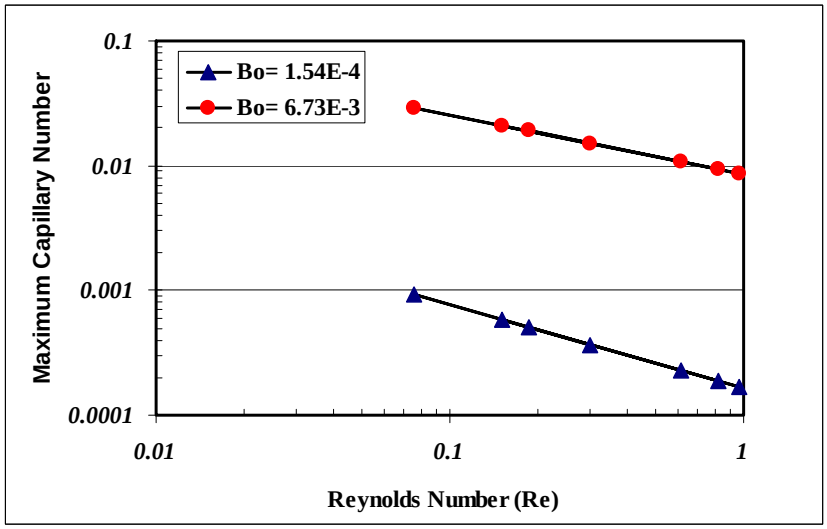

Figure 4.43: Effect of "Re" on "$Ca_{Max.}$" at two different values of Bond number.

According to these figures, it is clear that logarithm of dimensionless MPWR (i.e. maximum Capillary number) changes linearly with "K_f/K_m", Bond number, and maximum Reynolds number (Reynolds number associated with MPWR or maximum drainage velocity, "$v_{Max.}$"). Logarithm of dimensionless maximum withdrawal rate increases linearly with all the noted dimensionless groups except the maximum Reynolds number. Consequently, one could express the dimensionless maximum possible withdrawal rate in terms of the dimensionless parameters as follows:

$$Ca_{Max.} = \frac{v_{Maximum}.\mu_L}{\sigma} = f_2(Bo, \mathrm{Re}_{Max.}, \frac{K_f}{K_m}, Combination\ of\ these\ numbers)$$
$$\mathrm{Re}_{Max.} = \frac{\rho.v_{Maximum}.D_P}{\mu_L} \qquad (4.12)$$

Another point that can be concluded from Figures 4.41 to 4.43 is that the maximum Capillary number depends on the combination of all three of the dimensionless parameters, namely natural logarithms of Bond number, "K_f/K_m", and maximum Reynolds number. As a result, Equation 4.12 could be expressed in a more specific form:

$$Ln(Ca_{Max}) = a + b.Ln(Bo) + c.Ln(\mathrm{Re}_{Max}) + d.Ln(\frac{K_f}{K_m}) + e.\{Ln(Bo).Ln(\mathrm{Re}_{Max}).Ln(\frac{K_f}{K_m})\} \qquad (4.13)$$

Table 4.7 contains the numerical values of the coefficients of correlation provided in Equation 4.13 as well as the standard error, lower and upper limits of the coefficients obtained from the multiple linear regression analysis.

Table 4.7: Information table for linear regression model of maximum Capillary number

Coefficients	Numerical value	Standard Error	Lower 95%	Upper 95%
a	0.269179	0.511808	0.0712	1.409558
b	1.083895	0.075394	0.915908	1.251883
c	-0.02022	0.152268	-0.35949	-0.009057
d	0.058835	0.061108	0.07732	0.194992
e	0.00784	0.001896	0.003616	0.012065

According to Equation 4.13, the maximum drainage velocity is present on both sides of the equation, so in order to determine the MPWR, it is needed to perform the trial and error procedure similar to that presented in section 4.5.1 in order to obtain the maximum drainage velocity (i.e. MPWR).

4.5.3 Multiple linear regression analysis for dimensionless height: Elevation difference between G-L interface positions within matrix and fractured is another important parameter for evaluating the performance of a CGD process. Consequently, it was considered as one of the parameters which should be predicted statistically based on the multiple linear regression analysis using available system parameters. A relevant dimensionless objective function,

dimensionless height, has been defined as the ratio of model height to the elevation difference between G-L interface positions within matrix and fractures for each particular fractured system. In order to perform the statistical sensitivity analysis, one could examine the same method described in section 4.5.1 and Appendix C. Cross-plots of dimensionless height versus different affecting dimensionless groups (Figures 4.44 to 4.46) admit the linear dependency of dimensionless height to be of the following functional form:

$$\frac{L}{\Delta H} = f_3(Bo, Ca, \frac{K_f}{K_m}, Combination\ of\ these\ \ numbers) \qquad (4.14)$$

To present the data in a linear form regardless of their increasing and decreasing trends, the natural logarithm term would have been brought up in some of the terms. Accordingly, the combination term have been shown to be a multiplication of Bond number and logarithm of Capillary number as it was concluded from Figures 4.44 to 4.46:

$$\ln(\frac{L}{\Delta H}) = a + b.Ln(Ca) + c.Bo + d.\frac{K_f}{K_m} + e.\{Bo.Ln(Ca)\} \qquad \text{If } q \le q_{Critical} \quad (4.15)$$

$$\ln(\frac{L}{\Delta H}) = \ln(\frac{L}{\Delta H})_{Critical} \qquad \text{If } q > q_{Critical} \quad (4.16)$$

The correlation coefficients of Equation 4.15 have been presented in Table 4.8:

Table 4.8: Information table for linear regression model of dimensionless height

Coefficients	Numerical value	Standard Error	Lower 95%	Upper 95%
a	-3.7105	1.259318	-6.25191	-1.1691
b	-0.16571	0.120855	-0.4096	-0.106185
c	-164525	10411.7	-185537	-143513
d	9.65E-05	2.84E-05	3.92E-05	0.000154
e	-21904.4	1040.688	-24004.6	-19804.2

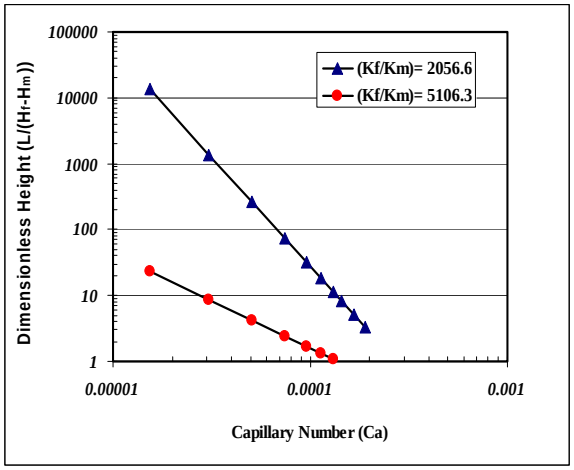

Figure 4.44: Dimensionless height against Capillary number ,"Ca", during controlled gravity drainage at various conditions

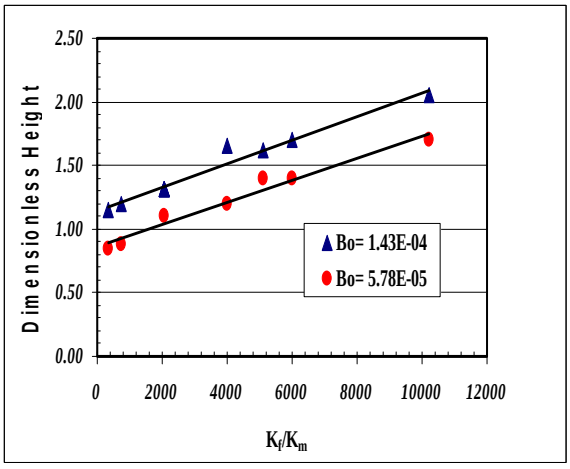

Figure 4.45: Effect of "K_f/K_m" on natural logarithm of dimensionless height (Ln(L/ΔH)).

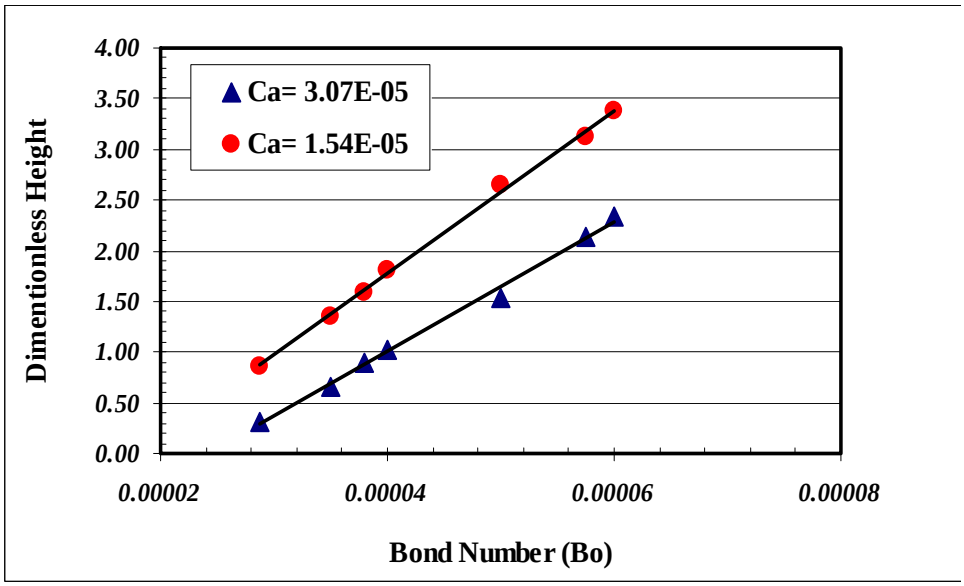

Figure 4.46: Effect of Bond number on "Ln (L/ΔH)" for Capillary numbers equal to 3.07E-05 and 1.54E-05, respectively

4.5.4 Multiple linear regression analysis for recovery factor: As the production performance of a CGD process would be evaluated based on the amount of recovered liquid with respect to the liquid initially present in place (i.e. recovery factor), it would be beneficial if one could estimate the amount of recovery factor having all the available system parameters in form of previously defined dimensionless groups. According to the same procedure presented in sections 4.5.1 through 4.5.3, for a fractured system analogous to the experimental schemes defined in section 4.3.1, one could suppose the recovery factor to have a functional relationship based on the defined dimensionless parameters as follows:

$$R.F = f_4(Bo, Ca, \frac{K_f}{K_m}, Combination\ of\ these\ \ numbers) \qquad (4.17)$$

Performing the standard statistical procedure described before, which could result in deducing relevant cross-plots of recovery factor versus affecting dimensionless groups (Figures 4.47 to 4.49), the final multi-variable regressing form of recovery factor is as follows:

$$RF = a + b.Ca + c.Bo + d.\frac{K_f}{K_m} + e.\{Ca.\frac{K_f}{K_m}\} + f.\{Ca.Bo.\frac{K_f}{K_m}\} \qquad \text{If} \quad q \le q_{Critical} \qquad (4.18)$$

$$RF = RF_{Critical} \qquad \text{If} \quad q > q_{Critical} \qquad (4.19)$$

It is worthwhile to note that the product of Bond and Capillary numbers as well as interaction of all three dimensionless numbers would affect the recovery factor parameter in the form of "combinatory impacts". Curve fitting based on the regression analysis results in determining the correlation coefficients as presented in Table 4.9:

Table 4.9: Information table for linear regression model of recovery factor

Coefficients	Numerical value	Standard Error	Lower 95%	Upper 95%
a	50.07562	2.325941	45.43302	54.71822
b	-271062	8651.818	-288331	-253793
c	218012.5	15589.04	186896.7	249128.4
d	0.001129	0.000256	0.000618	0.001641
e	-203.384	6.938715	-217.234	-189.535
f	1563333	59960.75	1443651	1683015

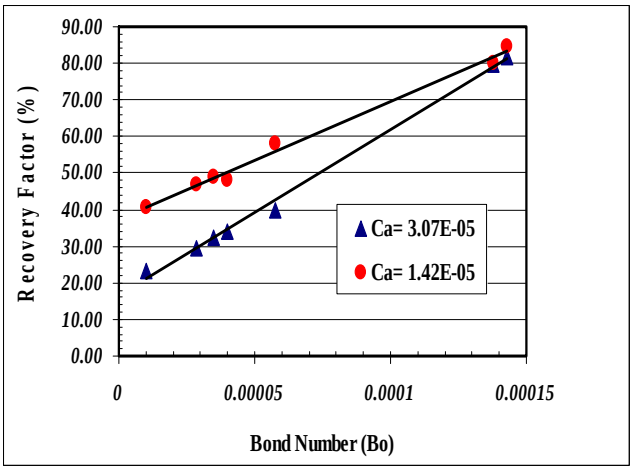

Figure 4.47: Impact of Bond number on production performance of the fractured porous media during the controlled gravity drainage.

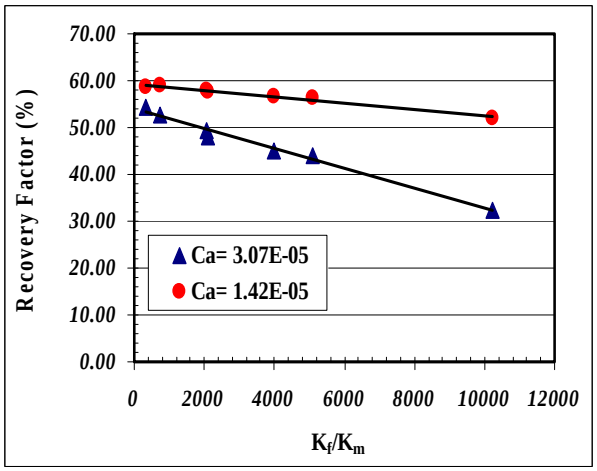

Figure 4.48: Recovery factor versus the ratio of fracture permeability to matrix permeability for two values of capillary number.

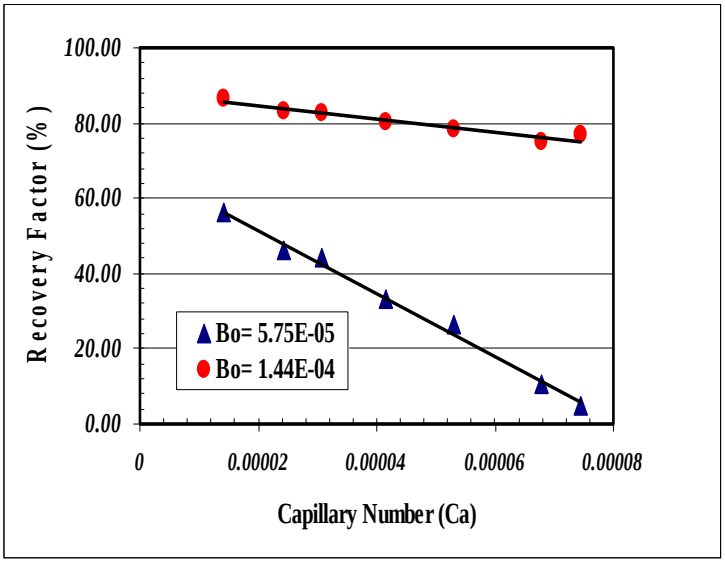

Figure 4.49: Linear plot of recovery factor versus Capillary number at two different magnitudes of Bond number.

Based on the analysis of residual errors illustrated in Appendix C, the multi-variable linear regression correlations are acceptable as they can predict the behaviors of the fractured porous media under the gravity drainage process well.

4.6 Limitations and Assumptions for the Empirical Correlations

The ranges of the dimensionless groups for, which the correlations of CPR, MPWR, R.F and ΔH are applicable, are given in Table 4.10. Moreover, Table 4.11 shows the limitations/restrictions associated with the correlations.

Table 4.10: Ranges of the dimensionless numbers

Dimensionless numbers	Range
Capillary number, Ca	0 – 0.00008
Permeabilities ratio, $\frac{K_f}{K_m}$	0 – 11000
Bond number, Bo	0 – 0.00015
Reynolds number, Re	0 – 5

Table 4.11: Limitations of the empirical equations in the current study

1) Porous medium is non-deformable so it has a constant porosity
2) Viscous drag tensor is neglected due to small pressure gradient
3) No source or sink terms exist for mass
4) Both liquid and gas phases are incompressible at the conditions (very small changes in temperature and pressure)
5) Two phases are immiscible
6) Physical properties of fluids are constant during the experiments
7) The studied case here is two dimensional flow in porous media, though fluid flow in gravitational direction is dominant in a vertical porous system under free fall and controlled gravity drainage processes
8) The correlations are valid just in the range of dimensionless number employed in the current study. Range of dimensionless groups in oil fields are almost the same as we have in the experimental work
9) Geometry of physical models doesn't have big effects on RF in gravity drainage; it just affects residual oil saturation slightly.
10) We had 8 porous media with different fracture patterns, and the correlations are giving very good results with high accuracy for the porous media having these kinds of fracture configuration. Therefore, only main limitation would be type of fracture configuration for the fractured porous media. It should be noted if we have effective fracture permeability for a porous medium with unknown fracture patterns, the obtained empirical equations can help to predict flow behaviour and recovery factor of the porous system somehow.

4.7 Conclusions

The following statements summarize the main results of the combined experimental and statistical research work for the fractured porous media undergoing the controlled gravity drainage (CGD) process.

- During controlled gravity drainage, elevation difference between gas-liquid interface locations in fracture and matrix remains constant while liquid is pumping out of the fractured system with constant withdrawal rate lower than associated Critical Pumping Rate (CPR).

- Pumping rate dictates the liquid communication between matrix and fractures, pressure, fluid flow regimes and also G-L interface movement in fractured porous media during the course of CGD experiments.
- Considering all experimental variables to remain unchanged, CPR is somehow sensitive to the magnitude of liquid viscosity.
- Maximum Possible Withdrawal Rate (MPWR) depends on the fractures' storage capacity, matrix flow properties (i.e. permeability), and also liquid flow properties (i.e. viscosity).
- During CGD experiments, rate of liquid communication from matrix into the fractures remains constant as long as a constant withdrawal rate is maintained.
- When the magnitude of fracture spacing increases, the liquid communication rate from matrix to fracture decreases, and as a result, the associated CPR decreases as well.
- Critical rate, maximum rate, recovery without gas breakthrough and difference of gas liquid interface positions in matrix and fracture were correlated by dimensionless numbers such as Bond number, Capillary, ratio of permeabilities and etc.
- Linear regression modeling presented in this paper can predict production history and flow behavior in our fractured porous media well for a wide range of dimensionless numbers. Therefore it helps us to understand the physics of controlled gravity drainage.

Chapter 5

Numerical Simulation of Gravity Drainage Processes Using COMSOL

5.1 Scope

The simulation of multiphase flow in subsurface porous media needs effective solution methods, and tools for managing the complicated structure of the media as well as for understanding of the transport phenomena in such porous systems. A complex two-phase flow (e.g., Air-Varsol) in porous media under gravity drainage process is studied here in this chapter. The numerical simulation of the gravity drainage process in homogeneous and fractured porous media were carried out using COMSOL. A new numerical modeling approach was proposed to simulate the time-dependent drainage in vertical porous physical models in order to investigate the important aspects of the gravity drainage (free fall or/and controlled gravity drainage) on oil saturation distribution and oil production history. The effect of permeability heterogeneity in the form of fractures on the drainage process was simulated by the fluid flow module of the software used. Furthermore, the evolution of relative permeability of the wetting and non-wetting phases, capillary pressure and some other significant parameters were investigated. The results obtained from this numerical simulation have been compared with the experimental data extracted from the laboratory tests published in the literature. Outputs from the numerical model generally show a very good agreement with the experimental results.

5.2 Governing Equations

Throughout this study, it is assumed that the porous medium has a constant porosity and the cross-product permeability terms associated with the viscous drag tensor can be neglected. It should be mentioned here that different models for deformable porous media with considering thermal and mechanical loads have been developed (Kueper et al., 1991; Chen et al., 1999). The general form of the two-fluid flow equations (without source–sink terms) is described by the two fluid, volume-averaged momentum and continuity equations (Chen et al., 1999) as following:

$$q_w = -\frac{K_w}{\mu_w}[\nabla p_w + \rho_w.g] \tag{5.1}$$

$$q_{nw} = -\frac{K_{nw}}{\mu_{nw}}[\nabla p_{nw} + \rho_{nw}.g] \tag{5.2}$$

$$\phi\frac{\partial(\rho_w.S_w)}{\partial t} + \nabla.(\rho_w.q_w) = 0 \tag{5.3}$$

$$\phi\frac{\partial(\rho_{nw}.S_{nw})}{\partial t} + \nabla.(\rho_{nw}.q_{nw}) = 0 \tag{5.4}$$

Equation (5.2) is the continuity equation of the wetting phase, where Equation (5.1) is the Darcy's equation for the oil phase. Equations (5.4) and (5.3) are the continuity equation and

Darcy's equation for non-wetting phase, correspondingly. In Equations (5.1), (5.2), (5.3) and (5.4), the subscripts w and nw denote the wetting and non-wetting fluids, respectively. Also, $p_i (i = w, nw)$, S_i, q_i, g, μ_i, ρ_i and K_i denote pressure, degree of saturation relative to the porosity, the volumetric flow rate vector, the gravitational acceleration vector, dynamic viscosity, density and the effective permeability tensor, respectively. The effective permeability is defined as the relation between intrinsic permeability (K) and relative permeability (k_{ri}) :

$$K_i = k_{ri}. K \tag{5.5}$$

Assuming that the porous media is non-deformable and with definition of volumetric fluid content as $\theta_i = \phi.S_i$ one can write:

$$S_w + S_{nw} = 1 \tag{5.6}$$

$$\theta_w + \theta_{nw} = \phi \tag{5.7}$$

In Equation (5.7), ϕ is the porosity of the porous media.
Assuming two-dimensional flow and that the wetting fluid is incompressible due to the small variation range of the pressure and then substitution of Equation (5.1) into Equation (5.2) and Equation (5.3) into Equation (5.4) gives:

$$\phi \frac{\partial S_w}{\partial t} = \frac{\partial}{\partial y}\left[\frac{K_w}{\mu_w}\left(\frac{\partial p_w}{\partial y} + \rho_w.g\right)\right] + \frac{\partial}{\partial x}\left[\frac{K_w}{\mu_w}\left(\frac{\partial p_w}{\partial x}\right)\right] \tag{5.8}$$

and similar equation for non-wetting phase,

$$\phi \frac{\partial S_{nw}}{\partial t} = \frac{\partial}{\partial y}\left[\frac{K_{nw}}{\mu_{nw}}\left(\frac{\partial p_{nw}}{\partial y} + \rho_{nw}.g\right)\right] + \frac{\partial}{\partial x}\left[\frac{K_{nw}}{\mu_{nw}}\left(\frac{\partial p_{nw}}{\partial x}\right)\right] \tag{5.9}$$

Equations (5.1) to (5.9) were written for matrix part, though those equations are valid for fractures if there is a fractured medium including two fractures on both sides.
p_{nw} and p_w are the non-wetting and wetting pressures, respectively. The capillary pressure p_C is defined by:

$$p_C = p_{nw} - p_w \tag{5.10}$$

The predefined Darcy's equations under the earth science module in COMSOL are stated for liquid phase and gas phase as follows:

$$\delta_{st}.C_p \frac{\partial p_w}{\partial t} + \nabla.\left[\delta_k \frac{K_w}{\mu_w}(\nabla p_w + \rho_w \vec{g} \nabla h)\right] = \delta_Q Q_w \tag{5.11}$$

$$\delta_{st}.C_p \frac{\partial p_{nw}}{\partial t} + \nabla.\left[\delta_k \frac{K_{nw}}{\mu_{nw}} (\nabla p_{nw} + \rho_{nw} \vec{g} \nabla h) \right] = \delta_Q Q_{nw} \qquad (5.12)$$

where the time scaling factor (δts), the flux scaling factor (δk), the source scaling factor (δQ), storage term ($C_p = d\theta_w / dh_c$), and, the source term (Q) are input parameters. $\delta ts = 0$ is valid for a steady state system and $\delta ts = 1$ is for a transient system. δk is the flux scaling factor which is unity in our gravity drainage system. Q is the source term. In this research, Q is equal to zero for both phases. The storage term (Cp) is a function of porosity (ϕ), residual wetting saturation (S_{wr}) and the effective wetting saturation and pressure.

Equations (5.11) and (5.12) for the pre-defined boundary conditions can be solved simultaneously. The functional description of the capillary pressure–saturation, $h_c(S_w)$, and permeability functions, $K_i(S_w)$, enables estimation of the evolution of wetting and non-wetting phases distribution. Also, to estimate the constitutive relations parameters properly, one can employ the obtained function into the governing equations (Parker et al., 1987; Chen et al., 1999; Zhang, 2002).

5.3 Capillary Pressure and Permeability Functions

The numerical model used the capillary pressure versus saturation curve to evaluate the saturation of the liquid. During the numerical simulation, both liquid and gas phases exist in the control volume. Therefore capillary pressure curve for our two phases should be taken into account during the simulation of the gravity drainage phenomena.
The scaling of capillary pressure curve of a particular porous medium in accomplished using the following relation:

$$\frac{P_{c1}}{P_{c2}} = \frac{\sigma_{og_1}}{\sigma_{og_2}} \sqrt{\frac{K_2}{K_1}} \qquad (5.13)$$

where σ_{og} is the interfacial tension of the oil-gas system. The capillary pressure of the porous medium is a function of interfacial tension and permeability. Therefore, the capillary pressure values will change as the properties of oil (or liquid) vary. This affects the capillary pressure curves that were used to evaluate the oil saturation in the particular position of the system.
The developed constitutive models to description of the capillary pressure–saturation, and permeability functions are listed in Table 5.1.

Table 5.1 : Two-fluid capillary pressure and permeability parametric models (Beckner, 1990; Kueper et al., 1991; Sahimi, 1995)

Parametric Model	Parameters	Capillary pressure functions	Relative Permeability functions
VGM (Van Genuchten)	$\theta_{ws}, \theta_{wr}, k, \alpha_{vg}, n, m, \eta$ where, m=1-1/n	$S_{ew} = \frac{1}{\left[1+(\alpha_{vg}h_c)^n\right]^m}$	$k_{rw} = S_{ew}^{\eta}\left[1-(1-S_{ew}^{\frac{1}{m}})^m\right]^2$ $k_{rnw} = (1-S_{ew})^{\eta}\left[1-S_{ew}^{\frac{1}{m}}\right]^{2m}$
BCM (Brook and Corey)	$\theta_{ws}, \theta_{wr}, k, h_e, \lambda, \eta$	$S_{ew} = (\frac{h_e}{h_c})^{\lambda}$	$k_{rw} = S_{ew}^{\eta+2+2/\lambda}$ $k_{rnw} = (1-S_{ew})^{\eta}\left[1-S_{ew}^{1+1/\lambda}\right]^2$
BRB (Brutsaert–Burdine)	$\theta_{ws}, \theta_{wr}, k, \beta, \gamma$	$S_{ew} = \frac{\beta}{\beta+h_c^{\gamma}}$	$k_{rw} = S_{ew}^2\left[1-(1-S_{ew})^{1-2/\gamma}\right]$ $k_{rnw} = (1-S_{ew})^{3-2/\gamma}$
GDM (Gardner–Mualem)	$\theta_{ws}, \theta_{wr}, k, \alpha_g$	$S_{ew} = (1+0.5\alpha_g h_c)e^{-0.5\alpha_g h_c}$	$k_{rw} = e^{-\alpha_g h_c}$ $k_{rn} = (1-e^{-0.5\alpha_g h_c})^2$

In this study, the Van Genuchten equation (VG) is employed to compute capillary pressure and relative permeability in the numerical modeling (Van Genuchten, 1980):

$$S_{ew} = [1+(\alpha h_c)^n]^{-m} \tag{5.14}$$

where S_{ew} denotes the effective saturation of the wetting fluid, $S_{ew} = \frac{(\theta_w - \theta_{wr})}{(\theta_{ws} - \theta_{wr})}$.

θ_{ws} and θ_{wr} are the saturated and residual wetting fluid content, respectively; α and n are fitting parameters, that are inversely proportional to the non-wetting fluid entry pressure value and the width of pore-size distribution, respectively. It is assumed that m=1-1/n and that the effective saturation of the non-wetting fluid (S_{en}) is derived from S_{en} =1-S_{ew}.

The capillary pressure–saturation function can be considered a static rock property, while the permeability function is a hydrodynamic property describing the ability of the medium to conduct a fluid. The basic assumption behind the capillary pressure–permeability prediction models are from conceptual models of flow in capillary tubes combined with pore-size distribution knowledge which are derived from the capillary pressure–saturation relationship. A typical representation of this type of model follows Mualem's formulation (Van Genuchten, 1980) which is as the following:

$$k_{rw} = S_{ew}^n \left[\frac{\int_0^{S_e} \frac{dS_e}{h_c}}{\int_0^1 \frac{dS_e}{h_c}}\right]^2 \tag{5.15}$$

$$k_{rn} = (1 - S_{ew})^n \left[\frac{\int_{S_e}^{1} \frac{dS_e}{h_c}}{\int_{0}^{1} \frac{dS_e}{h_c}} \right]^2 \tag{5.16}$$

Combining the Van Genuchten capillary pressure–saturation equation (5.14) with the Mualem (VGM) model-with introducing new parameter the tortuosity parameter (η) gives permeability functions as follows according to Mualem (1976):

$$k_{rw} = \frac{K_w}{K} = S_{ew}^{\eta} \left[1 - (1 - S_{ew}^{\frac{1}{m}})^m \right]^2 \tag{5.17}$$

$$k_{rnw} = \frac{K_{nw}}{K} = (1 - S_{ew})^{\eta} \left[1 - S_{ew}^{\frac{1}{m}} \right]^{2m} \tag{5.18}$$

For convenience in modeling and due to lack of information to the contrary, the η value was set equal to 0.5 for both the wetting and non-wetting permeability expressions throughout this study.Based on the research work of Chen et al (1998), it was found that the parameter changes from 0.45 to 0.6, depending on the size of glass beads.

The Corey's equation can be used to calculate relative permeability for numerical modeling. The following formulas show the relationship between saturation degree and relative permeability of each phase in Corey's analogy (Chatzis and Morrow, 1983; Saidi, 1987; Sahimi, 1995):

$$k_{rw} = \frac{K_w}{K} = S_{ew}^4 \times (h_c > 0) + 1 \times (h_c \le 0) \tag{5.19}$$

$$k_{rnw} = \frac{K_{nw}}{K} = (1 - S_{ew})^4 \times (h_c > 0) + 1 \times (h_c \le 0) \tag{5.20}$$

where h_c is capillary height.

The capillary pressure data for the experimental cases in this study were defined by the van Genuchten correlation for capillary pressure versus saturation. The capillary height curves shown in Figure 5.1 were curve fitted values using the van Genuchten and Brooks-Corey empirical models for the matrix part. The variables in van Genuchten and Brooks-Corey correlations for this research work are summarized in Table 5.2.

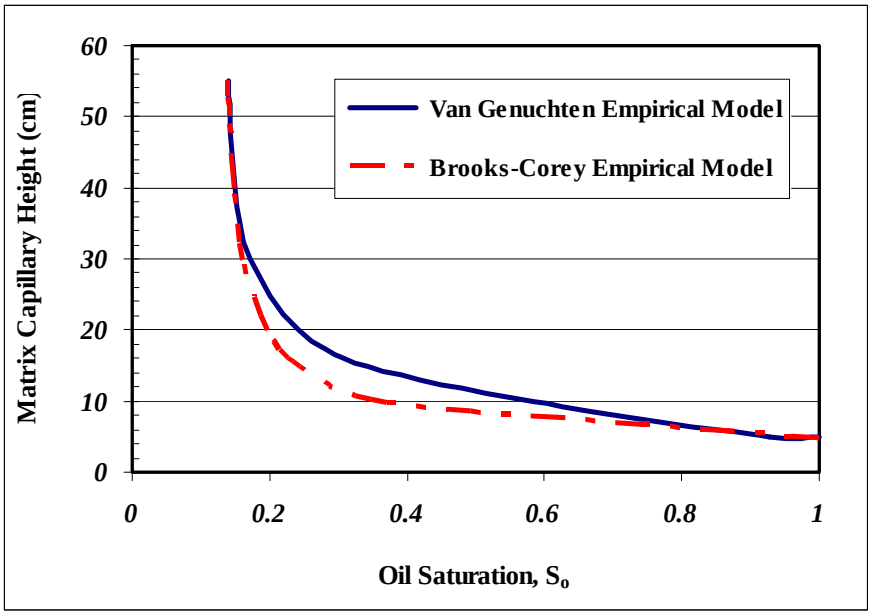

Figure 5.1: Capillary height curves for the matrix part saturated with Varsol oil based on two different empirical models (Matrix made with BT3 glass beads).

Table 5.2: The variables of the capillary pressure curves used in the numerical simulation

Parameter values		α	n	λ	m=1-1/n	Capillary threshold height (h_c), cm
h_c versus S_{ew}	van Genuchten	0.112	3.5	N/A	0.714	5
	Brooks-Corey	N/A	N/A	1.85	N/A	5

For the fracture part, the parametric models mentioned above for the capillary pressure–saturation and permeability functions were tested in their ability to fit the multi-step outflow experimental data. However none of them produced results with reasonable accuracy. Therefore in this case, the relative permeability constitutive equations tried are based on expressions proposed by Honarpour et al., (1982) which are as the following:

$$k_{rw} = k_{rw}^{0}\left[\frac{(S_w - S_{wr})}{(1 - S_{wr})}\right]^{n_o} \tag{5.21}$$

$$k_{rnw} = k_{rnw}^{0}\left[\frac{(1 - S_w)}{(1 - S_{wr})}\right]^{n_g} \tag{5.22}$$

In order to get results with lower absolute error percentage with respect to experimental findings, a set of required parameters are suggested for proposed empirical model. The parameters for the fitted curved are tallied in Table 5.3.

Table 5.3: Fit Parameters for fracture relative permeability in gravity drainage experiments

Parameters	Numeric value
k_{rw}^{0}	1.0 ± 0.15
n_o	2.0 ± 0.22
k_{rnw}^{0}	0.4 ± 0.08
n_g	3.1 ± 0.16

5.4 Numerical Simulation

A brief review of the state of the art literature concerning the numerical implementation of multiphase fluid flow model reflects that the finite element methods (FEM) are the general framework for numerical simulation in very large problems (Blunt and King, 1992; Kazemi and Gilman, 1993).

Flow in porous media is a subject of interest in many fields of the science and engineering, such as hydrogeology, petroleum engineering, and chemical engineering. The case of two-region heterogeneous media (e.g., fractured media) plays a fundamental role in numerical modeling of transport phenomena in porous media systems (Aziz and Settari, 1979). Many different theoretical models are implemented under COMSOL, using many of the original features of the software (COMSOL guide, version 3.5). These models correspond to direct simulation and macro-scale or large-scale models .In this section, some important aspects of the application of the COMSOL for a comprehensive analysis of transport through porous media which are either homogeneous or fractured ones are discussed. Also, a new numerical model for gravity drainage was developed to address certain limitations of the existing numerical simulation models. Instead of employing double porosity to deal with a complex term named communication rate between matrix and fracture, the new model considers matrix and fracture parts separately gridded properly in the modeling approach and then had continuity equation for each subdomain. Finally in order to apply communication between fracture and matrix, continuity was set in interior boundaries that mean pressure and velocity is identical for matrix and fracture parts. Therefore, the new model does not require a predefined equation for transfer rate which probably makes some errors due to various amounts for shape factor existing in the communication rate equation (Kazemi, 1990; Hoteit and Firoozabadi, 2008). In the following sections the numerical modeling along with the analysis of simulation outputs are presented and discussed in a great details. In the last section results obtained from the current numerical simulation are compared with the experimental data (Zendehboudi et al., 2008; Zendehboudi et al., 2009).

5.4.1 Subdomains, boundary and initial conditions: COMSOL 3.5® uses a graphic user interface (GUI) to model the problem analyzed. The GUI is simple to use and enables modeling of complex geometry. The analysis of the gravity drainage process is conducted using a 2-D rectangular control volume, constructed of 1 subdomain and 4 boundaries for homogeneous porous media and 3 subdomains and 6 boundaries for fractured unconsolidated media. The subdomain represents the control volume of the porous media. The dimension of the modeled control volume is same as the physical model (23.5 cm in width and 55 cm in height for the matrix part and 0.5 cm for aperture width and 55 cm in height for the fractures). The y axis is the

vertical axis with gravity acting in the "-y" direction. The permeability and porosity values for matrix are 3×10^{-10} m^2 and 0.38 respectively.

The combination of governing equations (5.7) and (5.8), the boundary and initial conditions (Figures 5.2 and 5.3 and Tables 5.4 and 5.5), and the constitutive relationships in equations (5.11 and 5.12) constitute the mathematical model of the system. The mathematical model has no analytical solution available because of the nonlinearity of the constitutive functions. Therefore, a numerical model should be adapted to simulate the two-fluid flow regime (Chen et al., 1999; Hoteit et al., 2008).

Initially, the control volume is assumed to be saturated with 100% oil phase. At $t > 0$, boundary 4 is exposed to air with atmospheric pressure and boundary 3 is opened for to the collection cylinder (see Figure 5.2). Since during free fall gravity drainage both the apparatus and the collection cylinder operate at identical system pressure equal to 1 atmosphere, the effect of pressure on the system is negligible. Therefore, in the upper bound of the geometry (Figure 5.2), air pressure equal to one atmosphere where the lower bound of the sample is in-transferable to non-wetting phase due to having capillary threshold height (Figure 5.2). The employed parameters for the porous media samples are shown in Table 5.6 which was used in the experimental work performed by Zendehboudi et al. (2008 & 2009).

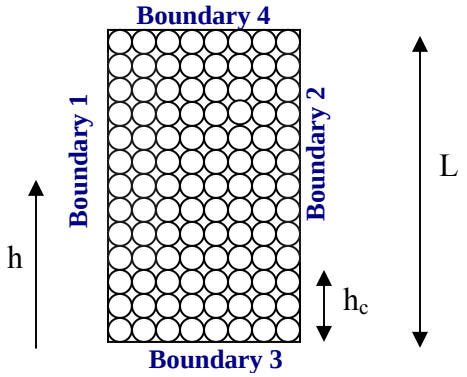

Figure 5.2: Boundaries of homogeneous porous media during FFGD and CGD for numerical modeling.

The procedure for doing a controlled gravity drainage experiment is the same as that for free fall gravity drainage except a constant flow rate is withdrawn during the gravity process, while in free fall gravity drainage the exit pressure is atmospheric.

Table 5.4: Boundary and initial conditions for homogeneous medium in COMSOL®

Boundary conditions	Free Fall Gravity Drainage(FFGD)		Controlled Gravity Drainage (CGD)	
	Wetting phase	Non-Wetting phase	Wetting phase	Non-Wetting phase
Boundary 1	Zero flux	Zero flux	Zero flux	Zero flux
Boundary 2	Zero flux	Zero flux	Zero flux	Zero flux
Boundary 3	$P_O=0$	Zero flux	$q_{Production}$=constant	Zero flux
Boundary 4	Zero flux	$P_O=0$	Zero flux	$P_O=0$
Initial conditions	$P(h,0) = P_{Bottom} - \rho_w.g.h$	$P(h,0)=\rho_{nw}.g.(L-h)$	$P(h,0) = P_{Bottom} - \rho_w.g.h$	$P(h,0) =\rho_{nw}.g.(L-h)$

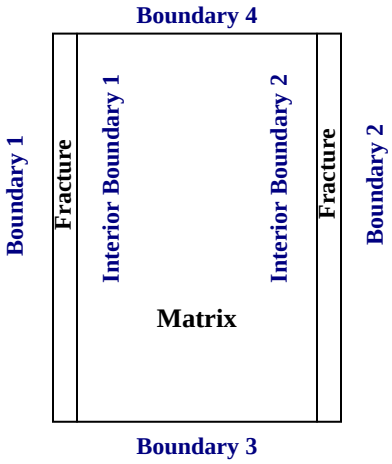

Figure 5.3: Boundaries of fractured porous media during FFGD and CGD for numerical modeling.

Table 5.5: Boundary and initial conditions for fractured medium in COMSOL®

Boundary conditions	Free Fall Gravity Drainage(FFGD)		Controlled Gravity Drainage (CGD)	
	Wetting phase	Non-Wetting phase	Wetting phase	Non-Wetting phase
Boundary 1	Zero flux	Zero flux	Zero flux	Zero flux
Boundary 2	Zero flux	Zero flux	Zero flux	Zero flux
Boundary 3	P_O=0	Zero flux	$q_{Production}$=constant	Zero flux
Boundary 4	Zero flux	P_O=0	Zero flux	P_O=0
Interior boundary 1	Continuity	Continuity	Continuity	Continuity
Interior boundary 2	Continuity	Continuity	Continuity	Continuity
Initial conditions	$P(h,0) = P_{Bottom} - \rho_w.g.h$	$P(h,0) = \rho_{nw}.g.(L-h)$	$P(h,0) = P_{Bottom} - \rho_w.g.h$	$P(h,0) = \rho_{nw}.g.(L-h)$

Table 5.6: Parameters required for employed porous media in numerical modeling

Type of the medium	Matrix permeability , Darcy	Test fluid	Oil viscosity , cp	Oil density, g/cm^3	Oil interfacial tension , mN/m	Fracture aperture, mm	Model height, cm
Homogeneous	300	Varsol	1.2	0.781	25	N/A	55
Fractured	300	Varsol	1.2	0.781	25	5	55

5.4.2 Mesh configurations: COMSOL 3.5 is a finite element analysis tool. Once all variables are input into the system and the subdomain is discretized into small elements. Typically, smaller mesh size produces more accurate numerical simulation; however, there is a limit to the mesh size used in the numerical model due to this fact that the smaller mesh size in the subdomain increases the number of elements in the numerical simulation. This will in turn increase the

computational efforts and time required for the numerical model. We use exponential distribution of mesh size for the numerical modeling of fractured porous medium as smaller meshes in the boundaries and bigger ones for middle parts of matrix are chosen. First, we fix the size for meshes (almost equal to mesh size in fracture) close to the boundary of matrix and fracture and size of meshes grows exponentially as we are approaching to the middle of matrix. Since fracture is small enough, the uniform mesh size was selected for the fracture parts.
To further understand the effect of mesh size on the numerical simulation result, two simulations were run with 39 mm (horizontal) by 37 mm (vertical) and 3.9 mm (horizontal) by 3.7 mm (vertical) mesh size to study the effect of the mesh size on the precision and accuracy of the numerical simulation. The effect of mesh size on the results are presented and discussed in section 5.5.4.

5.4.3 Method in analyzing the numerical results: The developed numerical model can evaluate the liquid saturation, the liquid cumulative production and the liquid velocity for each element and output the numerical results at some time intervals. The output data were analyzed before they were compared with the results from the experimental data. The focus of analysis of the results obtained from numerical model is the liquid saturation, velocity of liquid phase and the liquid production history.

5.4.3.1 Simulation runs of free fall gravity drainage: Figure 5.4 shows the results of the total velocity field calculation of COMSOL (solving of the PDEs by considering boundary condition) for homogeneous porous media under FFGD. As can be seen here, the velocity vectors of non-wetting phase (air), V_{nw}, follow a regular decreasing with the height of the sample in gravitational force direction. At the other hand, velocity of the wetting phase (V_w) increases as fluids are approaching the bottom of physical model. Also, due to blocking of the lower boundary condition for air flow as results of capillary threshold height, after 130 seconds there is a significant decrease in the rate of pressure and saturation degree changes for air as non-wetting phase. This is due to this fact that the air is a non-wetting phase here and cannot go through when gas-liquid interface reaches almost 5 cm of the model height relative to the bottom of the physical model. Also, the air saturation and air pressure would be in their minimum values.

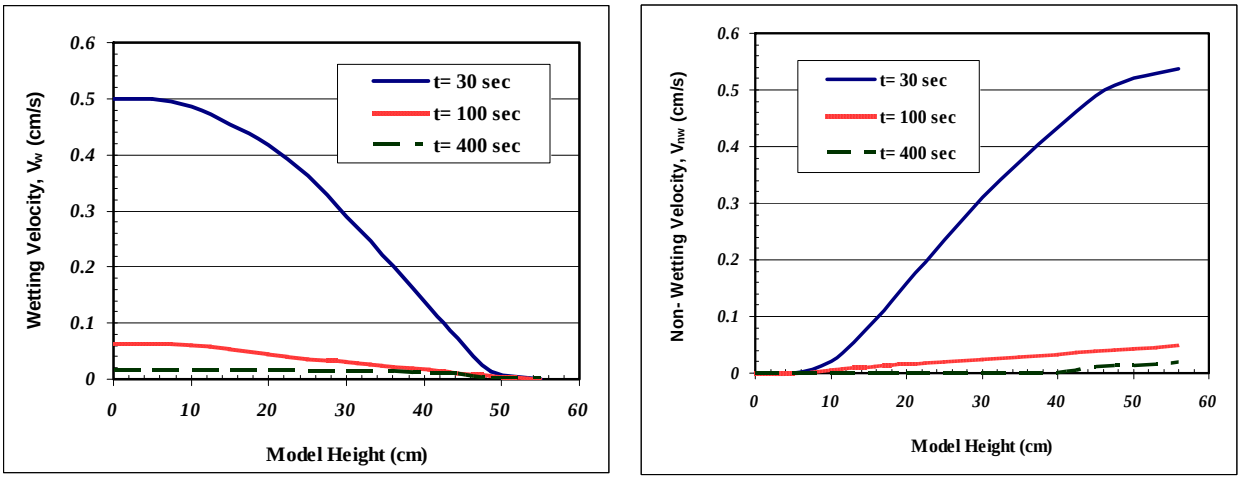

(a) (b)

Figure 5.4: Total Velocity versus height of homogeneous porous medium under FFGD, a) Wetting phase (V_w) b) Non-wetting phase (V_{nw}).

Figures 5.5a to 5.5c show the changes in non-wetting phase saturation for unfractured media which is drained in a free fall gravity drainage mode. The background color shows the extractable (effective) air volume fraction in which the red color is 100% air and blue is 0% air. The non-wetting phase across the reservoir pushes the Varsol oil in gravitational force direction during the process and flow direction of wetting phase is towards the bottom of the physical model. As the fluid reaches the production well, then the wetting phase velocity and also oil saturation degree increase at each particular time. It should be noted here that there are initial rapid changes in saturation followed by very slow drainage of the wetting phase. There are two features which help to describe the displacement pattern. First, gas rapidly reaches the equilibrium position (h_c) beyond which the column is saturated with the wetting phase. Second, at the later stages of the process the saturation profile is almost uniform with a distance from top of the h_c and then decreases slowly over the time.

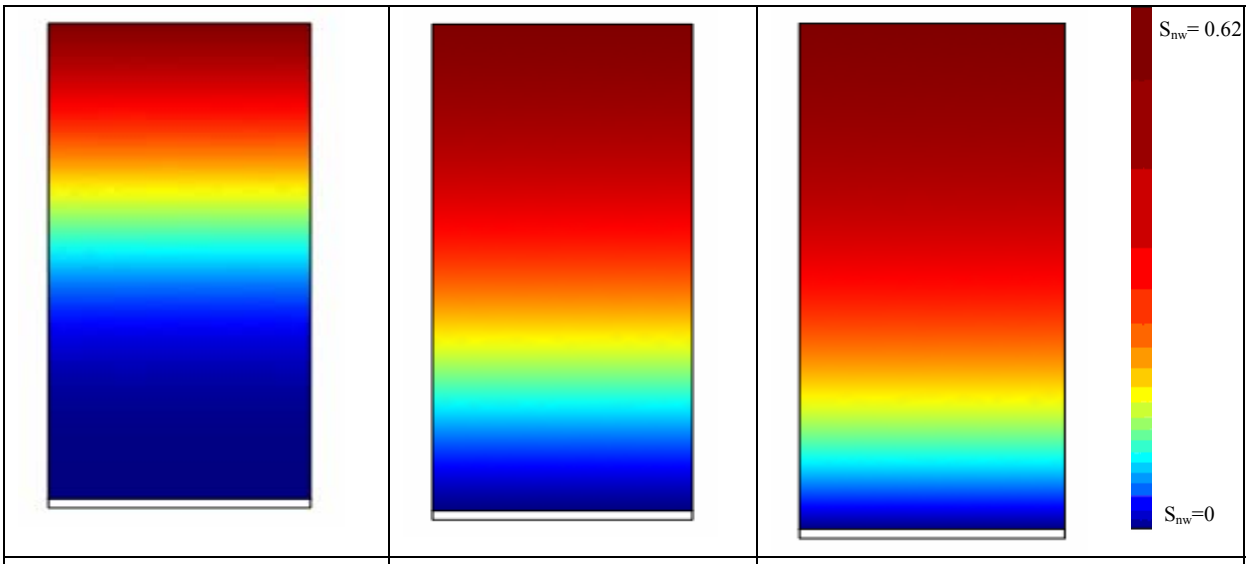

(a), @ t=40 sec | (b) , @ t=120 sec | (c) , @ t=400 sec

Figure 5.5: Effective saturation of non-wetting phase evolution during FFGD for homogeneous porous media.

Figures 5.6 and 5.7 demonstrate the distribution of the wetting fraction in a 55 cm-length volume of the fractured porous medium after 30 seconds and 120 seconds of FFGD, respectively. As shown in these figures, at time of 30 seconds there is still some oil phase in fracture and that this is why the percentage of residual oil saturation is 100% in the whole distance of 12 cm from the bottom of the fractured porous medium. However, as time goes on the gas-liquid interface advances more downward and finally after 120 seconds the fracture part gets empty and there is just drainage from porous matrix which provides the oil production. If more time is let the drainage process proceed, then the oil production will happen via oil film mechanism. If so, then lower average residual oil saturation value than what is seen in Figure 5.7 is attainable.

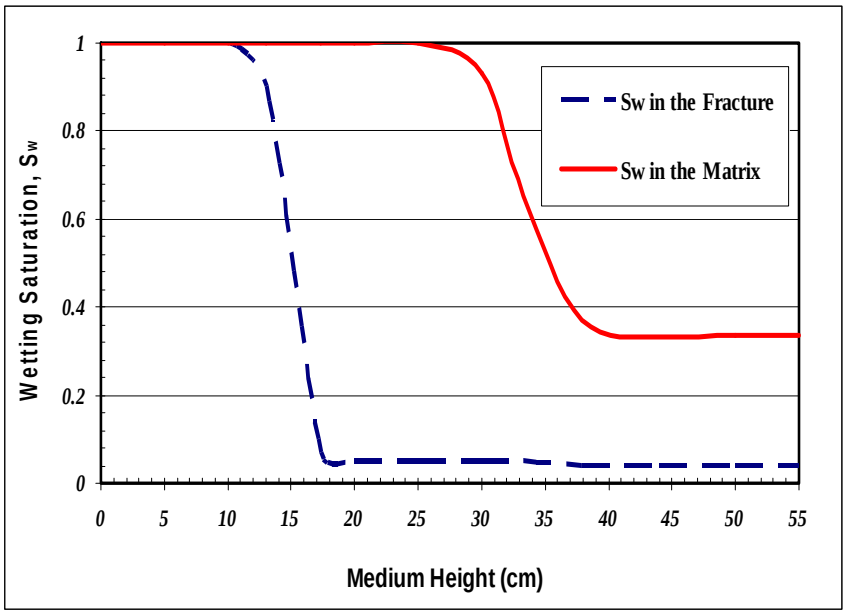

Figure 5.6: Wetting phase distribution curve along the model height after 30 seconds that free fall gravity drainage process proceeds in the fractured medium [BT3 glass beads, test fluid: Varsol oil, L= 55 cm , b=5 mm].

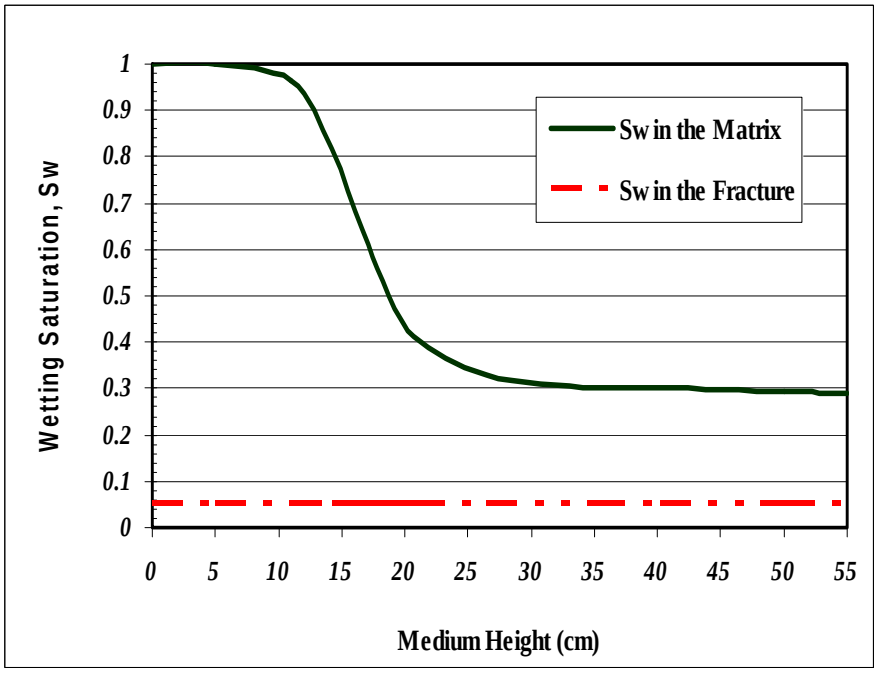

Figure 5.7: Oil saturation fraction versus height of a fractured porous medium saturated with Varsol under FFGD at t=120 sec [BT3 glass beads, L= 55 cm, b=5 mm].

Based on the two empirical models brought in Table 5.1, the numerical modeling data of relative permeability against wetting saturation were shown in Figure 5.8 for the homogeneous porous

media with permeability equal to 300 Darcy. According to Brooks-Corey correlation, a K_{rw} of about 0.4 can be calculated for a residual oil saturation of 0.8 (x=10 cm and y=40 cm). The relative permeability of each phase is proportional directly with the value of that phase's saturation degree. This means that the oil relative permeability will be higher at the points with higher residual oil saturation during free fall gravity drainage.

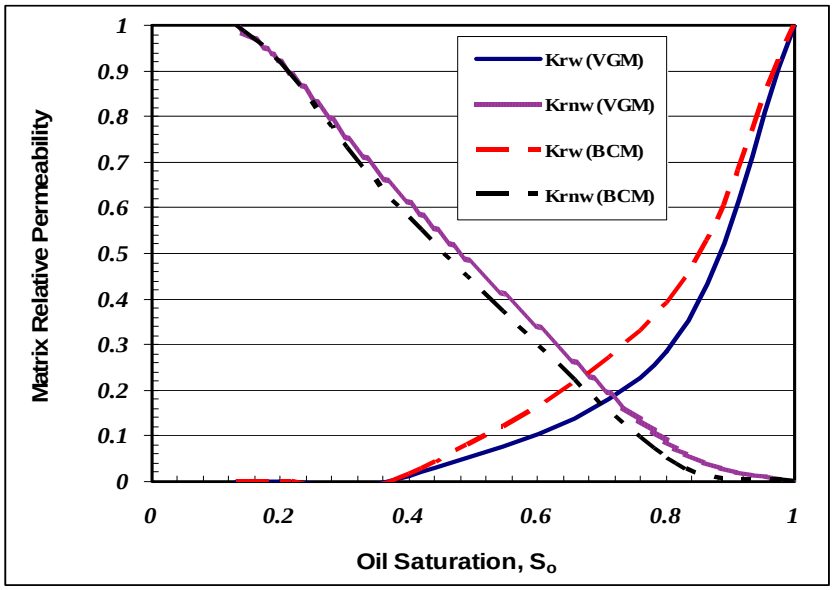

Figure 5.8: Oil and gas relative permeability versus wetting saturation degree for BT3 glass beads homogeneous porous medium fully saturated with Varsol.

As production starts in fractured oil reservoirs under gravity drainage, the oil in the fracture is first recovered and then gas from the gas cap or the free gas or injected gas replaces it. The oil in the matrix needs longer time to be drained by gravity into the fractures. This causes the fractures to become saturated with gas while the matrix contains mainly oil. Therefore the gas-oil contact (GOC) in fracture advances ahead of that in the matrix blocks. This difference in the contacts elevation in addition to the density difference between the oil in the matrix and the gas in the fracture provides the pressure difference required for the oil transferring from the matrix into the fractures. The final recovery factor from the matrix is determined by the balance between the capillary pressure and gravity forces. The numerical simulation of the FFGD experiment in a fractured medium during a time period of 30 seconds (Figure 5.9) shows the non-wetting phase distribution within the physical model. Since the fracture part of the model has a higher permeability, the air front moves further ahead in the fracture and it has a higher velocity initially. Therefore, it is not on the same level as in the matrix part.

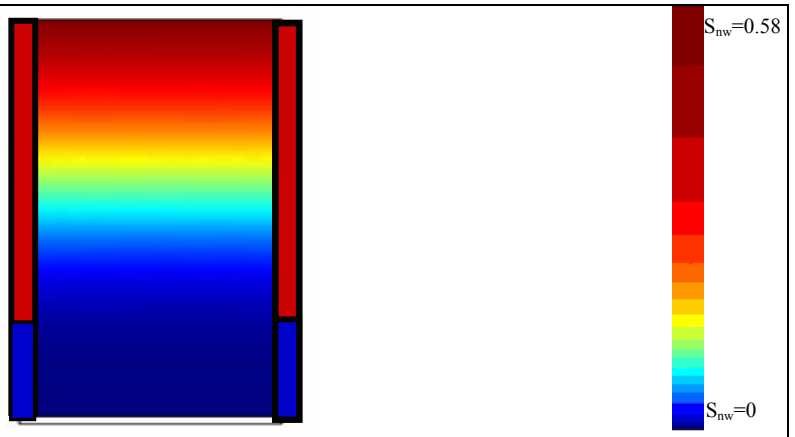

Figure 5.9: Non-wetting saturation distribution within two different parts of the fractured porous medium under FFGD [BT3 glass beads, b=5 mm , L=55 cm, t= 30 sec].

Figure 5.10 presents the field velocity profile versus model width for the fractured porous medium. The total velocity here is almost a flat line for the matrix part and there is a same velocity for the points located at the identical y-coordination. Furthermore, there is a considerable difference between velocity in fracture part and matrix part when the FFGD starts or the process is at the beginning of communication between matrix and fracture. The liquid velocity in the fracture is much higher than the matrix part. The liquid velocity in the fracture increases with increase in the fracture aperture. The dotted line in the Figure 5.10 represents the described velocity distribution. This phenomenon occurs when the elapsed time is 5 seconds in free fall gravity drainage mode. However as the process proceeds, more communication would be established between these two different parts of the medium, causing drainage of more liquids into the fracture and a bigger decline in movement rate of G-L interface in fracture towards the bottom of the physical model. However, this also depends on the magnitude of communication between matrix and fracture, and fracture dimensions. Such a process can occur in any of the following conditions:

1- Where the communication rate is very low (i.e. matrix permeability is small or oil phase is too viscous) and interfaces between matrix and fracture acts like an impermeable wall. Consequently, the liquid velocity still has a higher value in fracture than in the matrix.

2- Magnitude of the liquid transferred into the fracture is moderate as G-L interface positions move downward with a same velocity at both parts and there is no significant difference between them.

3- For the case of the present study, the matrix is highly permeable and the oil phase has a low viscosity. Therefore, the communication between matrix and fracture is strong enough allowing drainage of a considerable amount of oil into the fracture part. This transferring rate acts like a resistance force applying on side part of the fracture and this affects liquid velocity in fracture significantly leading to a lower G-L interface velocity in fracture even to values lower than the value of G-L interface velocity in the matrix (See Figure 5.9 for the velocity profile at 20 seconds).

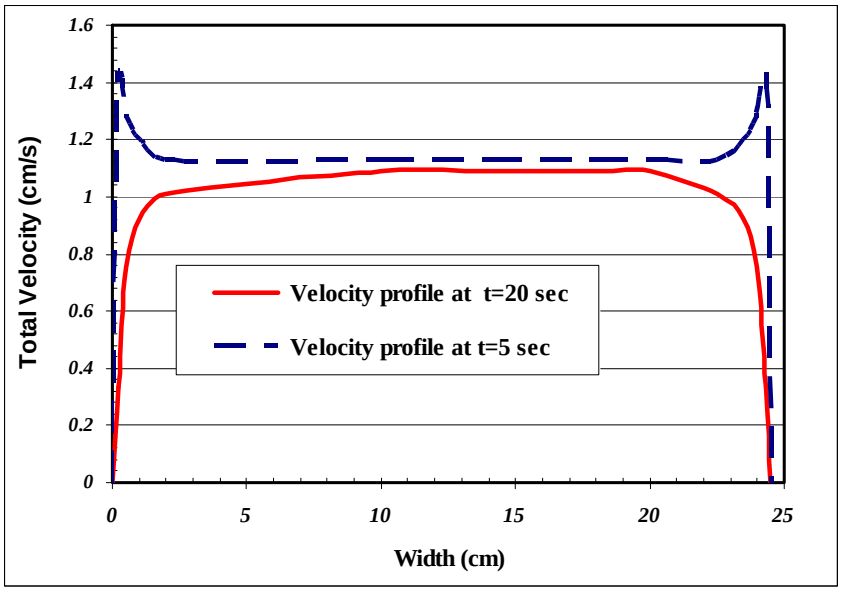

Figure 5.10 : Velocity profile along the width of the fractured porous medium saturated with Varsol oil for two different times of free fall gravity drainage [BT3 glass beads, L=55 cm , b=5 mm].

Figure 5.11 shows results for wetting and non-wetting phase relative permeabilities against oil saturation for the fracture part in the fractured porous media under FFGD. It should be emphasized here that the connate water saturation in this study is assumed to be equal to zero. This new approach is based on the continuity of capillary pressure at the fracture-matrix interface. This makes possible estimating physically correct relative permeability values for multiphase flow between fractures and the matrix. This new conceptual model overcomes a serious flaw that exists in most of the current simulation practices when estimating flow mobility for fracture-matrix flow term. Figure 5.11 conveys this message again that two-phase flow through the fractures can be modeled adequately by using a porous medium approach. In this approach, Darcy's law which governs the flow and phase interference is represented by a relative permeability variable. By choosing the appropriate fitting parameters (See Table 5.3) and applying them in a model proposed by Honarpour et al. (1982), a relative permeability model is obtained that is capable of predicting the fracture behaviour during the gravity drainage processes. There is an acceptable agreement between experimental results and the simulator outputs.

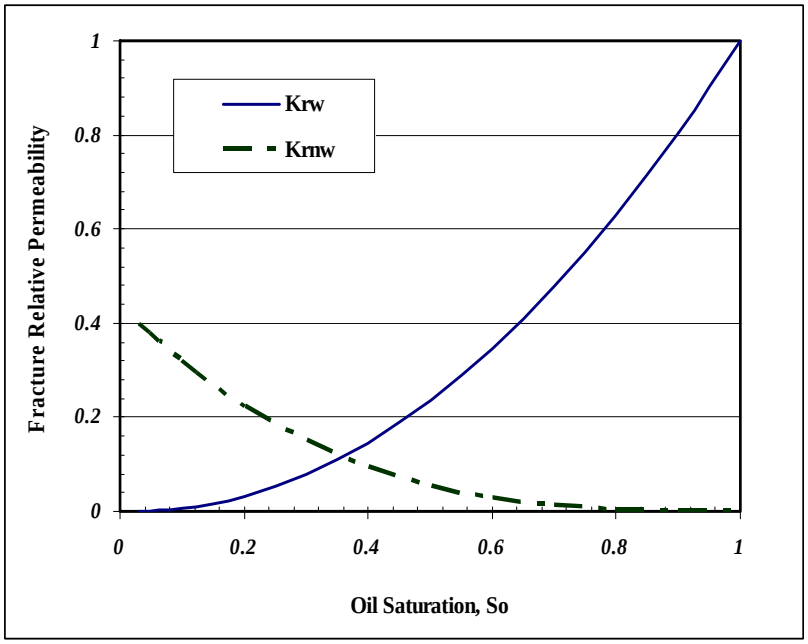

Figure 5.11: Oil and gas relative permeability curves for the fracture part based on the fitted Honarpour et al. expression for the case under study.

5.4.3.2 Simulation runs for controlled gravity drainage: The second problem addressed here is how to reproduce the flow behaviour in a controlled gravity drainage experiment in unconsolidated porous media under laboratory conditions. In Figures 5.12a to 5.12c, the numerical solutions for wetting saturation for an unfractured medium while pumping the oil from that medium with permeability of $3^* 10^{-10}$ m^2 and viscosity of 1.2 mPa.s for a time period of 2 minutes with different pumping rates are shown. The red colour and blue colour represent the maximum amount and minimum wetting phase saturation in Figures 5.12, respectively. It could be observed that there are various wetting saturation distributions for each withdrawal rate and lower pumping rate keeps higher amount of wetting phase in the porous media after elapsing a particular time of CGD.

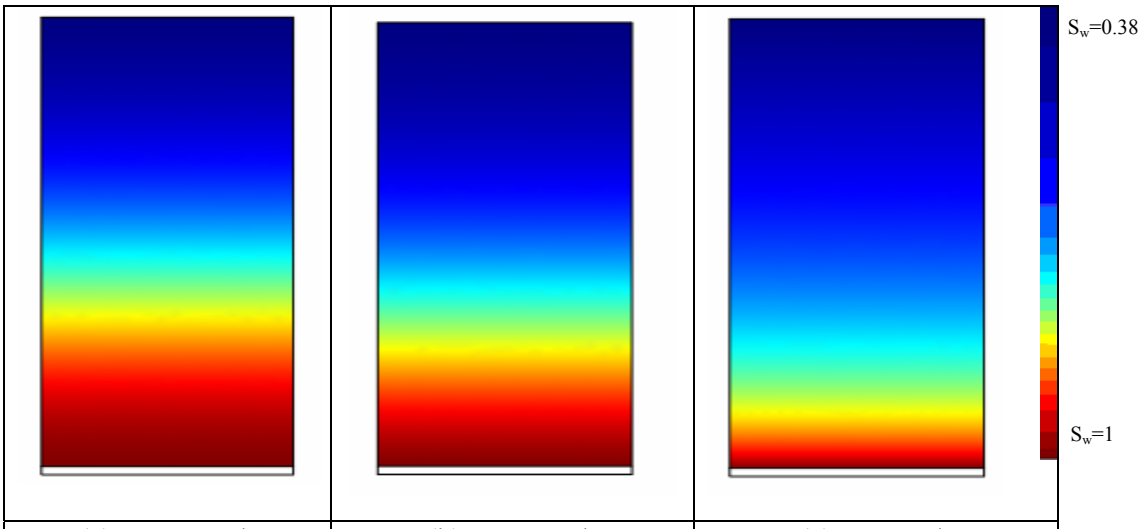

(a) q= 1.8 g/s	(b) q=2.2 g/s	(c) q= 3 g/s

Figure 5.12: Wetting phase evolution after 2 minutes of CGD process for the homogeneous porous medium saturated with Varsol oil at various volumetric flow rates [BT3 glass beads, L=55 cm].

Figures 5.13a to 5.13b present numerical solutions for the CGD process in fractured porous medium, in form of schematic cartons, to capture non-wetting phase front displacement and distribution of the residual oil saturation after 2 minutes. This graphical presentation shows that the gas-liquid interface moves faster in fractures compared with matrix at the initial stage of the process during which liquid has not been drained out of the matrix. In addition, Figure 5.13 indicates that when liquid withdrawal rate increases, assuming all other system parameters remain unchanged, the rate of G-L interface recession in both matrix and fractures increases, as well. This increase in the recession rate of interface also leads to increases in the elevation difference between interface positions within the matrix and fractures.

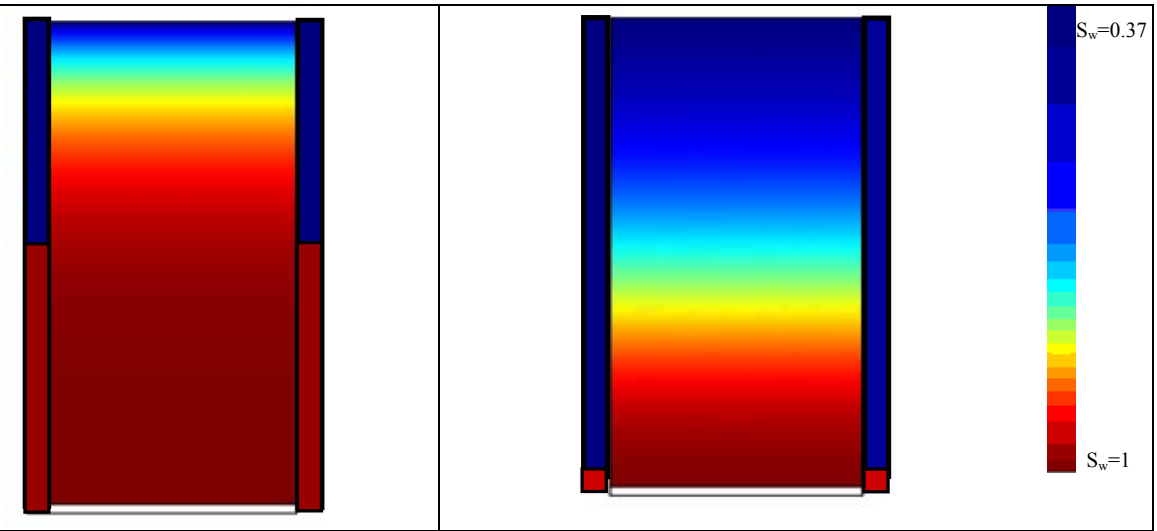

(a) q= 0.8 g/s	(b) q= 1.8 g/s

Figure 5.13: Gas front evolution in two different parts of the fractured porous medium for two withdrawal pumping rates at the time of 2 minutes of CGD [b=5 mm , L=55 cm].

Figure 5.14 presents change in wetting saturation along the model height at 60 sec and 260 seconds, respectively. These results explain well that during a short period of controlled gravity drainage, still a part of the porous medium has not become empty and oil saturation is 100% there. This means that non-wetting phase front still is placed behind the saturated part. However, as the process proceeds, the volume of fully saturated part would get smaller and finally it vanishes and gas-liquid interface touches the bottom of the porous medium. Such condition happens at 260 seconds and the residual oil saturation has the highest value close to production point. Also, the lowest residual oil saturation occurs at the top of the physical model. Therefore, as time goes on the average residual oil saturation decreases with time.

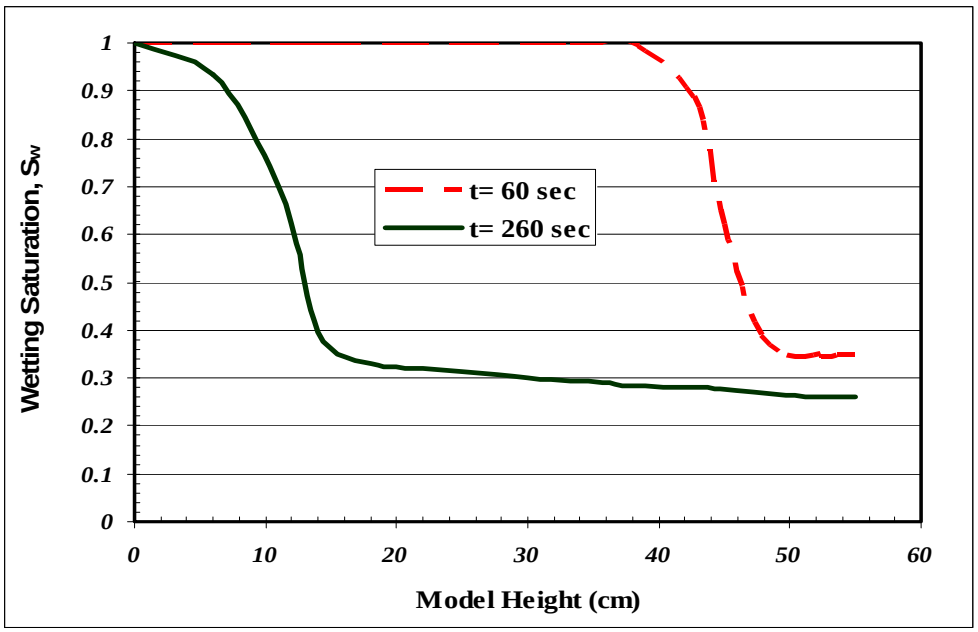

Figure 5.14: Oil saturation against model height under CGD at two different particular times [L= 55 cm, q= 1.4 g/s].

Figures 5.15 and 5.16 show velocity profile of the two immiscible-phase problem for the homogeneous porous medium and fractured one. As expected, field velocity for cross section of the medium at the bottom end part is the same as the withdrawal velocity identified in the simulation input data when the numerical modeling was set for homogeneous medium. Hence, in modeling of a fractured medium the same result came out and equal velocities for bother the fracture and matrix parts. These velocities are identical with outward velocity, but the volumetric flow rate of matrix part is much higher than the fracture part because of bigger cross sectional area of the matrix part. Such problems can exhibit good examples of the real phenomena related to oil velocities in petroleum reservoirs that can be in the forms of homogeneous or a porous medium with vertical fractures.

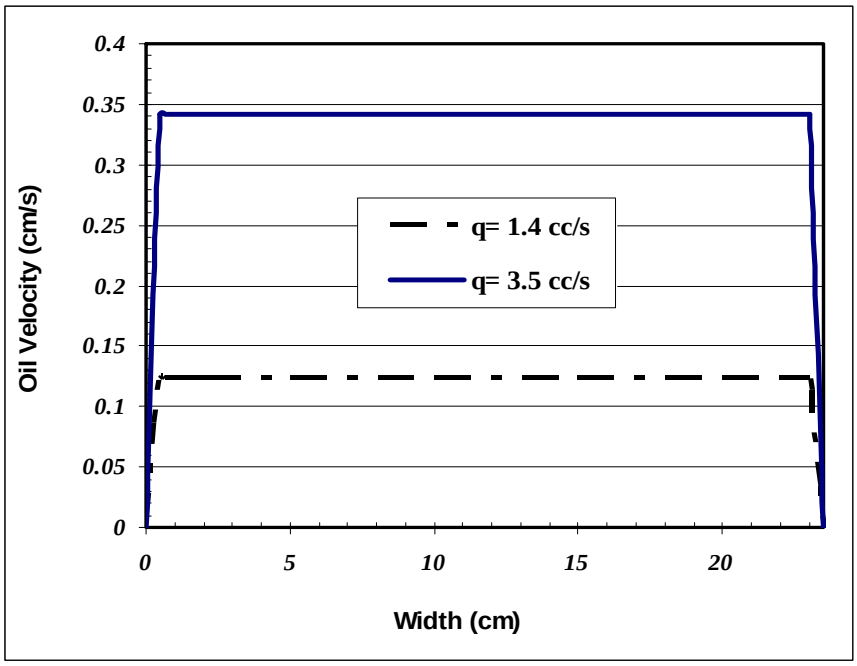

Figure 5.15 : Oil velocity distribution in the unfractured media during controlled gravity drainage for two withdrawal rates [BT3 glass beads, L=55 cm , fluid pair: Air-Varsol].

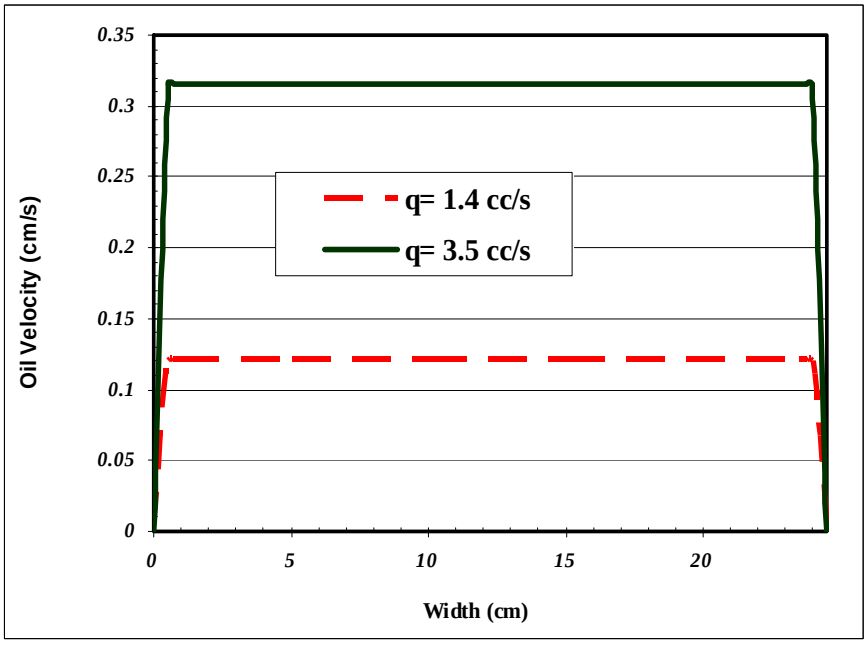

Figure 5.16: Velocity distributions in the fractured porous medium saturated with Varsol under CGD for volumetric flow rates equal to 1.4 cm^3/s and 3.5 cm^3/s [BT3 glass beads , L=55 cm , b=5 mm].

Figures 5.17 and 5.18 represent total velocity of the wetting phase versus model height for homogeneous and fractured porous media, respectively during controlled gravity drainage process with a constant pumping rate. These figures indicate that at a particular time the field

velocity for wetting phase is increasing as the fluid approaches the bottom of the physical model where production point is located. In this case, the porous medium is under controlled gravity drainage (CGD) and the pump drains the liquid out of the medium with constant volumetric flow rate.

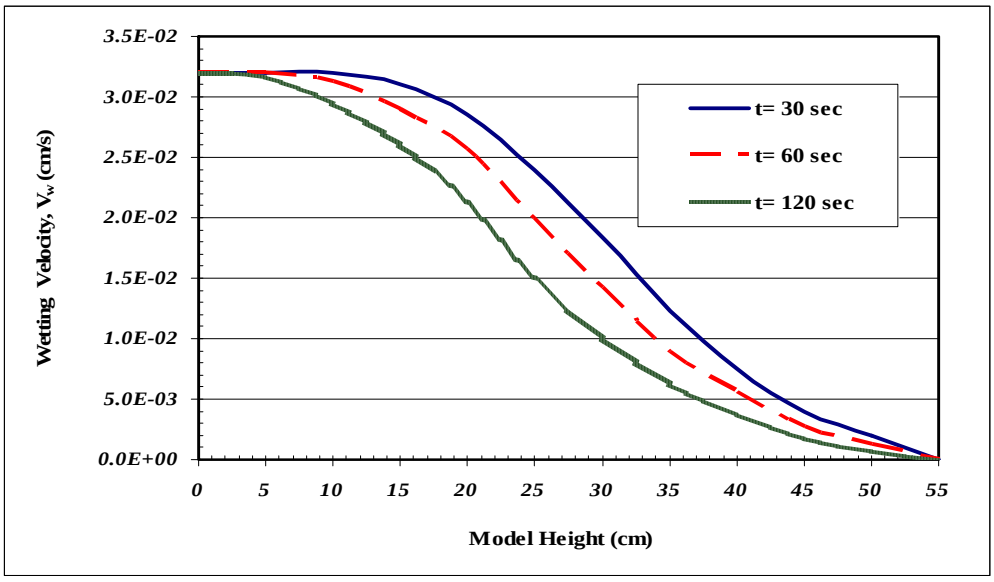

Figure 5.17: Total velocity profile along the unfractured medium height when pumping rate is 1 cm^3/s [BT3 glass beads, L=55 cm , fluid pair: Air-Varsol].

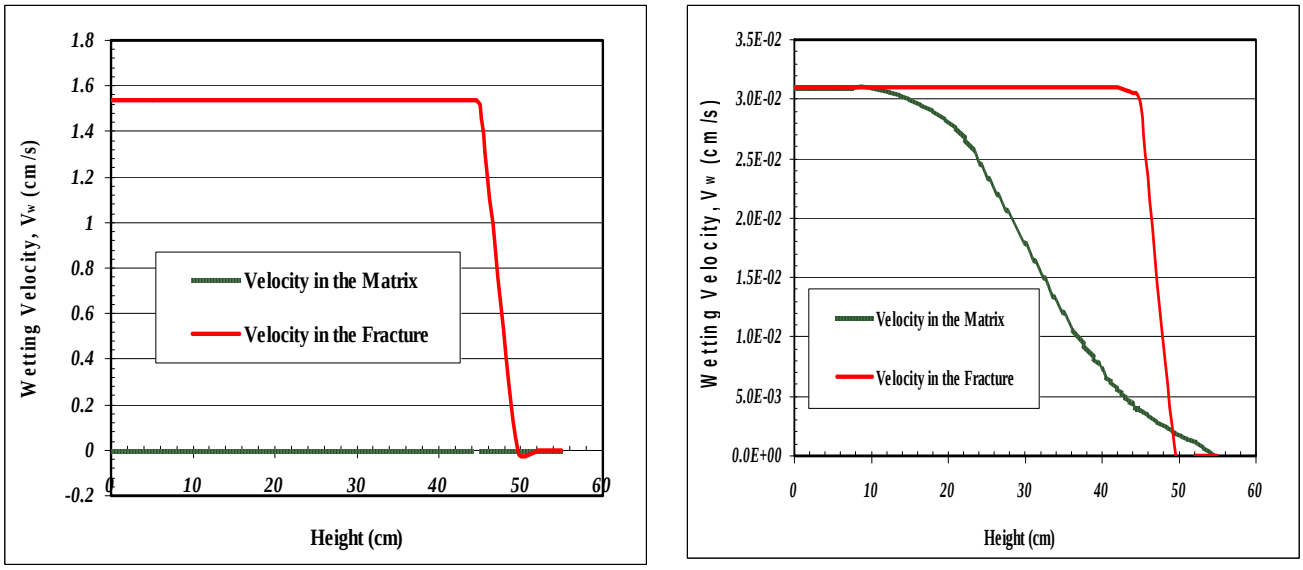

(a) @ t=10 sec (b) @ t=20sec

Figure 5.18: Total velocity distribution for matrix and fracture parts of the fractured porous model under CGD for two different process period [BT3 glass beads, b=5 mm, L=55 cm, test fluid: Varsol, q=1 cm^3/s].

5.5 Results and Discussions

Four numerical simulations with different boundary conditions were conducted in this study using the developed numerical model to investigate the gravity drainage processes in both homogeneous and fractured porous media. In all of the numerical simulations performed, the boundary conditions of the laboratory works were considered properly with varied mesh size to investigate the effect of mesh size on the numerical simulation results. In the following part some important numerical simulation results are presented and then compared with the experimental data in order to validate the selected approach for modeling implementation.

5.5.1 Evolution of saturation: Consider that we have a BT3 glass beads homogeneous porous media which is saturated with the Varsol oil. As the free fall gravity drainage process continues the saturation of wetting phase decrease in the porous medium and liquid saturation varies from a minimum value at the top of model to a maximum value at the model's bottom at any particular time. In order to depict this phenomenon numerically, a numerical simulation was done for a porous medium with the same properties as the physical experimental model. The software provides the saturation distribution along the model's height at various times. Figure 5.19 shows the simulation results for wetting phase saturation in the model.

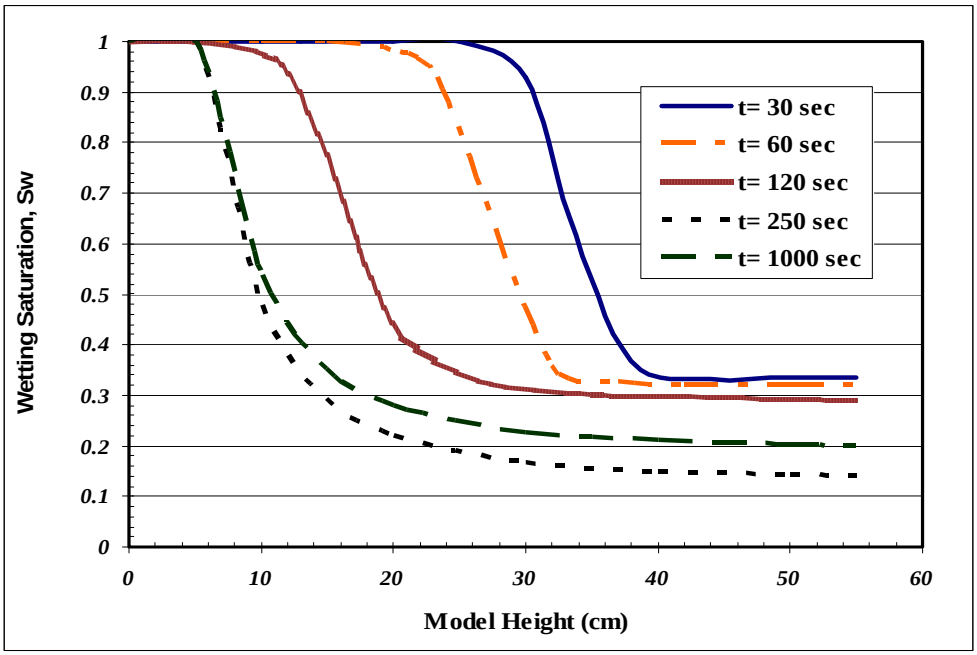

Figure 5.19 :Oil saturation distribution along the height of the homogeneous porous model during FFGD process at different time periods

It is possible to integrate and produce the amount of wetting liquid remaining in the invaded zone. This is shown in Figure 5.20.

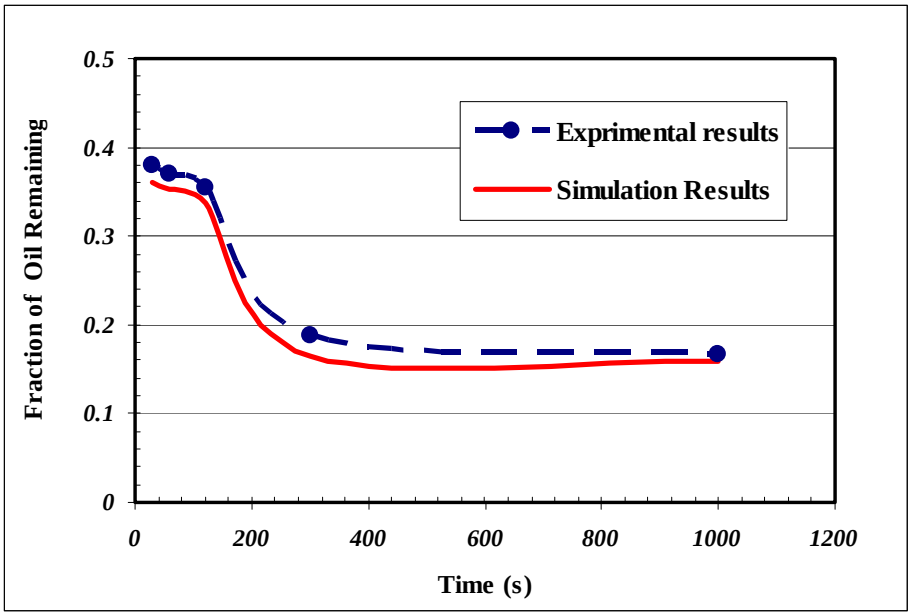

Figure 5.20: Comparison between simulation and experimental results for the fractured porous media saturated with Varsol oil under FFGD [BT3 glass beads, b= 5 mm , L=55 cm]

The gas-liquid interface movement versus time during the experiments was recorded using a camcorder under the gravity drainage conditions to obtain a good estimate of the average liquid saturation in the swept area in any specific time. Figure 5.20 shows the experimental findings along with numerical modeling outputs. Also, Figure 5.20 shows the relationship between the residual oil saturations at five specific times for the case of two-immiscible phase flow of oil-air in the fractured porous sample as determined by the COMSOL model and the experimental results. It can be seen that there is a reasonably good agreement between the two approaches as errors less than 10% in magnitude are observed. It should be noted here that as long as the bulk flow is the dominant mechanism in the gravity drainage process, the average remaining oil saturation will not change with time considerably in the gas invaded zone in a particular porous medium. However, after the process takes fairly long time, remaining oil saturation will have a big difference relative to when the bulk flow plays an important role in the production. Figure 5.20 confirms the statement made above.

The spatial variation of oil saturation during the controlled gravity drainage experiment is illustrated in Figures 5.21 and 5.22 and has similar trends to those observed during the experiment. The distribution of oil saturation before the gas breakthrough varies from ~ 0.36 at the top of the medium to 1 at the bottom when the pump is set on 1.4 g/s and the CGD lasts almost for 60 seconds for homogeneous porous media. The oil saturation profiles illustrate the gas/oil interface as it progressed through the porous medium.

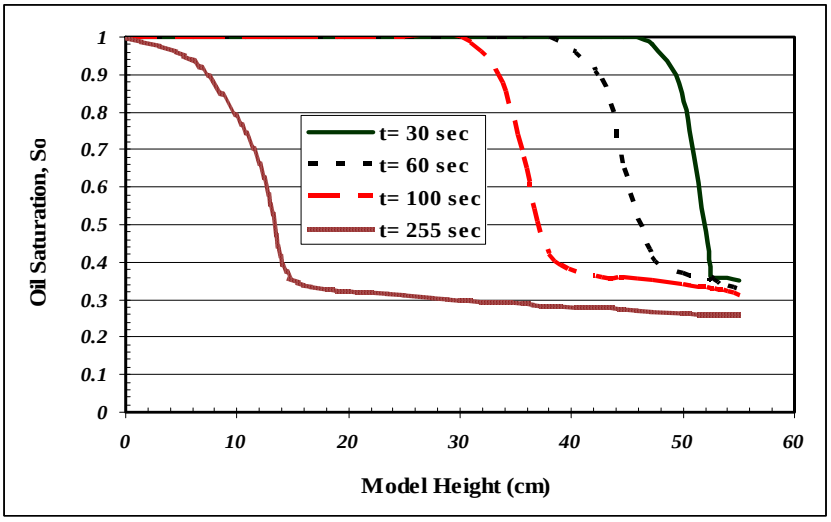

Figure 5.21: Oil saturation distribution in the homogeneous porous medium under CGD during different time periods [q= 1.4 g/s , L=55 cm, BT3 glass beads].

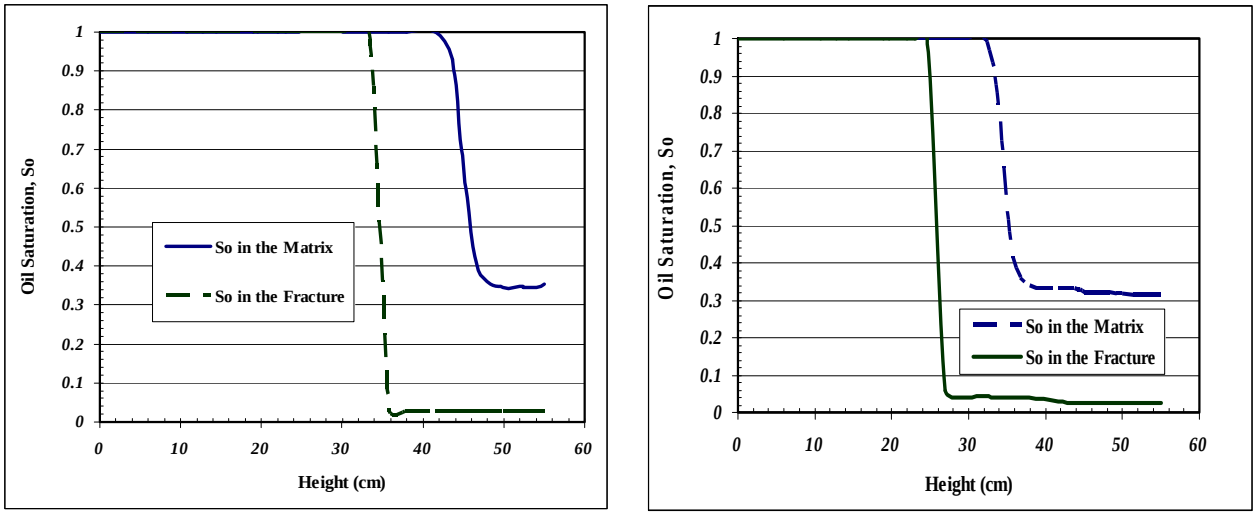

(a) @ t=60 seconds (b) @ t=100 seconds

Figure 5.22: Oil saturation versus height for the fractured porous medium saturated with Varsol undergoing CGD with withdrawal rate equal to 1.4 g/s [BT3 glass beads, L=55 cm, b=5 mm].

Figure 5.22 presents residual oil saturation for the fractured porous medium under the controlled gravity drainage at two different times. These plots demonstrate the gas front advancement change along the height of the fracture and the matrix versus time in the fractured medium.
In the case of fractured BT3 glass beads model, the value of the final residual oil saturation, S_{or}, (at gas breakthrough) obtained from the numerical modeling was 0.28 while experimental magnitude is 0.29 for the withdrawal rate of 1.4 g/s. Numerical modeling calculations say that the gas breakthrough was occurred after 170 seconds in homogeneous medium and 145 seconds in fractured one when the pumping rate was set on 2.5 g/s. Meanwhile, based on the experimental observations, those numbers were recorded 155 and 133 seconds for unfractured

and fractured porous samples, respectively. Therefore, it can be concluded that the simulation results are in good agreement with those obtained from experiments.

5.5.2 Liquid production history: The production histories for two numerical simulations are shown in Figure 5.23 and 5.24. The cumulative liquid production is based on 1.1 cm depth and one horizontal production well. During the free fall gravity drainage the liquid production rates were evaluated for three particular times, namely, 10, 20, and 60 seconds, respectively. The simulation results are in qualitative as well as quantitative agreement with the experimentally measured production history. Based on the simulation results, the cumulative liquid production is a linear function of time. Also, the experimental data show the same trend during the period which bulk flow dominates. The difference in the liquid production rates between the simulation run and the FFGD experiment is less than 10%. This indicates that the numerical model developed can successfully simulate the liquid production history of the gravity drainage experiments.
Figure 5.24 shows a plot of the experimental flow rates versus the flows modelled in COMSOL. As mentioned earlier in this text, the agreement between the model and the experiment is generally very good. In most cases, the absolute error is not greater than 12%. However, the magnitude of the lowest errors is actually not less than 10%. In free fall gravity drainage, a single porosity model was used to predict the experimental data of oil recovery from fractured media and the simulation results are shown in Figure 5.24. The solid lines represent the model results. Figure 5.24 shows that the model matches the experimental data of oil recovery remarkably. In the case of fractured BT3 glass beads model, the initial oil production rate calculated from numerical approach is 6.2 g/s compared to 5.7 g/s measured from the corresponding experiment.

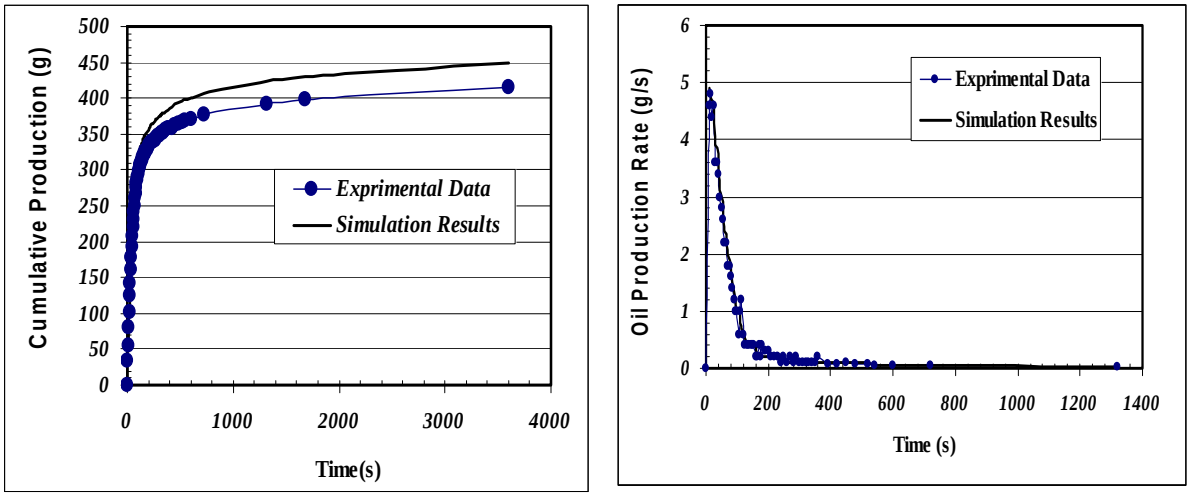

(a) (b)

Figure 5.23: a) production history b) Oil production rate versus time for the unfractured porous medium under free fall gravity drainage [BT3 glass beads, L=55 cm, fluid pair: Varsol-Air]

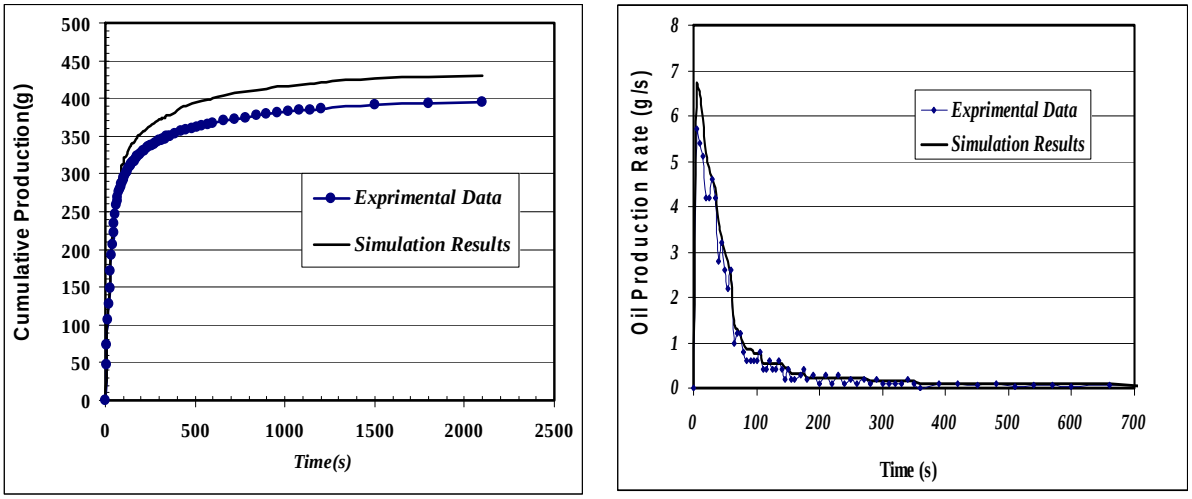

Figure 5.24: a) Oil cumulative production versus time b) oil outflow rate versus time for the fractured porous medium under free fall gravity drainage [BT3 glass beads, L=55 cm, b=5 mm, test fluid: Varsol]

Figures 5.23 and 5.24 indicate that at early times of gravity drainage processes, both the oil recovery and gas front position increases linearly with time. The gas moves down the packed model until it approaches the capillary/gravity equilibrium at a transition time, t. After this time period, the change of oil recovery and gas-liquid interface is not considerable as plot of oil recovery versus time (Figures 5.23 & 5.24) follows a flat trend, approximately.

Table 5.7 shows experimental and simulation results for the oil recovery factor after implementation of the gravity drainage with oil under atmospheric conditions for the both homogeneous and fractured media. As can be seen in Figures (5.23 & 5.24) and Table 5.7, the simulation results are in good agreement with those obtained from experiments. Also, the comparison between the experimental findings and the simulation results indicates that the suggested model works satisfactorily for gravity drainage in fractured porous media. As shown here, the oil recovery factor obtained after implementation of the gas gravity drainage changes with time and varies with different the height of the model changes. The experimental and simulation results obtained from all block heights in this work can be compared at the same time as shown in Table 5.8. The maximum simulation oil recovery factor could be attained using the gravity drainage with height almost equal to 80 cm. As mentioned before, the block height is important and can affect the oil recovery. For heights greater than 80cm, increasing model height does not change the magnitude of production performance, considerably.

Table 5.7: Experimental and Simulation results for the porous media under free fall gravity drainage (FFGD) [BT3 glass beads, fluid pair: Varsol-Air]

Production history	Homogeneous medium(L=55 cm)		Fractured medium (L=55 cm, b=5 mm)	
	Laboratory results	Simulation results	Laboratory results	Simulation results
Recovery Factor (%)	79.0 ± 0.9	80.5	80.0 ± 1.2	81.0
Maximum production rate , g/s	4.6 ± 0.7	4.9	5.7 ± 0.9	6.2
Production rate, g/s (@ t=10 sec)	4.5 ± 0.9	4.8	5.4 ± 0.3	6.0
Production rate, g/s (@ t=20 sec)	4.2 ± 0.5	4.4	4.3 ± 0.7	5.2
Production rate, g/s (@ t=60 sec)	2.2 ± 0.8	2.4	2.4 ± 0.6	2.6

Table 5.8: The amount of oil recovery factor for various block height of porous media according to laboratory and simulation works [BT3 glass beads, fluid pair: Varsol-Air]

Block height (cm)	Homogeneous medium		Fractured medium (b=5 mm)	
	Experimental recovery factor (%)	Simulation recovery factor (%)	Experimental recovery factor (%)	Simulation recovery factor (%)
28	68.5 ± 1.2	71.0	69.5 ± 2.0	72.0
40	74.0 ± 1.4	75.5	75.5 ± 1.5	77.0
55	79.0 ± 0.9	80.5	80.0 ± 1.2	81.0
80	80.5 ± 1.6	82.0	81.5 ± 0.8	83.0

5.5.3 Interface advancement: One of the goals of developing the numerical simulation was to enable the prediction of the gas-liquid advancement in the experiments. The gas-liquid interface positions of the simulations were extracted at 5 second-intervals. The interface corresponds to the elevations with 98% wetting phase in the simulation. Figures 5.25 and 5.26 are the G-L interface profiles extracted from the numerical simulations for different times in the porous medium under FFGD. These were then compared with the G-L interface profile of the experiment using the same plots. Interface velocity against time is shown in Figures 5.27 and 5.28 for homogenous porous medium and fractured medium, respectively. As can be seen in these figures, the interface velocities decrease with time during the free fall gravity. The difference between the interface velocity obtained from the simulation and the experiment is less than 12%, which is satisfactory. Figure 5.28 also confirms the relationship observed between the interface velocity in both fracture and matrix based on the magnitude of the communication rate. It should be noted that in the numerical simulation, the properties of the unconsolidated glass beads were assumed to be uniform.

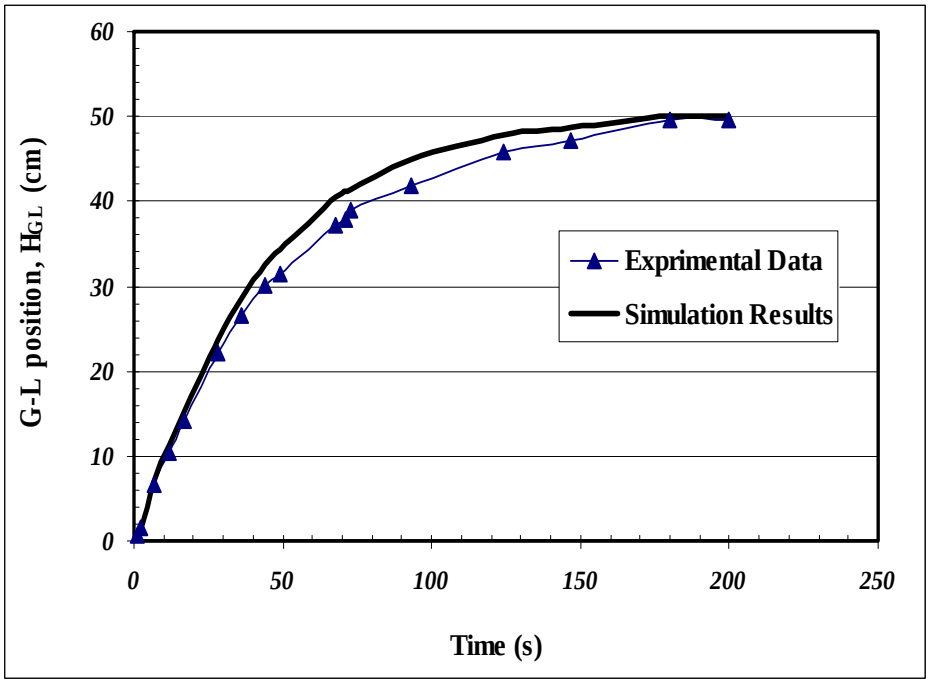

Figure 5.25: Gas-liquid interface position relative to top of model in the homogeneous porous medium under FFGD versus time [BT3 glass beads, L=55 cm, fluid pair: Air- Varsol]

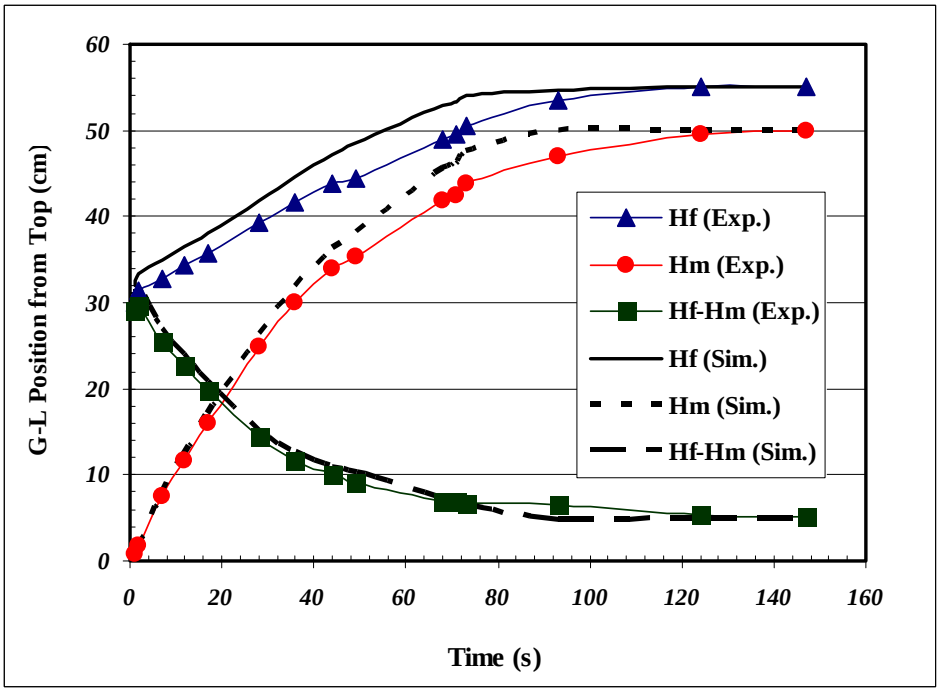

Figure 5.26: Comparison between simulation and experimental findings of FFGD process for gas-liquid contact locations in fracture and matrix [BT3 glass beads , model length =55 cm , fluid pair : Varsol -Air , b=5 mm]

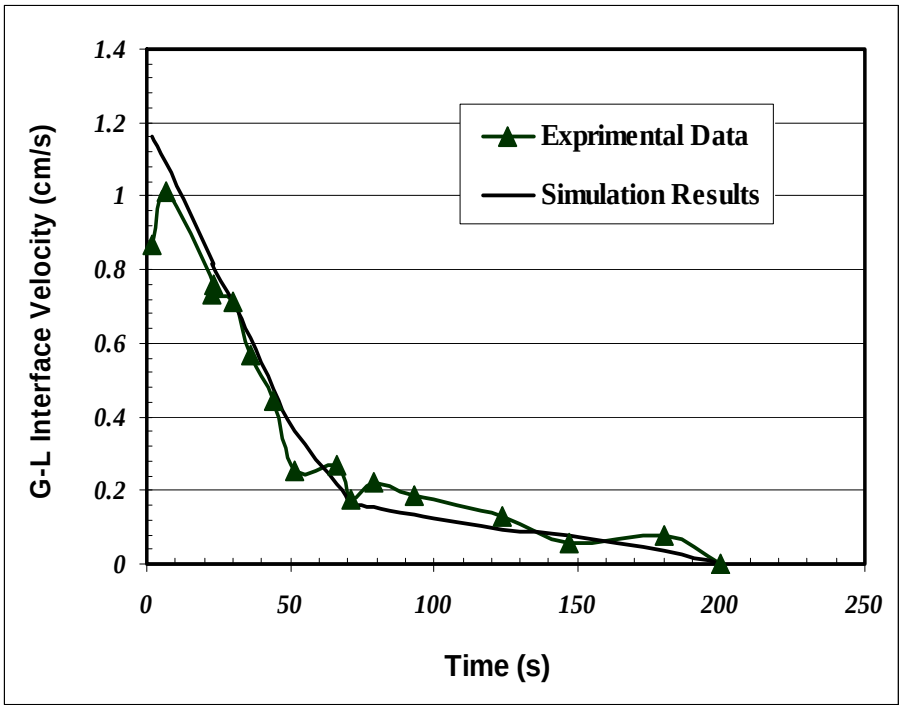

Figure 5.27: Interface velocity versus time during FFGD for a homogeneous BT3 glass beads medium saturated with Varsol, L=55 cm

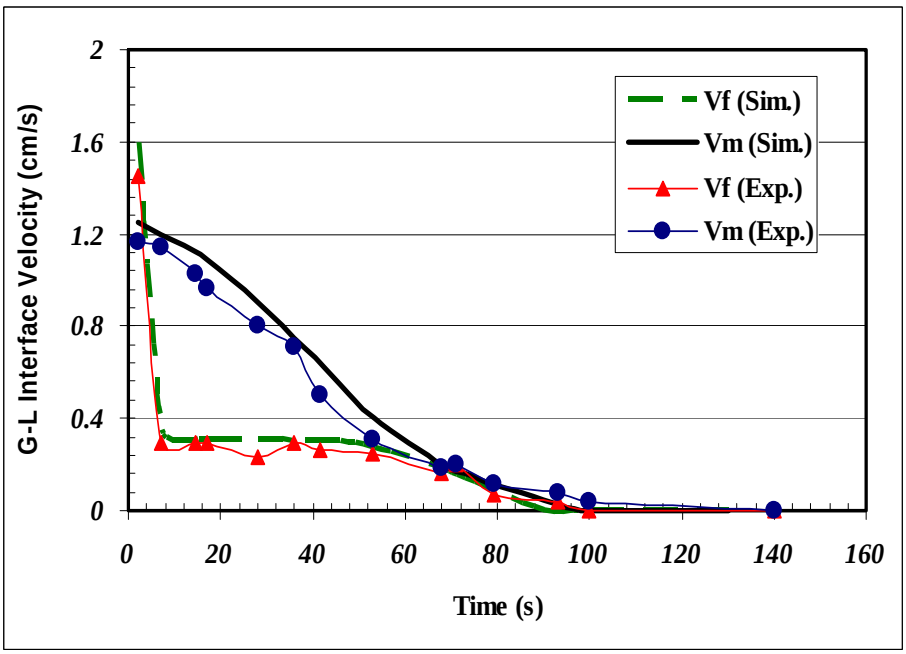

Figure 5.28: G-L interface velocity versus time for a fractured porous medium under FFGD [BT3 glass beads, L=55 cm , b=5 mm , Varsol oil-Air system]

For the controlled gravity drainage process, the vertical interface velocities obtained from the simulations are plotted in Figures 5.29 and 5.30. Since withdrawal rate is kept the same in this type of gravity drainage process, the rate of gas-liquid interface movement is constant throughout the controlled gravity drainage. It can be concluded here that under a constant withdrawal rate lower than the associated critical pumping rate (CPR), the elevation difference between gas-liquid interface locations in fracture and matrix remains constant while liquid is pumping out of the fractured system with. The same important point was extracted from the experiments conveying the message that there is a good agreement qualitatively between the numerical and experimental results as the numerical value for (H_f-H_m) is 8.2 cm for 1.8 g/s compared to 7.6 cm measured in the experiment. Quantitatively speaking, the difference between those two numbers is reasonable, indicating this is a good indicator for error evaluation. Results from the evaluation of the gravity drainage interface profile indicate that this numerical model can successfully simulate the gas-liquid interface movement of the experiments dealing with immiscible displacement in porous media.

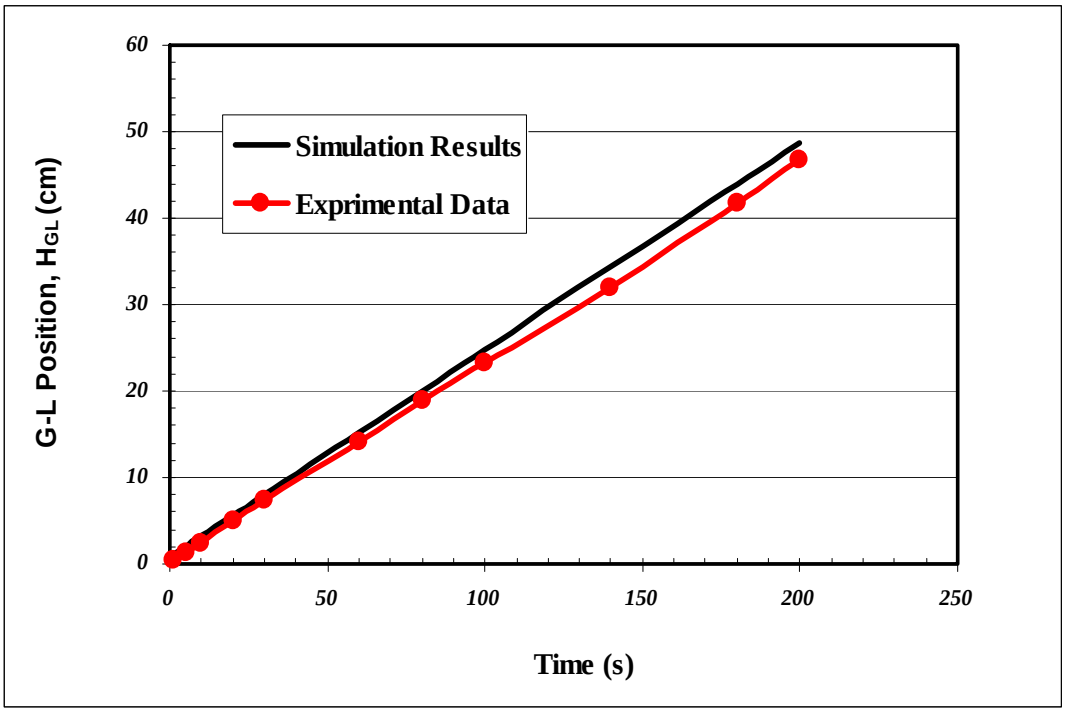

Figure 5.29: G-L position in the homogeneous porous medium made of BT3 glass beads during controlled gravity drainage based on the experiments and modeling part [q= 1.8 g/s , L=55 cm , test fluid: Varsol]

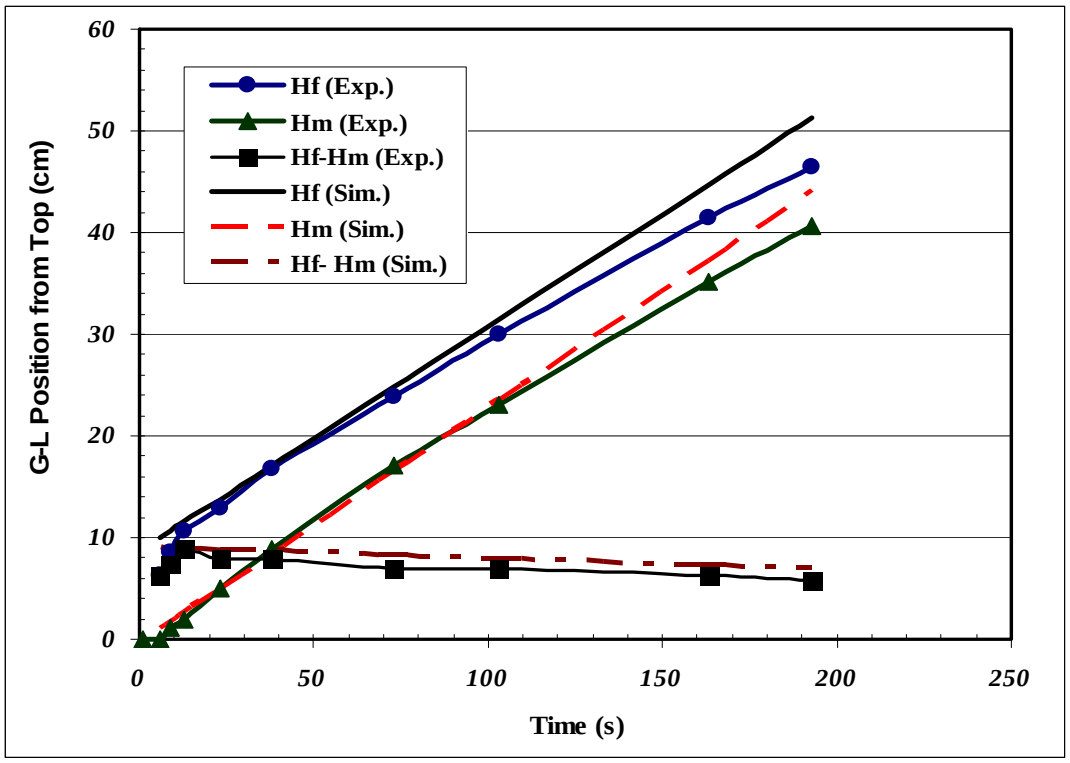

Figure 5.30:Comparison between experimental data and simulation results for G-L interface positions in matrix and fractures versus time; matrix filled with BT3 glass beads, withdrawal rate of q=1.8 g/s, [b= 5 mm, L= 55 cm, fluid pair: Air-Varsol]

5.5.4 Effect of mesh size: Two numerical simulations of the experiment were carried out using different mesh configurations to study the effect of mesh size on the numerical simulations results for free fall gravity drainage (FFGD). Simulation #1 was conducted with a 39 mm by 37 mm mesh size and the simulation #2 was conducted with a 3.9 mm by 3.7 mm mesh size. Simulation # 1 has a total of 96 elements and approximately 3700 degrees of freedom. The number of meshes increased to 9600 elements in the simulation #2 and the degrees of freedom increased to approximately 7900, which is more than double of that of simulation #1. Decreasing in the mesh size increases the memory requirement significantly. Furthermore, run time of simulation #1 was less than 15 min, while the runtime of simulation #2 was over 30 min. The initial (maximum) liquid production rates for simulations #1 and #2 were 5.1 g/s and 4.9 g/s, respectively. The oil production rate from simulation #1 was approximately 5% larger than that of simulation #2. The average residual oil saturation for simulations #1 and #2 were 0.14 PV and 0.12 PV, respectively. The residual oil saturation for simulation #1 is 16 % greater than that of simulation #2. Both the liquid production rate and the mean residual oil saturation for simulation #1 are greater than that of simulation #2. The reason can be accounted for by a higher numerical dispersion in simulation #1 than in simulation #2. Numerical dispersion happens when the gas goes into an element, and it is immediately dispersed throughout the element due the averaging of element properties. As a result, the larger the mesh size, the greater the numerical dispersion and less accurate the numerical simulation will be. The effect of the numerical dispersion on simulation #2, with a smaller mesh size, is less than that of simulation #1; hence, it is fair to conclude that the simulation results from simulation #2 are more accurate than that of simulation

#1. This also explains why both the oil production rate and the mean residual oil saturation for simulation #1 were larger than those of simulation #2 by 5% and 16%, respectively.

5.6 Conclusions

The main purpose of this study was to investigate the appeared complexity of two-phase flow (air/oil) using finite element method in homogeneous and fractured porous media where the supposed porous media was non-deformable media. The following five (5) conclusions can be made based on this study:

- A new 2-D numerical model of gravity drainage was developed using COMSOL 3.4. The new numerical design considered single porosity modeling approach to have separate governing equations for matrix and fractures parts and then solve them simultaneously. The numerical model developed is capable of modeling the production history and the gas-liquid advancement patterns of the experiments.
- By considering the capillary pressure-saturation and permeability functions as constitutive relations and governing equations, the unknown parameters such as the evolution of the model's wetting and non-wetting phases can be estimated.
- Four simulations with different model properties as well as different mesh configurations were carried out based on the properties of the experiments to validate the feasibility of the numerical model developed.
- The variation of mesh configuration in the numerical simulations indicates that the effect of mesh size on the liquid production rate was 5% and also its impact on residual oil saturations was by 16%.
- The main result of the present work was the implementation of a biphasic (Air-oil) flow model, including governing transport equations and capillary pressure functions in porous media, which coupled to fractured porous systems could be useful to study enhanced oil recovery (EOR) processes at laboratory scale.

Chapter 6

Conclusions and Recommendations

6.1 Conclusions

Based on two-phase flow experiments using free fall gravity drainage (FFGD) and controlled gravity drainage (CGD) conditions in fractured porous media, the experimental results were well matched by numerical simulation. Numerical simulations were also used to estimate the influence of variables like relative permeability, matrix capillary pressure, fracture aperture and test fluid properties. The results have shown that the capillary pressure function is very important in the simulation of gravity drainage processes. Knowledge of the capillary pressure function is critical in numerical modeling.

The combined experimental and simulation study resulted in a much better understanding of the physical processes that occur during two phases flow in a fractured system, compared to previous reported studies (Guzman and Aziz, 1993 ; Hughes, 1995). Significant conclusions that are based on experimental and simulation work presented in this thesis have as follows:

- Capillary continuity and communication between matrix and fracture strongly depend on fracture aperture, matrix physical properties and physical properties of test fluids. These two phenomena have high contribution in oil recovery and amount of final residual oil saturation in fractured petroleum reservoirs during production.
- According to the experimental results, fractured media with lower liquid viscosities have higher liquid transfer rate compared to those with higher liquid viscosities. This is because of the fact that as liquid viscosity decreases, the height difference between local positions of liquid interfaces within fractures and matrix becomes smaller. This condition of reduced viscosity and also $\Delta H(t)$ values would result in weakening the driving forces available for liquid communication from matrix towards the fractures.
- It has been observed for oil wet glass beads that a low value of interfacial tension for oil would increase overall recovery performance considerably because the capillary threshold height is shorter in comparison to the case when the model is saturated with oil of higher surface tension. Lower surface tension causes a decrease in the magnitude of residual oil saturation and it affects final oil recovery.
- It was proven that increasing the value of fracture aperture results in higher liquid production rates only during the initial period of the process, but it does not have any significant effect on the ultimate liquid recovery. The variation of the size of fracture aperture changes the magnitude of transfer rate between matrix and fracture as well as the value of height difference between interface locations in matrix and fractures.
- The experimental results show that an increase in matrix block height causes increase in matrix oil recovery by free fall gravity drainage, however the oil production performance approaches a limit by increasing the matrix height such that increasing the block height towards infinity makes an ignorable increase in production performance. This fact is related to capillary threshold height becoming negligible compared to porous medium length On the other hand, it is clear that the longer the model is, the higher would be the

- High density of fractures, especially vertical ones, within a porous medium accelerates recovery rate due to maintaining an increase in the overall effective permeability.
- Fractures affect more the recovery history of media with low matrix permeability compared to the case of high matrix permeability.
- Flow correction (F_{com}), which was introduced in order to consider all assumption made in formulation of communication rate, is a function of dimensionless time to calculate flow transfer rate between matrix and fracture during free fall gravity drainage and it is not right to assume a constant shape factor instead a variable correction factor for calculation of liquid communication in fractured porous media.
- In this study, an empirical model was developed to calculate recovery performance at different times of gravity drainage process that can be used for prediction of free fall gravity drainage in porous media if production history is available somehow.
- Pumping rate dictates the liquid transfer between matrix and fractures, pressure profile, fluid flow regimes and also the G-L interface recession rate in fractured porous media during the course of controlled gravity drainage (CGD) experiments.
- The elevation difference between G-L interface positions in matrix and fractures is a function of several parameters such as the petrophysical properties of the porous medium, fracture properties, physical properties of the liquid-in-place, and liquid withdrawal rate during controlled gravity drainage (CGD).
- Experimental data show that as long as the withdrawal rate is constant, the elevation difference between G-L interface positions in both matrix and fracture mediums remains unchanged during a particular controlled gravity drainage experiment.
- Pumping rate, mobility ratio and heterogeneities are three parameters that probably can cause viscous fingering depending on their values when we are dealing with immiscible displacement in fractured media.
- It is clear that models with larger fracture aperture show higher critical pumping rate (CPR) and maximum pumping withdrawal rate (MPWR) values. Since a model with higher fracture aperture has larger storage capacity, the corresponding MPWR would be higher as well compared to the model with smaller fracture aperture.
- Experiments indicate that the liquid level in fracture drops faster in the downwards direction (i.e. magnitude of "ΔH" increases with a steeper slope) when the liquid viscosity is higher in magnitude. The reason is that at higher liquid viscosities, the liquid communication rate between matrix and fractures would decrease and as a result, there is no liquid flow support from the matrix side to avoid excessive recession of the G-L interface within the fractures compared to that of matrix. In consequence, the rate of change of this elevation difference with respect to the drainage rate (i.e. $\frac{d(\Delta H_{F-M})}{dq}$) would be higher for the cases in which the liquid viscosity is higher as well.
- According to the physics of Controlled Gravity Drainage (CGD) process and experimental findings, the Bond number, Capillary number, permeability ratios, and dimensionless length are the main dimensionless numbers to carry out up scaling for fractured porous media under gravity drainage conditions.

- Aspects of gravity drainage process in porous media and saturation distribution were successfully modeled using COMSOL®, even though the model assumed that air and test fluids are incompressible. The model provided verification that the assumptions made about residual liquid saturation in fracture, relative permeability and capillary pressure functions were reasonable. It can be used for modeling multi-phase flow of fluids in fractured porous media when acceptable values for relative permeability, capillary pressure and model properties are available.
- Comparisons between experimental results and simulation outputs have shown a good agreement between them. This is encouraging for further developments in simulating oil production from heterogeneous porous media.

6.2 Recommendations

6.2.1 Experimental work: There are still some areas of further improvement. This study has relied on a simplistic description of fractured porous media. Although qualitative trends are possible using the simple fractured media structures employed in this research study, quantitative, predictive capability is possible only by using a more realistic model of fractured rocks. More research is needed to figure out effects of capillary continuity on recovery from fractured media during gravity drainage. Fracture aperture and type of test fluids are important parameters which should be taken into account for different fractured porous systems.

The impact of wettability on capillary continuity in fractured rocks is still not fully understood. Visualization methods, to measure the in situ fluid saturation development in fractured rocks, are recommended in order to study the impact of fractures and wettability on multiphase flow in fractured reservoirs. Visualization technique provides useful insights to local phenomena happening in fractured media during free and controlled gravity drainage processes.

Type of production well can affect recovery performance and gas breakthrough during gravity drainage processes and this subject requires more research and could be studied in future works.

Accurate modeling and characterization of underground flow in multi-fluid rock systems require development of a fast, reproducible experimental method that yields the information necessary to determine the parameters of the capillary pressure–saturation and relative permeability functions. Therefore it is needed to develop efficient parameter estimation approach to obtain relative permeability and capillary pressure for simulation softwares and numerical programs to study three-phase flow in homogeneous and fractured porous media.

Some particular fractures configurations in the fractured porous media to investigate different aspects of gravity drainage were used; therefore it would be interesting to have more fractures patterns in experimental runs and simulation part to figure out the influence of fracture patterns and interaction between fractures on recovery rate, gas-liquid interface downward rate and production performance.

6.2.2 Numerical modeling: The results from the numerical simulation indicate that the current model is capable of replicating the experimental results within a 12% difference. The accuracy of the numerical model depends on the quality of the input variables. In additional to mesh size,

other factors that may improve the numerical model include: 1) capillary pressure curve and coefficients, 2) mesh configuration, and 3) modeling technique

- **Capillary pressure curve**: Capillary pressure curve is critical to the algorithm of the numerical model. It is used to evaluate the liquid saturation of the system. The capillary pressure curves used in this model were calculated based on the capillary pressure curve of a water-air drainage system and scaled to the interfacial tension of air- Varsol oil. The capillary pressure data calculated were curve-fitted using the Van Genuchten correlations to describe the capillary pressure curve in the numerical model. The scaling and the curve-fittings of the water air capillary pressure curve to describe the Varsol oil drainage affect the accuracy of the capillary pressure curve inputted. Instead of curve fitting the capillary pressure curve using Van Genuchten correlation, it is recommended to measure capillary pressure data directly to reduce the inaccuracy in the capillary pressure data due to curve fitting of data.
- **Mesh configuration**: A quick study was conducted to understand the effect of mesh size on the production history, the mean residual oil saturation and the gas-liquid interface advancement of the numerical model. The disadvantage of the mesh configuration of the current numerical model is the inability to simulate gravity drainage in a very large fractured system. In field operation, the dimension of the control volume is in the order of kilometres rather than centimetres for lab scale. If the mesh size remains 1 mm by 1 cm or 0.67 mm by 6.7 mm, the total number of element and the total degrees of freedom will be exponential. A suggestion in minimizing such problem is to introduce a variable mesh configuration to the numerical model. The idea is to have smaller size meshes near the interface and boundaries and larger size meshes in middle areas.
- **Modeling Technique:** Regarding modeling of fractured media, dual porosity and dual permeability techniques in conjunction with experimental works should be performed to investigate the matrix-fracture transfer function in transient and steady-state flow.

References

Aborig, A., and Chatzis, J.: “Theoretical and experimental studies for critical cresting rate in horizontal wells”, M.Sc thesis, 2003.

Ahmadi, A., Remazeilles, V., Noetinger, B., and Quintard, M.: “Direct calculation of large-scale properties for one-phase flow in random fractured systems”, European conference on the mathematics of oil recovery, Leoben, Austria, September 1996.

Al-Hadhrami, H., and Blunt, M.: “Thermally induced wettability alteration to improve oil recovery in fractured reservoirs”, SPE Journal, SPE 1295, 179-181, 2001.

Ameri, H., and Wang, J.: “Effect of temperature on oil- water relative permeability”, SUPRI heavy oil research program, 8 annual report, SUPRI TR-47, 11-24, April 1985.

Ayatollahi, S., Boukadi, F., Wadhahi M., Maamari, R., and Bemani, A.: “Investigation of thermal gas-oil gravity drainage in fractured carbonate reservoirs”, SPE Journal, SPE 93585, March 2005.

Aziz, K., and Settari, A.: “Petroleum reservoir simulation” book, Elsevier science, New York, 1979.

Barenblatt, G.I., and Zheltov, J.P.: “On the basic equations of single phase flow of fluid through fractured porous media”, Dokl Akad Nauk SSSR, vol. 132 (3), 545–548, 1960.

Barenblatt, G.I., Entov, V.M., and Ryzhik, V.M: “Theory of fluid flows through natural rocks” book, Kluwer academic publishers, Dordrecht, 1990.

Barkve, T., and Firoozabadi, A.: “An analysis of reinfiltration in fractured porous media”, SPE 24900, SPE Annual technical conference and exhibition, Washington D.C., USA, 1992.

Batchelor, T., and Gutmanis, J.: “Hydrocarbon production from fractured basement reservoirs”, Department of Energy (DOE), February 2002.

Beckner, B.L.: “Improved modeling of imbibition matrix/fracture fluid transfer in Double porosity simulators”, PhD dissertation, Stanford University, July 1990.

Blunt, M., and King, M.J.: “Simulation and theory of two-phase flow in porous media”, Physical review A, vol. 46, 7680-7699, 1992.

Blunt, M., Zhou, D., and Fenwick, D.: “Three-phase flow and gravity drainage in porous media”, Journal of transport in porous media, vol. 20, 77-103, 1995.

Buckley, S.E., and Leverett, M.C.: “Mechanisms of fluid displacement in sands”, Transactions American institute of mining and metallurgical engineers, vol. 146, 107- 116, 1942.

Burns, R., and Toksöz, M.: “Characterization of in-situ stress and permeability in fractured reservoir”, Department of Energy (DOE), July 2004.

Carlson, M.: “Practical reservoir simulation”, Penn Well edition, 2004.

Chatzis, I., Morrow, N.R., and Lim, H.T.: “Magnitude and detailed structure of residual oil saturation”, Journal of petroleum science and engineering, vol. 23, 311–326, 1983.

Chatzis, I., Kantzas, A., and Dullien ,F.A.L. : “On the investigation of gravity drainage assisted inert gas injection using micromodels, Long Berea cores and computer assisted tomography”, SPE 18284 , 63rd Annual technical conference., Houston, Texas, October 1988.

Chatzis, I., and Ayatollahi, S.: “Investigation of the GAIGI process in stratified porous media for the recovery of waterflood residual oil”, no. 139, 6th Petroleum conference of the south Saskatchewan section, the petroleum society of CIM, Regina, Saskatchewan, October 1995.

Chen J., Hopmans J.W., and Grismer M.E.: “Parameter estimation of two-fluid capillary pressure–saturation and permeability functions”, Advances in water resources, vol. 22, no. 5, 479–493, 1999.

COMSOL Multiphysics: “COMSOL Multiphysics Modeling Guide: Version 3.5”, Porous media Lab., University of Waterloo, Canada

Da Sle,W.J., and Guo, D. S.: “Assessment of a vertical hydrocarbon miscible flood in the Westpem Nisku D Reef”, Journal of SPE reservoir engineering , 147-154, May 1990.

Dastyari, A., Bashukooh, B., Shariatpanahi, S.F., Haghighi, M., and Sahimi, M.:“Visualization of gravity drainage in a fractured system during gas injection using glass micromodel”, SPE Journal, SPE 93673, March 2005.

Dean, R.H., and Lo L.L.: “Simulations of naturally fractured reservoirs”, Journal of SPE reservoir engineering, 638-648, 1988.

Dernond, A.H., and Roberts, P.V.: “An examination of relative permeability relation for two-phase flow in porous media”, Water resource bulletin, American water resource association, vol. 23 (4), 617-628, 1987.

Dong, M., Dullien, F.A.L., and Chatzis, I.: “Imbibition of oil in film form over water present in edges of capillaries with an angular cross section”, Journal of colloid and interfaces Science, vol.172, 21-36, 1994.

Dullien, F.A.L., Chatzis, I., and Macdonald, I.F.: “Enhanced oil recovery process”, Canadian patent no. 1304675, July 1992, US patent no. 4953619, September 1990.

Dullien, F.A.L.: “Porous media, fluid transport and pore structure” book, 2nd edition, Academic press, San Diego, 1992.

Eclipse 100 User's Manual, Intera Information Technology Limited, Oxford shire, England, 1994.

Eshraghi, I.: "Reservoir engineering of fractured reservoirs" book, Elsevier edition press, 1995.

Fenwick, D.H., and Blunt, M.J.: "Three-dimensional modeling of three phase imbibition and drainage", Advance water resources, vol. 21 (2), 121-143, 1998.

Firoozabadi, A., and Markeset T.: "Fracture-liquid transmissibility in fractured porous media", SPE Journal, SPE 24919, December 1993.

Firoozabadi, A.: "Research program on fractured petroleum reservoirs", DE-FG22-93BC14875, Department of Energy (DOE), April 1994.

Firoozabadi A., and Markeset T.: "Laboratory study of reinfiltration for gas-liquid system in fractured porous media", SPE Journal, SPE 26129, November 1992.

Floyd Jerry, L.: "Carbonate reservoir characterization" book, Springer press, 1999.

Fung, Larry S.K., and Collins, D.A.: "An evaluation of the improved dual porosity model for the simulation of gravity effects in naturally fractured reservoirs", JPCT, vol. 30, no.3, 1991.

Gary, G.F.: "Essentials of multiphase flow and transport in porous media" book, Wiley press, 2008.

Gilman, J.R.: "An efficient finite-difference method for simulating phase segregation in the matrix blocks in double- porosity reservoirs", Journal of SPE reservoir engineering, 403-413, July 1986.

Granet, S., Fabrie, P., Lemonnier, P., and Quintard, M.: "A single-phase flow simulation of fractured reservoir using a discrete representation of fractures", European Conference on the mathematics of oil recovery, Peebles, Scotland, September 1988.

Grattoni, C.A., Jing, X.D., and Dawe, R.A.: "Dimensionless groups for three-phase gravity drainage flow in porous media", Journal of petroleum science and technology, vol. 29, 53–65, 2001.

Guzman, R.E., and Aziz, K.: "Design and construction of an experiment for two-phase flow in fractured porous media", SUPRI TR-95, Stanford petroleum research institute, Stanford, CA, June 1993.

Haghighi, M., and Yortosos, Y.C.: "Visualization of a steam injection in fractured system using micromodel", SPE Journal, SPE 37520, 1997.

Held, R.J., and Celia, M.A.: "Pore-scale modeling and up-scaling of non-aqueous phase liquid mass transfer", Journal of water resource research, vol.37 (3), 539–549, 2001.

Hoteit, H., and Firoozabadi, A.: “Numerical modeling of diffusion in fractured reservoirs”, SPE Journal, SPE 103292, 2006.

Hughes, R., and Blunt, M.: “Pore-scale modeling of multiphase flow in fractures and matrix/fracture transfer”, SPE Journal, SPE 71297, June 2001.

Jackson, M.D., Valvatne, P.H., and Blunt, M.J.: “Prediction of wettability variation and its impact on flow using pore- to reservoir-scale simulations”, Journal of petroleum science and technology, vol. 39, 231–246, 2003.

James, E. Gaiser: “PS-Wave Azimuthal anisotropy: Benefits for fractured reservoir”, Department of Energy (DOE), 1995.

Jean-François, T., and Pierre, M.: “Fractures and fracture networks” book, Springer edition, 1999.

Jerauld, G.R., and Salter, S.J.: “The effect of pore-structure on hysteresis in relative permeability and capillary pressure: pore-level modeling”, Journal of transport in porous media, vol. 5, 103-151, 1990.

Kantzas, A., Chatzis, I., and Dullien, F.A.L.: “Enhanced oil recovery by inert gas injection”, SPE 17379, SPE/DOE Symposium on enhanced oil recovery, Tulsa, OK, April 1988.

Kazemi, H., and Merrill, L.S.: “Numerical simulation of water imbibition in fractured cores”, SPE Journal, 175-182, June 1979.

Kazemi, H.: “Naturally fractured reservoirs”, Third International forum on reservoir simulation, Baden, Austria, 1990.

Kazemi, H., and Gilman, J.R.: “Multiphase flow in fractured reservoirs in flow and contaminant transport in fractured rock”, Bear, J.R., Tsang, C. F., and de Marsily, G (eds.), Academic press, San Diego, 267-323, 1993.

Keller, A.A., and Chen, M.: “Effect of spreading coefficient on three-phase relative permeability of nonaqueous phase liquids”, Journal of water resource research, vol. 39 (10), 1288-1298, 2003.

Keller, A.A., Blunt, M.J., and Roberts, P.V.: “Micromodel observation of the role of oil layers in three-phase flow”, Journal of transport in porous media, vol. 26, 277–297, 1997.

Kovscek A. R., Patzek T. W., and Radke C. J.: “Mechanistic foam flow simulation in heterogeneous and multidimensional porous media”, SPE Journal, SPE 39102, 511-526, December 1997.

Kueper B. H., Frind E. O.: “Two-Phase flow in heterogeneous porous media model development”, Journal of water resources research, vol. 27, 1049-1057, 1991.

Labastie, A.: “Capillary continuity between blocks of a fractured reservoir”, SPE 20515, 65th SPE Annual technical conference and exhibition, New Orleans, LA, September 1990.

Lefebvre du Prey, E.: “Gravity and capillary effects on imbibition in porous media”, SPE Journal, SPE 6192, 195-206, June 1978.

Lenormand, R., Zarcone, C., and Sarr, A.: “Mechanism of the displacement of one fluid by another in a network of capillary ducts”, Journal of Fluid mechanics, 337-53, 1983.

Leverett, M.C.: “Capillary behavior in porous solids”, Tulsa Meeting, 1940.

Li, H., Putra, E., Schechter, D.S., and Reid B. G.: “Experimental investigation of CO_2 gravity drainage in a fractured system”, SPE Journal, SPE 64510, October 2000.

Li, K., and Horne, R.: “Characterization of spontaneous imbibition into gas saturated rocks”, SPE 62552, SPE/AAPG Western regional meeting, Long Beach, June 2000.

Mercer, J.W., and Cohen, R.M.: “A review of immiscible fluids in the subsurface: properties, models, characterization and remediation”, Journal of contaminant hydrology, vol. 6, 107-163, 1990.

Montgomery, D.C.: “Introduction to statistical quality control”, Amazon press, 2008.

Montgomery, D.C., and Runger, G.C.: “Applied statistics and probability for engineers, student solutions manual”, Amazon press, 2006.

Mora, C.A., and Wattenbarger, R.A.: “Analysis and verification of dual porosity and CBM shape factors”, JCPT, vol. 48, no. 2, Feb. 2009.

Mualem, Y.: “A new model for predicting the hydraulic permeability of unsaturated porous media”, Journal of water resources research, vol.12, 513-522, 1976.

Nelson, R.: “Geological analysis of naturally fractured reservoirs”, Hardcover edition, April 2001.

Oliveira, L.I., and Demond, A.H.: “Estimation of primary drainage three-phase relative permeability for organic liquid transport in the vadose zone”, Journal of contaminant hydrology, vol. 66, 261-285, 2003.

Øren, P.E., and Pinczewski, W.V.: “Fluid distribution and pore-scale displacement mechanisms in drainage dominated three-phase flow”, Journal of transport in porous media, vol. 20, 105-133, 1995.

Pan, X., and Wong, R.C.: “Steady state two-phase in a smooth parallel fracture”, 47th Annual technical meeting of the petroleum society, Calgary, Alberta, Canada, June 1996.

Parker, J.C., Lenhard, R.J., and Kuppusany, T.: “A parametric model for constitutive properties governing multiphase flow in porous media”, Journal of water resource research, vol. 23, 618-624, 1987.

Paul, P., and Zoback, M.: “Fluid flow in a fractured reservoir using a geomechanically-constrained Fault Zone Damage Model for reservoir simulation”, SPE 110542, SPE Annual technical conference and exhibition, Anaheim, California, U.S., November 2007.

Persoff, P., Pruess, K., and Myer, L.: “Two-phase flow visualization and relative permeability measurement in transparent replicas of rough-walled rock fractures”, 6th Workshop on geothermal reservoir, Stanford University, January 1991.

Piri, M., and Karpyn, Z.T.: “Prediction of fluid occupancy in fractures using network modeling and x-ray microtomography. II: Results”, Journal of physical review E, vol.76, 163-172, 2007.

Pooladi-Darvish, M., and Firoozabadi, A.: “Cocurrent and countercurrent imbibition in a water-wet matrix block”, SPE journal, SPE 38443, vol. 234, 3-11, 2000.

Purcell, W. R.: “Capillary pressures - Their measurement using mercury and the calculation of permeability”, Trans, AIME, vol.186 (39), 1949.

Quintard, M., and Whitaker, S.: “Transport in chemically and mechanically heterogeneous porous media”, Advances in water resources, vol. 19(1), 29-60, 1996.

Rangel-German, E., and Kovscek, A.: “Matrix-fracture interaction in single matrix blocks”, 25th Workshop on geothermal reservoir engineering, Stanford University, Stanford, CA, January 2000.

Rangel-German, E., and Kovscek, A.: “Experimental and analytical study of water infiltration in fractured systems”, Annual geothermal resources congress, San Francisco, September 2000.

Rangel-German, E., and Kovscek, A.: “Water infiltration in fractured systems: Experiments and analytical model”, SPE 71618, SPE Annual technical conference and exhibition, New Orleans, October 2001.

Reeves, P.C., and Celia, M.A.: “A functional relationship between capillary pressure, saturation, and interfacial area as revealed by a pore-scale model”, Journal of water resource research, vol.32 (8), 2345-2358, 1996.

Reis, J., and Cil, M.: “Analytical models for capillary imbibition: One-dimensional matrix blocks”, In Situ, vol. 23(3), 243-270, 1999.

Reis, J.C., and Haq, S.A.: “Water advance in a single fracture in the presence of capillary imbibition into adjacent matrix blocks”, In Situ, vol. 23 (3), 271- 295, 1999.

Robert, W. M.: “Oil recovery mechanisms at different wettability conditions in fractured reservoirs”, Department of Energy (DOE), 2002.

Rossen, R.H., and Shen E.I.: “Simulation of gas/oil drainage and water/oil imbibition in naturally fractured reservoirs”, SPE 16982, SPE Annual technical conference and exhibition, Dallas, Texas, September 1987.

Sagar, N.S., and Castanier, L.M.: “Oil-foam interactions in a micromodel,” SUPRI TR- 110, Stanford University, November 1997.

Sahimi, M.: “Flow and transport in porous media and fractured rock” book, Elsevier press, 2nd edition, March 1995.

Saidi, A.M.: “Reservoir engineering of fractured reservoir- Fundamental and practical aspects” book, Total edition press, Paris, 1987.

Saidi, A.M., Tehrani, D.H., and Wit, K.: “Mathematical simulation of fractured reservoir performance”, 10th World petroleum congress, Romania, 1979.

Saidi, A.M: “Effect of gas pressure on the recovery of the Iranian fractured limestone reservoirs”, 9th World energy conference, Detroit, 1974.

Saidi, M.: “Simulation of naturally fractured reservoirs”, SPE Journal, SPE 12270, 1983.

Saidi, M.: “Mathematical simulation model describing Iranian fractured reservoirs and its application to Haft-Kel field”, Proceeding 9th world petroleum congress, Tokyo, 1995.

Sajjadian, A.V., Danesh, A., and Tehrani, D.H.: “Laboratory study of gravity drainage mechanism in fractured carbonate reservoir-Reinfiltration”, SPE Journal, SPE 54003, April 1999.

Salimi, H., and Bruining, J.: “Improved prediction of oil recovery from waterflooded fractured reservoirs”, SPE 115361, SPE Annual technical conference and exhibition, Denver, Colorado, US, September 2008.

Schechter, D.S., Zhou, D., and Orr, F.M.: “Low IFT drainage and imbibition”, Journal of petroleum science and engineering, vol. 11, 283–300, 1994.

Schechter, D.S., and Guo, B.: “Mathematical modeling of gravity drainage after gas injection into fractured reservoirs”, SPE 35170, SPE Improved oil recovery symposium, Tulsa, April 1996.

Shariatpanahi, S.F., Dastyari A., Bashukooh, B., Haghighi, M., Sahimi, M., and Ayatollahi, S.S.: “Visualization experiments on immiscible gas and water injection by using 2D-Fractured glass micromodels”, SPE Journal, SPE 93437, March 2005.

Srivastava, R., Kumar, G., and Srivastava, K. K.: “Properties of CMC”, Biotechnology letters, vol. 12, 541–545, 1990.

Suffridge, E.E., and Renner, R.A.: “Diffusion and gravity drainage tests to support the development of a dual porosity simulator”, 6th European IOR Symposium, Stavanger, May 1994.

Suicmez, V.S., Piri M., and Blunt, M.J.: “Effects of wettability and pore-level displacement on hydrocarbon trapping”, Advances in water research, vol. 31, 503–512, 2008.

Suicmez, V.S., Piri M., and Blunt, M.J.: “Pore scale modeling of three-phase WAG injection: Prediction of relative permeabilities and trapping for different displacement cycles”, SPE Journal, SPE 95594, 2006

Tan, J.C.T., and Firoozabadi, A.: “Dual-porosity simulation incorporating reinfiltration and capillary continuity concepts, Part one: single grid cell”, SPE 29113, l3th SPE Symposium on reservoir simulation, San Antonio, Texas, US, 1995.

Tavassoli, Z., Zimmerman, R.W., and Blunt, M.J.: “Analytic analysis for oil recovery during counter-current imbibition in strongly water-wet systems”, Journal of transport in porous media, vol. 58, 173–189, 2005.

Tavassoli, Z., Zimmerman, R.W., and Blunt, M.J.: “Analysis of counter-current imbibition with gravity in weakly water-wet systems”, Journal of petroleum science and engineering, vol. 48, 94–104, 2005.

Thomas, L.K., Dixon, T.N., and Pierson, R.G.: “Fractured reservoir simulation”, SPE Journal, SPE 147, 42-54, 1983.

Todd, A., Jim Douglas, Jr., and Ulrich, H.: “Modeling of naturally fractured reservoirs by formal homogenization techniques” book, Cite Seer press, 1991.

Todd, A.: “The double porosity model for single phase flow in naturally fractured reservoirs” book, Springer-Verlag New York, 1987.

Trivedi ,J., and Babadagli, T.: “Scaling miscible displacement in fractured porous media using dimensionless groups”, Journal of petroleum science and engineering, vol. 61, Issues 2-4, August 2008.

Van Genuchten, M.Th.: “A closed-form equation for predicting the hydraulic conductivity of unsaturated soils”, Journal of soil science, vol. 44, 892-898, 1980.

Warren, J.E., and Root, P.J.: “The behavior of naturally fractured reservoirs”, SPE Journal, SPE 3, 245–255, 1963.

Wilkinson D.: “Percolation effects in immiscible displacement”, Journal of physical review A, vol. 34, 1380, 1986.

Zendehboudi, S., Mohammadzadeh, O., and Chatzis , I.: “Investigation of gravity drainage in fractured porous media using rectangular macromodels”, Canadian international petroleum conference/SPE gas technology symposium joint conference (the Petroleum society’s 59th annual technical meeting), Calgary, Alberta, Canada, June 2008, accepted be published in JCPT.

Zendehboudi, S., Mohammadzadeh, O., and Chatzis, I.: “Experimental study of controlled gravity drainage in fractured porous media”, CIPC, Calgary, Canada, 2009, accepted to be published in JCPT.

Zhang, D.: “Stochastic methods for flow in porous media: coping with uncertainties” book, Academic press, San Diego, ISBN 012–7796215, 350- 370, 2002

Zhou, D., and Blunt, M.J.: “Effect of spreading coefficient on the distribution of light non-aqueous phase liquid in the subsurface”, Journal of contaminant hydrology, vol. 25, 1–19, 1997.

Zhou, D., and Blunt, M.: “Wettability effects in three-phase gravity drainage”, Journal of Petroleum engineering and science, 203-211, 1998.

Zhi-An L., and Dong Y.: “Some theoretical aspects of gravity drainage in naturally fractured reservoirs”, SPE Journal, SPE 28641, September 1994.

Zimmerman, R.W., and Bodvarsson, G.S.: “A simple approximate solution for horizontal infiltration in a Brooks–Corey medium”, Journal of transport phenomena in porous media, vol. 6, 195–205, 1991.

Appendix A: CMC Information

A.1 Product Description

Product name: Carboxy methyl cellulose (CMC) sodium salt
Product number: C 5678
Company name: Sigma-Aldrich Canada, Ltd
Store: at room temperature
CAS number: 9004-32-4
Molecular weight: 90 kDa
Degree of polymerization: 400
Sodium content: Approximately 8% by weight.
Purity: 99.5%
Synonym: CMC

This product is a low viscosity carboxy methyl cellulose (CMC); viscosity of CMC solution (2%) changes from 5 cp to around 12 cp. Moreover, the viscosity of a 4% solution in water at 25 °C is 50 - 200 centipoises. The viscosity is both concentration and temperature dependent. As the temperature increases, the viscosity decreases. As the concentrations increases, the viscosity increases.

All kinds of Carboxy methyl cellulose (CMC) are used as suspending agents. Low viscosity CMC is usually used in "thin" aqueous solutions. Medium viscosity CMC is used to make solutions that look like a syrup. High viscosity CMC is used to make a mixture, which resembles a cream or lotion.

A.2 Precautions and Disclaimer

For laboratory use only. Not for drug, household or other uses.

A.3 Preparation Instructions

The product is soluble in water (40 mg/ml). The key to dissolving carboxy methyl cellulose is to add the solid carefully to the water so that it is well dispersed (well-wetted). Adding the solid in portions may be necessary. Adding water to the dry solid produces a "clump" of solid that is very difficult to dissolve; the solid must be added to the water. Stir gently or shake intermittently; do not stir constantly with a magnetic stirring bar. High heat is not needed and may actually slow down the solubilization process. A mixing device, such as an impeller-type agitator which produces a vortex, would allow the powder to be drawn into the liquid, but it may produce some shearing.

A.4 Storage/Stability

Under normal conditions, the effect of temperature on solutions of this product is reversible, so slight temperature variation has no permanent effect on viscosity. However, long periods of

heating CMC solutions at high temperatures (autoclaving) will degrade the product and permanently reduce viscosity. CMC is therefore very difficult to sterilize.
γ-Irradiation, like heating, will degrade CMC. High viscosity CMC is more adversely affected by autoclaving and irradiation than is low viscosity CMC. Filtering CMC solutions tends to leave a gel behind because the material is fibrous, so solutions cannot be sterile filtered.

A.5 Procedure to Measure Viscosity

To measure the viscosity of CMC solutions: 1) Prepare a 2% (w/w) solution of CMC in water. 2) Heat for several hours at 37 ^{o}C. 3) Place in a shaker for one to two days at 2-8 °C to completely dissolve the product. 4) Bring the solution back to 25 C. 5) Measure the viscosity with a Brookfield viscometer

A.6 CMC Rheology

It has been reported in the literature that the CMC solution is a non-Newtonian fluid and its viscosity is a function of the shear rate. The solution is a power-law fluid which is in the category of pseudoplastic liquids. Figure A.1 shows shear stress versus shear rate for this kind of non-Newtonian fluids. However, in this thesis, the CMC solution has been considered as a Newtonian fluid with a constant viscosity. Because, CMC exhibits Newtonian behaviour at extreme shear rates, both low and high. For CMC solution (2%), if apparent viscosity is plotted against shear rate, we can see a curve like Figure A.2.

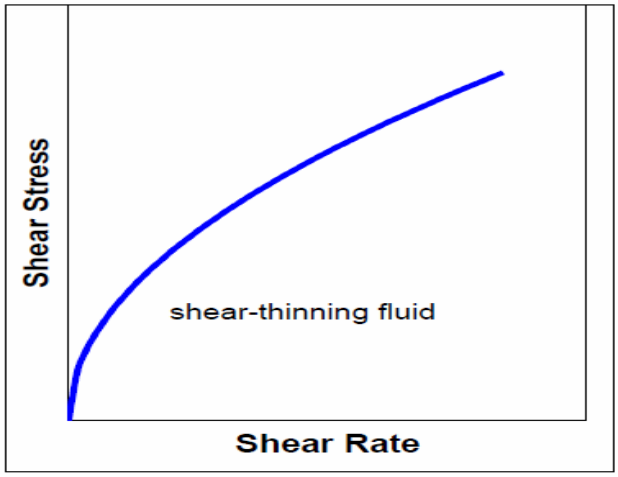

Figure A.1: Variation of shear stress with respect to shear rate for shear-thinning fluid

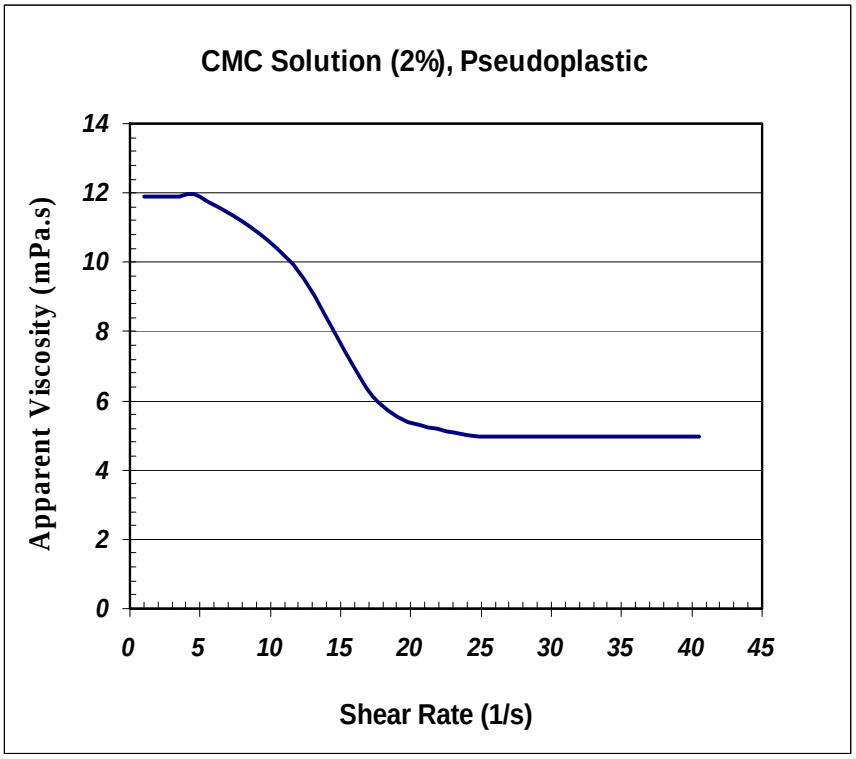

Figure A.2: Apparent viscosity versus shear rate for CMC solution (2%)

There are two reasons for assuming CMC solutions as Newtonian fluids:

1) During the experiments, velocity gradient is negligible for the main parts of the matrix medium, however shear rate is in the range of 0 – 5 1/s within the portion of matrix part which is adjacent to the side parallel fractures. Based on the viscosity measurement, the liquid behaves still Newtonian fluid in the domain of low velocity gradient established in the fractured porous media as seen in Figure A.2.
2) As obtained in the current study and also transport phenomena in porous media, velocity is small enough that we can consider Darcian flow regime for the gravity drainage experiments. Therefore, this assumption is valid for CMC solutions to be taken account as Newtonian fluids according to magnitude of Reynolds number and velocity gradient for both free fall and controlled gravity drainage processes.

Appendix B: Measurement of Physical Properties

B.1 Viscosity

There are a number of laboratory instruments for measuring viscosity. Here, two of them, which were employed in this study, are explained briefly.

B.1.1 Coaxial cylinder viscometer: A coaxial viscometer is used for measuring the viscosity of the test fluids. The type of viscometer is Fann® Model 34 series. The solution is sheared in the annular space between the coaxial cylinders by rotating the outer cylinder at a known speed. The torque, generated on the inner stationary cylinder due to viscous drag exerted by the solution, is transmitted to a spring. The deflection of this spring is measured on a dial indicator. The calibration of dial-reading vs. rotational speed has been done for two known viscosities for this viscometer and following equation was obtained:

$$\tau = 0.1047 * (Dial\ \text{Re}ading) - 0.5196 \qquad \text{(B.1)}$$

B.1.2 U-Capillary tube: There is a simple method to measure viscosity. First we make a U-capillary tube. In one arm of the U is a container of our liquid and there is another container down on the other arm. By making suction, liquid is flown down through the capillary into the lower container. During a certain time period, we measure cumulative liquid and then calculated flow rate. By calibration of this simple viscometer, we find out value of viscosity for the liquid with unknown viscosity. Equation (B.2) shows the relationship between viscosities of two liquids for this type of viscometer.

$$\frac{q_1}{q_2} = \frac{\mu_2}{\mu_1} \qquad \text{(B.2)}$$

where q and μ are the volumetric flow rate and the viscosity, respectively.

It should be noted that Equation (B.2) is valid when the test fluid exhibits Newtonian behavior and also flow regime is laminar.

B.2 Surface Tension

There are two common methods for measuring surface tension which were used in our research study.

B.2.1 Capillary rise method: The end of a capillary is immersed into the solution. The height at which the solution reaches inside the capillary is related to the surface tension by the equation as follows:

$$h = \frac{2\sigma.\cos\theta}{\rho.g.r} \qquad \text{(B.3)}$$

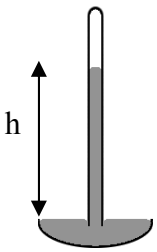

Figure B.1: Capillary rise method for measuring interfacial tension

where h is the height the liquid is lifted, σ is the liquid-air surface tension, ρ is the density of the liquid, r is the radius of the capillary, g is the acceleration due to gravity, and θ is the angle of contact.

Contact angle is measured by a goniometer (Model 190 CA Goniometer) using an optical subsystem to capture the profile of a pure liquid on a solid substrate. This method is called the sessile drop. The angle formed between the liquid/solid interface and the liquid/vapor interface is the contact angle. Older systems were using a microscope optical system with a back light. In this methodology, high resolution cameras and software are employed to capture and analyzed the contact angle.

For the purpose of modeling drainage process, it is reasonable to assume θ = 0°, since most rocks are water wet in their original depositional environment (Berg, 1975).

B.2.2 Wilhelmy plate method: A universal method especially suited to check surface tension over long time intervals. A vertical plate of known perimeter is attached to a balance, and the force due to wetting is measured.

$$\sigma = \frac{F}{l.\cos\theta} \qquad \text{(B.4)}$$

where l is the wetted perimeter of the Wilhelmy plate. Figure B.2 shows a simple schematic of the apparatus.

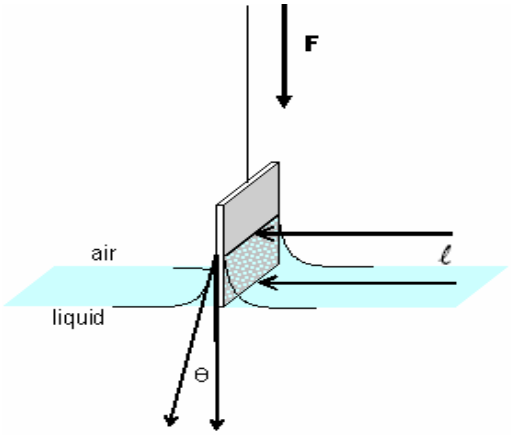

Figure B.2: Schematic of Wilhelmy plate model equipment

B.3 Density

The basic way to measure density is to weigh a known volume and densitometer is another option if high accuracy needed

Appendix C: Multi-Variable Regression Analysis

Design of a regression analysis procedure is important for modeling the response of a process. To do so, one need "good" estimates of the model parameters, i.e. the contributing parameters should have a minimum in the statistical variance and they should be unbiased in nature. In other words, if one wishes to design an appropriate regression model, some primary elements should be considered such as implementing a precise model, logical generalization of modeling results, and quantifying the dependency of response variable(s) on all process inputs. There are three main steps to perform such a statistical modeling which are described briefly in the following sections:

C.1 Dimensionless Numbers

In this section, the dimensionless numbers which play important role in the upscaling of the experimental results are discussed. There are three independent dimensions and fifteen (15) or sixteen (16) variables, depending on the response variable; therefore, thirteen or fourteen different dimensionless numbers can be defined based on the Buckingham π theorem or any of the dimensionless analysis analogies. Table C.1 lists the variables associated with the experiments carried out and Table C.2 lists the dimensionless groups that can be found.

Table C.1 : Dependent and independent variables used for Buckingham-Pi theorem

Variable	Dimension	Variable	Dimension
Particle diameter (D_p)	$M^0 L^1 T^0$	Matrix porosity (ϕ_m)	$M^0 L^0 T^0$
Liquid density (ρ_l)	$M^1 L^{-3} T^0$	Gas liquid surface tension (σ)	$M^1 L^1 T^{-2}$
Gas density (ρ_g)	$M^1 L^{-3} T^0$	Withdrawal velocity (v)	$M^0 L^1 T^{-1}$
Matrix permeability (K_m)	$M^0 L^2 T^0$	Fracture aperture (b)	$M^0 L^1 T^0$
Fracture permeability (K_f)	$M^0 L^2 T^0$	Gravitational force (g)	$M^0 L^1 T^{-2}$
Liquid viscosity (μ_L)	$M^1 L^{-1} T^{-1}$	Matrix width (W)	$M^0 L^1 T^0$
Gas viscosity (μ_g)	$M^1 L^{-1} T^{-1}$	Position difference between gas liquid interface in matrix and fracture (ΔH)	$M^0 L^1 T^0$
Model height (L)	$M^0 L^1 T^0$	Recovery factor (R.F)	$M^0 L^0 T^0$
Fracture porosity (ϕ_f)	$M^0 L^0 T^0$		

Table C.2: Dimensionless groups obtained using Buckingham-Pi analysis

Dimensionless Group	Dimensionless Group
$\frac{\rho_l}{\rho_g}$	$\frac{\mu_L}{\mu_g}$
$\frac{W}{L}$	$\frac{b}{L}$
$\frac{\phi_f}{\phi_m}$	$\frac{K_f}{K_m}$
$\frac{K_m.\Delta\rho.g}{\sigma}$	$\frac{v.\mu_L}{\sigma}$
$\frac{K_m.g^2}{v^4}$	$\frac{\rho_l.v.D_p}{\mu_L}$
R.F	ϕ_m
$\frac{L}{\Delta H}$	$\frac{g.L^3.\rho_l^2}{\mu^2}$

Since some of above variables are constant in the experimental work, the following table shows the required dimensionless groups for our cases.

Table C.3: Dimensionless groups used in the CGD experimental data analysis

Dimensionless Group	Dimensionless Group
R.F = Recovery factor	$\frac{K_f}{K_m}$ = Permeabilities ratio
$\frac{K_m.\Delta\rho.g}{\sigma}$ = Bond number	$\frac{v.\mu_L}{\sigma}$ = Capillary number
$\frac{L}{\Delta H}$ = Dimensionless height	$\frac{\rho_l.v.D_p}{\mu_L}$ = Reynolds number

It should be noted that six dependent variables are taken account as significant dimensional variables for recovery factor at gas breakthrough and elevation difference between G-L interface positions in matrix and fractures. Also five dependent variables are considered as effective parameters affecting the magnitudes of critical pumping rate and maximum withdrawal rate.

C.1.1 Capillary Number: In fluid mechanics, the Capillary number represents the relative importance of viscous forces compared to the surface tension forces acting across a particular interface between the liquid and gas phase, or between two immiscible liquid phases (Grattoni et al, 2001). It is defined as:

$$Ca = \frac{v.\mu_L}{\sigma} \qquad \text{(C.1)}$$

where "μ_L" is the liquid viscosity, "*v"* is a characteristic velocity (which could be considered as the withdrawal rate considering the current experimental study, , and "σ" is either the surface or interfacial tension between the two fluid phases. As a general rule of thumb, one can consider the fluid flow in a porous medium to be dominated mainly by capillary forces if the associated value of capillary number is equal to or less than 10^{-5} (Gray, 2008). As it was stated before in Section 4.4.2 of Chapter 4, liquid viscosity and the withdrawal rate have profound effect on the recovery factor, as well as on the G-L interface locations within matrix and fractures. Defining the capillary number as one of the contributing dimensionless numbers in the regression analysis, one could incorporate the importance of these two independent variables on the statistical modeling response.

C.1.2 Bond Number: As explained in Chapter 3, the Bond number is a dimensionless number expressing the ratio of body forces (often gravitational) to capillary forces.

$$Bo = \frac{\Delta\rho.g.l^2}{\sigma} \qquad \text{(C.2)}$$

where "Δρ" is the density difference between two fluids, "*g"* is the gravity acceleration in the direction of flow , "*l"* is the characteristic length scale (often taken as the average grain radius and "σ" is the surface tension across the interface (Morrow et al., 1988)). In this study, the (K_m) is used instead of (l^2).

For a vertical displacement, *Bo* takes into account the balance between gravity and capillary forces and is directly proportional to the advance of the displacing phase front. Understanding importance of the Bond number value is essential for investigating different aspects of gravity drainage process. It is wise to consider it as one of the reference dimensionless groups. This makes it possible to realize its importance on the different aspects of CGD process defined previously in section 4.4.2 of Chapter 4, including CPR, MPWR, and elevation difference between G-L interface positions in matrix and fractures.

C.1.3 Reynolds Number: For non-Darcy flow in porous media, it is similar to turbulent flow in a conduit. The Reynolds number for identifying turbulent flow in conduits was adapted to describe non-Darcy flow in porous media (Chilton et al , 1931). The researchers conducted fluid flow experiments on packed particles, and redefined the Reynolds number, *Re*, as

$$\mathrm{Re}_p = \frac{\rho.v.D_p}{\mu_L} \qquad \text{(C.3)}$$

where *D*p is the diameter of particles. In practically all cases, Darcy's law is valid as long as the Reynolds number based on average grain diameter does not exceed some value between 1 and 10. Also, some experimental works in porous media have shown that the critical Reynolds number for non-Darcy flow to become significant is in the range of 40-80 (Levy, T., 1975). To be consistent with the majority of the open literature cases in which this dimensionless number have been defined, macroscopic discharge velocity (i.e. withdrawal rate in case of flow under gravity drainage process) was used in our analogy regarding dimensionless analysis of CGD process.

C.1.4 Ratio of fracture permeability to matrix permeability, ($\frac{K_f}{K_m}$): This ratio is the main factor affecting fluid flow in both matrix and fractures during the course of CGD process. It could be beneficial to consider the importance of this driving force in the dimensional analysis. As the medium permeability (either matrix or fracture) contributes significantly to the flow potential within that particular medium, the ratio of fracture to matrix permeability, which is a dimensionless parameter) could represents the flow potential contrast between these two flow-related media. In addition, the contrast between fracture and matrix permeabilities also involves liquid flow exchange between these two media. Moreover, it has profound effect on the final recovery factor values as well as on the amount of gas invasion into the matrix. As a result, this dimensionless parameter was considered as one of the groups required for the dimensionless analysis of CGD process performance.

C.1.5 Dimensionless height, (L/ΔH): In order to fulfill the sufficient numbers of dimensionless groups required for the dimensionless analysis, the dimensionless height has been defined as the ratio of the magnitude of model height, "L" (which is constant for each particular packing height) to the magnitude of elevation difference between G-L interface positions within matrix and fractures, "ΔH", in each particular fractured medium. The latter is dictated by the value of withdrawal rate which has been set for each particular CGD process. The main reason for defining this dimensionless parameter is to figure out how the height difference between liquid level positions within fractures and matrix would be influenced by changing the main independent parameters of noted CGD experiments.

C.1.6 Recovery factor (R.F): As common in petroleum reservoir engineering, this dimensionless parameter is defined as the ratio of recoverable oil to the oil in place in a reservoir. It is accepted that recovery factor estimation is a tool for rapid assessment of suitability of recovery methods at given conditions. To ease evaluation, the results are ranked by recovery factor

C.2 Multiple Linear Regression Models

In many applications of regression analysis, it is common that there are more than one regressor variable. A regression model which contains more than one regressor variable is called a multiple regression model. As it was described in section C.1, the proposed dimensionless analysis contains six dimensionless groups, namely:

1) Bond number, 2) Capillary number, 3) Reynolds number, 4) $\frac{K_f}{K_m}$, 5) H/Δh, and, 6) Recovery factor

There are four important objective parameters for each CGD experiment, namely CPR, MPWR, Recovery Factor, and elevation difference between G-L interface positions within fractures and matrix. These four objective functions should be statistically modeled as functions of the defined dimensionless groups. In order to perform the multiple linear regression analysis, these four objective functions should be expressed explicitly in the dimensionless form.

As the nature of both of CPR and MPWR is drainage liquid velocity, they could be expressed in terms of the capillary number. Hence, two corresponding capillary numbers would be defined: Critical Capillary number, associated with the CPR, and Maximum Capillary number, associated with MPWR. Recalling the definition of Capillary number presented in section C.1.1, Critical Capillary number would be the ratio of viscous forces associated with the critical pumping velocity (or critical pumping rate) to the capillary forces applied across the gas-liquid interface. Similarly, Maximum Capillary number is also defined as the viscous forces associated with the MPWR, divided by the capillary forces associated with the G-L interface. As a result, these two important parameters (CPR and MPWR) or their equivalent dimensionless groups (Critical Capillary number or dimensionless CPR, and Maximum Capillary number or dimensionless MPWR) could be estimated statistically in terms of the other mentioned dimensionless groups.

The "Recovery Factor" objective function is dimensionless in nature. The elevation difference between G-L interface positions within matrix and fractures would also be altered to the dimensionless form by introducing the "dimensionless height" group. In other words, height of each particular model divided by the elevation difference between interface positions within matrix and fractures forms this forms this dimensionless objective function.

In order to perform the multiple linear regression analysis, it is primarily assumed that each of these dimensionless objective functions is a sole function of every each of the defined dimensionless groups. In other words, in order to figure out the dependency of a particular dimensionless objective function upon a particular dimensionless group, they should be plotted against each other for the range of all of the experimental data which are available. As a result, the absolute effect of each of the dimensionless groups (Capillary number, Bond number, Reynolds number, $\frac{K_f}{K_m}$) on the dimensionless objective functions could be investigated. Doing so, it was primarily assumed that there is no interaction term between defined dimensionless predictor variables. In other words, each particular objective function is only a sole function of different singular dimensionless predictor values, and not a function of an interaction term, consisting of a combination of some of those predictor variables.

Following plotting each particular dimensionless objective function versus each particular dimensionless group, two different schemes could appear. If the resulting graph would have a unique linear trend, it shows that the dimensionless objective function is a function of that particular dimensionless group itself and the dependency could be figured out using the multiple linear regression analysis. However, if the resulting graph would have multiple different linear trends, it means that not only the objective function has functional dependency upon that particular dimensionless group, but also there is a combined functional dependency between the objective function and a combination of dependent parameters. This combined dependant parameter consists of every other dimensionless group whose sole functional relationship with that particular objective function consists of multiple (i.e. more than one) linear graphs.

Following determination of the functionality of each particular dimensionless objective function to different dimensionless groups and/or their combination, the coefficients of the resulting correlation could then be obtained using multiple linear regression analysis. In general, the dependent variable or response (i.e. dimensionless objective function in our case) may be related to "k" regression variables using the following model:

$$y = \beta_o + \beta_1 x_1 + \beta_2 x_2 + ... + \beta_k x_k + e \qquad \text{(C.4)}$$

This relation is called a "multiple linear regression" model with "*k"* regressor variables (x_1 to x_k). The parameters "β_0 to β_k" are called the regression coefficients, x_1, x_2,…,x_k are the dimensionless numbers, and "y" is the actual response variable (i.e. objective function). According to the procedure mentioned above about considering the combined effect of dimensionless groups on the objective functions (and their related figures which are discussed later), and based on the physics of the CGD process which have already been reviewed in the first part of Chapter 4, it is found that combination of dependent dimensionless groups have also major contribution in the magnitudes of all the objective functions. As a result, regression models should include the term related to the "effect of interaction between the dependent dimensionless groups" as well. An interaction between two dependent variables can be represented by a cross-product term in the regression model, such as:

$$y = \beta_o + \beta_1 x_1 + \beta_2 x_2 + \beta_{12} x_1 x_2 + e \qquad \text{(C.5)}$$

in which "e" is the random error term (or experimental error), which is defined as the difference between actual dependent variable and predicted dependent variable obtained by the regression model. As far as the curve fitting procedure using multiple linear regression analysis is concerned, it is much more convenient to express the mathematical operations using matrix notation. Suppose there are "*k*" regressor variables and "*n*" observations, and the model relating the regressors to the response is as follows:

$$y_i = \beta_o + \beta_1 x_{i1} + \beta_2 x_{i2} + ... + \beta_k x_{ik} + e_i \qquad i = 1,2,....,n \qquad \text{(C.6)}$$

This model could be represented as a system of "*n*" equations; hence it could be expressed in the matrix notation as:

$$y = X\beta + e \qquad \text{(C.7)}$$

where:

$$y = \begin{bmatrix} y_1 \\ y_2 \\ \vdots \\ y_n \end{bmatrix}, \quad X = \begin{bmatrix} 1 & x_{11} & x_{12} & \cdots & x_{1k} \\ 1 & x_{21} & x_{22} & \cdots & x_{2k} \\ \vdots & \vdots & \vdots & & \vdots \\ 1 & x_{n1} & x_{n2} & \cdots & x_{nk} \end{bmatrix}, \quad \beta = \begin{bmatrix} \beta_1 \\ \beta_2 \\ \vdots \\ \beta_k \end{bmatrix}, \quad and \quad e = \begin{bmatrix} e_1 \\ e_2 \\ \vdots \\ e_n \end{bmatrix}$$

Respectfully, the least square estimate of "β" parameter is:

$$\hat{\beta} = (X'X)^{-1} X'y \qquad \text{(C.8)}$$

C.3 Analysis of the Multi-Variable Regression Modeling

The regression modeling, which is based on the assumption of validity of experimental data and as such the precision of preliminary DOE, should be checked accordingly in order to examine the curve fitting procedure and validity of the preliminary employed DOE. Three major validity indicators have been relied on in this section to check the suitability of the multi-variable linear regression analysis, namely as ANOVA tables, residual analysis, and squared of residuals' analysis (Montgomery and Runger, 2006; Montgomery, 2008).

C.3.1 ANOVA tables: The analysis of variance (ANOVA) table includes data from a standard sum of the squares of the variance analysis for regression. The relevant ANOVA table for CPR has been shown as Table C.4. As it is depicted in this Table, each particular ANOVA table includes the relevant data for each of three sources of deviation consisting of Regression, Residuals and Total (i.e. first column). The source of variation of each data is either due to the deviation of each predicted data from its group mean value (i.e. Regression), or due to the deviation of each predicted value from its observed value (i.e. Residuals). The sum of these two sources of deviation would be expressed as the Total source of deviation. For each of these three sources of deviations, four measures of variance (i.e. columns 2 to 5, Table C.4) could be described as follows:

a) Degrees of freedom (i.e. DF, 2nd column of Table C.4): For each particular regression analysis, this parameter could be determined as the number of correlation coefficients, "N", respect to the number of regressor variables used in each particular model. The higher is the degree of freedom for each particular model, the more reliable would be the regression model.

b) Sum squares (i.e. SS, 3rd column of Table C.4): Summation of the squared deviations, which are predicted from the observed data, is a measure of variance for each particular regression analysis. Total Sum Square is the summation of the squares of the residuals with the sum of the squares due to the regression.

c) Mean squares (i.e. MS, 4th column of Table C.4): This column contains the sum of squares (i.e. SS) corrected for the degrees of freedom (i.e. DF).

d) F-test (i.e. F, 5th column of Table C.4): This is a variance-related statistical parameter which compares two models that are different from each other by one or more regressor variables to figure out if the more complex model would be also more reliable than the less complex one. If the "F" value is greater than a standard (i.e. critical) tabulated value, the more complex equation would be considered significant. By default, the significance level is set at 0.05.

According to the above descriptions, Table C.4 is the ANOVA table for CPR, and since $F_{observed}$, which is equal to 478.027, is greater than the critical value (3.48), all of the considered parameters in multi-variable linear regression analysis of CPR (i.e. Critical Capillary number) and their attributed effects are of great significance, and consequently cannot be ignored to simplify the related statistical analysis.

Table C.4 : ANOVA table for CPR (i.e. $Ca_{Cr.}$) regression analysis

	DF	SS	MS	F
Regression	4	8.01E-08	2E-08	478.0275273
Residual	10	4.19E-10	4.19E-11	
Total	14	8.05E-08		

According to the same statistical analogy, ANOVA tables could also be created for MPWR (i.e. Maximum Capillary number) as it is depicted in Table C.5. It is clear that due to the higher magnitude of "F" function compared to its tabulated critical value (3.48), all the dimensionless groups considered for the multi-variable linear regression analysis of MPWR are of great importance and can be neither ignored nor reduced. In addition, it is concluded that there is at least one nonzero correlation coefficient in the proposed regression model.

Table C.5: ANOVA table for MPWR (i.e. $Ca_{Max.}$) regression analysis

	DF	SS	MS	F
Regression	4	9.022047	2.255512	256.1864
Residual	10	0.088042	0.008804	
Total	14	9.110089		

The same procedure has been followed to establish the ANOVA table for the other two objective functions of regression analysis, dimensionless height and recovery factor just before gas breakthrough into the production side. Tables C.6 and C.7 show the strong dependency of noted objective functions to the dimensionless groups used for statistical analysis based on the high magnitude of observed "F" function compared to the tabulated critical values. In addition, these two tables show good accuracy of the regression analysis for both of these objective functions.

Table C.6: ANOVA table for dimensionless height regression analysis

	DF	SS	MS	F
Regression	4	193.8636	48.46591	637.6914973
Residual	42	3.192089	0.076002	
Total	46	197.0557		

Table C.7 : ANOVA table for recovery factor regression analysis

	DF	SS	MS	F
Regression	5	26670.56648	5334.113	876.8266
Residual	67	407.5898002	6.08343	
Total	72	27078.15628		

C.3.2 Residual analysis: The difference between the observed value of the dependent variable (y) and its predicted value ($\hat{y}$) is called the residual parameter (i.e. "*e"*) attributed to that

particular dependent variable. Each data point has one attributed residual value based on the following definition:

Residual = Observed value - Predicted value (C.9)

A residual plot is a graph that shows the residual magnitudes for each particular variable on the vertical axis and the magnitudes of independent variable on the horizontal axis. If the data points in a residual plot would be randomly dispersed around the horizontal axis, that particular linear regression model is statistically appropriate, i.e. it predicts the dependant variable precisely enough compared to the actual values reported based on the experimental observations; otherwise, it is recommended to use a non-linear regression model instead of the linear one. In this section, residual plot studies have been performed for all the statistical regression analyses presented in section 4.5.2 of Chapter 4 to check for their validity and accuracy besides the accuracy check done in section C.3.1.

Residual plots for critical Capillary number regression analysis: Figures C.1 and C.2 are the residual plots for critical capillary number (i.e. CPR) with respect to "K_m/K_f" as well as with respect to the related combined interaction component (i.e. combination of Bond number, Reynolds number, and permeability ratio) respectively, which were included here as two samples of the residual plots for the critical capillary number. As it is clear in these two Figures, the residual data spread randomly all along the horizontal axis. In other words, the proposed linear regression is valid in terms of these two particular dependant variables. In addition, Figure C.3 and C.4 are the comparison chart between actual (i.e. experimentally measured) and predicted values of critical capillary number against its related interaction term (combination of Bond number, Reynolds number, and the permeability ratio) and Bond number (Bo) correspondingly. As it is depicted in these Figures, there is a good compatibility between the actual and predicted values of critical capillary number, showing reliable performance of the proposed regression analysis.

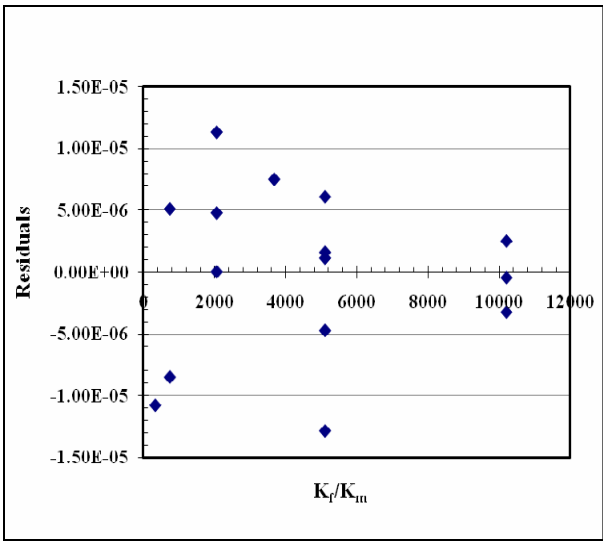

Figure C.1: Residual plots for "$Ca_{Cr.}$" with respect to "K_f/K_m" dimensionless number

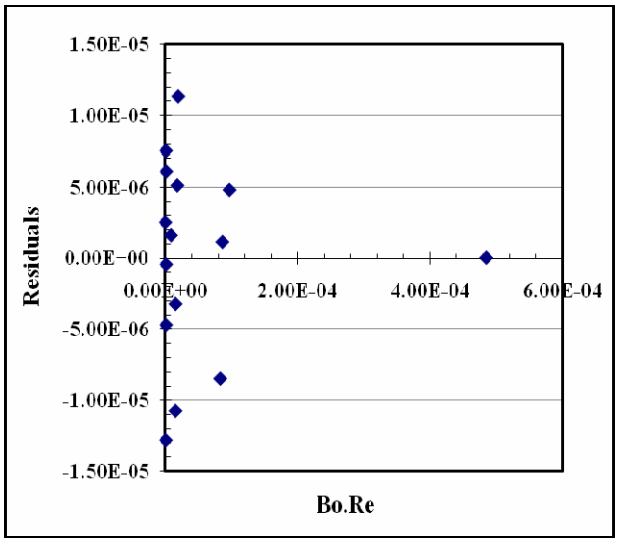

Figure C.2: Residual plots for "$Ca_{Cr.}$" with respect to interaction component [Bo.Re]

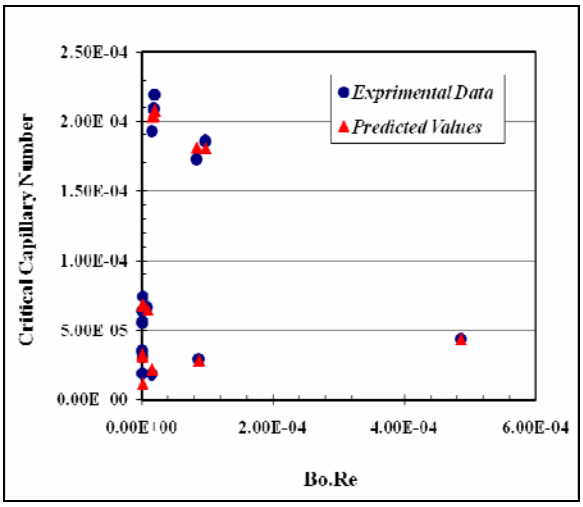

Figure C.3: Comparison chart of predicted versus actual "$Ca_{Cr.}$" against the interaction term

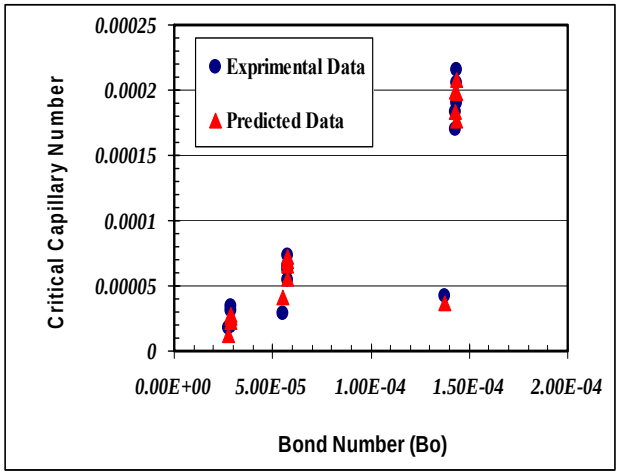

Figure C.4: Comparison chart of predicted versus actual "$Ca_{Cr.}$" against Bond number

Residual plots for maximum Capillary number regression analysis: In order to check the validity of the regression analysis performed for maximum capillary number (i.e. MPWR), two related residual plots have been presented as well. Figures C.5 and C.6 show the residual plots for maximum capillary number with respect to "$Ln(K_f/K_m)$" as well as its values with respect to another dimensionless parameter, i.e. the related combined interaction term, respectively. As these two residual plots do not present a certain trend with respect to the values provided in the "x-axis", it is concluded that the proposed linear regression relationship is appropriately valid for predicting maximum Capillary number using available experimental data for a system analogous to our proposed fractured systems.

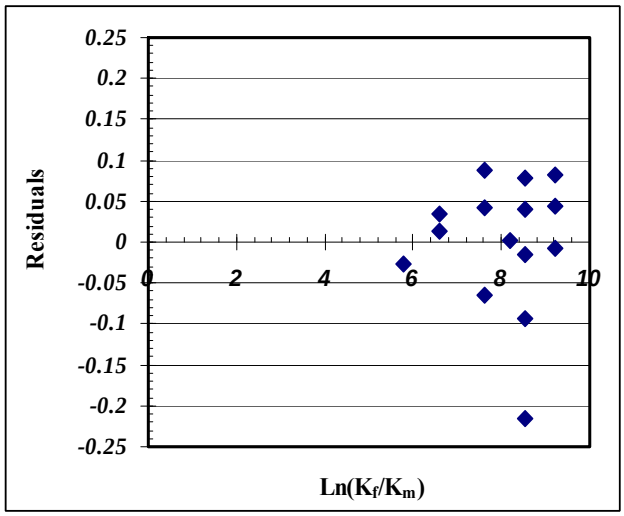

Figure C.5: Residual plots for "$Ca_{Max.}$" with respect to "$ln(K_f/K_m)$"

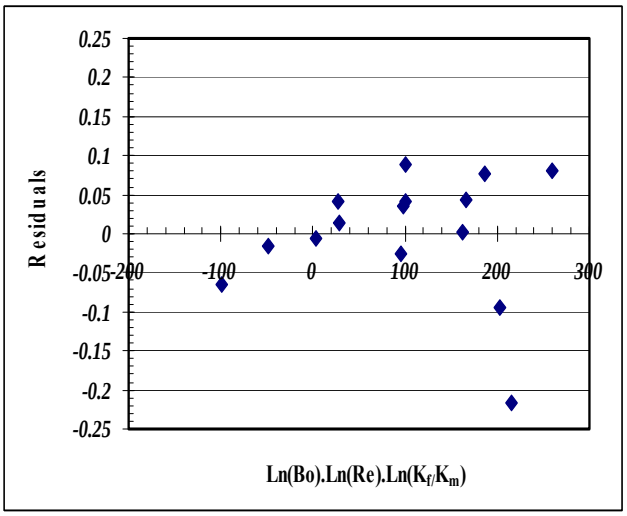

Figure C.6: Residual plot for "$Ca_{Max.}$" with respect to its related interaction component [i.e. $Ln(Bo).Ln(Re_{Max.}).Ln(K_f/K_m)$]

As well, a comparison between predicted and actual values of maximum Capillary number has been shown in Figures C.7 and C.8 as a function of two of the previously defined dimensionless groups to correlated "$Ca_{Max.}$", i.e. the combined interaction and K_f/K_m terms provided in Equation 4.13 in Chapter 4. As it is clear in the Figures, there is a precisely acceptable match between the values calculated based on the experimentally measured parameters and the values predicted by the regression analysis. In other words, Equation 4.13 could predict the maximum Capillary number (related to the MPWR) precisely for a system similar to the fractured models employed in our experimental approach.

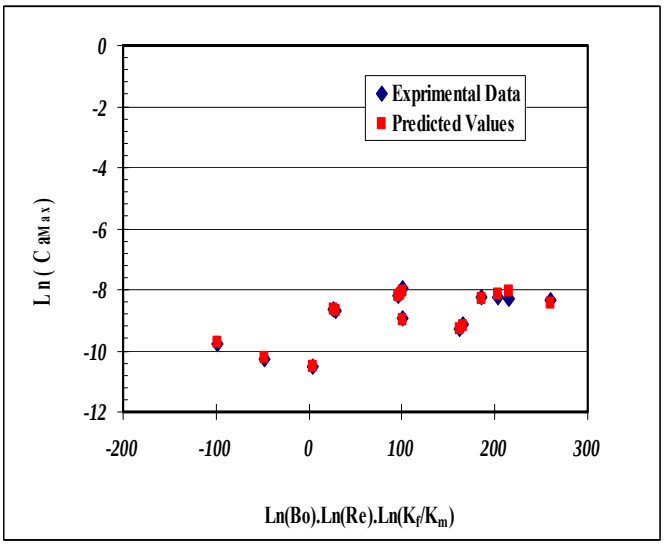

Figure C.7: Comparison chart of predicted versus actual "$Ca_{Max.}$" against the related interaction term

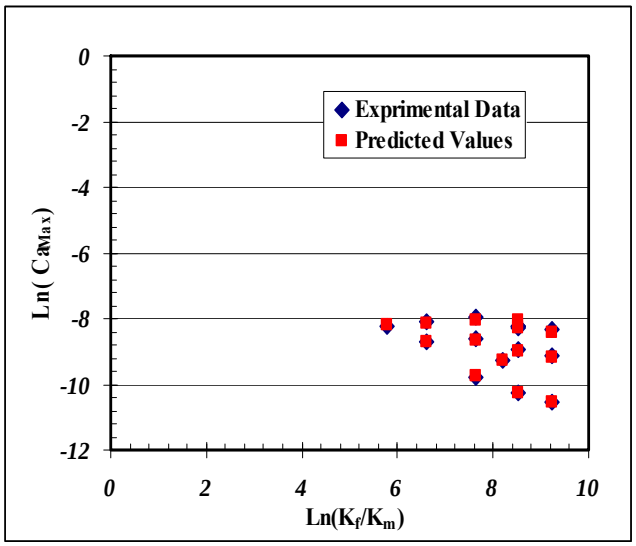

Figure C.8: Comparison chart of predicted versus actual "$Ca_{Max.}$" against the term named, K_f/K_m

Residual plots for dimensionless height regression analysis: Two consecutive plots, Figures C.9 and C.10, show the random spread of residual values attributed to the dimensionless height against two of the contributing dimensionless groups, provided previously in order to linearly regress it based on Equation 4.15 of Chapter 4. According to the logic provided in section C.3.2, it would be concluded that the regression analysis presented by Equation 4.15 accurately predict related values of dimensionless height based on the provided measurable experimental parameters for a system analogous to our fractured prototypes undergoing a particular CGD process. As usual, this accuracy could also be double checked by comparing the calculated dimensionless height values (based on the measurable experimental parameters) against its predicted values (using Equation 4.15) in presence of two of the contributing dimensionless groups according to Equation 4.15 (which is happened to be capillary number and the combined interaction term, (i.e. "Bo.Ln (Ca)"), as it is presented in Figures C.11 and C.12. It is clear that the achieved agreement has high levels of accuracy in terms of the statistical parameters.

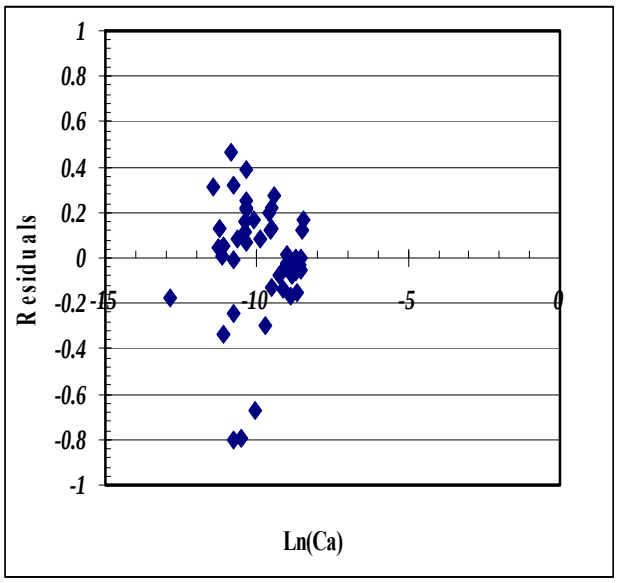

Figure C.9: Residual plot for dimensionless height with respect to "Ln(Ca)"

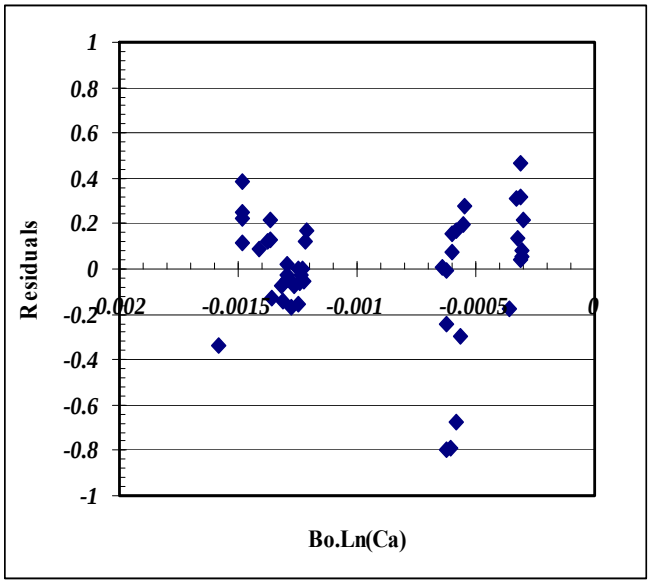

Figure C.10: Residual plot for dimensionless height with respect to its related combined interaction term (i.e. Bo.Ln (Ca))

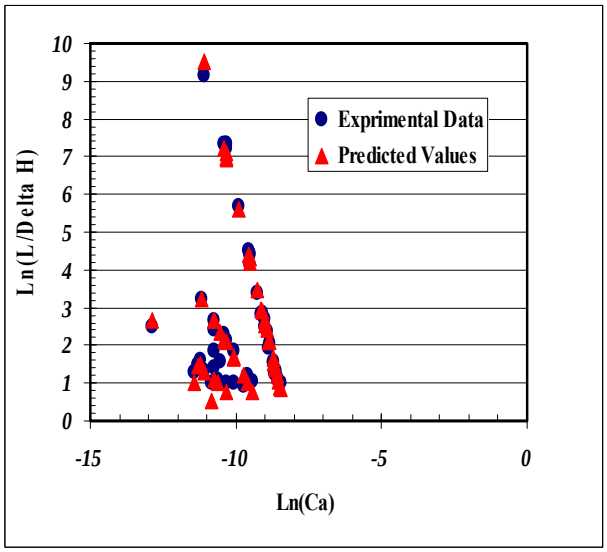

Figure C.11: Comparison chart of predicted versus actual dimensionless height against capillary number

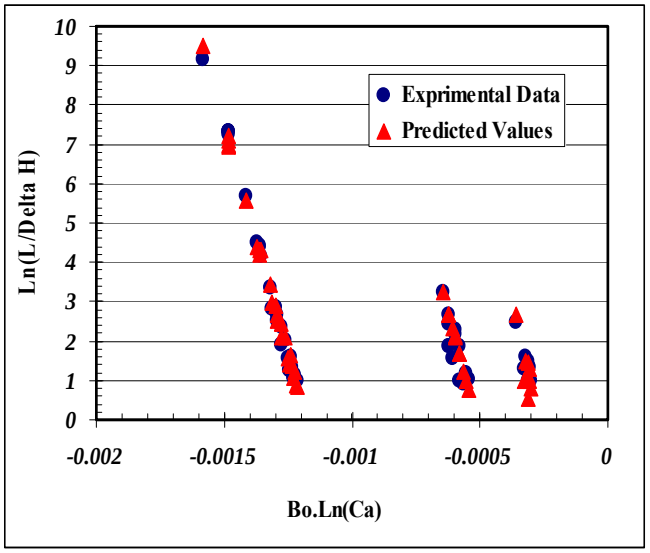

Figure C.12: Comparison chart of predicted versus actual dimensionless height against its combined interaction parameter (i.e. Bo.Ln(Ca))

Residual plots for recovery factor regression analysis: Figures C.13 and C.14 show the residual plots of recovery factor versus two selected contributing dimensionless groups based on Equation 4.18 (in Chapter 4), namely as fracture to matrix permeability ratio and also combined interaction term in terms of a multiplication of Capillary and Bond numbers respectively. As it is depicted in these two Figures, the data points are scattered randomly around the x-axis, showing

that the representation of the dependent variable based on that particular independent variable is valid within the range of change of noted independent variable. In other words, the proposed linear regression analysis provided to predict the recovery factor values is precisely valid for a system analogous to our experimental fractured system. The accuracy of Equation 4.18 to estimate the recovery factor values could also be examined by comparing the predicted and calculated actual recovery factor values. This is the theme of Figures C.15 and C.16, in which the calculated recovery factor values (i.e. obtained from experimentally measured parameters) are in good agreement with the predicted ones using Equation 4.18 when then have been plotted against each of the independent variables, such as capillary number and the combined interaction parameter as they are the cases for these Figures.

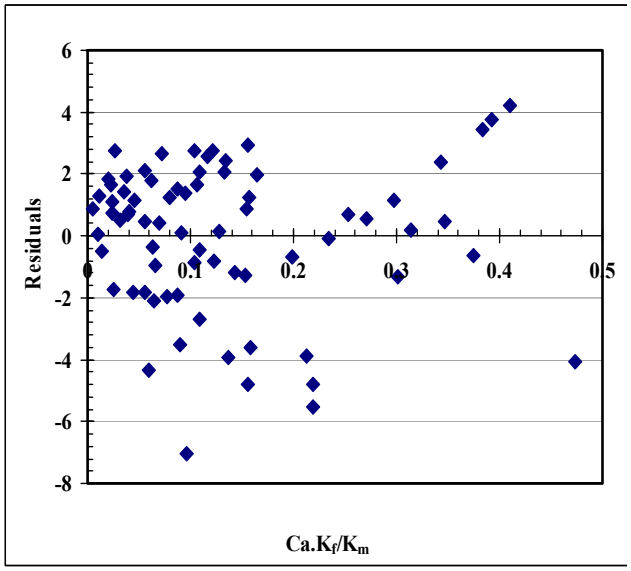

Figure C.13: Residual plot for recovery factor with respect to the dimensionless number named, $Ca.K_f/K_m$

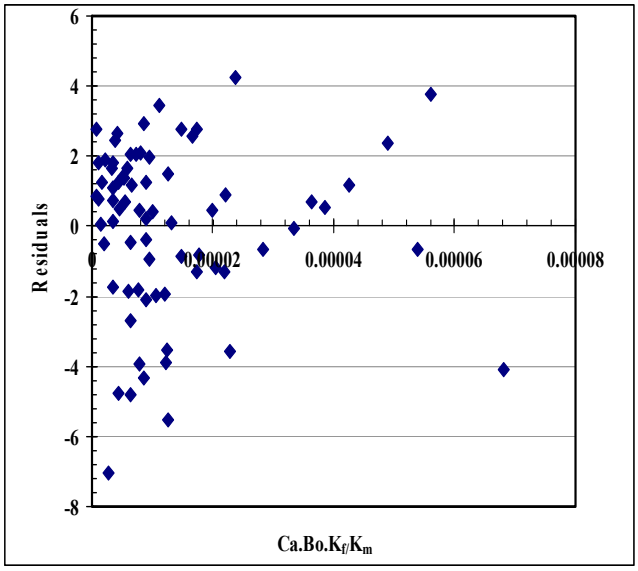

Figure C.14: Residual plot for recovery factor with respect to the combined dimensionless number $Ca.Bo.K_f/K_m$

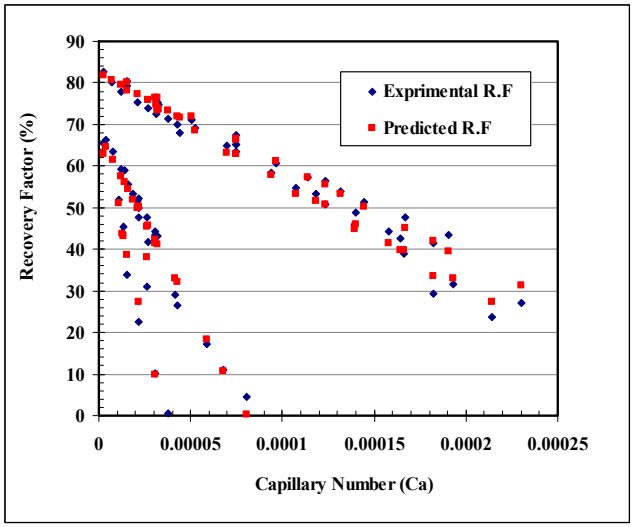

Figure C.15: Comparison chart of predicted versus actual recovery factor against capillary number

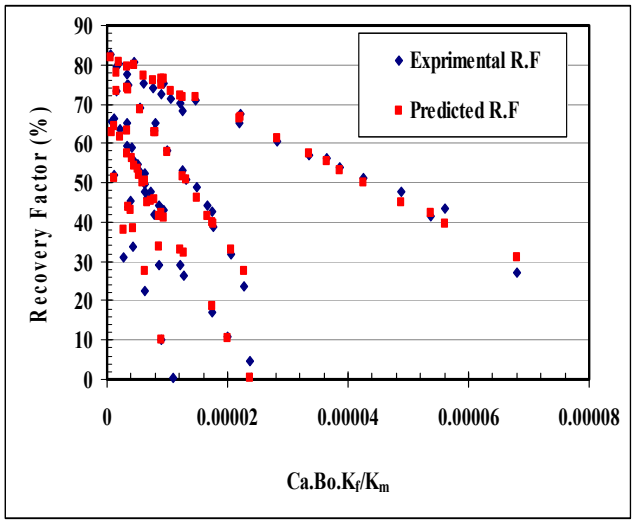

Figure C.16: Comparison chart of predicted versus actual recovery factor values against the combined interaction term (i.e. $Ca.Bo.K_f/K_m$)

Squared residuals analysis: One of the simplest methods to check the accuracy of a particular linear regression is to look at the magnitudes of squared residuals. These values for the proposed linear regressions have been presented in Table C.8. Our results from experimental and linear regression analyses are showing reasonable compatibility between measured and predicted values. In other words, small values of residuals as well as appreciable magnitudes of squared residual indicate that the proposed linear regression curves works well for the experimental conditions noted previously.

Table C.8: Summary of the statistical linear regressions

Objective function	Multiple R	R square	Standard Error	Number of observations
CPR	0.998	0.997	4.83E-06	19
MPWR	0.999	0.998	3.2E-02	19
(H_f-H_m)	0.997	0.995	14.38E-2	59
Recovery Factor	0.998	0.996	21.3E-2	59

Appendix D: Model Report from COMSOL

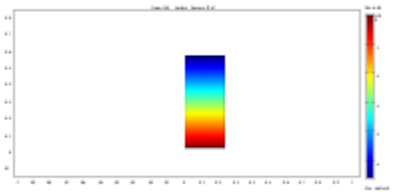

D.1 Table of Contents

D.2 Model Properties

Property	Value
Model name	Two Phase Flow of Air and Oil
Author	Sohrab Zendehboudi
Company	University Of Waterloo
Department	Department of Chemical Engineering
Reference	Copyright (c) 1994-2007 by COMSOL AB
URL	www.comsol.com
Saved date	Jul 5, 2010 10:32:12 PM
Creation date	Sep 6, 2008 8:35:56 AM
COMSOL version	COMSOL 3.5

File name: C:\Users \Desktop\Homogenious.mph (**Simulation Modeling of Two Phase Flow of Air and Oil)**

Application modes and modules used in this model:

- Geom1 (2D)
  - Darcy's Law (Earth Science Module)
  - Darcy's Law (Earth Science Module)

D.2.1 Model description

Two Phase Flow of Air and Oil

This two-phase flow example for air and oil builds on the two-phase flow model for an air-water system. The switch from air-water to air-oil is accomplished with Leverett scaling of interfacial tensions for the different fluid pairs.

D.3 Constants

Name	Expression	Value	Description
rhowater	1000[kg/m^3]		Density, water
rhow	803[kg/m^3]		Density, wetting fluid
etaw	0.00392*hour[Pa*s]		Dynamic viscosity, water
rhonw	1.28[kg/m^3]		Density, nonwetting fluid
etanw	0.0000181*hour[Pa*s]		Dynamic viscosity, nonwetting fluid
hour	3600		
sigma_ao	0.00259		
sigma_aw	0.00681		

D.4 Geometry

Number of geometries: 1

D.4.1 Geom1

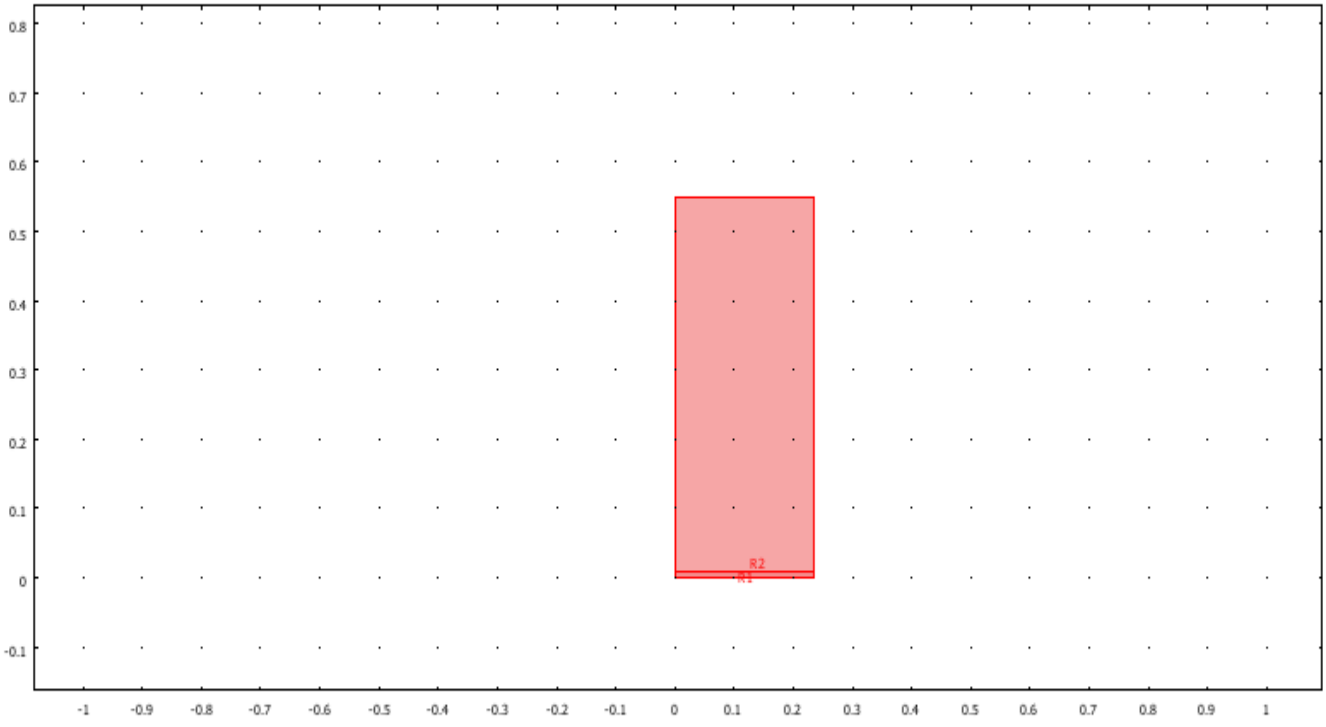

D.4.1.1 Point mode

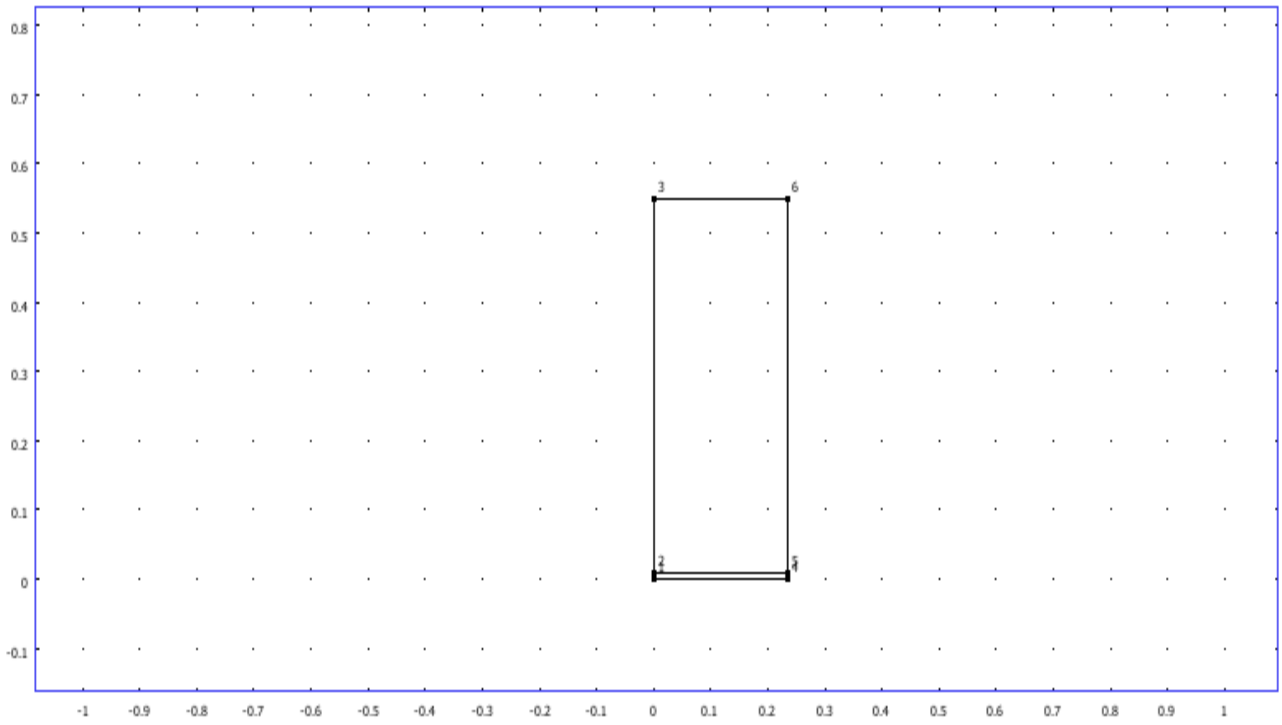

D.4.1.2 Boundary mode

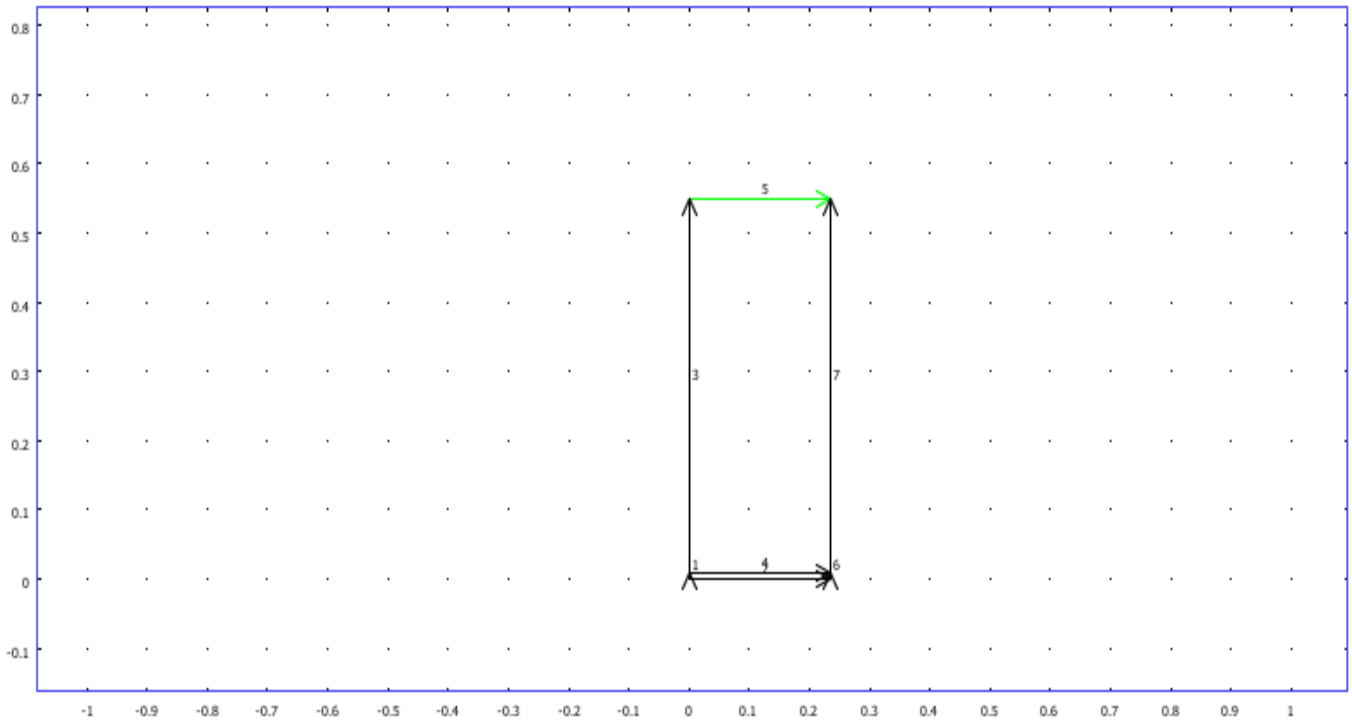

D.4.1.3 Subdomain mode

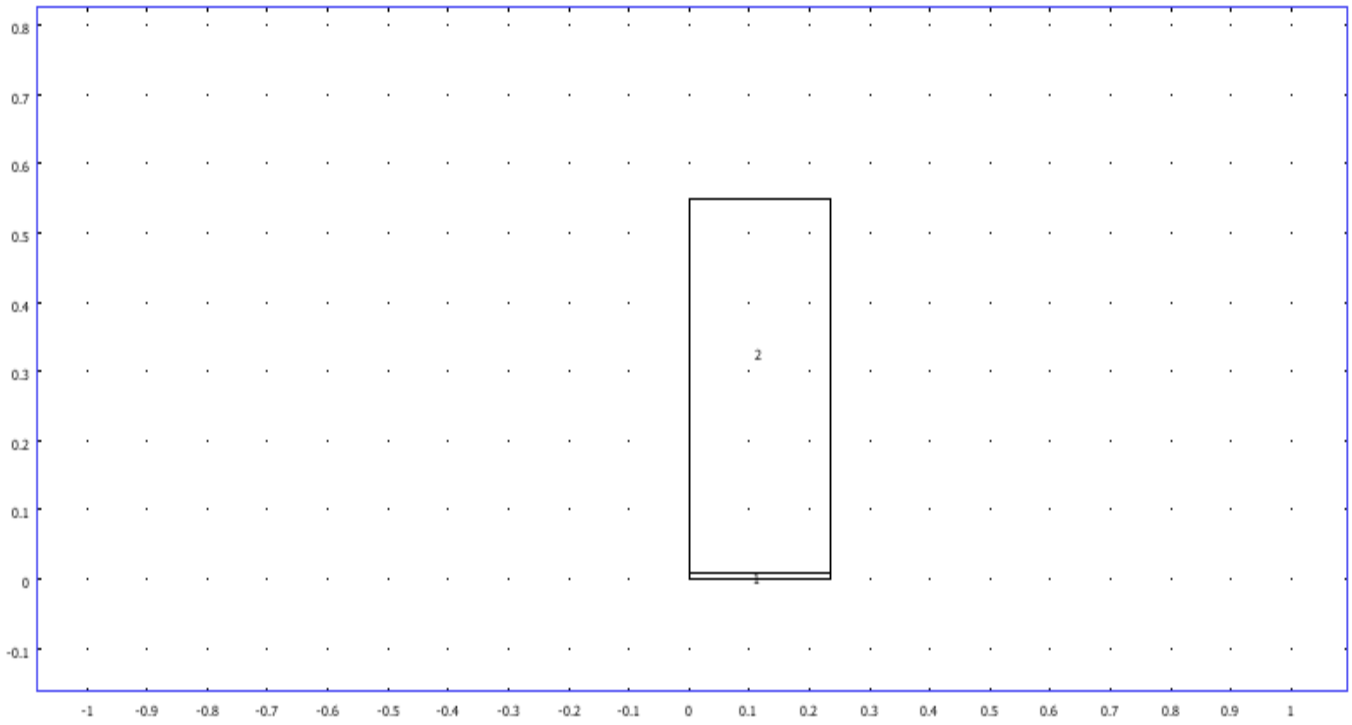

D.5 Geom1

Space dimensions: 2D

Independent variables: x, y, z

D.5.1 Scalar Expressions

Name	Expression	Unit	Description
pnw_top	0.2[m]*rhowater*g_nw*sigma_ao/sigma_aw	Pa	
pnw_in	pnw_top+(0.55-y)*rhonw*g_w	Pa	
pw_in	-rhow*g_w*y	Pa	
pw_t	5		
Hc	(pnw-pw)/(rhowater*g_w)	m	
Sew	(1+abs(alpha*Hc)^N)^(-M)*(Hc>0)+1*(Hc<=0)		
thetaw	(thetar+Sew*(thetas-thetar))*(Hc>0)+thetas*(Hc<=0)		
krw	((Sew^L*(1-(1-Sew^(1/M))^M)^2)+eps)*(Hc>0)+1*(Hc<=0)		
Cp	1/rhowater/g_w*((alpha*M/(1-M)*(thetas-thetar)*Sew^(1/M)*(1-Sew^(1/M))^M))*(Hc>0)		
Senw	1-Sew		
thetanw	thetas-thetaw		
krnw	((1-Sew)^L*(1-Sew^(1/M))^(2*M))*(Hc>0)+eps		

D.5.2 Expressions

D.5.2.1 Subdomain Expressions

Subdomain		1	2
kaps	m^2	3e-010[m^2]	3e-010[m^2]
thetas		0.38	0.38
thetar			0.003
alpha			0.112
N			3.5
L			0.5
M			1-1/N

D.5.3 Mesh

D.5.3.1 Mesh Statistics

Number of degrees of freedom	31304
Number of mesh points	4586
Number of elements	8800
Triangular	8800
Quadrilateral	0
Number of boundary elements	605
Number of vertex elements	6
Minimum element quality	0.665
Element area ratio	0

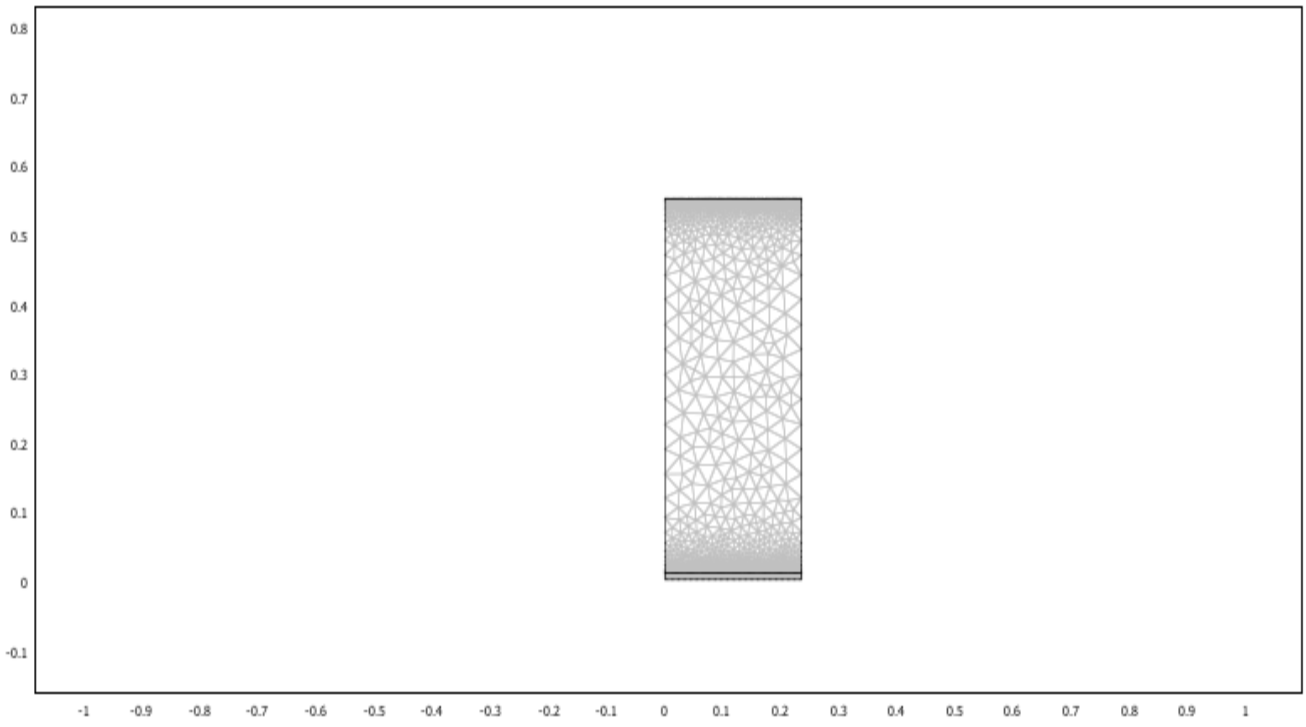

D.5.4 Application Mode: Darcy's Law (w)

Application mode type: Darcy's Law (Earth Science Module)

Application mode name: w

D.5.4.1 Scalar Variables

Name	Variable	Value	Unit	Description
tscale	tscale_w	1e-5	s	Heaviside scaling factor
g	g_w	9.82*hour*hour	m/s^2	Gravity
D	D_w	y	m	Elevation/vertical axis

D.5.4.2 Application Mode Properties

Property	Value
Default element type	Lagrange - Quadratic
Variable	Pressure analysis
Analysis type	Transient
Frame	Frame (ref)
Weak constraints	Off
Constraint type	Ideal

D.5.4.3 Variables

Dependent variables: pw

Shape functions: shlag(2,'pw')

Interior boundaries not active

D.5.4.4 Boundary Settings

Boundary		1, 3, 5-7	2
Type		Zero flux/Symmetry	Pressure
Pressure (p0)	Pa	0	**6**
Inward flux (N0)	m/s	0	**-9e-4**

D.5.4.5 Subdomain Settings

Locked Subdomains: 2

Subdomain		1	2
Storage term (S)	1	**0**	**Cp**
Saturated permeability (kaps)	m^2	**kaps**	**kaps*krw**
Density, fluid (rhof)	kg/m^3	**rhow**	**rhow**
Viscosity, fluid (eta)	$Pa \cdot s$	**etaw**	**etaw**

Subdomain initial value		1	2
Pressure (pw)	Pa	pw_in	pw_in

D.5.5 Application Mode: Darcy's Law (nw)

Application mode type: Darcy's Law (Earth Science Module)

Application mode name: nw

D.5.5.1 Scalar Variables

Name	Variable	Value	Unit	Description
tscale	tscale_nw	1e-5	s	Heaviside scaling factor
g	g_nw	9.82*hour*hour	m/s^2	Gravity
D	D_nw	y	m	Elevation/vertical axis

D.5.5.2 Application Mode Properties

Property	**Value**
Default element type	Lagrange - Quadratic
Variable	Pressure analysis
Analysis type	Transient
Frame	Frame (ref)
Weak constraints	Off
Constraint type	Ideal

D.5.5.3 Variables

Dependent variables: pnw

Shape functions: shlag(2,'pnw')

Interior boundaries not active

D.5.5.4 Boundary Settings

Boundary		3-4, 7	5
Type		Zero flux/Symmetry	Pressure
Pressure (p0)	Pa	0	**6**

D.5.5.5 Subdomain Settings

Locked Subdomains: 2

Subdomain		2
Storage term (S)	1	**Cp**
Saturated permeability (kaps)	m^2	**kaps*krnw**
Density, fluid (rhof)	kg/m^3	**rhonw**
Viscosity, fluid (eta)	$Pa \cdot s$	**etanw**

Subdomain initial value		2
Pressure (pnw)	Pa	pnw_in

D.6 Interpolation Functions

D.6.1 Interpolation Function: Hpnw_t

Interpolation method: Linear

Data source type: Table

x	**f(x)**
0	0.4
21.2	0.4
21.25	0.6
45.2	0.6
45.25	0.8
68.95	0.8
69	1
92.95	1
93	1.5
122.45	1.5
122.5	2
154.95	2
155	4
200	4

D.7 Solver Settings

Solve using a script: off

Analysis type	Transient
Auto select solver	On
Solver	Time dependent
Solution form	Automatic
Symmetric	auto
Adaption	Off
Optimization	Off

D.7.1 Direct (UMFPACK)

Solver type: Linear system solver

Parameter	**Value**
Pivot threshold	0.1
Memory allocation factor	0.7

D.7.2 Time Stepping

Parameter	**Value**
Times	0: 0.1:120
Relative tolerance	0.01
Absolute tolerance	0.0010
Times to store in output	Specified times
Time steps taken by solver	Free
Manual tuning of step size	Off
Initial time step	0.0010
Maximum time step	1.0
Maximum BDF order	5
Singular mass matrix	Maybe
Consistent initialization of DAE systems	Backward Euler
Error estimation strategy	Include algebraic
Allow complex numbers	Off

D.7.3 Advanced

Parameter	Value
Constraint handling method	Elimination
Null-space function	Automatic
Assembly block size	5000
Use Hermitian transpose of constraint matrix and in symmetry detection	Off
Use complex functions with real input	Off
Stop if error due to undefined operation	On
Store solution on file	Off
Type of scaling	Automatic
Manual scaling	
Row equilibration	On
Manual control of reassembly	Off
Load constant	On
Constraint constant	On
Mass constant	On
Damping (mass) constant	On
Jacobian constant	On
Constraint Jacobian constant	On

D.8 Postprocessing

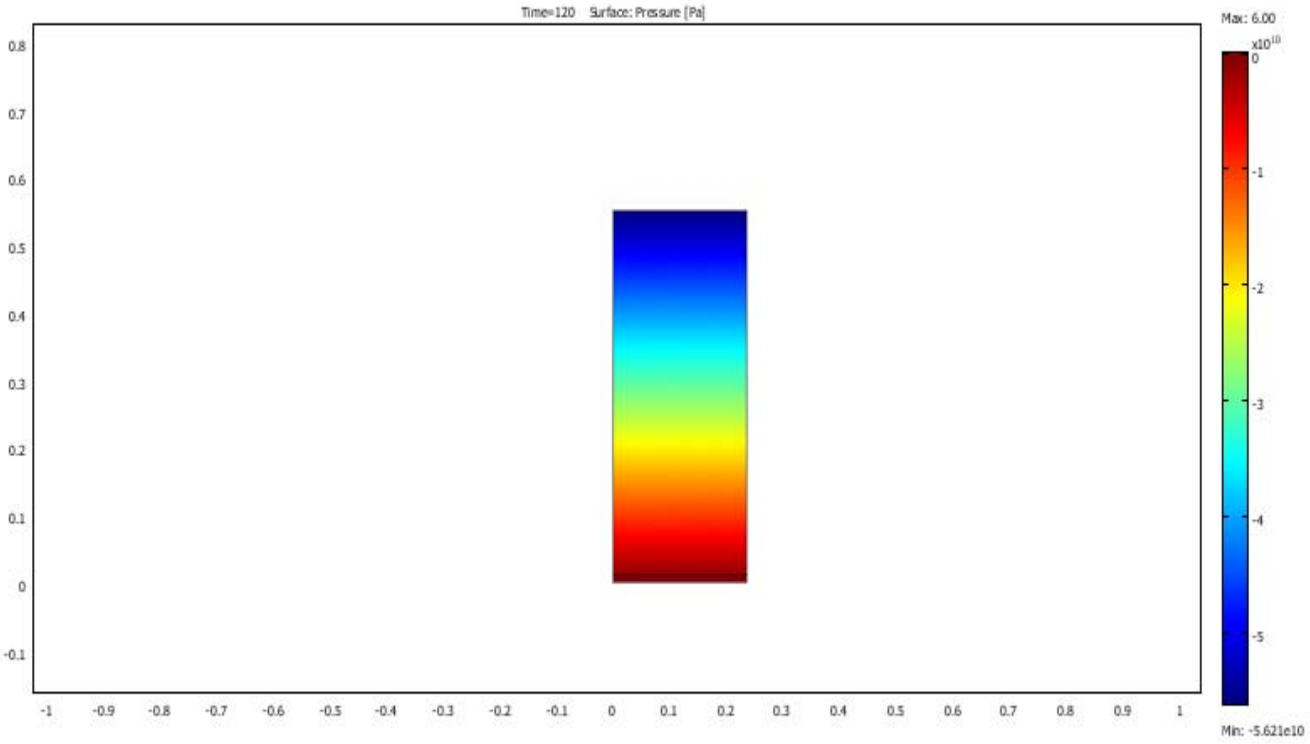

D.9 Equations

D.9.1 Subdomain

Dependent variables: pw, pnw

D.9.1.1 Subdomain: 2

Diffusion coefficient (c)

pw	pnw
-diff(kap_w*(-pwx/eta_w-rhof_w*g_w*diff(D_w,x)/eta_w),pwx), -diff(kap_w*(-pwy/eta_w-rhof_w*g_w*diff(D_w,y)/eta_w),pwx), -diff(kap_w*(-pwx/eta_w-rhof_w*g_w*diff(D_w,x)/eta_w),pwy), -diff(kap_w*(-pwy/eta_w-rhof_w*g_w*diff(D_w,y)/eta_w),pwy)	-diff(kap_w*(-pwx/eta_w-rhof_w*g_w*diff(D_w,x)/eta_w),pnwx), -diff(kap_w*(-pwy/eta_w-rhof_w*g_w*diff(D_w,y)/eta_w),pnwx), -diff(kap_w*(-pwx/eta_w-rhof_w*g_w*diff(D_w,x)/eta_w),pnwy), -diff(kap_w*(-pwy/eta_w-rhof_w*g_w*diff(D_w,y)/eta_w),pnwy)
-diff(kap_nw*(-pnwx/eta_nw-rhof_nw*g_nw*diff(D_nw,x)/eta_nw),pwx), -diff(kap_nw*(-pnwy/eta_nw-rhof_nw*g_nw*diff(D_nw,y)/eta_nw),pwx), -diff(kap_nw*(-pnwx/eta_nw-rhof_nw*g_nw*diff(D_nw,x)/eta_nw),pwy), -diff(kap_nw*(-pnwy/eta_nw-rhof_nw*g_nw*diff(D_nw,y)/eta_nw),pwy)	-diff(kap_nw*(-pnwx/eta_nw-rhof_nw*g_nw*diff(D_nw,x)/eta_nw),pnwx), -diff(kap_nw*(-pnwy/eta_nw-rhof_nw*g_nw*diff(D_nw,y)/eta_nw),pnwx), -diff(kap_nw*(-pnwx/eta_nw-rhof_nw*g_nw*diff(D_nw,x)/eta_nw),pnwy), -diff(kap_nw*(-pnwy/eta_nw-rhof_nw*g_nw*diff(D_nw,y)/eta_nw),pnwy)

Damping/Mass coefficient (da)

pw	pnw
Cp+eps	-Cp+eps
-Cp+eps	Cp+eps

Conservative flux convection coeff. (al)

pw	pnw
-diff(kap_w*(-pwx/eta_w-rhof_w*g_w*diff(D_w,x)/eta_w),pw), -diff(kap_w*(-pwy/eta_w-rhof_w*g_w*diff(D_w,y)/eta_w),pw)	-diff(kap_w*(-pwx/eta_w-rhof_w*g_w*diff(D_w,x)/eta_w),pnw), -diff(kap_w*(-pwy/eta_w-rhof_w*g_w*diff(D_w,y)/eta_w),pnw)
-diff(kap_nw*(-pnwx/eta_nw-rhof_nw*g_nw*diff(D_nw,x)/eta_nw),pw), -diff(kap_nw*(-pnwy/eta_nw-rhof_nw*g_nw*diff(D_nw,y)/eta_nw),pw)	-diff(kap_nw*(-pnwx/eta_nw-rhof_nw*g_nw*diff(D_nw,x)/eta_nw),pnw), -diff(kap_nw*(-pnwy/eta_nw-rhof_nw*g_nw*diff(D_nw,y)/eta_nw),pnw)

Conservative flux source term (ga)

kap_w*(-pwx/eta_w-rhof_w*g_w*diff(D_w,x)/eta_w), kap_w*(-pwy/eta_w-rhof_w*g_w*diff(D_w,y)/eta_w)
kap_nw*(-pnwx/eta_nw-rhof_nw*g_nw*diff(D_nw,x)/eta_nw), kap_nw*(-pnwy/eta_nw-rhof_nw*g_nw*diff(D_nw,y)/eta_nw)

Initial value (init)

pw	pw_in
pnw	pnw_in

D.10 Variables

D.10.1 Point

D.10.1.1 Point 1, 4

Name	Description	Unit	Expression
rhof_w	Density	kg/m^3	rhow
rhof_nw	Density	kg/m^3	

D.10.1.2 Point 2-3, 5-6

Name	Description	Unit	Expression
rhof_w	Density	kg/m^3	rhow
rhof_nw	Density	kg/m^3	rhonw

D.10.2 Boundary

D.10.2.1 Boundary 1-2, 6

Name	Description	Unit	Expression
nU_w	Normal velocity	m/s	u_w * nx_w+v_w * ny_w
flux_w	Outward flux	m/s	u_w * nx_w+v_w * ny_w
nU_nw	Normal velocity	m/s	
flux_nw	Outward flux	m/s	

D.10.2.2 Boundary 3-5, 7

Name	Description	Unit	Expression
nU_w	Normal velocity	m/s	u_w * nx_w+v_w * ny_w
flux_w	Outward flux	m/s	u_w * nx_w+v_w * ny_w
nU_nw	Normal velocity	m/s	u_nw * nx_nw+v_nw * ny_nw
flux_nw	Outward flux	m/s	u_nw * nx_nw+v_nw * ny_nw

D.10.3 Subdomain
D.10.3.1 Subdomain 1

Name	Description	Unit	Expression
S_w	Storage term	1/Pa	0
Qs_w	Liquid source	1/s	0
K_w	Hydraulic conductivity tensor	m/s	Ks_w * CKs_w
Kxx_w	Hydraulic conductivity tensor	m/s	K_w
Kxy_w	Hydraulic conductivity tensor	m/s	0
Kyx_w	Hydraulic conductivity tensor	m/s	0
Kyy_w	Hydraulic conductivity tensor	m/s	K_w
kap_w	Permeability tensor	m^2	kaps_w * CKs_w
kapxx_w	Permeability tensor	m^2	kap_w
kapxy_w	Permeability tensor	m^2	0
kapyx_w	Permeability tensor	m^2	0
kapyy_w	Permeability tensor	m^2	kap_w
gradP_w	Pressure gradient	Pa/m	sqrt(pwx^2+pwy^2)
u_w	x-velocity	m/s	(-kapxx_w * (pwx+diff(rhof_w * g_w * D_w,x))-kapxy_w * (pwy+diff(rhof_w * g_w * D_w,y)))/eta_w
v_w	y-velocity	m/s	(-kapyx_w * (pwx+diff(rhof_w * g_w * D_w,x))-kapyy_w * (pwy+diff(rhof_w * g_w * D_w,y)))/eta_w
U_w	Velocity field	m/s	sqrt(u_w^2+v_w^2)
S_nw	Storage term	1/Pa	
Qs_nw	Liquid source	1/s	
K_nw	Hydraulic conductivity tensor	m/s	
Kxx_nw	Hydraulic conductivity tensor	m/s	
Kxy_nw	Hydraulic conductivity tensor	m/s	
Kyx_nw	Hydraulic conductivity tensor	m/s	
Kyy_nw	Hydraulic conductivity tensor	m/s	
kap_nw	Permeability tensor	m^2	
kapxx_nw	Permeability tensor	m^2	
kapxy_nw	Permeability tensor	m^2	

kapyx_nw	Permeability tensor	m^2	
kapyy_nw	Permeability tensor	m^2	
gradP_nw	Pressure gradient	Pa/m	
u_nw	x-velocity	m/s	
v_nw	y-velocity	m/s	
U_nw	Velocity field	m/s	

D.10.3.2 Subdomain 2

Name	Description	Unit	Expression
S_w	Storage term	1/Pa	Cp * CSs_w
Qs_w	Liquid source	1/s	0
K_w	Hydraulic conductivity tensor	m/s	Ks_w * CKs_w
Kxx_w	Hydraulic conductivity tensor	m/s	K_w
Kxy_w	Hydraulic conductivity tensor	m/s	0
Kyx_w	Hydraulic conductivity tensor	m/s	0
Kyy_w	Hydraulic conductivity tensor	m/s	K_w
kap_w	Permeability tensor	m^2	kaps_w * CKs_w
kapxx_w	Permeability tensor	m^2	kap_w
kapxy_w	Permeability tensor	m^2	0
kapyx_w	Permeability tensor	m^2	0
kapyy_w	Permeability tensor	m^2	kap_w
gradP_w	Pressure gradient	Pa/m	sqrt(pwx^2+pwy^2)
u_w	x-velocity	m/s	(-kapxx_w * (pwx+diff(rhof_w * g_w * D_w,x))-kapxy_w * (pwy+diff(rhof_w * g_w * D_w,y)))/eta_w
v_w	y-velocity	m/s	(-kapyx_w * (pwx+diff(rhof_w * g_w * D_w,x))-kapyy_w * (pwy+diff(rhof_w * g_w * D_w,y)))/eta_w
U_w	Velocity field	m/s	sqrt(u_w^2+v_w^2)
S_nw	Storage term	1/Pa	Cp * CSs_nw
Qs_nw	Liquid source	1/s	0
K_nw	Hydraulic conductivity tensor	m/s	Ks_nw * CKs_nw

Kxx_nw	Hydraulic conductivity tensor	m/s	K_nw
Kxy_nw	Hydraulic conductivity tensor	m/s	0
Kyx_nw	Hydraulic conductivity tensor	m/s	0
Kyy_nw	Hydraulic conductivity tensor	m/s	K_nw
kap_nw	Permeability tensor	m^2	kaps_nw * CKs_nw
kapxx_nw	Permeability tensor	m^2	kap_nw
kapxy_nw	Permeability tensor	m^2	0
kapyx_nw	Permeability tensor	m^2	0
kapyy_nw	Permeability tensor	m^2	kap_nw
gradP_nw	Pressure gradient	Pa/m	sqrt(pnwx^2+pnwy^2)
u_nw	x-velocity	m/s	(-kapxx_nw * (pnwx+diff(rhof_nw * g_nw * D_nw,x))-kapxy_nw * (pnwy+diff(rhof_nw * g_nw * D_nw,y)))/eta_nw
v_nw	y-velocity	m/s	(-kapyx_nw * (pnwx+diff(rhof_nw * g_nw * D_nw,x))-kapyy_nw * (pnwy+diff(rhof_nw * g_nw * D_nw,y)))/eta_nw
U_nw	Velocity field	m/s	sqrt(u_nw^2+v_nw^2)